University of Alberta

Developments and Mechanistic Investigations of Ester, Imide, and Ketone Hydrogenations

by

Satoshi Takebayashi

A thesis submitted to the Faculty of Graduate Studies and Research
in partial fulfillment of the requirements for the degree of

Doctor of Philosophy

Department of Chemistry

Examining Committee

Dr. Steven H. Bergens, Department of Chemistry

Dr. Derrick L. J. Clive, Department of Chemistry

Dr. Martin Cowie, Department of Chemistry

Dr. Eric Rivard, Department of Chemistry

Dr. Natalia Semagina, Department of Chemical and Material Engineering

Dr. R. Tom Baker, Department of Chemistry, University of Ottawa

To my loving family

Abstract

The Noyori-type catalyst *trans*-[Ru((*R*)-BINAP)(H)$_2$((*R*,*R*)-dpen)] (**6**) and its analogues are among the most active and enantioselective ketone hydrogenation systems reported to date. Its applications towards other types of carbonyl compounds are, however, understudied. This dissertation describes the first applications of this catalyst system towards hydrogenations of esters and imides under mild reaction conditions. Further, a detailed mechanistic study of this system is presented using ketones, esters, and imides as substrates.

The dihydride **6** was highly active towards the hydrogenation of esters. Stoichiometric reactions between **6** and lactones proceeded at –80 °C to form the net hydride insertion products, Ru-hemiacetaloxides. The hemiacetaloxides were further hydrogenated at –40 °C under ~2 atm of H$_2$ to form the corresponding Ru-alkoxides. Catalytic hydrogenations could be carried out, even at –20 °C under 4 atm of H$_2$, however, these hydrogenations slowed over time due to deactivation of the catalyst by primary alcohol products.

The first homogeneous monohydrogenation of imides was developed using **6** and related compounds as catalysts. Further, upon optimization of reaction conditions and imide structure, *meso*-cyclic imides were desymmetrized in high ee via the monohydrogenation to form kinetically unfavoured *trans*-hydroxy lactams with up to 5 stereogenic centres. Furthermore, the number of stereogenic centres was increased

from 5 to 7 using *N*-acyliminium ion chemistry. A model for the origin of enantioselection was proposed using substrate-catalyst steric interactions. Low temperature NMR studies revealed that base catalyzes the rapid cis-trans isomerization to form the thermodynamically more stable *trans*-isomer. It was proposed that this rapid isomerization prevents racemization of a product.

Transition states for the formation of Ru-alkoxides from addition between **6** and acetophenone were studied using an intramolecular trapping experiment. Addition between **6** and 4-hydroxymethylacetophenone at –80 °C exclusively formed the net hydride insertion product, Ru-secondary-alkoxide. Combined with controlled experiments, this result is strong evidence for the formation of a Ru–O interaction in the transition state, which supports concerted formation of the Ru-alkoxides from **6** and acetophenone.

Acknowledgements

Table of contents

Chapter 3

Ru Catalyzed Enantioselective Desymmetrization of *meso*-Cyclic Imides via Monohydrogenation

Chapter 4

Intramolecular Trapping Experiments to Investigate the Bifunctional Addition Step in Noyori-type Enantioselective Ketone Hydrogenations.

Chapter 5

Conclusions and Future Directions

References

List of Tables

Chapter 4

No Tables

Chapter 5

No Tables

List of Figures

Chapter 3

Chapter 4

Chapter 5

List of Schemes

Chapter 4

Chapter 5

List of Equations

List of Abbreviations

Å	angstrom
2-PrOH	2-propanol
Ac	acetyl
acac	acetylacetonate
AcOH	acetic acid
atm	atmosphere(s)
BINAP	2,2'-bis(diphenylphosphino)-1,1'-binaphthyl
Bn	benzyl
Boc	*tert*-butoxycarbonyl
BSA	*N*,*O*-bis(trimethylsilyl)acetamide
Bu	butyl
calcd	calculated
cm	centimeter(s)
COD	cyclooctadiene
Cp	cyclopentadienyl
Cp*	pentamethylcyclopentadienyl
Cy	cyclohexyl
d.r.	diastereomeric ratio
daipen	1,1-bis(4-methoxyphenyl)-3-methyl-1,2-butanediamine
δ	chemical shift(s)
DIBAL-H	diisobutylaluminum hydride
dpen	1,2-diphenylethylenediamine

dppp	1,3-bis(diphenylphosphino)propane
ee	enantiomeric excess
en	Ethylenediamine
equiv	equivalent(s)
ESI	electrospray ionization
ESI-MS	electrospray ionization mass spectrometry
Et	Ethyl
FTIR	fourier transform infrared spectroscopy
GC	gas chromatography
gCOSY	gradient correlation spectroscopy
gHMBC	gradient heteronuclear multiple bond correlation
gHSQC	gradient heteronuclear single quantum coherence
gTOCSY	gradient total correlation spectroscopy
h	hour(s)
HOMO	highest occupied molecular orbital
HPLC	high-performance liquid chromatography
HRMS	high resolution mass spectrometry
Hz	Hertz
i.d.	internal diameter
i-Pr	Isopropyl
IR	infrared spectroscopy
KIE	kinetic isotope effect
LUMO	lowest occupied molecular orbital

M.p.	melting point
Me	methyl
MeOH	methanol
mg	milligram(s)
MHz	megahertz
μL	microliter(s)
min	minute(s)
mL	milliliter
mM	millimolar
mm	millimeter
mmol	millimole
mol%	mole percent
NMR	nuclear magnetic resonance spectroscopy
ORTEP	Oak Ridge thermal-ellipsoid plot
Ph	phenyl
pica	2-aminomethylpyridine
psi	pounds per square inch
Py	pyridine
RT	room temperature
t-Bu	*tert*-butyl
t-BuOH	*tert*-butyl alcohol
TFA	trifluoro acetic acid
THF	tetrahydrofuran

TMS   Tetramethylsilane

TOF   turnover frequency

TON   turnover number

Ts   *p*-toluenesulfonyl

UV   Ultraviolet

Chapter 1

Introduction

The development of organic synthesis in industry

Since Wohler's preparation of urea from ammonium isocyanate in 1828,[1] organic synthesis has become a central component of modern academic and industrial chemistry.[2] The methodologies for synthesizing complex molecules are extensively developed, and the high level of synthetic sophistication now available allows the production and commercialization of many complex compounds, such as (+)-discodermolide, a potent anti-cancer drug that contains 13 stereogenic centres (Figure 1-1).[3] Surprisingly, 60 g of this compound was made in 39 steps by Novartis International AG in 2004 for phase 1 clinical trials.[4]
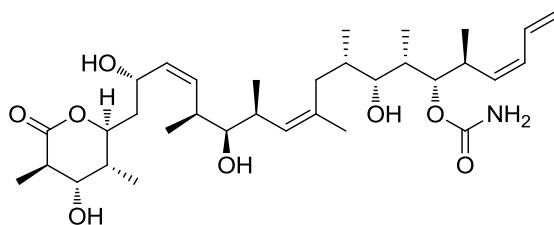
Figure 1-1. Chemical structure of a potent anticancer drug (+)-discodermolide.

The modern fine chemical and pharmaceutical industries are established upon the tremendous advances made in organic synthesis over the last century. Since many well-established methodologies were developed in an era when the toxicities of many reagents were unknown,

and/or when minimization of waste was not a paramount priority, industrial-scale synthesis is often associated with negative environmental impacts. These negative impacts are the incentive for the development of Green Chemistry, and the minimization or elimination of environmental harm by industrial chemistry is among the highest priorities of modern organic chemistry.[5]

Green chemistry in the fine chemical and pharmaceutical industries

The term "Green Chemistry" was coined by Anastas of the US Environmental Protection Agency in 1993.[6] Its concise definition is as follows: *Green chemistry efficiently utilizes raw materials, eliminates waste and avoids the use of toxic and/or hazardous reagents and solvents in the manufacture of chemical products.*[5] One issue raised by this definition is how to evaluate the efficiency of chemical processes. There are several metrics used to assess the efficiencies of chemical processes such as atom economy,[7] Process Mass Intensity (PMI),[8] E factor,[9] and others. The E factor is among the most frequently used by industry and is formulated as the mass of waste per mass of desired product. The ideal chemical process should thus have E factor of 0. Table 1-1 shows typical E factors for representative segments of chemical industry.[9]

Table 1-1. E factors for various chemical industries.

Industries	Annual production (t)	Waste produced (t)	E factor
Oil refining	10^6 - 10^8	10^5 - 10^7	< 0.1
Bulk chemicals	10^4 - 10^6	10^4 - 5×10^6	< 1 - 5
Fine chemicals	10^2- 10^4	5×10^2 - 5×10^5	5 - 50
Pharmaceuticals	10 - 10^3	2.5×10^2 - 10^5	25 - 100

These data show that the E factor increases from the oil refining to the pharmaceutical industries. There are three major reasons for the high E factor in the fine chemical and pharmaceutical industries. First, the profit margin in those industries is much higher than those of the oil/bulk industries. As a result, minimization of the cost associated with waste management is often not the highest priority in these industries. In addition, the production volume of these industries is relatively small compared to the others. Thus, even though the E factors of fine chemical and pharmaceutical industries are high, the amount of waste produced is relatively small (Table 1-1). Second, unlike oil/bulk chemicals, fine chemicals and pharmaceuticals are often produced via multi-step synthesis, often with each step producing waste. For example, one of the most cost-effective processes to produce the anti-inflammatory drug naproxen consists of five synthetic steps with waste products that include CH_2Cl_2, HBr, NaBr, and MgX_2 (X = Br or Cl) (Scheme 1-1).[10] Another example is the large scale synthesis of (+)-discodermolide described in page 1. Even if

each step of this 39-step synthesis proceeds in 90% yield, the yield of final product is 1.6%.

Scheme 1-1. A relatively cost-effective process for the production of (*S*)-naproxen.
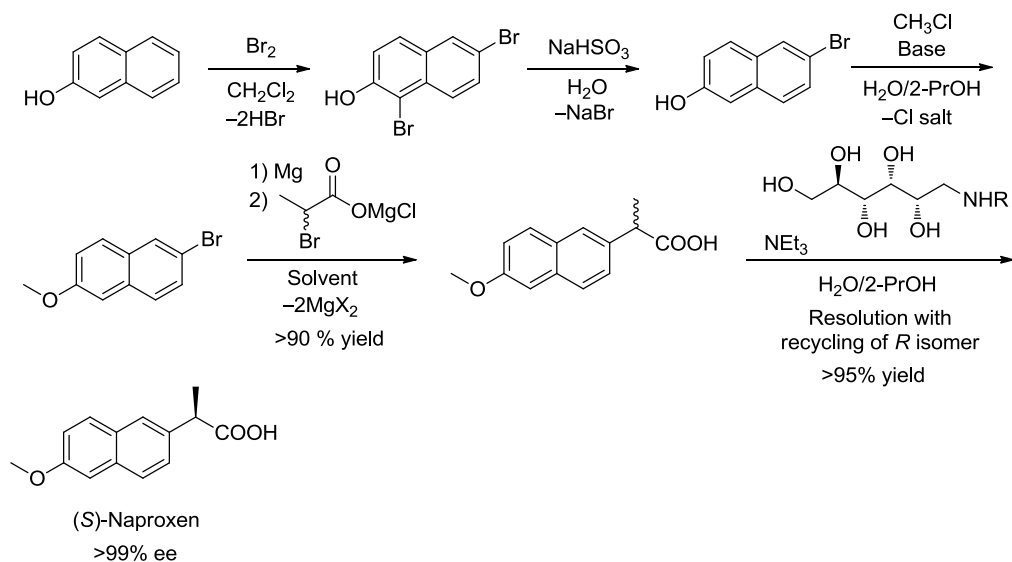
Furthermore, the purity of fine chemicals and pharmaceuticals must be near absolute, as the products are meant for human consumption. For example, naproxen is currently produced as the enantiomerically pure *S* isomer because presence of the less active *R* isomer is associated with liver damage.[11] The requirement for higher purities translates into more purification steps with increasing waste production, mainly as solvent. The third reason for the larger E values in the fine chemical and pharmaceutical industries is the need for quick product development, resulting from a competitive market place, and from shorter life cycles of products compared to that of bulk chemicals. This time factor is one of the major

obstacles to replace well established, yet wasteful processes with new environmentally (and often economically) superior processes, especially when developing a process for a first-in-class drug.[12]

The increasing environmental concerns regarding chemical industry have, however, changed the situation since the 90's. In fact, the 2005 Nobel Prize in chemistry was awarded to Y. Chauvin, R. H. Grubbs, and R. R. Schrock for the development of step-reducing, metathesis methodologies in organic synthesis.[13] A number of methods are under development in both academia and industry to reduce waste production in the fine chemical and pharmaceutical industries.[14(a)] For example, a new cost-efficient and environmentally superior process to produce (*S*)-naproxen was developed by Albemarle in 1998 using the Heck and carbonylation reactions (Scheme 1-2).[14(b)] This new process eliminated the MgX_2 waste associated with the Grignard reaction, and it is now used in commercial production on the 500 ton/year scale.[15]

Scheme 1-2. New catalytic process for the production of (*S*)-naproxen.

5
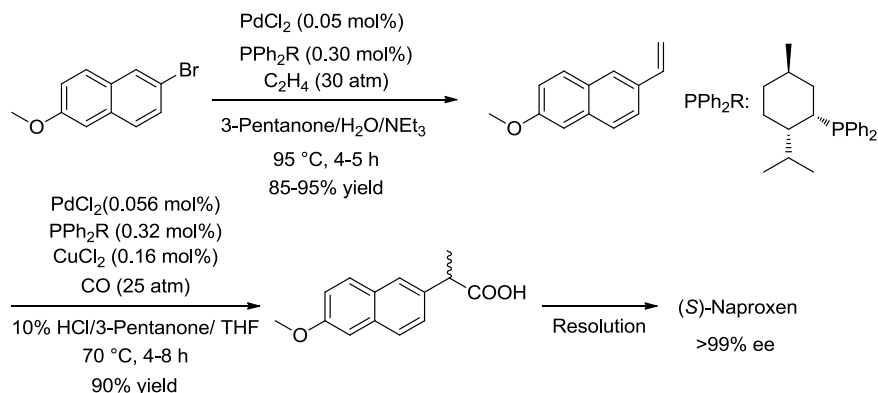
The major approaches to reduce waste production in large-scale synthesis include catalysis, alternate reaction solvents, and one-pot/cascade reactions.[5] Each of these approaches has examples adopted by industry as an environmentally superior method. For example, Pfizer received a Presidential Green Chemistry Challenge Award in 2002 for the switch to environmentally friendly solvents for the synthesis of antidepressant sertraline.[16] In this process, they replaced three solvents (THF, toluene, and hexanes) with ethanol. As a result, they achieved a 24% reduction of the volume of solvents used, and eliminated the processes required to recover three different solvents. In addition, ethanol is less toxic than THF, toluene, and hexanes (Scheme 1-3).

Scheme 1-3. More environmentally friendly sertraline process.

Sertraline HCl salt
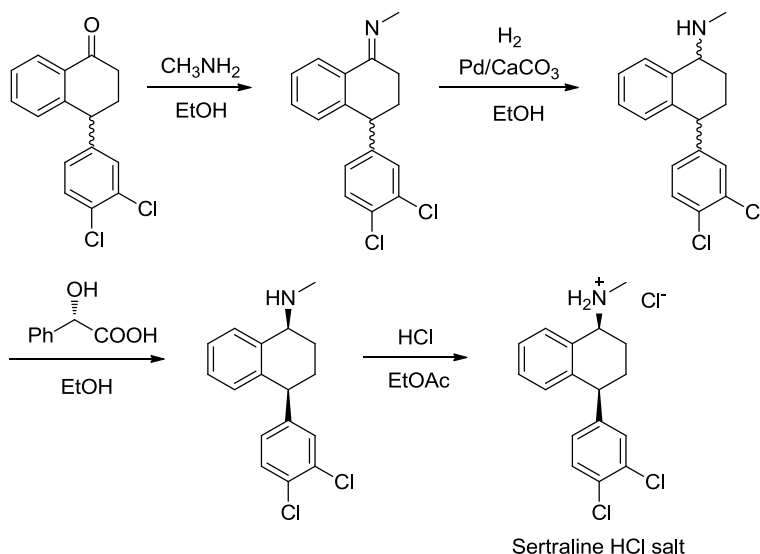
Catalysis in the fine chemical and pharmaceutical industries

The largest advantage of catalysis is its high atom efficiency. For

example, catalytic reduction and oxidation can eliminate waste generated by stoichiometric reagents such as Na and NaBH$_4$ for reductions, and chromium reagents for oxidations. The major challenge in fine chemical catalysis is the development of processes based on H$_2$, O$_2$, H$_2$O$_2$, CO, CO$_2$, and NH$_3$ as abundant and clean sources of H, O, C, and N.

Scheme 1-4. Classical and new ibuprofen processes.
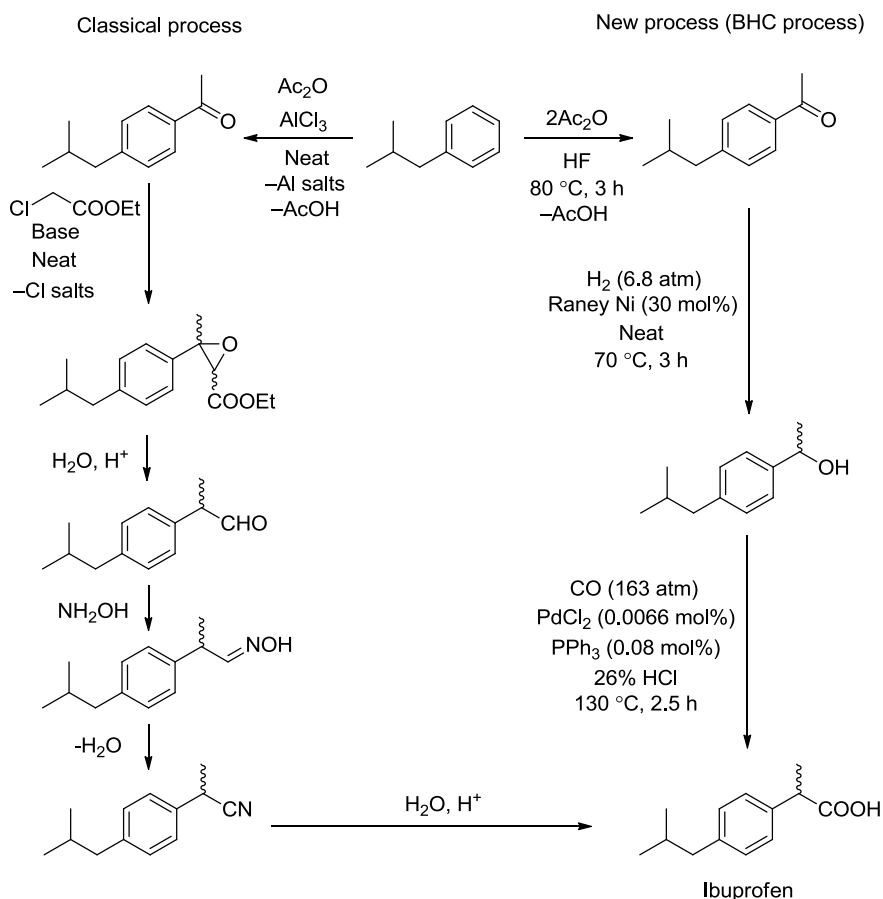
An excellent example of an atom-efficient process utilizing catalysis is that developed by the Boots-Hoechst-Celanese (BHC) Company for the production of the anti-inflammatory drug ibuprofen.[5,17]

Scheme 1-4 shows both the classical and new processes for the production of ibuprofen. Note the exact reaction conditions used in the production scale are a trade secret, and the reaction conditions given in Scheme 1-4 are adopted from a patent.

The classical route consists of six steps with stoichiometric reagents that proceed with the formation of inorganic salts. As a result, the atom utilization of this process is less than 40%. The new route developed by BHC is a three-step synthesis with two catalytic reactions. Furthermore, the catalytic reactions utilize H_2 and CO respectively as a source of H and CO. The catalytic carbonylation reaction in the third step of BHC process is proposed to proceed via formation of the corresponding chloride from the starting alcohol, followed by oxidative addition of the C–Cl bond, CO insertion, and reductive elimination to form ibuprofen (Scheme 1-5).[18]

Scheme 1-5. Proposed catalytic cycle of the carbonylation reaction.
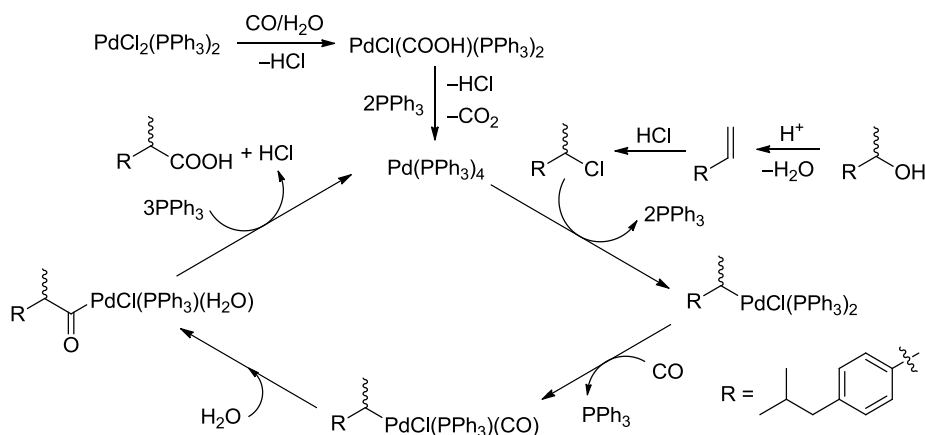
This process operates with nominal overall atom utilizations of 80%, and can reach nearly 99% by recycling acetic acid and hydrogen fluoride.

8

Even though (*S*)-ibuprofen is the active enantiomer, racemic ibuprofen is produced because ibuprofen is known to racemize under physiological conditions.[11] The BHC process was commercialized in 1992 in a ca. 4000 ton/year facility, and received the Presidential Green Chemistry Challenge Award in 1997.

Another major challenge in catalysis is producing high chemo-, regio-, diastereo-, and enantioselectivity. The development of enantioselective catalytic process is a high priority in the fine chemical and pharmaceutical industries since the announcement of regulations from the U.S. Food and Drug Administration (FDA) regarding stereoisomeric drugs in 1992.[19] This announcement stated that pharmacological activities of all stereoisomers should be investigated in animals and/or in humans. Usually the additional cost of producing enantiomerically pure drugs is lower than that of investigating pharmacological activities of unwanted enantiomers.[20] As a result, many pharmaceutical companies have started producing enantiomerically pure drugs since the regulation was implemented. In fact, the major form of stereoisomeric drugs marketed before the new legislation was introduced was racemic. As Figure 1-1 shows, racemic drugs are nearly no longer marketed.[20]
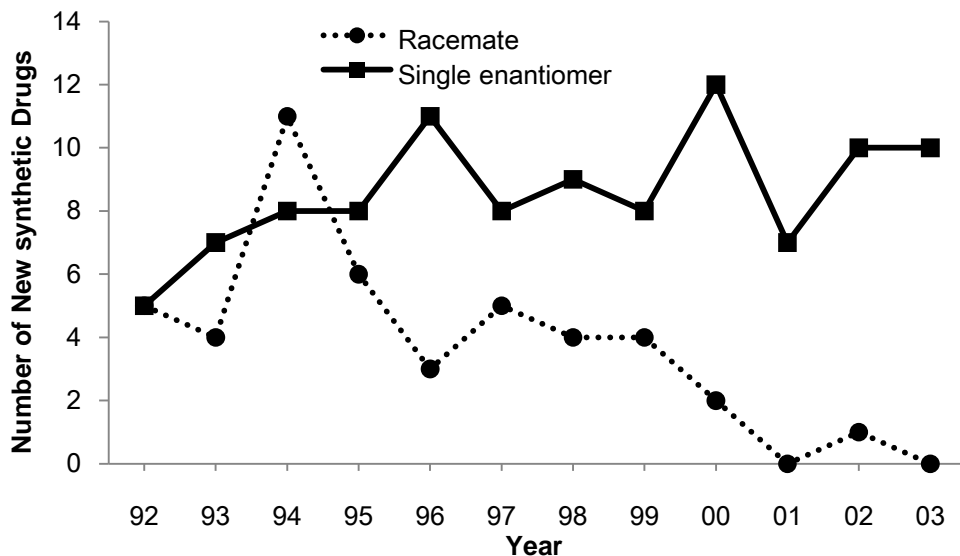
Figure 1-2. Number of marketed racemic/enantiomerically pure synthetic drugs.[20]

The three major methods utilized to produce enantiomerically pure products in industry are chiral pool, resolution, and enantioselective catalysis. Currently, more than half of industrial asymmetric synthesis is based on the use of starting materials from the chiral pool or the use of resolution.[20] Although technically easy, these methods are often associated with low atom efficiencies, and relatively narrow applicability. Conversely, enantioselective catalysis is atom-efficient, and it is a widely applicable method. Among the industrial enantioselective catalytic reactions currently in operation, hydrogenation is the most widely used. According to a recent review by Blaser and co-workers, at least 18 out of 38 catalytic asymmetric transformations in the fine chemical and pharmaceutical industries are asymmetric hydrogenations of C=C, C=O, or C=N functionalities.[21] The

popularity of asymmetric hydrogenation is mainly due to its simplicity, its broad scope, its high turnover number (TON) and turnover frequency (TOF), and its high degree of chemo-, regio-, diastereo-, and enantioselectivity. TON is the number of moles of product produced per mole of catalyst; TOF is TON per unit time. Hydrogenation is one of the few catalytic processes with which both atom efficiency and selectivity meet the level of sophistication required for pharmaceutical production.

Hydrogenation of carbonyl compounds

The reduction of carbonyl compounds to alcohols is a fundamental process in organic synthesis because the alcohol functionality is ubiquitous in nature. A wide variety of B-H and Al-H reagents, with well-established reactivities and selectivities have been developed since the discovery of $NaBH_4$ as a reducing agent in the 1940s.[22] The use of these stoichiometric hydride reagents in industry, however, has several disadvantages. First, these reagents are hazardous because they are highly reactive toward moisture. Second, and more importantly, these reagents generate stoichiometric amounts of boron or aluminum waste. From both an economic and environmental viewpoint, hydrogenation is preferred by industry. The following sections present recent developments in hydrogenation of ketones, esters, and imides with emphasis on mechanism and applicability. There are relatively few recent advances in the hydrogenation of acid anhydrides, carboxylic acids, and amides.[23,93] Hydrogenation of amides is discussed in Chapter 5.

11

Hydrogenation of ketones

There are a large number of heterogeneous and homogeneous catalysts that hydrogenate ketones. The typical choice of catalysts for heterogeneous ketone hydrogenation in industry includes Pd, Pt, Raney Ni, and Cu-Cr catalysts.[24] For enantioselective heterogeneous hydrogenations, Raney Ni with tartaric acid modifiers and Pt with cinchona alkaloids modifiers are the most common catalysts for β- and α-functionalized ketones respectively. These systems, however, show low enantioselectivity and TOF towards hydrogenation of simple ketones likely due to weaker coordination ability of simple ketones. One of the recent developments in this field is a heterogeneous Ir-PPh$_3$-cinchona alkaloids catalyst system that hydrogenates simple ketones under basic conditions with high enantioselectivity (typically > 80%), however, with low TOF (< 67/h) (Typical reaction conditions: 0.5 mol% catalyst, LiOH 40 mol%, 30 °C, 60 atm H$_2$).[25]

Typical homogeneous catalyst systems use Mo, W, Fe, Pd, Cu, Ru, Ir, or Rh as the metal centre.[26] Among them, Ru, Ir, and Rh catalysts with chiral bidentate phosphine ligands are the most common. Of this subset, Ru catalysts with chiral diphosphine ligands have proved to be the most versatile.[25(b)] For example, Ru(diphosphine)(X)$_2$ (X = halides) catalysts hydrogenate α- or β-functionalized ketones under neutral or acidic conditions with high enantioselectivities (Equations 1-1 and 1-2).[27]
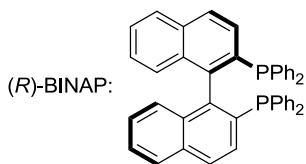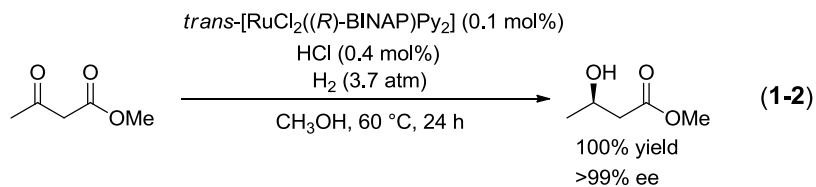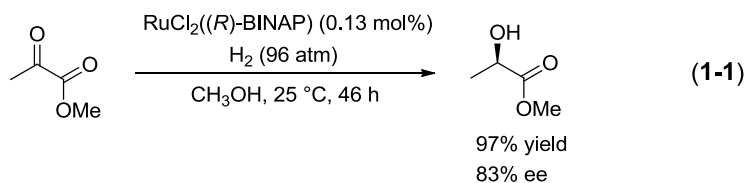
More recently, Noyori and co-workers discovered that the complexes *trans*-[Ru(diphosphine)(X)(Y)(diamine)] (X and/or Y = H, Cl, or BH$_4$) hydrogenate weakly coordinating, non-functionalized ketones with high TON, chemo-, and enantioselectivities. Examples include unsaturated ketones and sterically hindered *tert*-alkyl ketones under neutral or basic conditions (Equations 1-3 and 1-4).[28] With these two versatile classes of catalyst systems, Ru catalysts have become the most used chiral catalysts for ketone reduction in the fine chemical and pharmaceutical industries. Several chiral key alcohol-containing intermediates are produced using Ru-catalyzed ketone hydrogenations on industrial scales. Examples occur in the production of rivastatin (cholesterol-lowering agent),[29] (*S*)-oxfloxazin (bactericide),[21] carbapenem (antibiotic),[30] and vitamin B$_5$.[21]
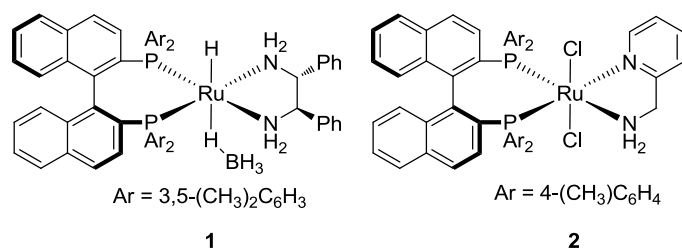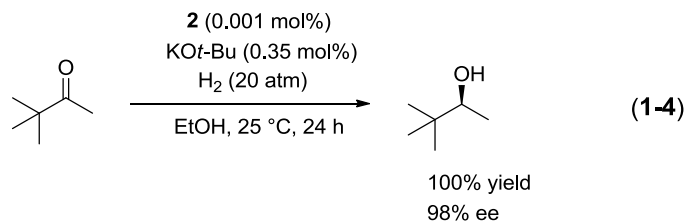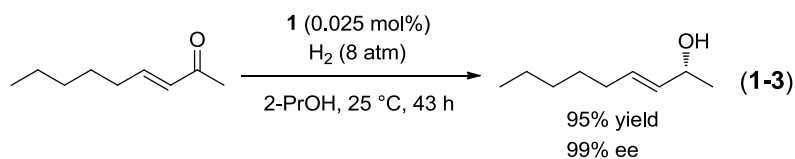
Reaction mechanism for Ru-catalyzed enantioselective ketone hydrogenation

The reaction mechanisms for the Ru(diphosphine)$(X)_2$ and the Ru(diphosphine)$(X)_2$(diamine) systems have been extensively studied by kinetic, computational, and stoichiometric methods.[31] Scheme 1-6 shows the proposed catalytic cycle for the Ru(diphosphine)$(X)_2$ system under acidic condition that takes into account all of the presently available mechanistic data.[27a]

Scheme 1-6. Proposed mechanism of Ru-diphosphine-X$_2$ catalyzed hydrogenation of ketones under acidic condition.
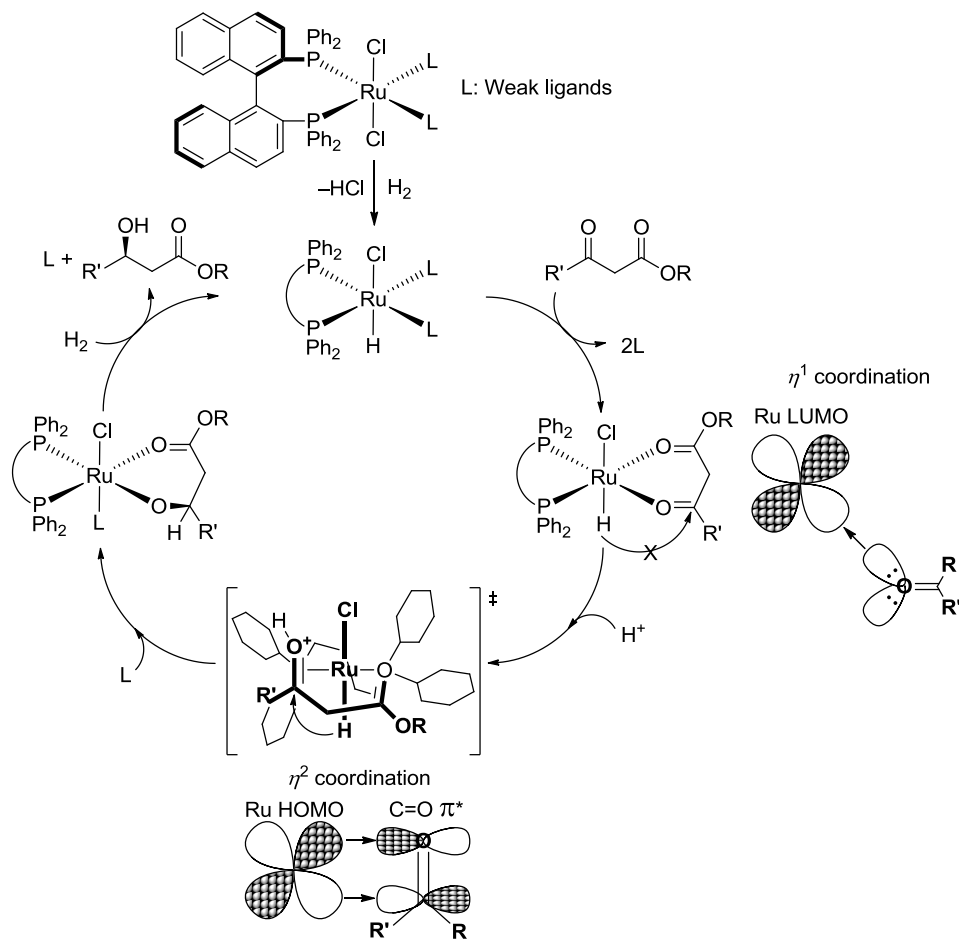
This cycle includes two important features that explain the reactivity of the catalysts. One is that the ketone needs to coordinate to the Ru centre prior to hydride insertion. This system thus proceeds via a so-called inner coordination sphere mechanism.[32] This requirement provides an explanation for the high reactivity and enantioselectivity of these systems towards functionalized ketones, but not towards weakly

15

coordinating, non-functionalized ketones. This requirement also provides an explanation for the poor C=O/C=C selectivity of these systems, as olefin hydrogenation also proceeds in the presence of a vacant coordination site. It is proposed that the ketone first coordinates as an η^1 (σ) ligand with electron donation from an oxygen lone pair to Ru(II) because η^1 coordination is preferred by electron deficient metal centres.[33] The coordination mode of the carbonyl then likely changes from η^1 to η^2 (π) to facilitate insertion into the M–H bond (Scheme 1-6). The acid additives increase the reaction rate. The rate increase is proposed to occur by increasing electrophilicity of carbonyl-carbon via protonation of carbonyl-oxygen.[27a]

Part of this proposed mechanism was directly observed by Daley and Bergens using NMR.[34] They used [Ru((R)-BINAP)(H)(CH$_3$CN)-(sol)$_2$]BF$_4$ (sol = THF or CH$_3$OH) (**3**) as a model for the Ru-H active catalyst in the proposed catalytic cycle, and observed insertions of the Ru-H into α,β-functionalized ketones at –30 °C to form Ru alkoxides **4** without observable pre-coordination of ketones (Equation 1-5). Thus, the Ru-H insertion is faster than the ketone coordination even without the assistance of protonation of the ketone. Further, they observed that stoichiometric hydrogenolysis of Ru-alkoxide **4** to form an alcohol product and **3** is slow (50 atm H$_2$, 50 °C, 1h, 100% yield), and has a similar rate to the rate of a catalytic reaction.

Sol = MeOH or THF

R = Me, *i*-Pr, *t*-Bu

−30 °C

3 **4** **(1-5)**
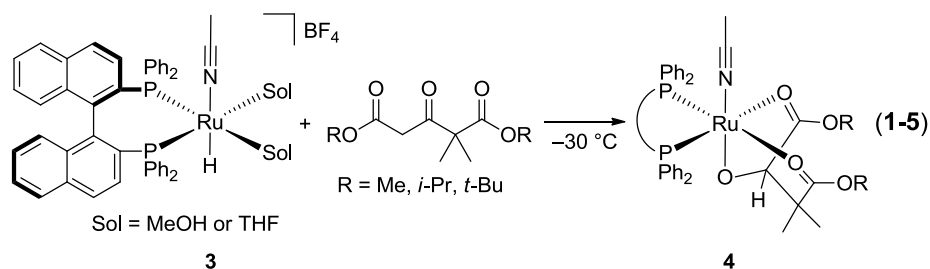
Based on these observations and observation of Ru-alkoxide **4** as the major Ru species in catalytic reaction mixture, they concluded that Ru–H insertion is not the rate limiting step, but hydrogenolysis of Ru-alkoxide to regenerate **3** is the rate limiting step in this catalyst system. They also observed rapid formation of an alcohol product and $[Ru((R)\text{-BINAP})(CH_3CN)_4](BF_4)_2$ upon addition of $HBF_4 \cdot OEt_2$ to a solution of Ru-alkoxide **4**. The acid additive, thus, possibly increases the reaction rate not by increasing the rate of Ru–H insertion, but by increasing the rate of turnover limiting Ru–O bond cleavage. This assumption is, however, oversimplified since protonation of **4** forms new cationic Ru(II) species that have to regenerate active Ru–H species.

Scheme 1-7 shows the proposed general catalytic cycles for the *trans*-$[Ru((R)\text{-BINAP})(Cl)_2((R,R)\text{-dpen})]$ catalyzed ketone hydrogenation in the presence of a base.[35] The active catalyst in these systems is *trans*-$[Ru((R)\text{-BINAP})(H)_2((R,R)\text{-dpen})]$ (**6**), formed by reaction of the dihalide precursor with base via formation of a Ru-dihydrogen complex **5**.

Scheme 1-7. Proposed general mechanism for the *trans*-[Ru((*R*)-BINAP)(Cl)$_2$((*R*,*R*)-dpen)]-catalyzed hydrogenation of ketones in the presence of a base.
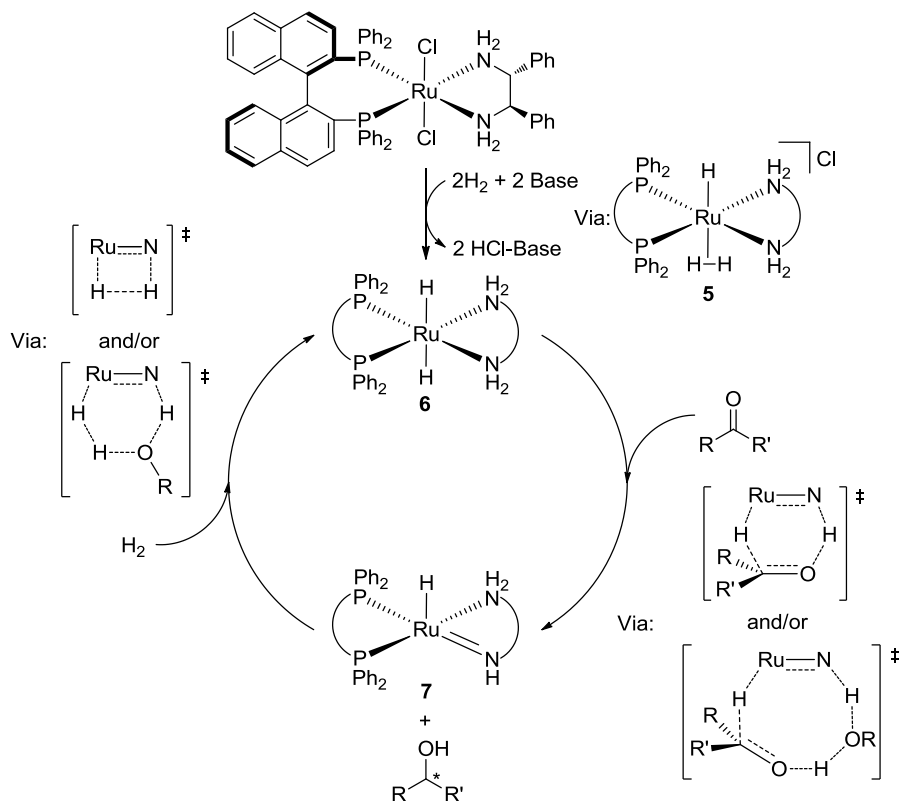
Unlike the Ru(diphosphine)(X)$_2$ system, ketones do not need to coordinate to Ru to undergo addition reaction with the Ru-hydride. Indeed, the Ru-dihydride cannot coordinate ketones prior to the insertion because it is a coordinatively saturated 18-electron complex. Instead of coordination, it is proposed that the Ru–H insertion occurs via ligand-assisted, bifunctional addition of nucleophilic Ru–H and protic N–H to a ketone carbonyl carbon and oxygen through a six-membered pericyclic transition state. Alternatively, in the presence of alcohol, a transition state with

solvent assistance is also proposed (Scheme 1-7). This system thus proceeds via an outer coordination sphere mechanism,[31] and hydrogenates both functionalized and non-functionalized ketones with high enantioselectivity because the pericyclic nature of the transition state minimizes conformational freedom, thereby maximizing the net asymmetric induction. Also, this system can selectively hydrogenate ketones in the presence of C=C bonds (Equation 1-3) because active Ru-dihydride **6** is coordinatively saturated. It is proposed that the addition of **6** and a ketone forms Ru-amide **7** and a free alcohol product. **7** then heterolytically cleaves H_2 to regenerate Ru-dihydride **6** via a four-membered transition state and/or a six-membered transition state mediated by a hydrogen-bonded alcohol molecule.

Morris and co-workers studied the reaction mechanism using *trans*-[Ru((R)-BINAP)(H)(Cl)(NH$_2$CMe$_2$CMe$_2$NH$_2$)] (**8**).[35a,b] They prepared Ru-dihydride **9** and Ru-amide **10** by reacting **8** with KOi-Pr in the presence or absence of H_2 respectively. They observed that Ru-dihydride **9** and 1 equiv of acetophenone reacted to form Ru-amide **10** and free product alcohol in C_6D_6 at room temperature. Further, they observed **10** reacted with H_2 to regenerate Ru-dihydride **9** at –60 °C (Equation 1-6). Based upon these observations as well as computational studies they proposed a reaction mechanism similar to that shown in Scheme 1-7. They proposed formation of a hydrogen bond between Ru-amide **10** and a product alcohol before formation of Ru-amide and the free alcohol (Equation 1-6).
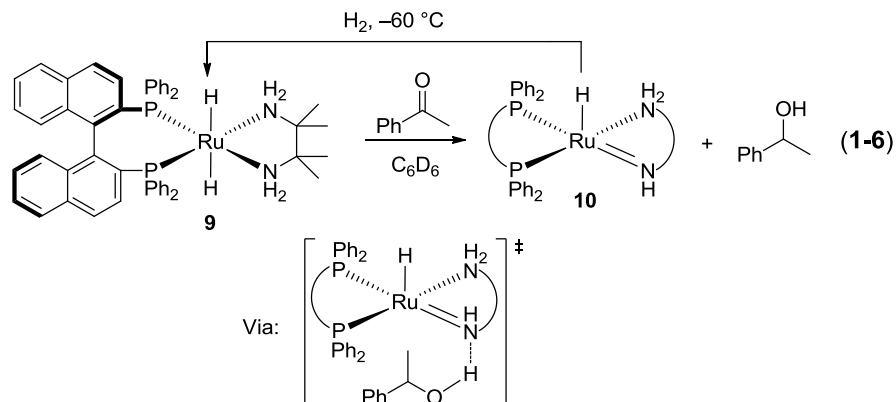
Noyori et al. studied related, *trans*-[Ru(diphosphine)(H)-(BH$_4$)(diamine)] catalyzed ketone hydrogenation that does not require base. They proposed the following catalytic cycle based on kinetic, mass spectrometric, and kinetic isotope effect experiments (Scheme 1-8).[35c] They proposed two catalytic cycles, namely cycle I and cycle II, to explain 25-fold enhancement of reaction rate when they used [KO*t*-Bu] = 10–15 mM, and 4–5-fold enhancement when [KO*t*-Bu] =20–130 mM compared to the rate under base-free conditions. They explained that cycle I has a larger relative contribution under base-free or lower [KO*t*-Bu] conditions, and deprotonation of Ru-dihydrogen complex **5** by 2-PrOH solvent or added base to form Ru-dihydride **6** is the turnover limiting step. The observed 25-fold rate enhancement is then explained by increased rate of the rate-limiting deprotonation step. The 4–5-fold rate enhancement under higher [KO*t*-Bu] was then explained by increased relative contribution of cycle II since higher [KO*t*-Bu] enhances deprotonation of 16 electron species **11** to form Ru-amide **7**, and hence lower [**5**] and relative contribution of cycle I. They proposed that rate of cycle II is lower than

20

cycle I because coordinatively saturated **7** is less reactive than coordinatively unsaturated **11** towards H_2.

Scheme 1-8. A proposed mechanism for the *trans*-[Ru(diphosphine)(H)-(BH$_4$)(diamine)] catalyzed hydrogenation of ketones.
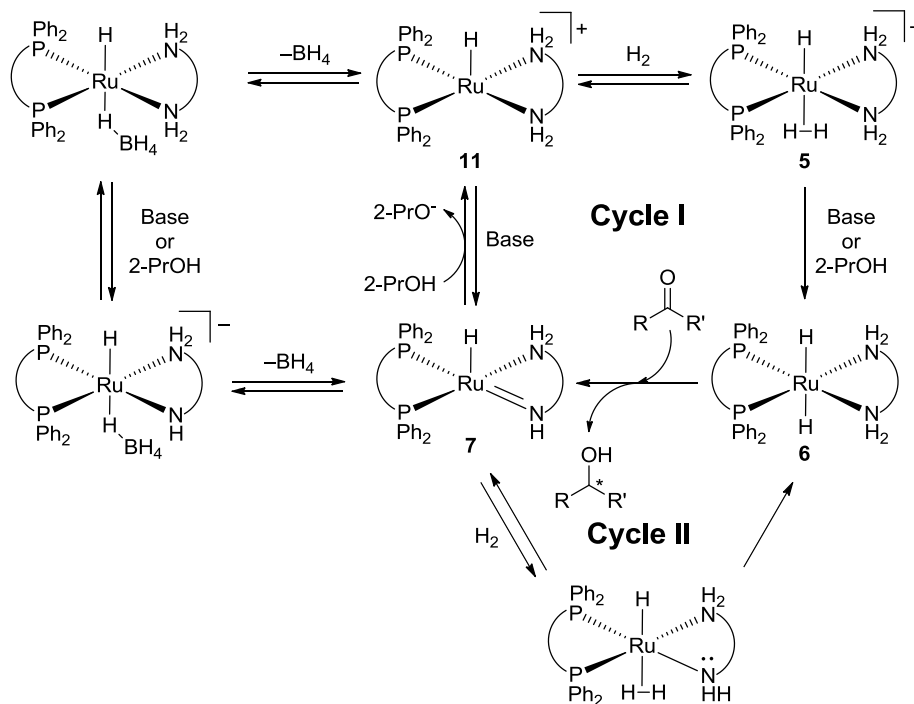
These catalytic cycles are further supported by *in situ* (0.05 mol% catalyst, [KO*t*-Bu] = 8.3 mM, 4 atm H_2, 30 °C) observation of 16 electron species **11** using ESI-MS, and change in kinetic isotope effect (KIE) of the catalytic reactions by the addition of base (KIE = 55 under [KO*t*-Bu] = 0 mM, KIE = 2 under [KO*t*-Bu] = 82 mM). Larger KIE under the base-free conditions was explained by the rate limiting step being deprotonation of Ru-dihydrogen complex **5**. ESI-MS is a good tool to detect cationic species in a reaction mixture, however it is not the optimal way of detecting neutral

complexes such as **6** and **7**.[36] Further, observation of the cationic, 16 electron species **11** could be due to the decomposition of other species under the conditions of ESI-MS.

Scheme 1-9. Reactivities of putative intermediates in asymmetric ketone hydrogenation.
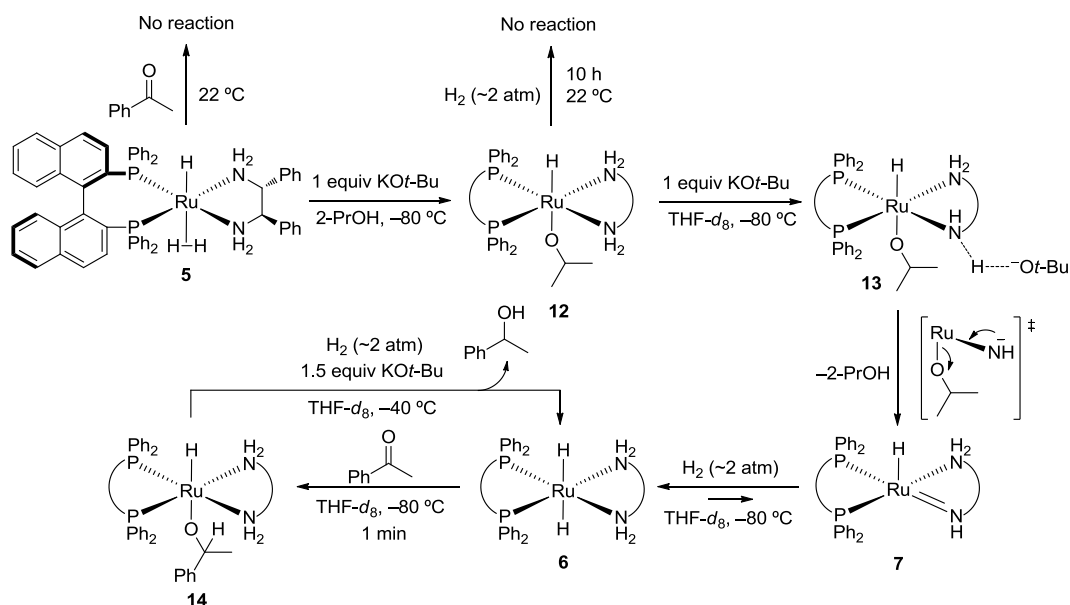
The most extensive stoichiometric study of this system under both base-free and basic conditions was done by Hamilton and Bergens.[35d-f] They prepared putative intermediates **5**, **6** and **7** shown in Scheme 1-8 independently, and examined the reactivity of each intermediate with low-temperature NMR experiments. Unlike the proposed catalytic cycle, they did not observe formation of **6** from **5** in neutral 2-PrOH solutions. Further, they observed that **5** does not hydrogenate acetophenone in neutral 2-PrOH solution under stoichiometric conditions (~2 atm H_2, 22 °C)

nor under catalytic conditions (0.05 mol% **5**, 4 atm H_2, 30 °C, 3 h, ~0.1%

yield). They observed dramatic accelerations of the reaction, however, in

the presence of either $NaBH_4$ (0.05 mol% **5**, 0.05 mol% $NaBH_4$, 4 atm H_2,

30 °C, 3 h, 32% yield) or KO*t*-Bu (0.05 mol% **5**, 0.05 mol% KO*t*-Bu, 4 atm

H_2, 30 °C, 3 h, 25% yield) (Scheme 1-9). These results showed that the

Ru-dihydrogen compound **5** requires added base to be active towards the

hydrogenation.[35d]

A possible mechanism by which base enhances the rate of these

hydrogenations was discovered by further reactions. In 2-PrOH, the

reaction of **5** and 1 equiv of KO*t*-Bu (~2 atm H_2, –80 °C) forms the

Ru-alkoxide **12**. The proposed formation of the Ru-dihydride **6** from

deprotonation of **5** (Scheme 1-8, Cycle I) was not observed upon

prolonged exposure of **12** to H_2 in 2-PrOH (~10 h, ~2 atm, 22 °C). However,

12 formed **6** upon addition of 1 equiv KO*t*-Bu (~2 atm H_2, –80 °C, <10 min)

in THF-d_8 via formation of *t*-BuO⁻ hydrogen bonded Ru-alkoxide **13**. The

transformation from **13** to **6** is proposed to proceed via the Ru-amide **7**,

formed by a base-catalyzed elimination reaction. Indeed, **7** was

independently prepared, and reacted with H_2 reversibly (~2 atm, –80 °C, <5

min) to generate **6** quantitatively (Scheme 1-9). The added base thus likely

accelerates the hydrogenation by promoting formation of active

Ru-dihydride **6** from the catalyst resting state Ru-alkoxide.[35e]

These stoichiometric studies also showed that the Ru-dihydride **6**

reacts with acetophenone at –80 °C (~2 atm H_2, <1 min). **6** is thus

extremely reactive towards reduction of carbonyl compounds. The net insertion products, however, were not the Ru-amide **7** and product alcohol predicted by the bifunctional addition reaction (Scheme 1-7), instead it was the Ru-alkoxide **14**. Ru-alkoxide **14** was also prepared independently by reacting **7** with (±)-1-phenylethanol. This observation was unexpected since Morris and co-workers observed formation of Ru-amide and a free product alcohol in their mechanistic study (Equation 1-6). Finally, **14** regenerated the dihydride **6** under H_2 (~2 atm) at –40 °C in the presence of 1.5 equiv of excess KO*t*-Bu, presumably via the base assisted formation of the product alcohol and Ru-amide **7**.[35f] A complete, kinetically competent catalytic cycle was thus observed at low temperatures.

Possible mechanisms for the formation of Ru-alkoxide 14

There are four possible reaction pathways to explain the formation of Ru-alkoxide **14** (Scheme 1-10). These pathways can be divided into two groups; either they proceed via concerted addition of RuH and NH to carbonyl carbon and oxygen respectively, or via transfer of RuH without NH bond cleavage. There are three possible pathways that proceed via concerted transfer. One pathway is that the concerted addition forms Ru-amide **7** and a free product alcohol as proposed by Noyori and Morris, and the subsequent reaction between **7** and the free alcohol forms **14** (Scheme 1-10, path A).[35a-c] Other pathways are that the concerted addition forms amide **7** and the free alcohol within the solvent cage (path B), or that the concerted addition forms **7** with a strong hydrogen bond between the

product alcohol and the amide nitrogen (path C). These species then collapse to **14** without formation of the free alcohol. A possible pathway that proceeds via RuH insertion without NH bond cleavage is that proceeds via concerted formation of a Ru–O bond and C–H bond with the assistance of a NH hydrogen bond to the carbonyl oxygen to form **14** (Scheme 1-10, path D).

Scheme 1-10. Possible pathways to form Ru-alkoxide **14**.
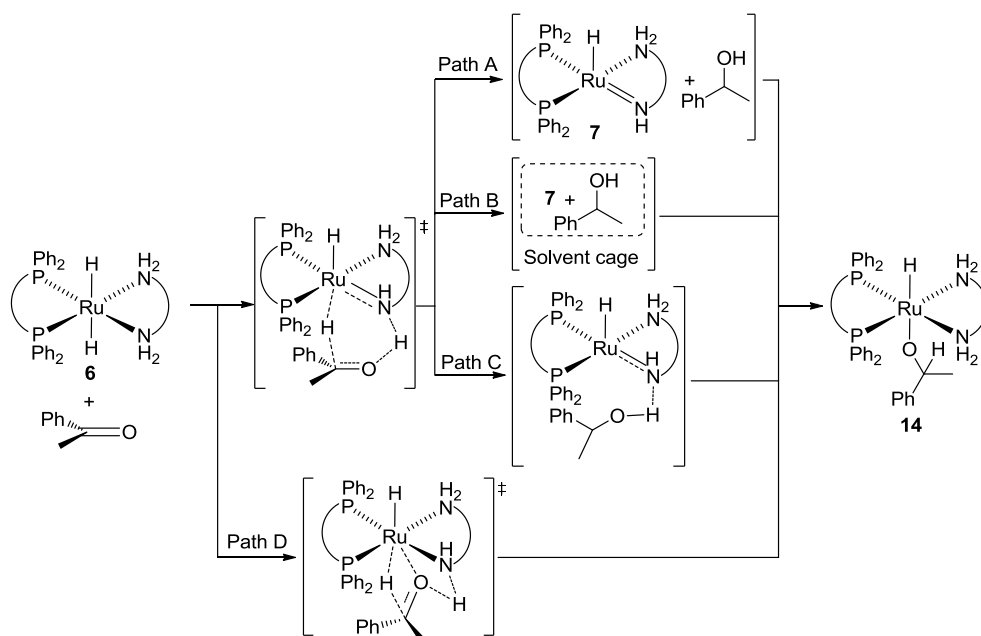
There are numerous computational as well as experimental studies that support concerted transfer of RuH and NH (Scheme 1-10, paths A–C) in Ru(diphosphine)(X)$_2$(diamine) and related catalyst systems. Morris, Catlow, and Harvey reported computational studies on Ru(diphosphine)(X)$_2$(diamine) catalyst systems.[35b,37] Their calculation under gas-phase conditions using *trans*-[Ru(PH$_3$)$_2$(H)$_2$(en)] (en is

ethylenediamine) as a model catalyst showed that the most stable Ru species is a Ru-amide that has a hydrogen bond with a product alcohol via the amide nitrogen. This species then collapses into the Ru-amide and the free alcohol. Their calculations thus support reaction paths A and C.

A similar mechanism as the path C is proposed by Baratta and co-workers to explain their observation of a Ru-alkoxide complex.[38] They observed that the related Ru-CNN pincer complex $[Ru(PPh_2(CH_2)_4PPh_2)-(H)(CNN)]$ (**15**) (see Equation 1-7 for the structure of CNN ligand) reacts with 1 equiv of benzophenone at 20 °C in C_6D_6 to form a Ru-alkoxide **16**. It was proposed that **16** has a hydrogen bond with one of the NH groups because one of the NH signals in the ^1H NMR is shifted downfield.

(**1-7**)
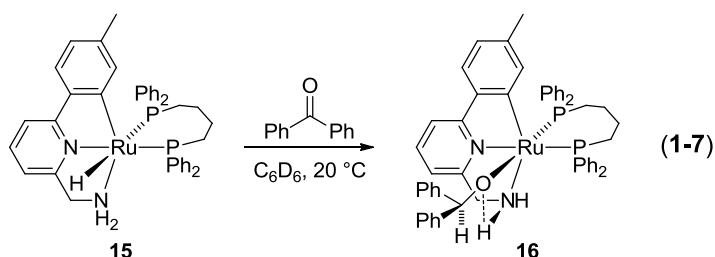
Baratta proposed that the alkoxide **16** formed via a mechanism that involves: Formation of a hydrogen bond between the catalyst NH_2 group and the oxygen of benzophenone that activates the carbonyl group towards nucleophilic attack; Nucleophilic attack of Ru–H to benzophenone to form the product alkoxide anion that remains hydrogen-bonded to the NH group; Finally, migration of the alkoxide anion from the NH group to the Ru centre. They, however, could not rule out another possible pathway that

involves dissociation of the NH_2 group followed by coordination of benzophenone, and hydride insertion via the inner coordination sphere mechanism.

Related transfer/H_2 ketone hydrogenation catalysts RuH(arene)-($XCH_2CH_2NH_2$) (X = O or NTs) (Ts is $SO_2C_6H_4$-*p*-CH_3) and Shvo's system, are also proposed to proceed via a concerted addition mechanism. Several research groups independently studied reaction mechanisms of RuH(arene)($OCH_2CH_2NH_2$) catalyzed transfer hydrogenation of ketones using computational methods, and all of them came to similar conclusions.[39] Figure 1-3 shows an energy diagram of the reaction mechanism calculated by Noyori and co-workers under gas-phase conditions using RuH(C_6H_6)($OCH_2CH_2NH_2$) and formaldehyde.[39b,d] All of the computational studies found that this catalyst system most likely proceeds via the concerted addition of RuH and NH to the carbonyl carbon and oxygen respectively (Figure 1-3, **TS**), and predicted that the most stable Ru species in the catalytic cycle is the Ru-amide **17** that has a hydrogen bond with a product alcohol via the amide nitrogen.[39] This prediction agrees with Morris' computational study.[35b] The majority of the computational studies found that the Ru-alkoxide, Ru(OCH_3)(C_6H_6)-($OCH_2CH_2NH_2$) (**18**), forms from the hydrogen bonded Ru-amide **17** or from Ru-amide and a free alcohol. They found formation of **17** from **18** is thermodynamically favoured (ΔG = −7.3 to −10.8 kcal/mol), and **18** is the most stable Ru complex that can form in and out of the catalytic cycle. It is

proposed that the alkoxide **18** is stabilized by an intramolecular Ru–O⋯H–N hydrogen bond, and is a catalyst resting state.
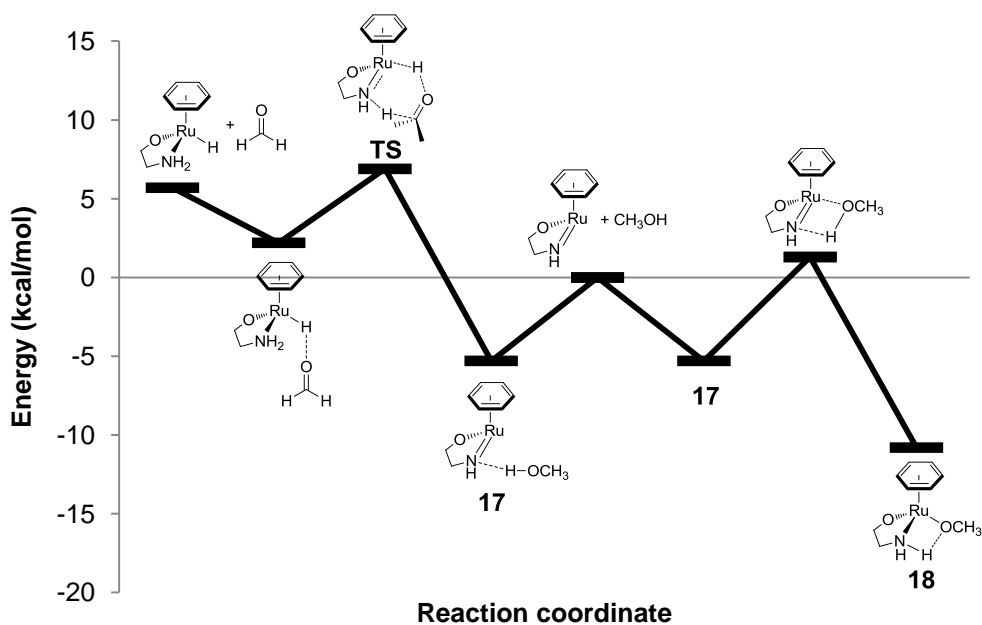
Figure 1-3. An energy diagram of $RuH(C_6H_6)(OCH_2CH_2NH_2)$ catalyzed transfer hydrogenation of formaldehyde under gas-phase conditions.

An experimental study that supports concerted RuH and NH addition was reported by Casey and Johnson using the reverse reaction, i.e. dehydrogenation of an alcohol by a Ru-amide **19** to form a corresponding Ru-hydride and a ketone.[40] The authors determined kinetic isotope effects (KIE) of dehydrogenation reaction using Ru-amide **19** and isotopomers of 2-PrOH: (($CD_3)_2CHOH$, $(CD_3)_2CHOD$, $(CD_3)_2CDOH$, and $(CD_3)_2CDOD$) (Equation 1-8). They found KIE for the reaction of $(CD_3)_2CDOH$ and **19** (KIE_{CDOH} = 2.86 ± 0.20), for the reaction of $(CD_3)_2CHOD$ and **19** (KIE_{CHOD} = 1.79 ± 0.07), and for the reaction of

$(CD_3)_2CDOD$ and **19** ($KIE_{CDOD} = 4.88 \pm 0.41$). The observation of KIE for transfer of both CH(D) and OH(D) indicates that dehydrogenation of alcohols proceeds via concerted addition of CH and OH to Ru and N respectively. As a further support of the concerted mechanism, the authors found that KIE_{CDOD} was within experimental error of the product of KIE_{CDOH} and KIE_{CHOD} ($2.86 \times 1.79 = 5.11$). Reaction paths A and B are, thus, supported by those computational and experimental studies of $RuH(arene)(XCH_2CH_2NH_2)$ (X = O or Ts) catalyzed transfer hydrogenations.
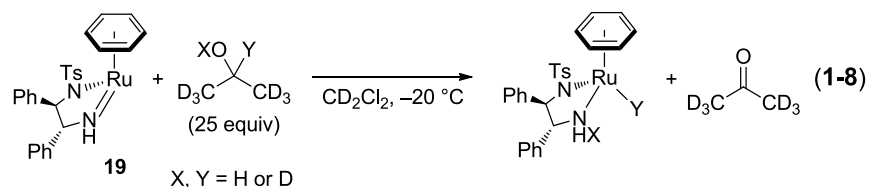
A mechanism of related Shvo's catalyst systems has also been investigated extensively by Casey and Bäckvall.[41-43] There are two proposed catalytic cycles for this system, one proposed by Casey and the other proposed by Bäckvall (Scheme 1-11). Casey proposed that this catalyst system proceed via an outer coordination sphere mechanism without coordination of a substrate before RuH insertion. Conversely, Bäckvall proposed that this system proceeds via an inner coordination sphere mechanism with coordination of a substrate by $\eta^5 \rightarrow \eta^3$ ring slippage of a cyclopentadienyl (Cp) ligand.

Scheme 1-11. Proposed mechanisms for Shvo's system.
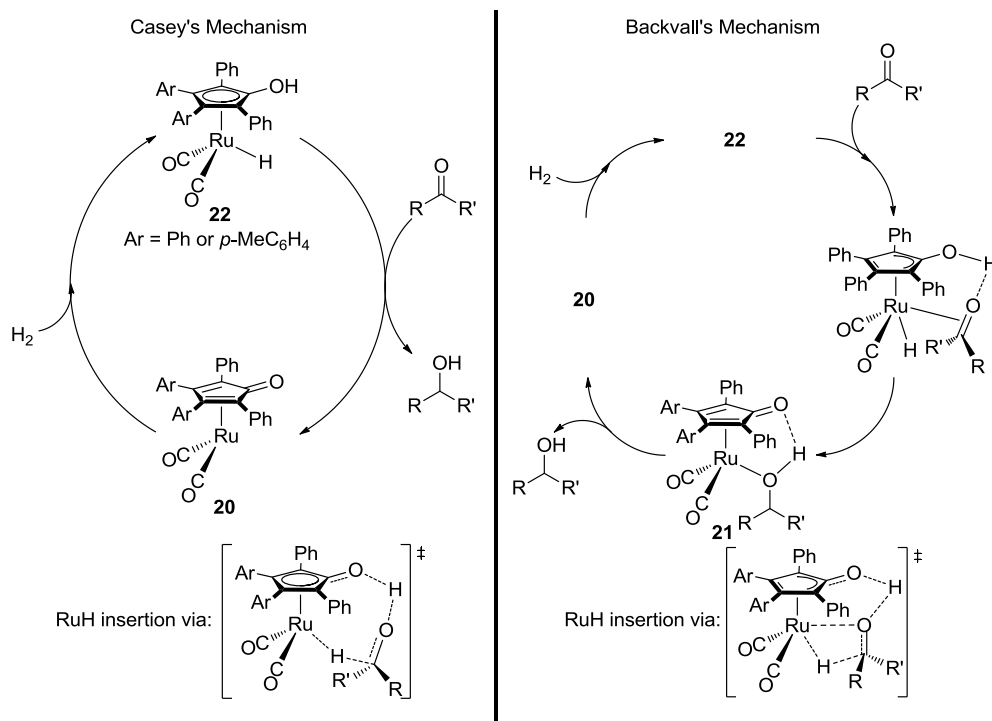
Both of them proposed that the addition of RuH and OH proceeds via concerted mechanism. Their proposed RuH and NH net addition products are, however, different. Casey proposed formation of 16 electron species **20**. Conversely, Bäckvall proposed formation of an alcohol adduct **21**. They studied these reaction mechanisms using computational, KIE, and trapping experiments using aldehydes, ketones, and imines.

In the case of aldehyde and ketone hydrogenation, Casey and co-workers studied addition of RuH and OH to a carbonyl carbon and oxygen using KIE experiments that are similar to Equation 1-8 with isotopomers of Ru-hydride **22** and benzaldehyde.[41a] The authors found both RuD (2.2 ± 0.1) and OD (1.5 ± 0.2) showed positive KIE's, and the

product (2.2 x 1.5 = 3.3) is within experimental error of the combined KIE measured for RuDOD (3.6 ± 0.3). Similar observations were also made using acetophenone. They concluded that RuHOH addition to an aldehyde or a ketone is concerted based on these observations. Bäckvall and Johnson also carried out similar KIE experiments using dehydrogenation of isotopomers of (±)-2-(p-fluorophenyl) ethanol.[42a] They also found that both CD (2.57 ± 0.26) and OD (1.87 ± 0.17) of the alcohol showed positive KIE, and the product of these KIE's (2.57 x 1.87 = 4.80) was within experimental error of combined KIE measured for CDOD (4.61 ± 0.37). Thus, the reverse reaction also proceeds via a concerted mechanism. These KIE experiments, thus, support reaction paths A–C that proceed via concerted transfer of both RuH and NH, however, it does not differentiate between the outer and inner coordination sphere mechanisms proposed by Casey and Bäckvall respectively.

Lledós and co-workers studied these mechanisms by computational methods using model compound $[Ru(\eta^5\text{-}C_4H_4COH)(CO)_2H]$ (23) and formaldehyde.[44] They found that Casey's outer coordination sphere mechanism is more favoured, however they did not consider the effects of aromatic groups on Cp ligands that are known to facilitate ring slippage of Cp ligands.

Similar arguments are also made for the imide hydrogenation. In the case of imide hydrogenation, however, KIE experiments were difficult to interpret since magnitudes of KIE's change significantly ($KIE_{RuDOD} = 0.56$ to

3.32) upon change of substrate structures.[41b,42b,c] Also, unlike ketone hydrogenation, product amines formed Ru-amine complexes due to stronger coordination ability of product amines than alcohols (See Equation 1-9 for a structure of Ru-amine complexe). Casey and Bäckvall carried out inter- and intramolecular trapping experiments to distinguish the outer and inner coordination sphere mechanisms.

(1-9)
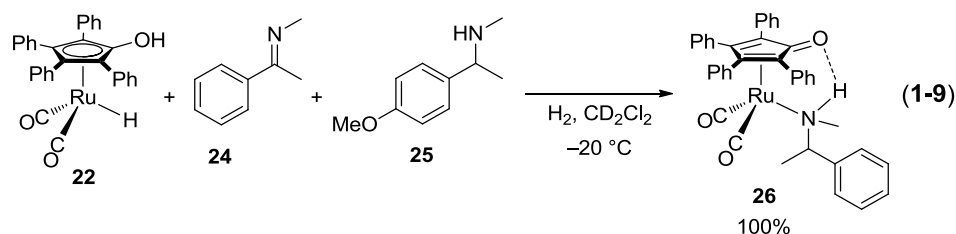
Bäckvall and co-workers conducted an intermolecular trapping experiment using Ru-hydride **22**, imine **24**, and trapping amine **25** under H_2 to prevent competitive dehydrogenation reaction of **25** (Equation 1-9).[42e] If the RuH insertion proceeds via the outer coordination sphere mechanism such as the path A in Scheme 1-10, the insertion forms product amine and 16 electron Ru species **20**. The coordinatively unsaturated **20** should then be trapped by both a product amine and a trapping amine. Conversely, if the insertion proceeds via inner coordination sphere mechanism, the insertion will form only Ru-amine complex of product amine. The authors found only Ru-amine complex of the product amine **26** formed at −20 °C. The concerted mechanism that produces free amine and 16 electron species **20** (an analogue of path A in Scheme 1-10) is thus not likely.

Casey also conducted similar experiments, and observed

formation of Ru-amine complexes of product amines exclusively.[41d] These results of intermolecular trapping experiments can be, however, explained using outer coordination sphere mechanisms such as paths B and C. Thus, if there is a strong hydrogen bond or solvent cage effect between 16 electron species **20** and a product amine, the observation of intermolecular trapping experiments can be explained by an outer coordination sphere mechanism. To distinguish these variations of the outer coordination sphere mechanism and the inner coordination sphere mechanism. Intramolecular trapping experiments were carried out by both Casey and Bäckvall,[41d,f,42e]

Table 1-2. Results of intramolecular trapping experiments (Ru*: complex **20**).

entry	amino imines	T (°C)	Ru-amine complexes
1		−20<	50% + 50%
2		0	85% + 15%
3		−8<	100%

Table 1-2 summarizes results of their intramolecular trapping experiments. The observations of two Ru-amine species in entry 1 and 2

33

suggest the outer coordination sphere mechanisms. Conversely, the absence of a trapped product in entry 3 indicates the inner coordination sphere mechanism. These incoherent results might indicate change of reaction mechanisms by changing imide substrate, which is observed in KIE experiments.

There are relatively few reports that support the mechanism that involves RuH insertion without NH bond cleavage (Scheme 1-10, path D). Morris recently reported a computational study of the Ru(diphosphine)(X)$_2$(diamine) catalyst system in the presence of 2-PrOH using *trans*-[Ru(PH$_3$)$_2$(H)$_2$(pica)] (pica is α-picolylamine) and acetone.[45] In the presence of 2-PrOH, they found that 2-PrOH-assisted transfer of Ru–H to the acetone carbonyl carbon proceeds via alcohol assisted transition states, and formed Ru-2-propoxide *trans*-[Ru(PH$_3$)$_2$(H)(OCH(CH$_3$)$_2$)(pica)] as the most stable intermediate without cleavage of the N–H bond. This observation thus supports path C. Morris and Bergens suggested that the stability of the Ru-alkoxides are attributed to the intra- and/or intermolecular hydrogen bonds between the NH group and RO$^-$ ligand and/or alcohol solvent molecules.[35e, 45] In fact, recently Morris reported a solid state structure of related Ru-alkoxide, *trans*-[Ru(PPh$_3$)$_2$(H)(OPh)-(NH$_2$CMe$_2$CMe$_2$NH$_2$)]·HOPh, in which a phenol molecule forms a six-membered RuO···HO(Ph)···NH ring via intermolecular hydrogen bonds.[46]

To investigate the possibility of path A, Hamilton and Bergens

carried out an intermolecular trapping experiment (Equation 1-10).[35f] They carried out the addition reaction between the Ru-dihydride **6** and acetophenone at –80 °C in the presence of ~5 equiv 2-PrOH as an internal trap, and observed only **14** as the Ru-alkoxide product. No formation of Ru-2-propoxide **12** was observed during the addition.

$$(1\text{-}10)$$
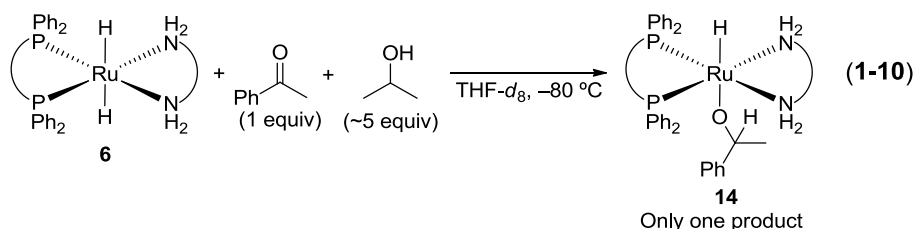
They also carried out a control experiment by adding a mixture of 2-PrOH (~5 equiv) and 1-phenylethanol (1 equiv) to Ru-amide **7**, and observed both Ru-alkoxides **12** and **14** in a ~1:1 ratio. Based upon these two experiments they proved that the free Ru-amide **7** is not the product of addition reaction between Ru-dihydride **6** and acetophenone, and hence eliminated the possibility of reaction path A. Further intramolecular trapping experiments using ketones that have alcohol functionalities will be able to distinguish reaction paths B–D. KIE experiments such as these described above will also be able to distinguish path B–D.

Hydrogenation of carboxylic acids and their derivatives

Unlike the hydrogenation of ketones, there are only a few catalyst systems that can hydrogenate carboxylic acids and their derivatives, even though these functionalities are as ubiquitous in nature as ketones. The lower reactivity of these functionalities towards hydrogenation can be

attributed to the lower electrophilicity at carbon, and the lower π-acidity of the ester carbonyl group relative to ketones. It is known that electrophilicity of the carbonyl carbon decreases in the order of acid halides > aldehydes > ketones > acid anhydrides > carboxylic acids, esters > amides > carboxylate ions due to inductive and resonance effects.[47] In fact, unlike aldehydes and ketones, esters and amides usually are not reduced using $NaBH_4$, instead they are usually reduced using stronger, and hence more hazardous, reducing agents such as $LiAlH_4$. Additionally, the lower π-acidity weakens η^2 (π) coordination of esters to a metal centre, which is believed to be the necessary step in Ru catalyzed ketone hydrogenation via the inner coordination sphere mechanism. In fact, there are no reports of η^2-carboxylic acid complexes (η^2-C=O coordination complex), and few reports of η^2-carboxylic acid derivatives. All of these reports utilize powerful π-basic metal centres to compensate for the lower π-acidity of carboxylic acid derivatives.[48] For example, Harman and co-workers showed that esters, acid anhydrides, imides, and amides form η^2 (π) complexes with highly π-basic Re(I)[48b], Mo(0)[48d], and W(0)[48c,d] complexes (Equation 1-11).

(1-11)

R = OMe, NMe$_2$
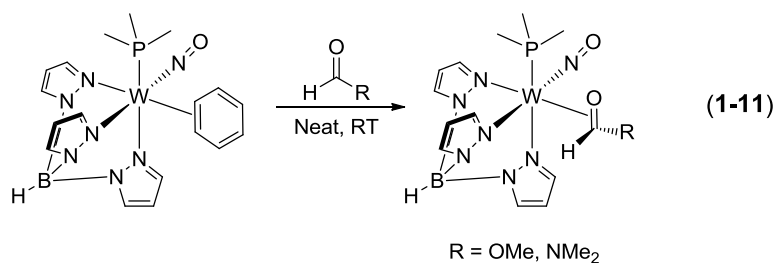
Hydrogenation of esters

All of the catalytic ester hydrogenations developed to date hydrogenates the esters completely to give the corresponding primary alcohols. Unlike B–H or Al–H reagents such as DIBAL-H, there is no example of a catalyst that can hydrogenate esters to hemiacetals or aldehydes since hemiacetals and aldehydes are usually in equilibrium, and aldehydes are more reactive towards hydrogenation than esters. The most common heterogeneous catalyst for the hydrogenation of esters is copper-containing mixed-oxides such as copper chromite, $CuCr_2O_4$.[24,49] The major application of these catalysts is hydrogenation of long-chain alkyl esters, such as vegetable oils and animal fats, to produce aliphatic alcohols that have several applications including emulsifiers in cosmetics and food industries.[49] The catalyst is usually used under harsh conditions, typically 200–300 °C and 200–300 atm H_2 (Equation 1-12). As a result, the applicability of this catalyst system to the synthesis of multi-functional fine chemicals and pharmaceuticals is limited.
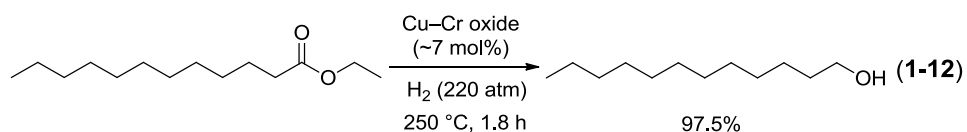
There are relatively few homogeneous catalysts that can hydrogenate esters. Interestingly, all of them are Ru complexes. In 1981, Grey and co-workers reported the first homogeneous ester hydrogenation system using anionic Ru complex, $K[RuH_2(PPh_3)_2(PPh_2C_6H_4)]$ (**27**), and

$K_2[Ru_2H_4(PPh_2)(PPh_3)_3] \cdot (diglyme)_2$ (**28**).[50] The chemical formula of complex **28** was proposed based on ^{31}P NMR data, and formation of $Ru_2Cl_4(PPh_3)_3(PPh_2H)$ and $4H_2$ upon addition of HCl to the complex. These catalysts were capable of hydrogenating activated esters such as trifluoroethyl tirfluoroacetate (0.3 mol% **27** or **28**, 6.1 atm H_2, 90 °C, 4–12 h, 100% yield) and dimethyloxalate (0.3 mol% **28**, 6.1 atm H_2, 90 °C, 20 h, 70% yield), however hydrogenation of unactivated esters, such as methyl acetate, was sluggish (0.3 mol% **28**, 6.1 atm H_2, 90 °C, 20 h, 22% yield). Halpern and co-workers studied a reaction mechanism of this system using a ketone, and found Ru-dihydride species $RuH_2(L)(PPh_3)_3$ is the actual active species for the hydrogenation of ketones.[51] However, mechanistic studies using esters have not been done to date.

Matteoli and coworkers also reported the hydrogenation of dimethyloxalate in the 80's utilizing the Ru-carbonyl complex $Ru(CO)_2(CH_3COO)_2(PBu_3)_2$ as catalyst.[52] This hydrogenation produced methyl glycolate in high TON under forcing conditions (0.0065 mol% catalyst, 130 atm H_2, 180 °C, 50 h, 100% yield, TON = 15000). The application of this catalyst to unactivated esters has not been reported.

The most well studied system in both academia and industry for ester hydrogenation uses $Ru(III)(acac)_3$ with phosphine ligands as catalyst.[53] Typically 3 equiv of PBu_3 or 1 equiv of $MeC(CH_2PPh_2)_3$ are used as phosphine ligands. For example, Elsevier and co-workers reported one of the earliest examples of homogeneous hydrogenation of unactivated

esters using Ru(III)(acac)$_3$ with 1.15–1.65 equiv. MeC(CH$_2$PPh$_2$)$_3$ as catalyst.[53a] They hydrogenated benzyl benzoate (PhCOOBn) in high TON under forcing conditions in the presence of base (0.046 mol% catalyst, 9 mol% NEt$_3$, 85 atm H$_2$, 120 °C, 16 h, 95% yield, TON = 2071). Interestingly, the TON was higher in 1,1,1,3,3,3-hexafluoropropan-2-ol solvent (maximum TON = 2071) than in 2-PrOH (maximum TON = 105). The authors postulated that this increase in TON is due to the formation of PhCOOCH(CF$_3$)$_2$ by transesterification. The Ru(III)(acac)$_3$ with MeC(CH$_2$PPh$_2$)$_3$ system has been patented by several chemical companies, which is an indicator of the importance of ester hydrogenation in industry.[53b,c] One of the recent applications of this system is transformation of biomass into economically more valuable chemicals using tandem dehydration/hydrogenation. Leitner and co-workers reported tandem dehydration/hydrogenation of levulinic acid and itaconic acid to form diols, or cyclic ethers (Equation 1-13).[54]
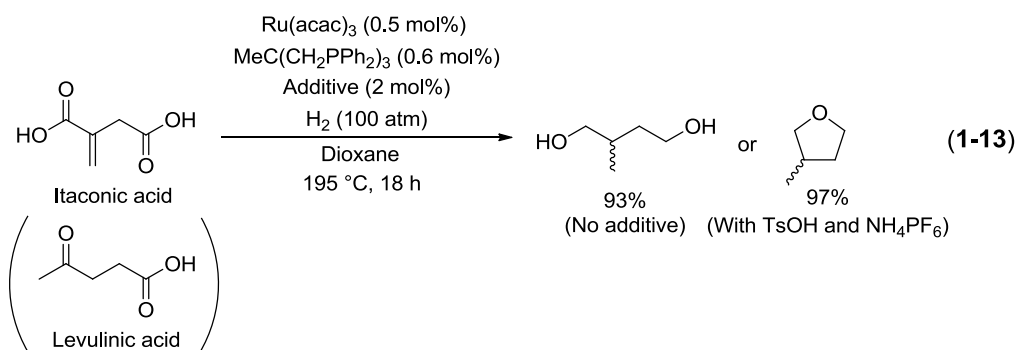
These systems described above likely proceed via inner coordination sphere mechanisms that are similar to that proposed for

ketones with the Ru(diphosphine)(X)$_2$ catalysts. Commonly these systems require high temperatures (120–180 °C) and high H$_2$ pressures (85–130 atm) for the hydrogenation of unactivated esters. This requirement of harsher reaction conditions likely results from the lower reactivity of esters towards hydrogenation. In fact, most of these catalyst systems hydrogenate activated esters in high TON but not unactivated esters.

In a recent breakthrough, Milstein and co-workers reported a ruthenium-PNN pincer complex that hydrogenates a series of unactivated esters under relatively low H$_2$ pressure (5.3 atm) to give the corresponding alcohol products (Equation 1-14).[55] This reaction, however, requires relatively high catalyst loading and temperature (1 mol% catalyst, 115 °C).
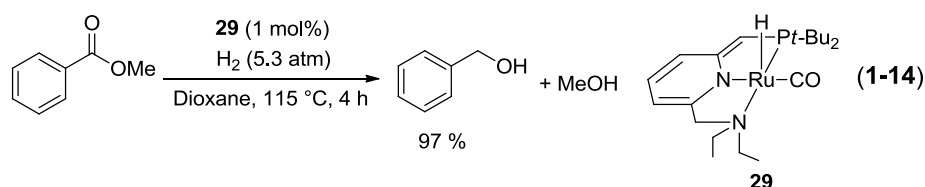
The authors proposed an inner coordination sphere mechanism with ligand-assisted heterolytic cleavage of H$_2$ by **29** to form *trans*-Ru-dihydride **30** (Scheme 1-12). In fact, these authors observed formation of **30** from **29** upon exposure to H$_2$. Dissociation of the hemilabile NEt$_2$ group, and coordination of the ester forms **31** most likely via η^1 coordination. Change of coordination mode (η^1 to η^2), followed by Ru-H insertion forms Ru-hemiacetaloxide **32**. Deprotonation of the acidic benzylic proton next to the Pt-Bu$_2$ group in **32** by the hemiacetaloxide

40

ligand regenerates **29** and a free hemiacetal. The hemiacetal tautomerizes

to the corresponding aldehyde which is further hydrogenated via the same

catalytic cycle to form primary alcohol products. The importance of the

hemilabile NEt_2 group was proposed based upon observations that the

PNP analogue of **29** showed lower catalytic activity towards the

hydrogenation of ethyl benzoate (1 mol% catalyst, 5.3 atm H_2, 115 °C,

7.5 % yield (PNP analogue, 16 h) vs. 99.2 % yield (**29**, 4 h)). Catalyst **29**

(Milstein Catalyst) and its analogue [RuHCl(PPh$_2$(CH$_2$)$_2$NH(CH$_2$)$_2$PPh$_2$)-

(CO)] (Ru-MACHO^{TM}) developed by Takasago are now commercially

available from Strem.[56]

Scheme 1-12. A reaction mechanism proposed by Milstein and

co-workers.
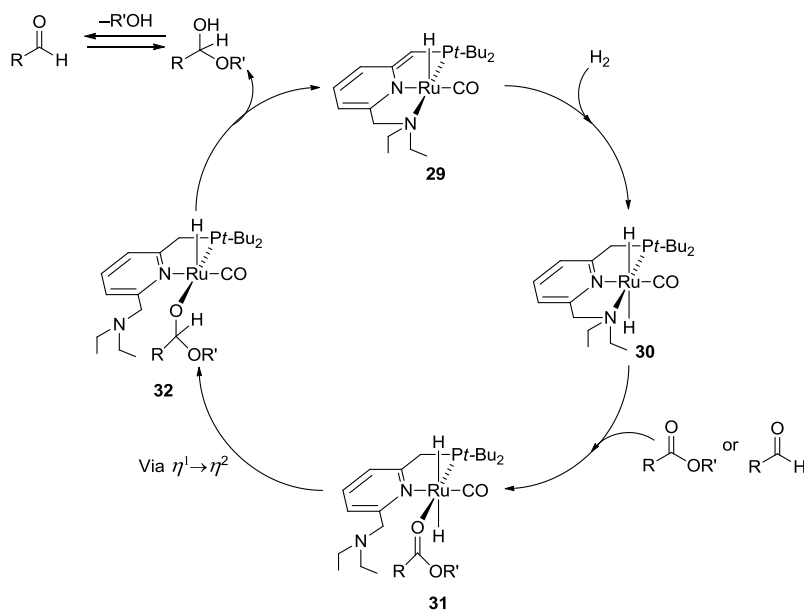
Recently Saudan and co-workers from Firmenich SA reported several Ru(diphosphine)(X)$_2$(diamine)-type catalyst systems that hydrogenate unactivated esters with high TOF and high TON under relatively forcing conditions in the presence of a large amount of base (typically 0.05 mol% catalyst, 100 °C, 50 atm H$_2$, 1–4 h, 5 mol% NaOMe, in THF, 82–99% yield) (Figure 1-4).[57] For example, this system was capable of hydrogenating sterically hindered aromatic esters, and electron-rich alkyl esters in high yields and TOF. The authors proposed that this catalyst system likely proceeds via an outer coordination sphere mechanism because high C=O/C=C selectivity was observed in hydrogenation of several unsaturated esters. Interestingly, they found that RuCl$_2$(P–N)$_2$ or RuCl$_2$(PNNP) systems work better than the Noyori-type RuCl$_2$(P–P)(N–N) systems. This observation could be explained by the stronger coordination abilities of P–N or PNNP ligands that prevent decomposition of the catalyst under high temperatures.
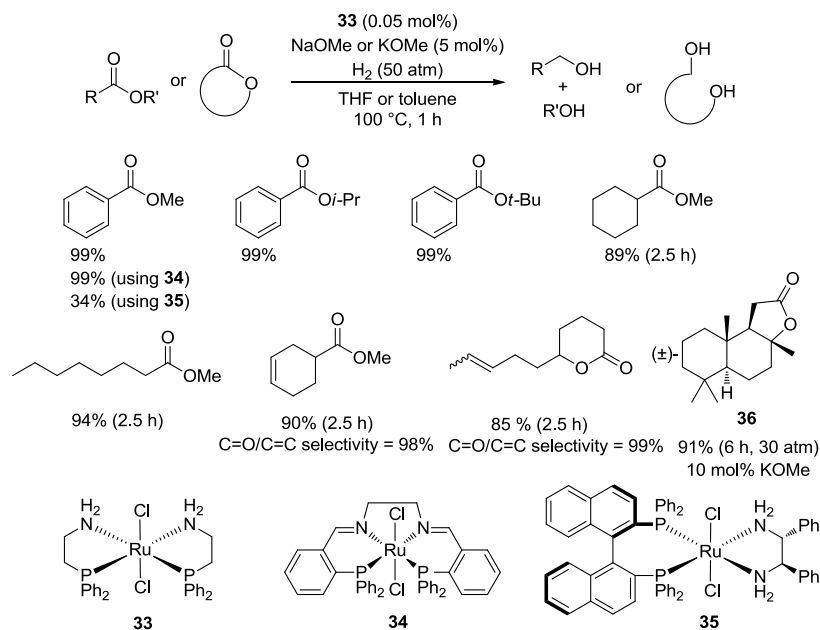
Figure 1-4. Hydrogenation of unactivated esters reported by Saudan and co-workers.

They also observed decreases in catalyst activity towards hydrogenation of methyl benzoate (0.05 mol% **33**, 5 mol% NaOMe) under lower H_2 pressure (100 °C, 10 atm H_2, 4 h, 47% yield) or lower temperature (60 °C, 50 atm H_2, 2 h, 90% yield). These systems thus have to be used under relatively forcing conditions (100 °C, 50 atm) to achieve high TON and TOF. Another interesting observation is the solvent dependency of this system. For example, the catalyst activity towards hydrogenation of methyl benzoate (0.05 mol% **33**, 100 °C, 50 atm H_2, 1 h, 5 mol% NaOMe) decreases significantly when primary alcohols are used as solvent (36% yield (EtOH), 1% yield (MeOH)), however almost no change in catalyst activity was observed when 2-PrOH was used as solvent (95% yield). The catalyst system was active in a wide range of aprotic solvents such as

43

ethers (92–99% yield), toluene (83% yield), and hexanes (68% yield). As a potential commercial application, this hydrogenation system was applied to the hydrogenation of the lactone **36**, a precursor for CETALOX® (a major ingredient of the smell of amber) (Figure 1-4).[57e] Catalyst **33** is also commercially available from Strem.[56]

Ino and co-workers from Takasago International Corp. also reported several Ru(diphosphine)(X)$_2$(diamine)-type catalyst systems for ester hydrogenation in the absence of base (Typically, 1 mol% catalyst, 80 °C, 50 atm H$_2$, 16 h, in THF, 45–95% yield).[58] Their focus is on hydrogenation of chiral esters to chiral alcohols without racemization. They found a Noyori-type base-free catalyst, RuH(BH$_4$)(dppp)((S,S)-dpen) (**37**) (dppp is 1,3-bis(diphenylphosphino)propane, (S,S)-dpen is (1S,2S)-(–)-1,2-diphenylethylenediamine)[ref] hydrogenates α- and β-chiral esters without racemization (Equation 1-15). Interestingly, a significant decrease in catalyst activity was observed when an unprotected α-amino ester was hydrogenated (0% yield), that did not occur when a β-amino (53% yield), ester was used as substrate. This observation could be interpreted as relatively weak coordination of the N–N ligand in the catalyst that can be replaced by the chelating product, 1,2-aminoalcohol. This catalyst system requires forcing conditions as well as relatively high catalyst loadings. The observed slow hydrogenation could be explained by the report of Hamilton and Bergens regarding rate acceleration by the addition of base in Ru(diphosphine)(X)$_2$(diamine)-type catalyst systems.

44
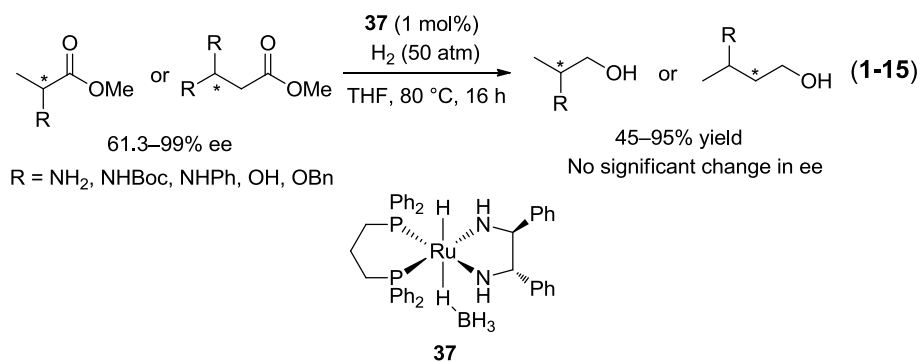
Recently, Ikariya and co-workers reported Ru-Cp*(P–N) complexs (Cp*: η^5-C$_5$Me$_5$) that hydrogenate esters with lower TOF in the presence of large amount of base (Typical reaction conditions: 1 mol% catalyst, 100 °C, 50 atm H$_2$, 21 h, 25 mol% NaOMe, in THF, 85–99% yield).[59] Interestingly, they tried dynamic kinetic resolution of α-substituted esters using chiral Ru-Cp*(N–N) complex, however, the ee was unsatisfactory (Equation 1-16). Morris et al. also recently reported analogous catalyst system using a Ru-Cp* (N-NHC) (NHC is *N*-heterocyclic carbene) complex.[60]
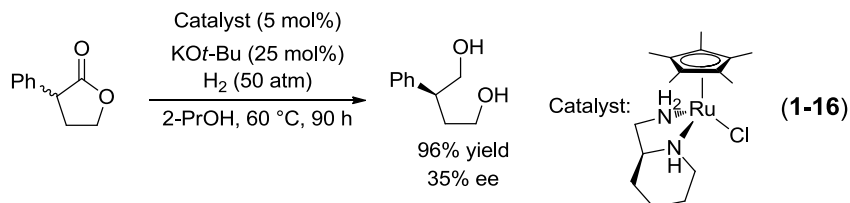
These Milstein, Ino, and Ikariya's systems likely proceed via outer coordination sphere mechanisms that are similar to that proposed for ketones with the Ru(diphosphine)(X)$_2$(diamine) catalysts. This system potentially has an advantage over previously reported Ru(diphosphine)-(X)$_2$-type systems because this system does not require electronically less

favourable η^2 coordination of esters. Developmental homogeneous ester hydrogenation chemistry in both academia and industry has begun to produce practical homogeneous catalyst systems. Mechanistic studies of both Ru(diphosphine)(X)$_2$-type and Ru(diphosphine)(X)$_2$(diamine)-type systems have not been reported likely due to the forcing conditions required to observe catalytic activity.

Hydrogenation of imides

The hydrogenation of imides can produce several products as shown in Scheme 1-13. Path A involves hydrogenation of one of the imide C=O bonds. Products of this reaction could be either an aldehyde and amide or the corresponding hydroxy-amide. Further hydrogenation of the mixture of aldehyde and amide gives the corresponding primary alcohol and amide (path B). In contrast, further hydrogenation of hydroxy-amide via hydrogenolysis of C–OH bond forms the corresponding amide (path C). Finally, complete hydrogenation of all C=O bonds gives several products (path D).

Scheme 1-13. Possible products of hydrogenation of imides.
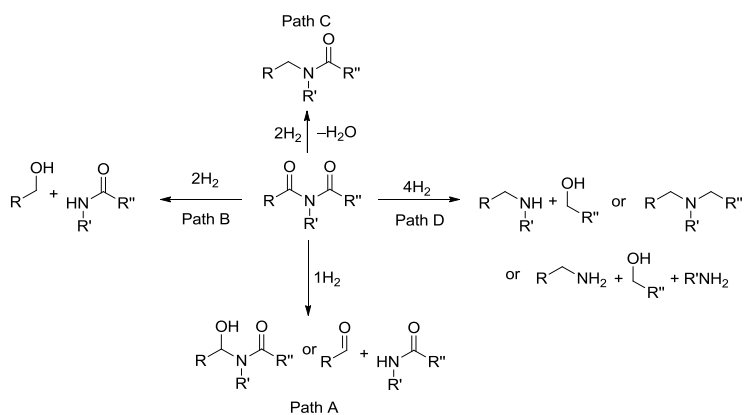
Cyclic imides can be hydrogenated using heterogeneous catalyst such as copper chromite, or Raney Ni under harsh conditions (typically 200–300 °C, 200–300 atm H_2). The products are typically lactams which formed via reaction pathway C in Scheme 1-13.[24] Two exceptions are the PtO_2- and Pd/C-catalyzed hydrogenation of imides.[61] These catalysts can hydrogenate activated imides such as *N*-acetylphthalimide under ambient conditions (20 °C, 1 atm H_2) to form monohydrogenated *N*-substituted hydroxyl lactams via reaction pathway A, however, they are inactive towards unactivated imides such *as* *N*-alkylphthalimide under these conditions. These catalysts also hydrogenate aromatic C=C bonds, as illustrated in Equation 1-17.

$$\text{(1-17)}$$

1 g
R = Me, OEt, OMe, NMe_2

(Racemate)
0.21–0.80 g
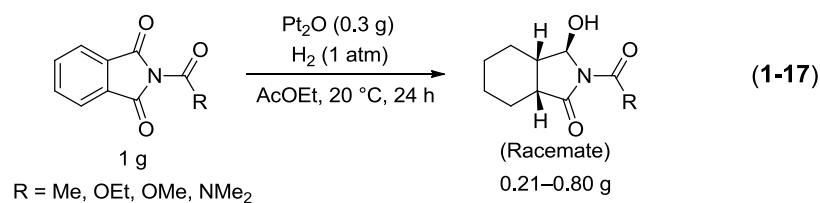
Until recently, there were only two reports of homogeneous systems that hydrogenate imides (Equation 1-18).[62] Both of them use Ru(II) as catalysts, and hydrogenate unactivated imides to form lactams via reaction pathway C. The possible *in situ* formation of heterogeneous Ru catalyst is unlikely since addition of mercury did not affect the catalyst activity. This catalyst system most likely proceeds via an inner coordination sphere mechanism because this system also hydrogenates aromatic C=C bonds.
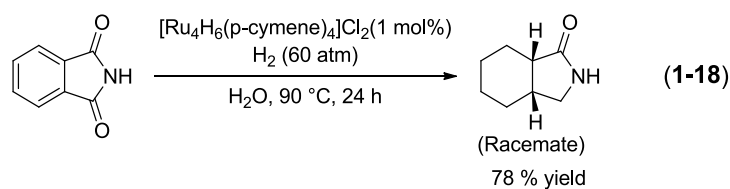
$$[Ru_4H_6(p\text{-cymene})_4]Cl_2(1 \text{ mol}\%)$$
$$H_2 \text{ (60 atm)}$$
$$H_2O, 90\ °C, 24\ h$$

(1-18)

(Racemate)
78 % yield

Recently, Ikariya and co-workers reported Ru-Cp*(P–N) complexes that hydrogenate cyclic imides in the absence of excess base (Typical reaction conditions: 10 mol % catalyst, 80 °C, 30 atm H_2, 18-24 h, in 2-PrOH, >99 % yield) (Figure 1-5).[63] The products were dihydrogenated, ring-opened alcohol-amides formed via reaction pathway B. Further, they reported the first enantioselective desymmetrization of cyclic imides using chiral Ru-Cp*(P–N) catalyst. They observed moderate to excellent ee (62–98%) in high yields (>99%). The TOF was, however, low (0.42/h). This system likely proceeds via an outer coordination sphere mechanism. Homogeneous hydrogenations of imides via the reaction pathway A as well as mechanistic study of imide hydrogenation were not reported before this research.
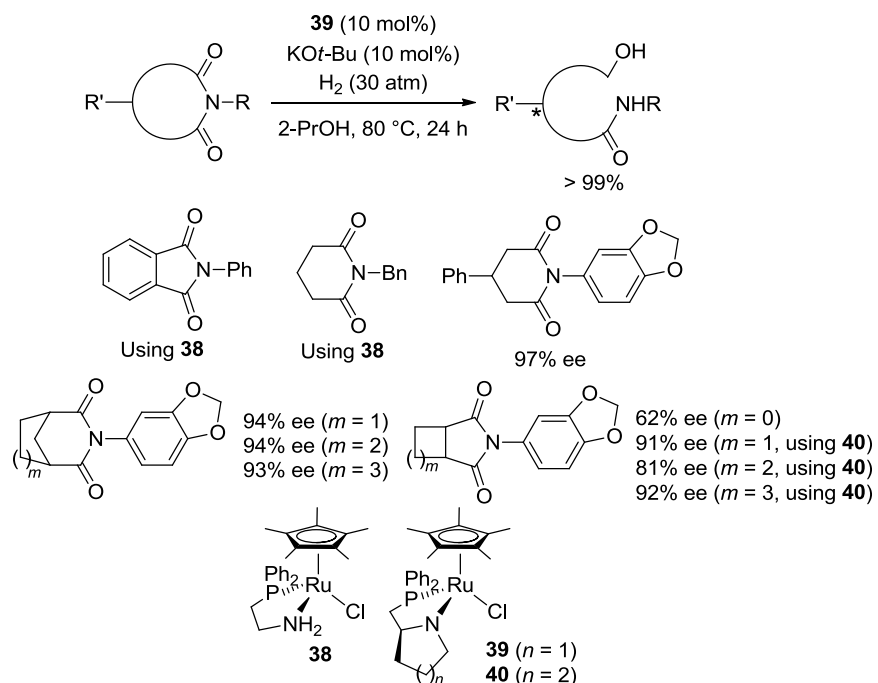
Figure 1-5. Dihydrogenation of imides reported by Ikariya and co-workers.

Research objectives

As illustrated in this review Ru catalyzed homogeneous hydrogenation of the C=O functionality is one of the most environmentally (and economically) superior synthetic methods to produce alcohols that are ubiquitous in nature, and hence important products in fine chemical and pharmaceutical industries. In the case of asymmetric ketone hydrogenation, there are two types of well-studied Ru catalyst systems, namely the Ru(diphosphine)(X)$_2$ system and the Ru(diphosphine)(X)$_2$(diamine) system. Both of these catalyst systems have been studied extensively by the Bergens group using stoichiometric reactions of putative catalytic intermediates.[34,35d-f] One of the most important findings during the course of those mechanistic studies is remarkable reactivity of the Ru-dihydride **6**

49

towards ketone hydrogenation (Scheme 1-8).[35f]

Unlike ketone hydrogenation, there are only a few reports of Ru catalysts that hydrogenate more challenging carbonyl compounds such as esters and imides. With rational considerations of reaction mechanisms based on previous studies, and the high reactivity of **6** in hand, the first objectives of my research ware the development and mechanistic investigation of a highly active catalyst system towards hydrogenation of esters and imides under mild reaction conditions.

Another important observation from previous studies is the observation of a net Ru-H insertion product Ru-alkoxide **14**.[35f] Understanding of reaction pathways that lead to formation of **14** is important since this complex is most likely a catalyst resting state as predicted by computational studies of related $RuH(arene)(XCH_2CH_2NH_2)$ system. Previously the reaction mechanism of the formation of **14** was studied using an intermolecular trapping experiment (Equation 1-10). The second objective of my research was thus elucidation of a reaction mechanism that leads to the formation of alkoxide **14** using intramolecular trapping experiments. The findings presented in this thesis are the breakthrough towards development of C=O bond hydrogenations that would enable industries to develop more sustainable processes.

Chapter 2

Ru Catalyzed Hydrogenation of Esters under Mild Conditions. The First Direct Observation of Intermediates

Introduction

As described in Chapter 1, the extensive hydrogenation of esters to give alcohol products is a relatively difficult transformation in both heterogeneous and homogeneous catalysis. This hydrogenation, however, offers significant benefits because it can remove the requirement for stoichiometric amounts of hazardous and wasteful metal-hydride reagents to reduce esters. Recently, Saudan and co-workers reported a Noyori-type $RuCl_2(P–N)_2$ catalyst that can hydrogenate esters in high TON and TOF (Figure 1-4).[57] This reaction, however, has to be carried out under relatively forcing conditions (100 °C, 50 atm H_2) to achieve these high TON and TOF. As a consequence, a detailed mechanistic investigation of this system to improve the catalyst performance is unavailable to date.

Hamilton and Bergens recently reported the most extensive mechanistic investigation of Noyori ketone hydrogenation catalyzed by *trans*-[Ru((*R*)-BINAP)(Cl)$_2$((*R*,*R*)-dpen)] in the presence of a base.[35d-f] During the course of this study they developed a high-yield, low temperature preparation of several key Ru putative intermediates (Figure 2-1), and found that the dihydride **6** is an active carbonyl reducing agent. For example, **6** reacts with 1 equiv of acetophenone on mixing at –80 °C to form the alkoxide *trans*-[Ru((*R*)-BINAP)(H)(OCH(CH$_3$)(Ph))((*R*,*R*)-dpen)]

(**14**), the net product of ketone-hydride insertion.[35f] With this reactivity in hand Chapter 2 discusses the low temperature and pressure hydrogenation of esters using **6** and its analogues in the presence of base, and the first direct observations of catalytic intermediates in lactone/ester hydrogenations.
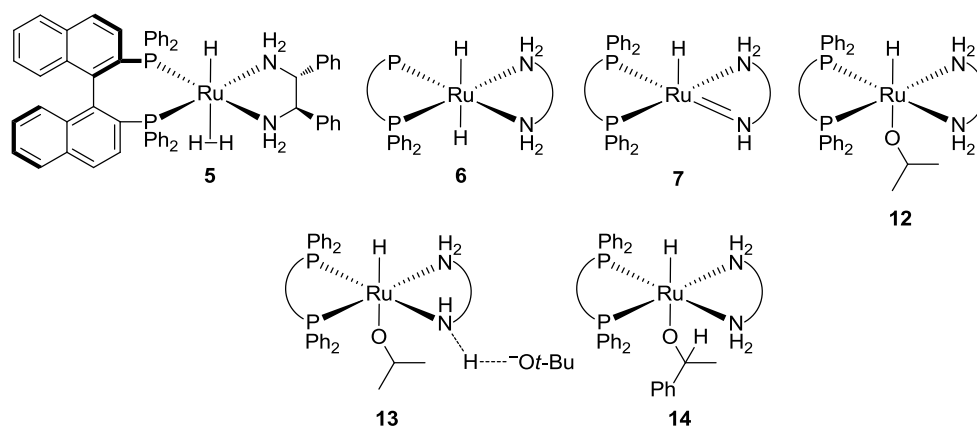
Figure 2-1. Ru putative intermediates prepared by Hamilton and Bergens.

Results and discussion

We prepared solutions of Ru-dihydride **6** and its ethylenediamine (en) analogue *trans*-[Ru((*R*)-BINAP)(H)$_2$(en)] (**41**) for this study by reacting *trans*-[Ru((*R*)-BINAP)(H)(η^2-H$_2$)(diamine)]BF$_4$ with 1.5–20 equiv of KN(Si(CH$_3$)$_3$)$_2$ or KO*t*-Bu under H$_2$ (~2 atm) at –78 °C in THF.[35e] As 1 equiv of base is consumed to prepare **6** or **41**, the amount of base quoted in this thesis is that remaining after **6** or **41** is prepared. We found that **6** was inactive for ester hydrogenations in 2-PrOH, the most common solvent for ketone hydrogenation catalyzed by Ru(diphosphine)(X)$_2$(diamine).[27a] For example, hydrogenation of acetophenone and benzaldehyde proceed

quantitatively in 2-PrOH (0.5 mol% **6**, 5.5 mol% KO*t*-Bu or KN(Si(CH$_3$)$_3$)$_2$, 4 atm H$_2$, 40 °C, overnight). Under identical condition, hydrogenation of methyl benzoate did not form the desired alcohol products. The transesterification product, isopropyl benzoate, was observed (92% yield) instead. Compound **6** was, however, active in THF (the solvent used in previous reports under harsh conditions (typically 100 °C, 50 atm H$_2$)) under low pressures and temperatures. For example, the hydrogenation of ethyl hexanoate at –20 °C under 4 atm H$_2$ formed 1-hexanol and ethanol as the sole organic products in 23% yield. The yield increased to 55% upon increasing the temperature to 0 °C (Equation 2-1). Thus, the lower intrinsic reactivity of esters does not impede their hydrogenation under very mild conditions with these catalysts.
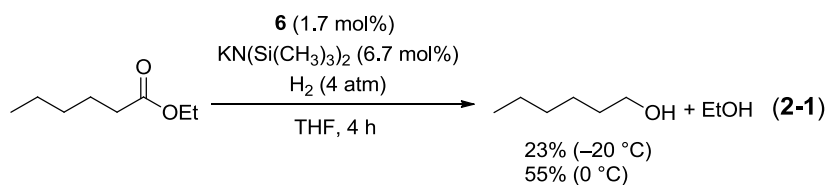
The hydrogenation did, however, slow over time. For example, hydrogenation of methyl benzoate using Ru-dihydride **41** (100 equiv of ester, 9 equiv of KO*t*-Bu, 23 °C, 4 atm H$_2$) showed a significant decrease in TOF over time (Figure 2-2).
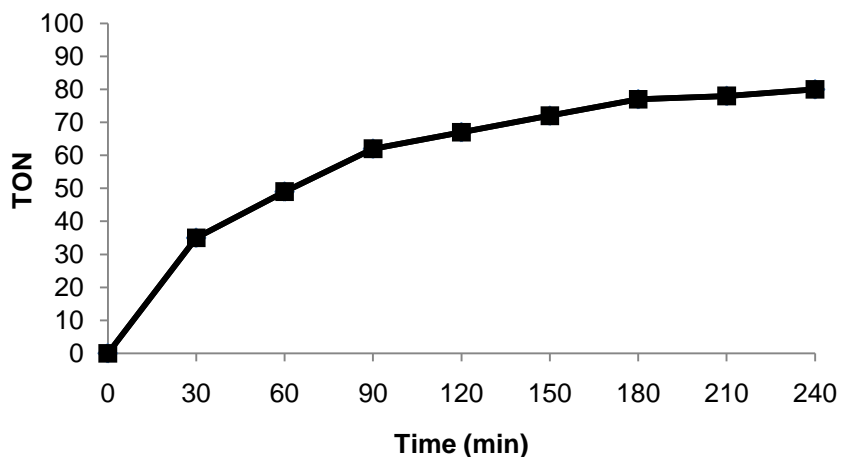
Figure 2-2. Plot of TON vs. time for hydrogenation of methyl benzoate.

TOF (h^{-1}) decreased from 49 for the first hour to 3 for the last hour. The following control experiment was conducted to distinguish between this phenomenon and the exponential decrease of reaction rate that might be observed if this hydrogenation has first order kinetics in [ester]. Hydrogenation of methyl benzoate were carried out under the same conditions, as those used in Figure 2-2 in the presence of 80 equiv added methanol and 80 equiv of benzyl alcohol. The observed TOF (h^{-1}) of 17 (for the first hour) confirms that product inhibition is the origin of the rate decrease over time.

We investigated the high intrinsic activity of this catalyst, and the product inhibition, by carrying out the stoichiometric addition of γ-butyrolactone (**42**) to Ru-dihydride **6** at –80 °C (THF-d_8, ~3 equiv of **42**, ~2 atm H_2, 0.5 equiv of $KN(Si(CH_3)_3)_2$ or 2 equiv of KOt-Bu). Excess base was added to prevent formation of *trans*-[Ru((*R*)-BINAP)(H)(OR)-((*R*,*R*)-dpen)] (R = H (**43**)[35e] or *t*-Bu (**44**)) that forms via reaction of

54

Ru-amide (**7**) and trace water or *t*-BuOH if KO*t*-Bu is used. The addition formed the Ru-hemiacetaloxide **45**, the result of a net carbonyl-hydride insertion, in 55% yield over ~3 min. No intermediates were detected during the bifunctional addition of **6** to **42** (Equation 2-2).
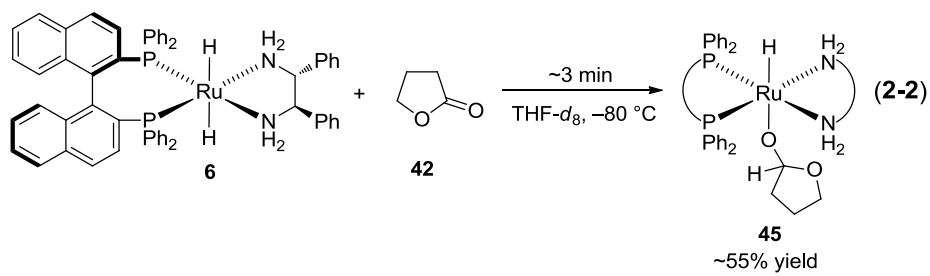
Stoichiometric transition metal-ester chemistry is less studied than that of ketones. Most reports are of the ester ligand coordinating through the carbonyl oxygen.[64] There are fewer reports of coordination through the alkoxide oxygen,[65] and there are only four reports of an ester coordinating as a π-ligand.[48] This is the first observation of a transition metal-hemiacetaloxide compound formed from addition of a lactone or ester substrate. The hemiacetaloxide **45** was identified with ^{1}H, ^{31}P, ^{1}H–^{13}C gHSQC, ^{1}H–^{1}H gCOSY and 2D gTOCSY NMR experiments. Figure 2-3 shows key α-CH correlation of the hemiacetaloxide group in ^{1}H–^{13}C gHSQC NMR spectra. The ^{1}H and ^{13}C signals of the CH peak were at δ 6.17 and 110.9 ppm, respectively, shifted down-field by 0.84 and 13.4 ppm from the free hemiacetal in THF-d_8 at –80 °C.
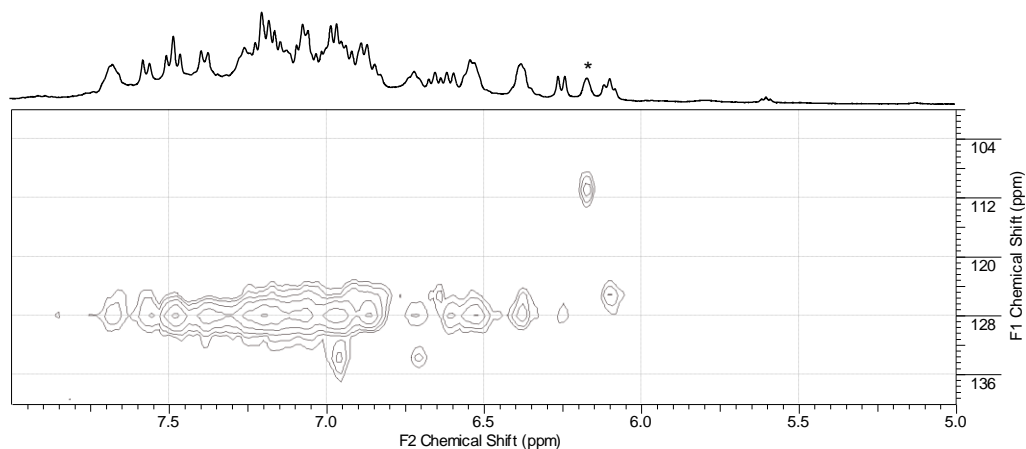
Figure 2-3. The key α-CH (marked by *) correlation of the hemiacetaloxide group in ^{1}H–^{13}C gHSQC NMR of **45**.

The identity of **45** was further confirmed by independent synthesis. Specifically, we showed previously that alcohols rapidly add to the Ru-amide **7** at low temperatures to form the corresponding Ru-alkoxide compounds (Scheme 1-9).[35e,f] The corresponding addition reaction between the free hemiacetal **46** (~1 equiv) and **7** also occurred rapidly at −78 °C to form **45** in a near quantitative yield (Equation 2-3).
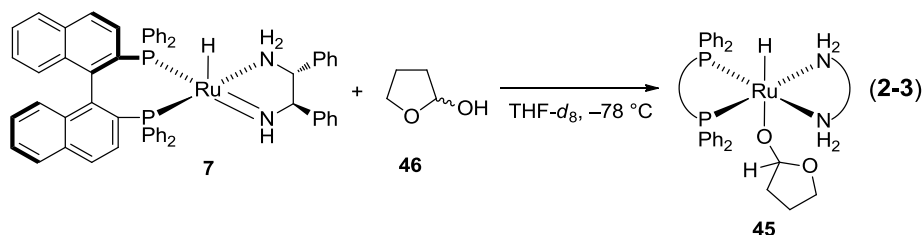
Phthalide (**47**) also added to **6**, forming the corresponding Ru-hemiacetaloxide **48** at −80 °C (Equation 2-4). The rate of this addition

56

was ~3x slower than the addition of γ-butyrolactone (**42**) to **6** likely due to the sterically bulkier **47**. The addition of methyl benzoate began at ~–60 °C to form mixtures of catalyst-alkoxide compounds. The order of reactivity towards **6** is, thus, **42** > **47** > methyl benzoate. This trend agrees with the more electrophilic nature of a lactone C=O bond due to lack of stereoelectronic stabilization by n–σ*(C=O) interaction.[66]
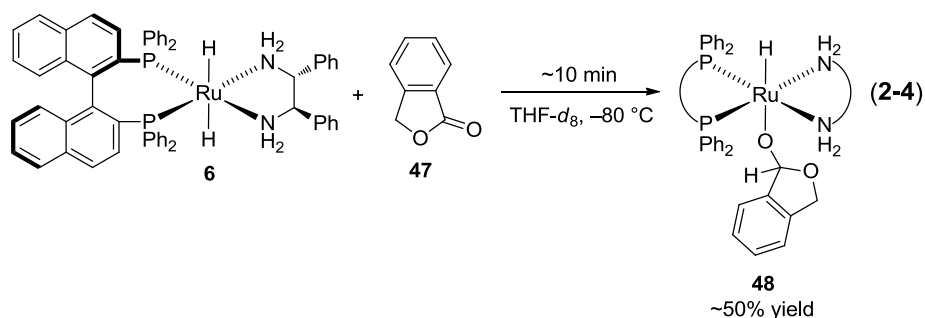
Our preliminary model for these unexpectedly facile additions of lactones and esters to **6** is that they proceed in a manner similar to the addition of ketones. Specifically, the additions either proceed in a bifunctional manner to form the hemiacetal that has a hydrogen-bond to the Ru-amide **7**, or exists with **7** as a hydrogen bonded species, which then collapses into Ru-hemiacetaloxide **45**. Alternatively, the bifunctional addition forms **45** directly through a partial Ru-oxygen bond in the transition state (Figure 2-4). These transition states have the same formal electron count. Both pathways may also occur in parallel.
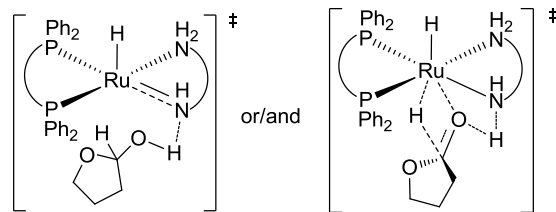
Figure 2-4. Possible transition states for the formation of Ru-hemiacetaloxide **45**.

Scheme 2-1. Transformation of the hemiacetaloxide **45** into Ru-alkoxide **49**.
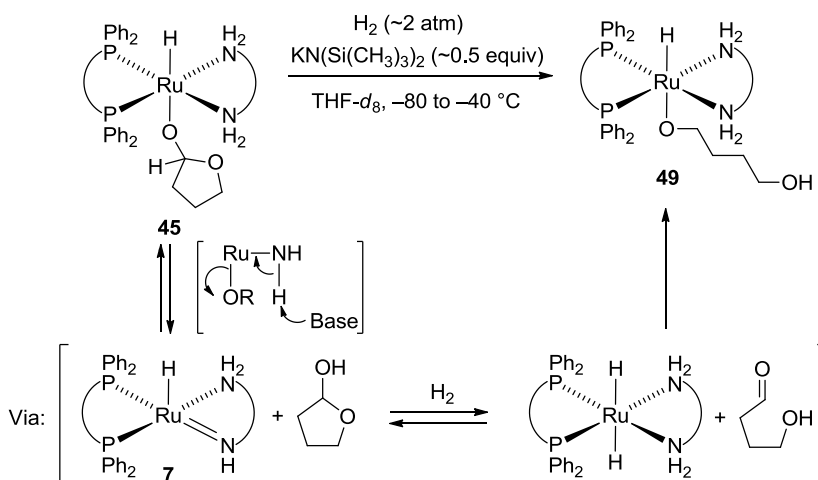
The hemiacetaloxide **45** transformed into the Ru-alkoxide **49** under hydrogen (~2 atm) (Scheme 2-1). This conversion occurs slowly at −80 °C, and quickly upon warming up to −40 °C. The alkoxide ligand in **49** is the diol that would result from complete reduction of the parent lactone. The hemiacetaloxide **48**, made by addition of phthalide **47** to **6**, underwent the same transformation at −40 °C to form the corresponding Ru-alkoxide **50**. Compounds **49** and **50** were identified with ^{1}H, ^{31}P, ^{1}H–^{13}C gHSQC, and

^{1}H–^{1}H gCOSY NMR experiments, and with independent synthesis by addition of the corresponding diols to the amide **7**. Interestingly, the OH ^{1}H NMR signal from coordinated diols appeared at unusually down-field (12.8 ppm for **49** and 13.3 ppm for **50**). These low-field shifts are probably because of a formation of an intramolecular hydrogen bond between an OH group of the alkoxide ligand (donor) and the Ru-oxygen group of the alkoxide ligand (acceptor).[67] An intermolecular hydrogen bond between excess base (KO*t*-Bu or KN(Si(CH$_3$)$_3$)$_2$) or the corresponding protonated base is unlikely since the same OH signals were observed no matter which base is used.

Scheme 2-2. A proposed origin of the product inhibition.
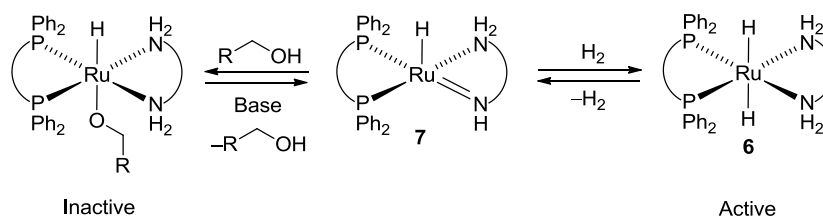
We have shown in our previous studies that alkoxides related to **45**, **48**, **49**, and **50** undergo a base-assisted elimination of the alkoxide ligand to generate the Ru-amide **7**,[35e] which also reacts quickly with H$_2$ to form **6**. We propose that a similar sequence of steps occurs as a part of the transformations of **45** and **48** into **49** and **50**, respectively, via the tautomerization of hemiacetals into aldehyde-alcohols (Scheme 2-2). If this mechanism is operative, a competition would be established during the

catalytic hydrogenations between the primary alcohol products that react with the Ru-amide **7** to form catalytically inactive Ru-alkoxides, and H_2 that reacts with **7** to form catalytically active Ru-dihydride **6**. In other words, as the concentration of primary alcohol products increases, the probability of the Ru-amide **7** reacting with the product alcohols increases. As a consequence, the concentration of catalytically active species **6** decreases. Additionally, primary alcohols are more reactive towards Ru-amide **7** since they are less hindered, and have more acidic OH groups than secondary or tertiary alcohols.[68] We propose that this competition of alcohols and H_2 toward **7** combined with higher acidity of primary alcohol products is the origin of the product inhibition. This proposal is further supported by the fact that the catalytic reaction did work in *t*-BuOH, a less acidic, and less coordinating alcohol solvent, (0.5 mol% **41**, 4.5 mol% KO*t*-Bu, 4 atm H_2, 23 °C, 2 h, 32% yield), unlike in 2-PrOH.

Hansen et al. proposed a similar product inhibition for their Rh catalyzed enamine hydrogenation.[125] They observed that the hydrogenation took ~3 times longer when 32 mol% of the product amine was added to the reaction mixture before the hydrogenation (Equation 2-5). Further, the hydrogenation was ~3 times faster in the presence of 200 mol% of $(Boc)_2O$ as the product amine trap, despite a 5-fold reduction in catalyst loading (Equation 2-6).

NH$_2$ O
          NHPh

2 mol% Chiral P-P
1 mol% [Rh(COD)Cl]$_2$
H$_2$ (32.6 atm)
—————————————
MeOH, 40 °C

NH$_2$ O
          NHPh

98% yield

3.6 h (without product amine)
11.3h (with 32 mol% product amine)

Fe — PPh$_2$, Pt-Bu$_2$

Chiral P-P

(2-5)

NH$_2$ O
          NHPh
+ 200 mol% t-BuO—C(O)—O—C(O)—Ot-Bu
(Boc)$_2$O

0.4 mol% Chiral P-P
0.2 mol% [Rh(COD)Cl]$_2$
H$_2$ (32.6 atm)
—————————————
MeOH, 40 °C
−CO$_2$, −t-BuOH

Ot-Bu
O—C(O)—NH O
                    NHPh
98% yield
1.1h

(2-6)
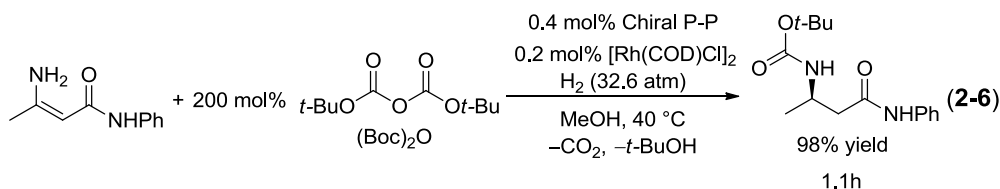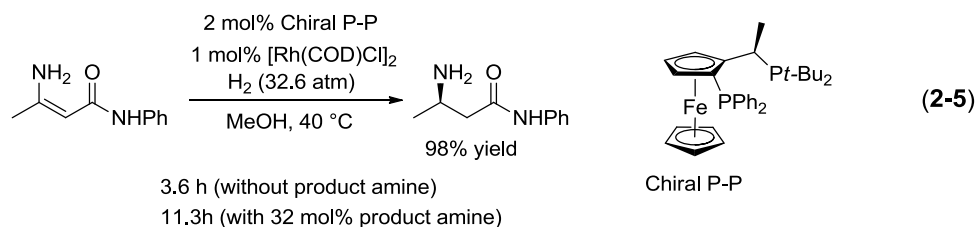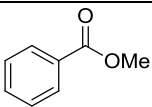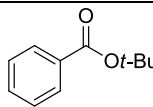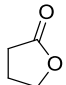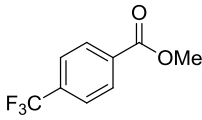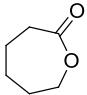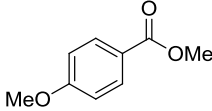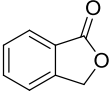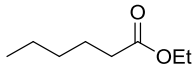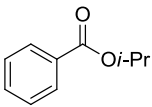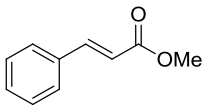
As described in Chapter 1, researchers at Firmenich and Takasago reported ester hydrogenation with high TON and TOF using Noyori-type, ketone hydrogenation catalysts under high H$_2$ pressure (50 atm), temperature (100 °C), and [base].[57,58] Based on our low temperature, stoichiometric study, these reaction conditions most likely contribute to the high TON and TOF by helping to overcome product inhibition.

Table 2-1 shows the results for hydrogenation of a series of esters and lactones under mild conditions using Ru-dihydride **41** as a catalyst. Several of these substrates were hydrogenated in 100% yield (entries 1–3) using 1 mol% **41** at 30 or 50 °C (9 equiv KOt-Bu, 4 atm H$_2$, 3 or 4 h). No significant difference in activity was observed between **6** and **41**. For example, hydrogenation of γ-butyrolactone (200 equiv, room temperature 4 atm H$_2$, 10 equiv KOt-Bu, 2 h) was 97% complete with **6**, and 85% with **41**. Lactones are less prone to product inhibition than acyclic esters (entries 2 and 3), possibly due to their higher reactivity towards Ru-dihydride **6** as seen in the low temperature, stoichiometric reactions, and fewer molecules

61

of alcohols produced per molecule of esters hydrogenated. The remaining substrates in Table 1 were hydrogenated using 2 mol% catalyst. Steric hindrance (entries 5 and 6) and more electron donating substituents (entries 8 and 9) retarded the yields as expected. Both the C=O and C=C bonds of methyl cinnamate were reduced in 100% yield possibly via concerted 1,4-addition of RuH and NH to β-carbon and carbonyl oxygen, or via reduction of carbonyl C=O followed by isomerization of an resulting allyl alcohol.

Table 2-1. Catalytic hydrogenation of esters and lactones.[a]

entry	ester/lactone	yield (%)[b]	entry	ester/lactone	yield (%)[b]
1[c]		100	6		75
2[d]		100	7		100
3[d]		100	8		84
4[e]		92	9		61
5		91	10		100

[a] Conditions: 50 equiv ester, 30 °C, 9 equiv KOt-Bu, 4 atm H_2, 3 h unless otherwise noted. [b] Determined by ^{1}H NMR. [c] 100 equiv ester, 50 °C. [d] 100 equiv ester, 4 h. [e] 4 h.

Conclusions

This Chapter presented the first direct observation and study of intermediates in the homogeneous hydrogenation of lactones and esters using the highly active Noyori ketone hydrogenation catalyst *trans*-[Ru((*R*)-BINAP)(H)$_2$((*R*,*R*)-dpen)] (**6**). Contrary to expectations, the intrinsic reactivity of Ru-dihydride **6** towards esters and lactones is high. It is product inhibition that limits the turnover number under low pressures and temperatures. Future catalyst development should be directed towards systems that minimize product inhibition and still retain a high intrinsic activity towards esters.

Experimental

Materials and Methods. All pressure reactions were carried out in a glass autoclave. All NMR experiments were carried out in NMR tubes fitted with a rubber septum under an atmosphere of argon or hydrogen using standard Schlenk and glovebox techniques unless stated otherwise. Deuterated solvents were obtained from Cambridge Isotope Laboratories. Common solvents were obtained from Fisher Scientific and distilled over appropriate drying reagents. THF was distilled over potassium/benzophenone before each experiment. THF-d_8 was distilled over potassium before each experiment. MeOH, 2-PrOH, *tert*-butanol, and benzyl alcohol were distilled over CaH$_2$. Common chemicals were obtained from Aldrich, TCI America, and Strem, and were used as received unless stated otherwise. Potassium *tert*-butoxide (KO*t*-Bu) was sublimed before use. All liquid esters and

lactones were distilled over molecular sieves type 4Å or CaH_2. γ-Butyrolactone (**42**) was distilled over molecular sieve type 4Å and passed through activated neutral alumina before use. Phthalide (**47**) was used as received. Ethylenediamine was distilled over KOH. *trans*-[Ru((*R*)-BINAP)-(H)$_2$((*R,R*)-dpen)] (**6**) and [Ru((*R*)-BINAP)(H)((*R,R*)-NH(CH(Ph))$_2$NH$_2$)] (**7**) were prepared using the method reported previously.[35e] 1,2-Benzenedimethanol was prepared by the LiAlH$_4$ reduction of **47**.[69] 2-Hydroxyfuran (**46**) was prepared by the DIBAL-H reduction of γ-butyrolactone.[70] Hydrogen gas was ultra high purity grade purchased from Praxair. ^{1}H, ^{13}C, and ^{31}P NMR spectra were recorded using Varian-Inova (400 MHz) spectrometers. ^{1}H and ^{13}C NMR chemical shifts are reported in parts per million (δ) relative to TMS with the solvent as the internal reference. [31]P chemical shifts are reported in parts per million (δ) relative to 85% H_3PO_4 as the external reference. NMR peak assignments were made using ^{1}H–^{1}H gCOSY, 2D gTOCSY, and ^{1}H–^{13}C gHSQC NMR experiments. Abbreviations for NMR spectra are s (singlet), d (doublet), t (triplet), q (quartet), dd (doublet of doublet), ddd (doublet of doublet of doublet), dt (doublet of triplet), tt (triplet of triplet), m (multiplet), and br (broad). Gas chromatography was performed using a Hewlett Packard 5890 chromatograph equipped with a flame ionization detector, a 3392A integrator, and a Beta Dex™ 120 fused silica capillary column (30m × 0.25mm × 0.25μm thickness, Supelco) using 20 psi He as carrier gas. The standard conditions used to determine yield of benzyl alcohol were: initial

oven temperature 100 °C increased at 1.0 °C/min. The retention times were t_R = 9.0 min for methyl benzoate, and t_R = 13.7 min for benzyl alcohol.

Preparation of the hemiacetaloxide 45 by reaction of trans-[Ru((R)-BINAP)(H)$_2$((R,R)-dpen)] (6) with γ-butyrolactone (42). A solution of **6** (0.011 mmol) was prepared in THF-d_8 (0.80 mL) using KN(Si(CH$_3$)$_3$)$_2$ (3.4 mg, 0.017 mmol) at –78 °C under H$_2$.[35e] Argon was then bubbled through the solution for 1 min at –78 °C to remove the excess H$_2$ used to prepare **6**. γ-Butyrolactone (**42**) (2.6 µL, 0.034 mmol) was then added at –78 °C using a syringe. The NMR tube was quickly removed from the –78 °C bath, shaken once, and returned to the bath. The sample was then introduced into the NMR probe pre-cooled to –80 °C. The first ^{1}H NMR spectrum showed that ~94% of the dihydride **6** had reacted to form a mixture of the hemiacetaloxide **45**, ~70% and the diol alkoxide **49**, ~24%. **45** was characterized at –80 °C using several ^{1}H, ^{31}P{^{1}H}, ^{1}H–^{1}H gCOSY, 2D gTOCSY, and ^{1}H–^{13}C gHSQC NMR experiments. ^{1}H NMR (399.95 MHz, THF-d_8, –80 °C): δ –17.6 (1H, t, $^2J_{P-H}$ = 24.0 Hz, Ru-H), 1.79 (1H, overlapping with a residual THF-d_8 peak, C$_B$HH), 1.95 (1H, overlapping with a C$_C$HH peak, C$_B$HH), 1.97 (1H, overlapping with a C$_B$HH peak, C$_C$HH), 2.46 (1H, br, overlapping with a γ-butyrolactone peak, C$_a$HNHH), 2.73 (1H, broad peak, C$_C$HH), 3.66 (1H, br, overlapping with a residual THF-d_8 peak, C$_b$HNHH), 3.87 (1H, br, overlapping with a free (R,R)-dpen peak, C$_D$HH), 3.97 (1H, br t, $^3J_{H-H}$ = 12.0 Hz, C$_b$HNHH), 4.23 (1H, br t, $^3J_{H-H}$ = 7.0 Hz, overlapping with a γ-butyrolactone peak, C$_a$HNHH), 4.47 (1H, br,

overlapping with a C_aHNHH peak, C_DHH), 4.55 (1H, br, overlapping with a C_DHH peak, C_aHNHH), 4.78 (1H, br, C_bHNHH), 6.17 (1H, s, C_AHO-Ru), 6-9.5 (overlapping peaks, aromatic). $^{13}C\{^1H\}$ NMR (100.6 MHz, THF-d_8, –80 °C, determined using ^1H–^{13}C gHSQC): δ 27.8 (C_CH$_2$), 38.3 (C_BH$_2$), 64.5 (C_DH$_2$), 64.4 (C_bHNH$_2$) 69.5 (C_aHNH$_2$), 110.9 (C_AHO-Ru), 126-136 (aromatic). $^{31}P\{^1H\}$ NMR (161.91 MHz, THF-d_8, –80 °C): δ 65.90 (d, $^2J_{P–P}$ = 41.9 Hz), 69.26 (d, $^2J_{P–P}$ = 41.9Hz). Figure 2-5 shows the ^{31}P NMR spectrum.

Preparation of the hemiacetaloxide 45 by reaction of trans-[Ru((R)-BINAP)(H)$_2$((R,R)-dpen)] (6) with γ-butyrolactone (42) using KOt-Bu as base. A solution of **6** (0.010 mmol) was prepared in THF-d_8 (0.80 mL) using KOt-Bu (3.7 mg, 0.033 mmol), and frozen in a liquid nitrogen bath.[35e] γ-Butyrolactone (**42**) (2.3 µL, 0.030 mmol) was then added at –78 °C using a syringe. The frozen solution was partially thawed and mixed by shaking once outside the bath. The sample was then introduced into the NMR probe pre-cooled to –80 °C. The first ^1H NMR spectrum (~3 min at –80 °C) showed that ~83% of the dihydride **6** had reacted to form a mixture of the hemiacetaloxide **45**, ~55%, the tert-butoxide compound **44**, ~17% ,and the diol alkoxide **49**, ~11%. The tert-butoxide compound was likely formed by reaction of **45** with the tert-butanol present from the preparation of **6**. The composition of the tert-butoxide compound was confirmed by an independent synthesis where the amide **7** was reacted with tert-butanol. The sample was then stored in

the NMR probe (–80 °C) for 30 min. The ^{1}H NMR spectrum taken after 30 min showed that a total of ~96% of the dihydride **6** had reacted to form a mixture of the hemiacetaloxide **45**, ~67%, the *tert*-butoxide compound **44**, ~15%, and the diol alkoxide **49**, ~14%. This rate roughly corresponds to 76% of the dihydride present when the first NMR was recorded reacting over 30 min at –80 °C. The hemiacetaloxide **45** converted into diol alkoxide **49** over several hours at –80 °C or upon warming up to –40 °C.

Preparation of the hemiacetaloxide 45 by reaction of [Ru((*R*)-BINAP)(H)((*R*,*R*)-NH(CH(Ph))₂NH₂)] (7) with 2-hydroxyfuran (46). A solution of **7** (0.015 mmol) was prepared in THF-d_8 (0.70 mL) using KN(Si(CH₃)₃)₂ (4.6 mg, 0.023 mmol), and frozen in a liquid nitrogen bath. 2-hydroxyfuran (**46**) (1.4mg, 0.016 mmol)[70] in THF-d_8 (0.10 mL) was then added into a frozen solution of **7** by cannula under argon pressure. Two frozen layers were partially melted and mixed by shaking once outside the bath. The sample was then introduced into the NMR probe pre-cooled to –80 °C. The first ^{1}H NMR spectrum (~3 min at –80 °C) showed that all compound **7** had reacted to form a mixture of the hemiacetaloxide **45**, ~91%, and the diol alkoxide **49**, ~9%. See Figure 2-6 – 2-8.

 Preparation of the hemiacetaloxide 48 by reaction of *trans*-[Ru((*R*)-BINAP)(H)₂((*R*,*R*)-dpen)] (6) with phthalide (47). A solution of **6** (0.015 mmol) was prepared in THF-d_8 (0.60 mL) using KN(Si(CH₃)₃)₂ (4.5 mg, 0.023 mmol) at –78 °C under H₂.[35e] Argon was then bubbled through the solution for 1 min at –78 °C to remove the excess H₂

67

used to prepare **6**. A solution of phthalide (**47**) (6.1 mg, 0.045 mmol) in THF-d_8 (0.20 mL) was then added at −78 °C by cannula under argon pressure. The NMR tube was quickly removed from the −78 °C bath, shaken once, and returned to the bath. The sample was then introduced into the NMR probe pre-cooled to −80 °C. The ^{1}H NMR spectrum showed that 89% of the dihydride **6** had reacted to form a mixture of the hemiacetaloxide **48**, ~73%, and the diol alkoxide **50**, ~16%. The hemiacetaloxide **48** was characterized at −80 °C using ^{1}H, ^{31}P{^{1}H}, ^{1}H–^{1}H gCOSY, and ^{1}H–^{13}C gHSQC NMR experiments. ^{1}H NMR (399.95 MHz, THF-d_8, −80 °C): δ −18.0 (1H, t, $^2J_{P-H}$ = 25.0 Hz, Ru-H), 2.46 (1H, br, C$_a$HN*HH*), 3.88 (1H, br, overlapping with a free (*R,R*)-dpen peak, C$_b$HN*HH*), 4.06 (1H, br quartet, C$_b$*H*NHH), 4.19 (1H, br quartet, C$_a$*H*NHH), 4.44 (1H, br, C$_b$HNH*H*), 4.87 (1H, br, overlapping with a CH*H* peak, C$_a$HNH*H*), 4.92 (1H, d, overlapping with a C$_a$HNH*H* peak, $^2J_{H-H}$ = 12.0 Hz, CH*H*), 5.28 (1H, d, overlapping with a phthalide peak, $^2J_{H-H}$ = 12.0 Hz, C*H*H), 7.35 (1H, s, C*H*O-Ru, overlapping with aromatic peaks), 6-10 (overlapping peaks, aromatic). ^{13}C{^{1}H} NMR (100.6 MHz, THF-d_8, −80 °C, determined using ^{1}H–^{13}C gHSQC): δ 63.2 (*C*$_a$HNH$_2$), 67.6 (*C*H$_2$), 69.7 (*C*$_b$HNH$_2$), 117.2 (*C*HO-Ru), 121-138 (aromatic). ^{31}P{^{1}H} NMR (161.91 MHz, THF-d_8, −80 °C): δ 66.32 (d, $^2J_{P–P}$ = 43.1 Hz), 68.80 (d, $^2J_{P–P}$ = 43.1 Hz). See Figures 2-9 – 2-11.

Preparation of the hemiacetaloxide 48 by reaction of *trans*-[Ru((*R*)-BINAP)(H)₂((*R,R*)-dpen)] (6) with phthalide (47) using

KO*t*-Bu as base. A solution of **6** (0.015 mmol) was prepared in THF-d_8 (0.60 mL) using KO*t*-Bu (5.0 mg, 0.045 mmol). A solution of phthalide (**47**) (5.7 mg, 0.043 mmol) in THF-d_8 (0.20 mL) was then added at –78 °C by cannula under H_2 pressure (~2 atm). The NMR tube was quickly removed from the –78 °C bath, shaken once, and returned to the bath. The sample was then introduced into the NMR probe pre-cooled to –80 °C. The first ^1H NMR spectrum (~10 min after the shake) showed that ~73% of the dihydride **6** had reacted to form a mixture of the hemiacetaloxide **48**, ~50%, the *tert*-butoxide compound, ~13%, the diol alkoxide **50**, ~1% and an uncharacterized ruthenium species, ~9%. The *tert*-butoxide compound was likely formed by reaction of **48** with the *tert*-butanol present from the preparation of **6**. The sample was then stored in the NMR probe (–80 °C) for 30 min. The ^1H NMR spectrum taken after 30 min showed that a total of ~80% of the dihydride **6** had reacted to form a mixture of the hemiacetaloxide **48**, ~53%, the *tert*-butoxide compound, ~15%, the diol alkoxide **50**, ~3%, and an uncharacterized ruthenium species, ~9%. This rate roughly corresponds to 26% of the dihydride present when the first NMR was recorded reacting over 30 min at –80 °C. This ruthenium hemiacetaloxide converted into the diol alkoxide **50** over several hours at –80 °C or upon warming up to –40 °C.

Reaction of *trans*-[Ru((*R*)-BINAP)(H)$_2$((*R*,*R*)-dpen)] (6) with methyl benzoate. A solution of **6** (0.011 mmol) was prepared in THF-d_8 (0.80 mL) using KN(Si(CH$_3$)$_3$)$_2$ (3.3 mg, 0.017 mmol).[35e] Methyl benzoate (3.9 µL,

0.031 mmol) was then added at –78 °C using a syringe. The NMR tube was quickly removed from the –78 °C bath, shaken once, and returned to the bath. The sample was then introduced into the NMR probe pre-cooled to –80 °C. ^{1}H and ^{31}P{^{1}H} NMR spectra was taken at –80, –60 and –40 °C. The reaction slowly started at –60 °C and all **6** was consumed when temperature reached –40 °C. The reaction products were a mixture of unidentified catalyst-alkoxide compounds.

Preparation of diol alkoxide 49 by reaction of *trans*-[Ru((*R*)-BINAP)(H)$_2$((*R*,*R*)-dpen)] (6) with γ-butyrolactone (42). The hemiacetaloxide **45** was prepared as described previously using KO*t*-Bu as base, and stored for 3 h in the NMR probe pre-cooled to –80 °C. NMR spectra showed this mixture consisted of the diol alkoxide **49**, ~61%, the hemiacetaloxide **45,** ~19%, the *tert*-butoxide compound **44**, ~18%, and the dihydride **6**, ~2%. Upon warming the NMR probe from –80 to –40 °C over ~10 min, the mixture consisted of **49**, ~86%, the *tert*-butoxide compound **44**, ~9%, and an unidentified ruthenium species, ~5%. **49** was characterized at –80 °C using several ^{1}H, ^{31}P{^{1}H}, ^{1}H–^{1}H gCOSY, and ^{1}H–^{13}C gHSQC NMR experiments. ^{1}H NMR (399.95 MHz, THF-d_8, –80 °C): δ –17.3 (1H, t, $^2J_{\text{P-H}}$ = 25.2 Hz, Ru-H), 1.47 (1H, overlapping with a cyclooctane peak (formed during the hydrogenation of [Ru((*R*)-BINAP)((1-5-η)-C$_8$H$_{11}$)]BF$_4$), C$_B$*H*H), 1.61 (1H, overlapping with a cyclooctane peak, C$_B$H*H*), 1.79 (2H, overlapping with a residual THF-d_8 peak, C$_C$*HH*), 2.51 (1H, br, C$_a$HN*H*H), 3.04 (1H, br, overlapping with a

70

C_bHNHH peak, $C_A$$H$HO-Ru), 3.11 (1H, br, overlapping with a $C_A$$H$HO-Ru peak, C_bHNHH), 3.53 (1H, overlapping with a residual THF-d_8 peak, C_AHHO-Ru), 3.65 (1H, overlapping with a residual THF-d_8 peak, $C_D$$H$HOH), 3.87 (1H, overlapping with a free (R,R)-dpen peak, C_DHHOH), 4.03 (1H, br, $C_b$$H$NHH), 4.26 (1H, overlapping with a γ-butyrolactone peak, C_aHNHH), 4.32 (1H, overlapping with a C_aHNHH peak, $C_a$$H$NHH), 4.45 (1H, br, C_bHNHH), 6-9.5 (overlapping peaks, aromatic), 12.8 (1H, s, C_DHHOH). ^{13}C{^{1}H} NMR (100.6 MHz, THF-d_8, −80 °C, determined using ^{1}H–^{13}C gHSQC): δ 36.0 (C_CH$_2$), 37.0 (C_BH$_2$), 62.6 (C_aHNH$_2$) 62.7 (C_DH$_2$), 69.2 (C_bHNH$_2$), 69.3 (C_AH$_2$O-Ru), 126-140 (aromatic). ^{31}P{^{1}H} NMR (161.91 MHz, THF-d_8, −80 °C): δ 68.98 (d, $^2J_{P–P}$ = 43.1 Hz), 73.76 (d, $^2J_{P–P}$ = 41.9 Hz). See Figures 2-12 – 2-14. This compound was also prepared using 1.5 equiv KN(Si(CH$_3$)$_3$)$_2$ instead of KOt-Bu to avoid the formation of ruthenium *tert*-butoxide compound.

Preparation of diol alkoxide 50 by reaction of *trans*-[Ru((R)-BINAP)(H)$_2$((R,R)-dpen)] (6) with phthalide (47). A solution of **6** (0.017 mmol) was prepared in THF-d_8 (0.60 mL) using KOt-Bu (5.7 mg, 0.051 mmol).[35e] A solution of phthalide (**47**) (7.7 mg, 0.057 mmol) in THF-d_8 (0.20 mL) was then added at −78 °C by cannula under H$_2$ pressure (~2 atm). The NMR tube was shaken for ~5 sec outside the −78 °C bath and then returned to the bath. This process was repeated nine times. ^{1}H, ^{31}P{^{1}H}, ^{1}H–^{1}H gCOSY, and ^{1}H–^{13}C gHSQC NMR spectra taken at −80 °C showed that the reaction was completed and formed ruthenium

alkoxide (**50**). Yield: 98% (based on ^{31}P NMR). ^{1}H NMR (399.95 MHz, THF-d_8, –40 °C): δ –17.4 (1H, t, $^2J_{\text{P-H}}$ = 25.6 Hz, Ru-H), 2.23 (1H, br, partially overlapping with a cyclooctene peak (formed during the hydrogenation of [Ru((*R*)-BINAP)((1-5-η)-C$_8$H$_{11}$)]BF$_4$), C$_a$HN*H*H), 3.83 (1H, d, $^2J_{\text{H-H}}$ = 11.5 Hz, C$_A$*H*HO-Ru), 3.91-4.00 (3H, overlapping multiplet, C$_a$*H*NHH, C$_b$*H*NHH and C$_b$HN*H*H overlapping with a free (*R,R*)-dpen peak), 4.11 (1H, br, C$_b$HNH*H*), 4.46 (1H, br, C$_a$HNH*H*), 4.72 (1H, br, C$_B$*H*HOH), 5.22 (1H, d, $^2J_{\text{H-H}}$ = 11.0 Hz, C$_A$H*H*O-Ru), 5.43 (1H, d, $^2J_{\text{H-H}}$ = 11.1 Hz, C$_B$*H*HOH), 6-10 (overlapping peaks, aromatic), 13.3 (1H, br, C$_B$HHO*H*). ^{13}C{^{1}H} NMR (100.6 MHz, THF-d_8, –40 °C, determined using ^{1}H–^{13}C gHSQC): δ 63.0 (*C*$_a$HNH$_2$), 66.7 (*C*$_A$H$_2$O-Ru), 69.8 (*C*$_b$HNH$_2$), 73.5 (*C*$_B$H$_2$OH), 126-138 (aromatic). ^{31}P{^{1}H} NMR (161.91 MHz, THF-d_8, –40 °C): δ 67.55 (d, $^2J_{\text{P–P}}$ = 46.9 Hz), 75.27 (d, $^2J_{\text{P–P}}$ = 46.9 Hz). This compound was also prepared using 1.5 equiv KN(Si(CH$_3$)$_3$)$_2$ instead of KO*t*-Bu to avoid the formation of the ruthenium *tert*-butoxide compound.

Preparation of diol alkoxide 49 by reaction of [Ru((*R*)-BINAP)(H)((*R,R*)-NH(CH(Ph))$_2$NH$_2$)] (7) with 1,4-butanediol. A solution of **7** (0.010 mmol) was prepared in THF-d_8 (0.80 mL) as we described previously using KN(Si(CH$_3$)$_3$)$_2$ (3.1 mg, 0.016 mmol).[35e] 1,4-Butanediol (1 µL, 0.011 mmol) was then added at –78 °C using a syringe. The NMR tube was shaken once outside the –78 °C bath and then returned to the bath. ^{1}H, ^{31}P{^{1}H}, ^{1}H–^{1}H gCOSY and ^{1}H–^{13}C gHSQC NMR

spectra showed formation of diol alkoxide **49**. Yield: ~100% (based on ^{31}P NMR).

Preparation of diol alkoxide 50 by the reaction of [Ru((R)-BINAP)(H)((R,R)-NH(CH(Ph))$_2$NH$_2$)] (7) with 1,2-benzenedimethanol. A solution of **7** (0.020 mmol) was prepared in THF-d_8 (0.60 mL) as we described previously using KN(Si(CH$_3$)$_3$)$_2$ (8.1 mg, 0.041 mmol).[35e] A solution of 1,2-benzenedimethanol (3.1 mg, 0.022 mmol) in THF-d_8 (0.20 mL) was then added at –78 °C by cannula under argon. The NMR tube was shaken for ~5 sec outside the –78 °C bath and then returned to the bath. This process was repeated nine times. ^{1}H, ^{31}P{^{1}H}, ^{1}H–^{1}H gCOSY, and ^{1}H–^{13}C gHSQC NMR spectra showed formation of diol alkoxide **50**. Yield: 100% (based on ^{31}P NMR). See Figures 2-15 – 2-17.

Preparation of a mixture of *trans*-[Ru((R)-BINAP)(H)$_2$-(ethylenediamine)] (41) and 9 equiv KO*t*-Bu for use as an ester hydrogenation catalyst. This compound was prepared using the method reported previously for the preparation of *trans*-[Ru((R)-BINAP)(H)$_2$-((R,R)-dpen)] (**6**).[35e] A solution of [Ru((R)-BINAP)((1-5-η)-C$_8$H$_{11}$)]BF$_4$ (9.2 mg, 0.010 mmol)[71] in THF (0.50 mL) was shaken under H$_2$ (~2 atm) in a NMR tube at 0 °C for 3 min. Ethylenediamine (1.0 µL, 0.015 mmol) was then added using a micro-liter syringe at –78 °C. An excess of ethylenediamine was used to overcome the losses associated with measuring and addition of the required 0.7 µL (0.010 mmol) of ethylenediamine. The NMR tube was then shaken for ~5 sec outside the

–78 °C bath and then returned to the bath. This process was repeated nine times. KOt-Bu (11.2 mg, 0.10 mmol) (KN(Si(CH$_3$)$_3$)$_2$ can be used as well) in THF (0.50 mL) was then added by cannula under H$_2$ pressure (~2 atm). The NMR tube was shaken for ~5 sec outside the –78 °C bath and then returned to the bath. This process was repeated nine times. The solution color changed from yellow to red during the addition of KOt-Bu. NMR spectra recorded at –20 °C showed formation of the ruthenium dihydride **41** as sole ruthenium containing product. **41** was characterized using ^{1}H, ^{31}P{^{1}H}, ^{1}H–^{1}H gCOSY, and ^{1}H–^{13}C gHSQC NMR. ^{1}H NMR (399.95 MHz, THF-d_8, –20 °C): δ –5.46 (2H, t, $^2J_{\text{P-H}}$ = 16.7 Hz, Ru-H), 1.68 (2H, broad peak, 2NHH, partially overlapping with a residual THF-d_8 peak), 2.40 (2H, broad peak, 2CHH, partially overlapping with the other 2CHH peak), 2.48 (2H, broad peak, 2CHH, partially overlapping with the other 2CHH peak and a free en peak), 3.27 (2H, broad peak, 2NHH), 6.0-9.5 (overlapping peaks, aromatic). ^{13}C{^{1}H} NMR (100.6 MHz, THF-d_8, –20 °C, determined using ^{1}H–^{13}C gHSQC): δ 46.4 (2CH$_2$), 123-135 (aromatic). ^{31}P{^{1}H} NMR (161.88 MHz, THF-d_8, –20 °C): δ 86.97 (s). See Figures 2-18 – 2-20. This mixture was then added by cannula under H$_2$ pressure (~2 atm) to a glass autoclave containing an appropriate ester (1.0 or 0.50 mmol) and 2.0 mL of freshly distilled THF.

Typical procedure for hydrogenation of esters. A glass autoclave was purged with H$_2$ before adding reagents. The appropriate ester (1.0 or 0.50 mmol) and 2.0 mL of freshly distilled THF were then injected into the

autoclave. A mixture of *trans*-[Ru((*R*)-BINAP)(H)$_2$(ethylenediamine)] (**41**) (0.010 mmol) and KO*t*-Bu (0.10 mmol) in THF (1.0 mL), prepared as described in the previous section, was then added by cannula under H$_2$ pressure (~2 atm). The reaction mixture was stirred at 30 °C for 3 h under 4 atm of H$_2$. Formation of small amount of solid was sometimes observed during the reaction. The autoclave was then vented. The reaction mixture was analyzed by NMR and/or GC.

TON vs. Reaction time for hydrogenation of methyl benzoate (Figure 2-2.). A glass autoclave was purged with H$_2$ before adding reagents. Methyl benzoate (0.13 mL, 1.0 mmol) and 2.0 mL of freshly distilled THF were injected into the autoclave. A mixture of *trans*-[Ru((*R*)-BINAP)-(H)$_2$(ethylenediamine)] (0.010 mmol) and KO^{t}Bu (11.6 mg, 0.10 mmol) in THF (1.0 mL) was then added by cannula under H$_2$ pressure (~2 atm). The reaction mixture was stirred at room temperature (~23 °C) for 4 h under 4 atm of H$_2$. Aliquot of the reaction mixture was taken every 30 min for 4 h and analyzed using GC. Yield: 35% (30 min), 49% (60 min), 62% (90 min), 67% (120 min), 72% (150 min), 77% (180 min), 78% (210 min), 80% (240 min). The turnover frequency of the first an hour and the last an hour were 49 h^{-1} and 3 h^{-1} respectively.

Hydrogenation of methyl benzoate in the presence of product alcohols. A glass autoclave was purged with H$_2$ before adding reagents. Methyl benzoate (0.130 mL, 1.03 mmol, 100 equiv), benzyl alcohol (0.086 mL, 0.83 mmol, 80 equiv), MeOH (0.034 mL, 0.84 mmol, 80 equiv), and 2.0

mL of freshly distilled THF were injected into the autoclave. A solution of

trans-[Ru((*R*)-BINAP)(H)$_2$(en)] (**41**) (0.010 mmol, 1 equiv) prepared using

[Ru((*R*)-BINAP)((1-5-*η*)-C$_8$H$_{11}$)]BF$_4$ (9.5 mg, 0.010 mmol) and KO*t*-Bu (11.6

mg, 0.094 mmol) in THF (1.0 mL) was then added to the autoclave under

H$_2$ pressure (~2 atm). The reaction mixture was stirred at room

temperature (~23 °C) for 1 h under 4 atm of H$_2$. The reaction mixture was

analyzed by NMR and GC. The mixture of methyl benzoate (18 %), benzyl

alcohol (30 %), and benzyl benzoate (52 %) was obtained. Benzyl

benzoate was formed via a base catalyzed transesterification. This ratio

was translated into the increased amount of benzyl alcohol from 80 equiv

to 97 equiv for 1 h by counting the benzyl benzoate as a product and a

reactant. This increase corresponds to TOF of 17 h^{-1}.

Preparation of Ru-*tert*-butoxide compound 44 by the reaction of

[Ru((*R*)-BINAP)(H)((*R,R*)-NH(CH(Ph))$_2$NH$_2$)] (7) with *t*-BuOH. A solution

of **7** (0.012 mmol) was prepared in THF-d_8 (0.60 mL) as we described

previously using KN(Si(CH$_3$)$_3$)$_2$ (3.7 mg, 0.019 mmol).[35e] *t*-BuOH (3.5 µL,

0.036 mmol) in was then added using a syringe at –78 °C. The NMR tube

was shaken for ~5 sec outside the –78 °C bath and then returned to the

bath. ^{1}H, ^{31}P{^{1}H}, ^{1}H–^{1}H gCOSY, and ^{1}H–^{13}C gHSQC NMR spectra

showed formation of diol alkoxide **44**. Yield: 75% (based on ^{31}P NMR). ^{1}H

NMR (399.95 MHz, THF-d_8, –80 °C): δ –16.3 (1H, t, $^2J_{P-H}$ = 23.8 Hz, Ru-H),

1.17 (9H, overlapping with a free *t*-BuOH peak, OC(C*H*$_3$)), 2.13 (1H, broad

peak, partially overlapping with a cyclooctene peak (formed during the

hydrogenation of [Ru((*R*)-BINAP)((1-5-η)-C$_8$H$_{11}$)]BF$_4$), C$_a$HN*H*H), 3.29 (1H, br, C$_b$HN*H*H), 3.98 (1H, br t, C$_b$*H*NHH), 4.33 (2H, br, overlapping C$_a$*H*NHH and C$_b$HNH*H*), 4.56 (1H, br, C$_a$HNH*H*), 6-10 (overlapping peaks, aromatic). ^{13}C{^{1}H} NMR (100.6 MHz, THF-d_8, –80 °C, determined using ^{1}H–^{13}C gHSQC): δ 31.8 (C(*C*H$_3$)), 62.3 (*C*$_a$HNH$_2$), 69.4 (*C*$_b$HNH$_2$), 126-138 (aromatic). ^{31}P{^{1}H} NMR (161.91 MHz, THF-d_8, –80 °C): δ 68.39 (d, $^2J_{P–P}$ = 41.9 Hz), 73.75 (d, $^2J_{P–P}$ = 40.8 Hz). See Figures 2-21 – 2-23.
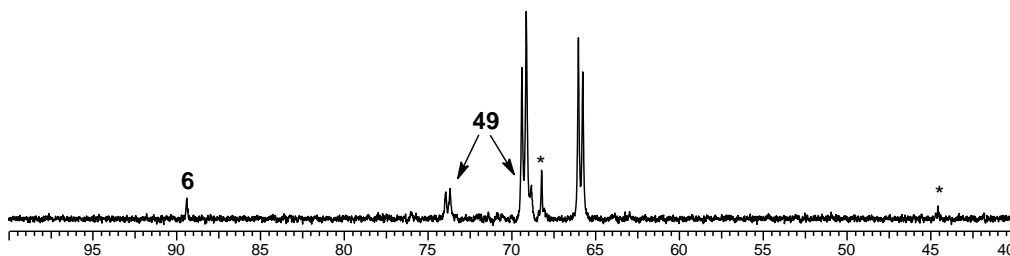
Figure 2-5. ^{31}P NMR spectrum (δ 100 to 40) of **45** prepared from **6** and **42** using KN(Si(CH$_3$)$_3$)$_2$ at –80 °C. * is Ru species formed during preparation of **6**.
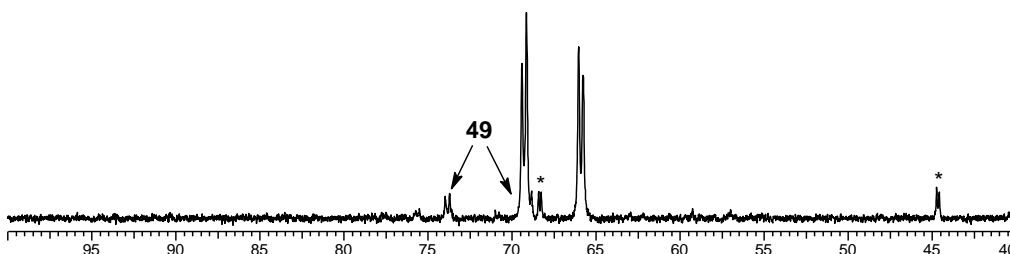
Figure 2-6. ^{31}P NMR spectrum (δ 100 to 40) of **45** prepared from **7** and **46** at –80 °C. * is Ru species formed during preparation of **7**.
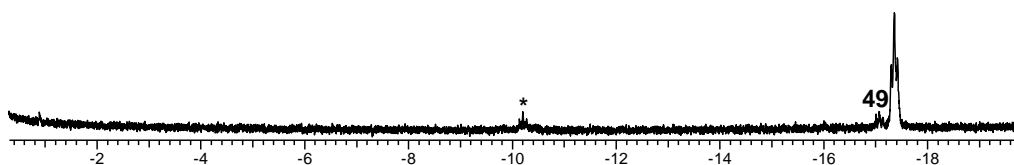
Figure 2-7. ^{1}H NMR spectrum (δ −0.5 to −20) of **45** prepared from **7** and **46** at −80 °C. * is Ru species formed during preparation of **7**.
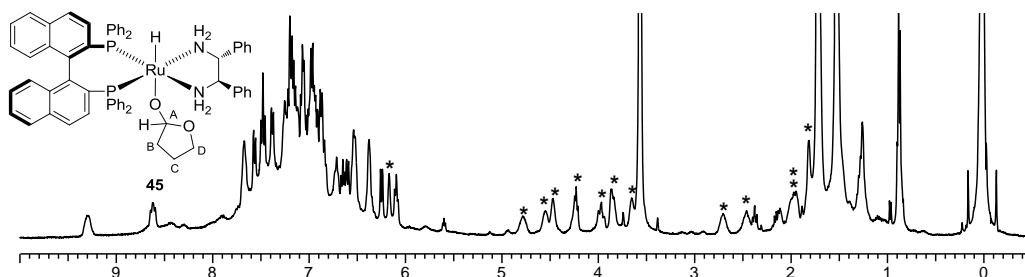
Figure 2-8. ^{1}H NMR spectrum (δ 10 to −0.5) of **45** prepared from **7** and **46** at −80 °C. The non-aromatic peaks assigned to **45** are marked with an asterisk. The remaining peaks are due to trace γ-butyrolactone (**42**) and **49,** residual protons in THF-d_8, KN(Si(CH$_3$)$_3$)$_2$, HN(Si(CH$_3$)$_3$)$_2$, cyclooctane and cyclooctene (formed during the hydrogenation of [Ru((R)-BINAP)((1-5-η)-C$_8$H$_{11}$)]BF$_4$) and hexanes, if present.
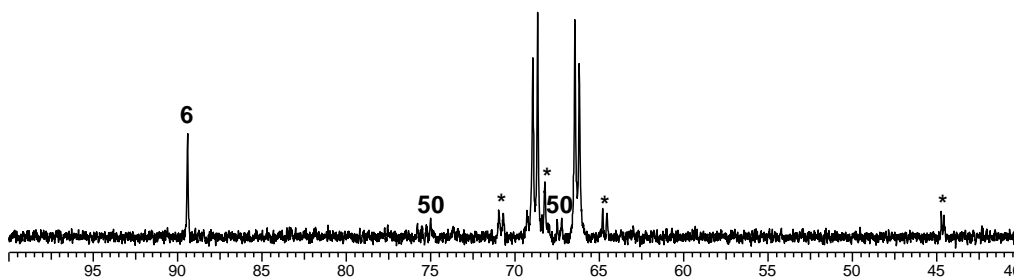
Figure 2-9. ^{31}P NMR spectrum (δ 100 to 40) of **48** prepared from **6** and **47** at −80 °C. * is Ru species formed during preparation of **6**.

78
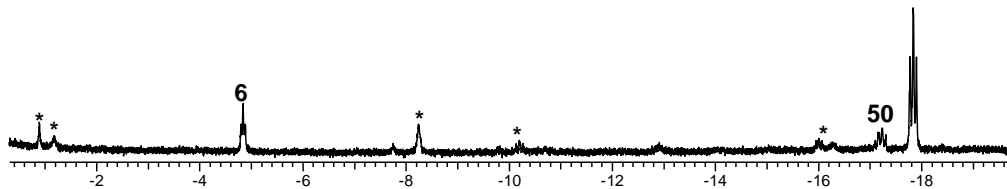
Figure 2-10. ^{1}H NMR spectrum (δ –0.5 to –20) of **48** prepared from **6** and **47** at –80 °C. * is Ru species formed during preparation of **6**.
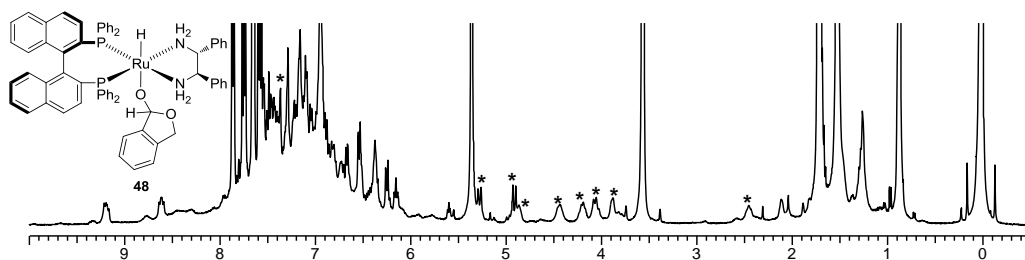
Figure 2-11. ^{1}H NMR spectrum (δ 10 to –0.5) of **48** prepared from **6** and **47** at –80 °C. The non-aromatic peaks assigned to **48** are marked with an asterisk. The remaining peaks are due to excess phthalide (**47**), trace **6** and **50**, residual protons in THF-d_8, KN(SiC(H$_3$)$_3$)$_2$, HN(Si(CH$_3$)$_3$)$_2$, cyclooctane and cyclooctene (formed during the hydrogenation of [Ru((*R*)-BINAP)((1-5-*η*)-C$_8$H$_{11}$)]BF$_4$) and hexanes, if present.
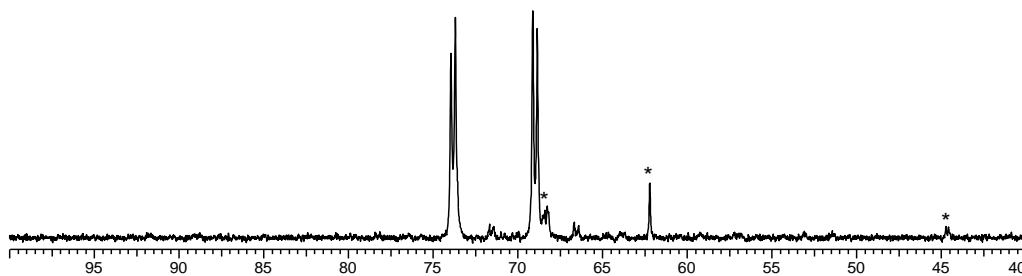
Figure 2-12. ^{31}P NMR spectrum (δ 100 to 40) of **49** prepared from **6** and **42**

at –80 °C. * is Ru species formed during preparation of **6**.
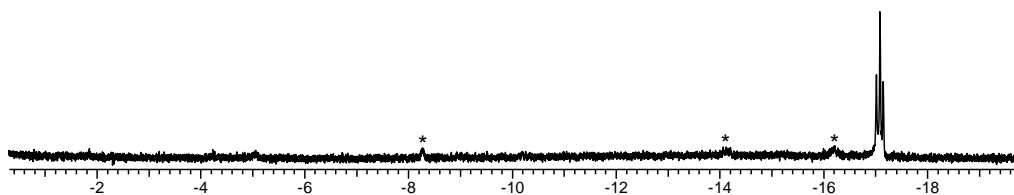
Figure 2-13. ^{1}H NMR spectrum (δ –0.5 to –20) of **49** prepared from **6** and **42** at –80 °C. * is Ru species formed during preparation of **6**.
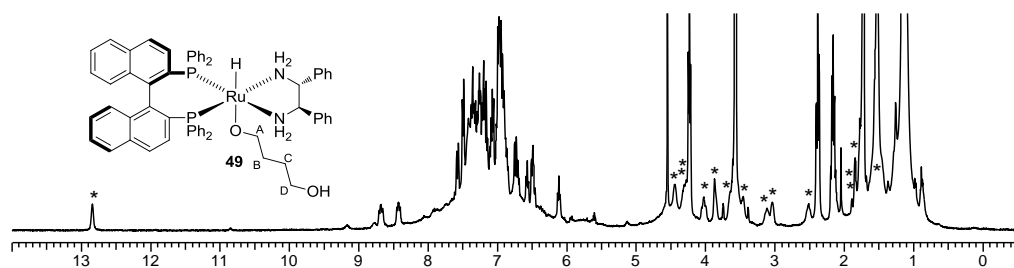
Figure 2-14. ^{1}H NMR spectrum (δ 14 to –0.5) of **49** prepared from **6** and **42** using KOt-Bu at –80 °C. The non-aromatic peaks assigned to **49** are marked with an asterisk. The remaining peaks are due to excess **42**, residual protons in THF-d_8, KOt-Bu, t-BuOH, H$_2$, cyclooctane and cyclooctene (formed during the hydrogenation of [Ru((R)-BINAP)((1-5-η)-C$_8$H$_{11}$)]BF$_4$) and hexanes, if present.
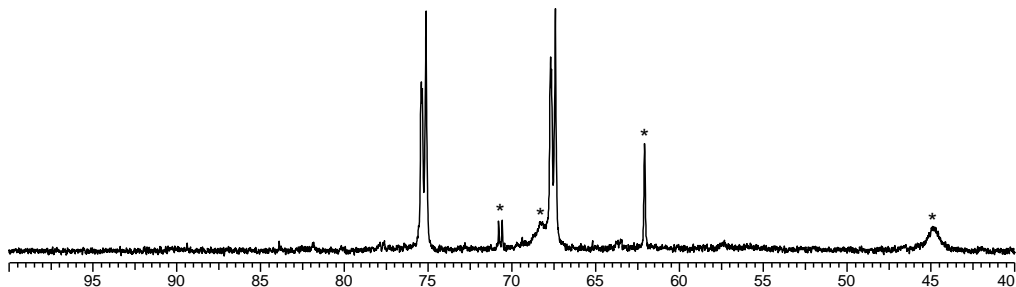
Figure 2-15. ^{31}P NMR spectrum (δ 100 to 40) of **50** prepared from **7** and 1,2-benzenedimethanol at –40 °C. * is Ru species formed during preparation of **7**.
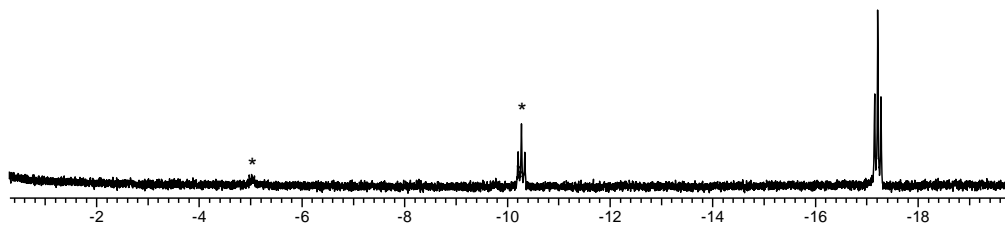
Figure 2-16. ^{1}H NMR spectrum (δ –0.5 to –20) of **50** prepared from **7** and 1,2-benzenedimethanol at –40 °C. * is Ru species formed during preparation of **7**.
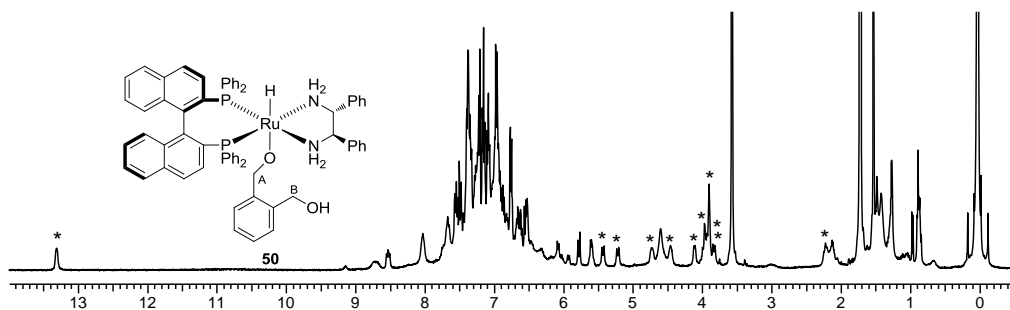
Figure 2-17. ^{1}H NMR spectrum (δ 14 to –0.5) of **50** prepared from **7** and 1,2-benzenedimethanol at –40 °C. The non-aromatic peaks assigned to **50**

are marked with an asterisk. The remaining peaks are due to excess 1,2-benzenedimethanol, residual protons in THF-d_8, KN(Si(CH$_3$)$_3$)$_2$, HN(Si(CH$_3$)$_3$)$_2$, cyclooctane and cyclooctene (formed during the hydrogenation of [Ru((R)-BINAP)((1-5-η)-C$_8$H$_{11}$)]BF$_4$) and hexanes, if present.
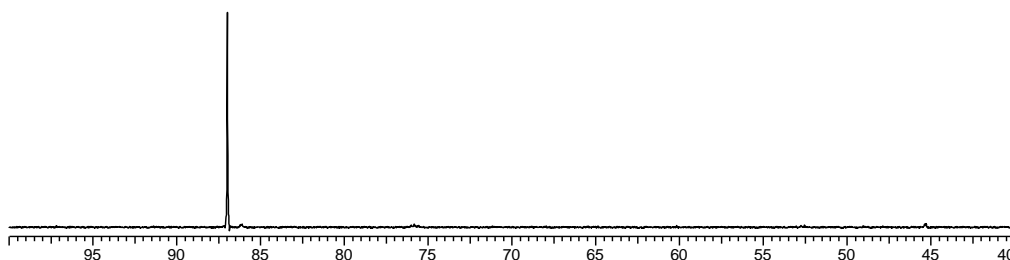
Figure 2-18. ^{31}P NMR spectrum (δ 100 to 40) of **41** prepared using KN(Si(CH$_3$)$_3$)$_2$ at –20 °C.
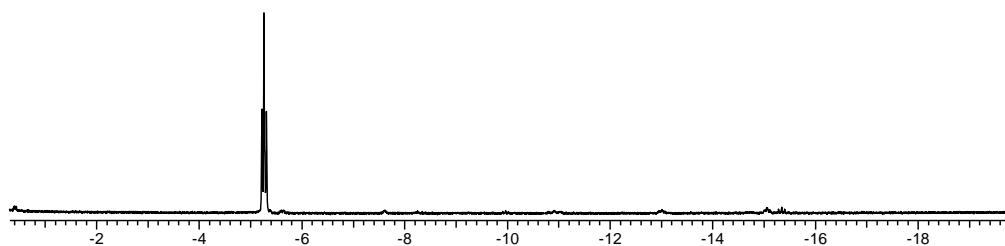
Figure 2-19. ^{1}H NMR spectrum (δ –0.5 to –20) of **41** prepared using KN(Si(CH$_3$)$_3$)$_2$ at –20 °C.
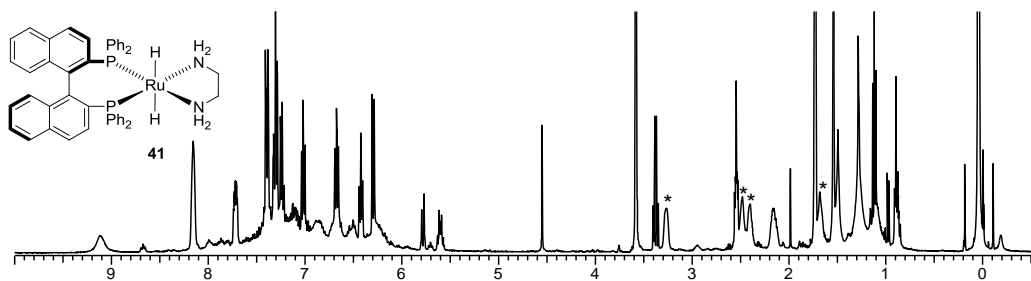
Figure 2-20. ^{1}H NMR spectrum (δ 10 to −0.5) of **41** prepared using KN(Si(CH$_3$)$_3$)$_2$ at −20 °C. The non-aromatic peaks assigned to **41** are marked with an asterisk. The remaining peaks are due to trace amount of excess ethylenediamine, residual protons in THF-d_8, KN(Si(CH$_3$)$_3$)$_2$, HN(SiC(CH$_3$)$_3$)$_2$, H$_2$, cyclooctane and cyclooctene (formed during the hydrogenation of [Ru((R)-BINAP)((1-5-η)-C$_8$H$_{11}$)]BF$_4$), diethyl ether and hexanes, if present.

Figure 2-21. ^{31}P NMR spectrum (δ 100 to 40) of **44** at −80 °C. * is Ru species formed during preparation of **7**.
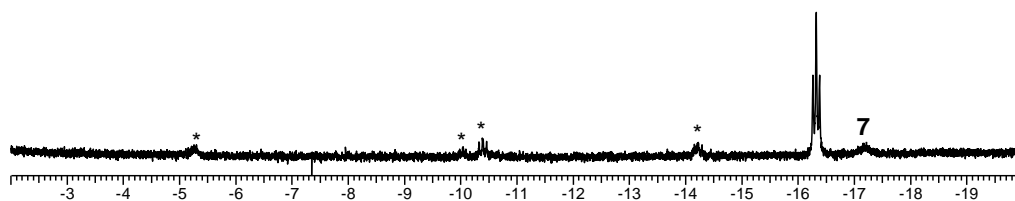
Figure 2-22. ^{1}H NMR spectrum (δ –2 to –20) of **44** at –80 °C. * is Ru species formed during preparation of **7**.
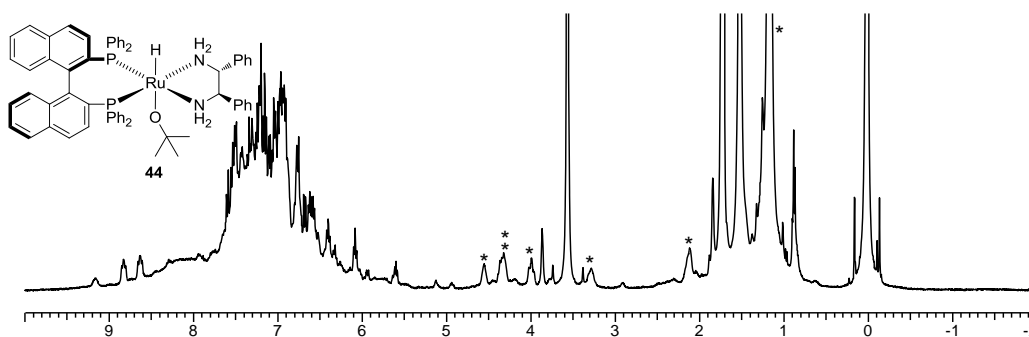
Figure 2-23. ^{1}H NMR spectrum (δ 10 to –2) of **44** at –80 °C. The non-aromatic peaks assigned to **44** are marked with an asterisk. The remaining peaks are due to trace amount of excess ethylenediamine, residual protons in THF-d_8, $KN(Si(CH_3)_3)_2$, $HN(Si(CH_3)_3)_2$, t-BuOH, cyclooctane and cyclooctene (formed during the hydrogenation of $[Ru((R)\text{-}BINAP)((1\text{-}5\text{-}\eta)\text{-}C_8H_{11})]BF_4)$, diethyl ether and hexanes, if present.

Chapter 3

Ru Catalyzed Enantioselective Desymmetrization of *meso*-Cyclic

Imides via Monohydrogenation

Introduction

Enantioselective desymmetrization of *meso*-compounds is an efficient method to form multiple stereogenic centres[72] with identical ee in one reaction from simple substrates such as *meso*-anhydrides, epoxides, dienes, and diols. Enantioselective desymmetrizations of anhydrides by esterification are among the most studied because of the ready availability of the corresponding *meso*-diacid starting materials, and because of the high electrophilicity of anhydrides.[72d] There are, in contrast, only a few reports of enantioselective desymmetrization of *meso*-imides. Among these, there is one report of imide desymmetrization by esterification,[73] and several reports of enantioselective desymmetrization of *meso*-cyclic imides using chiral M–H reagents.[74] Most of these M–H reductions utilize either chiral oxazaborolidine catalysts (CBS catalyst) + BH$_3$·THF, or (*R*)- or (*S*)-BINAL-H(MeOH), where BINAL-H(MeOH) is a 1:1:1 mixture of BINOL, LiAlH$_4$, and MeOH (BINOL is 1,1'-bi-2-naphthol). The products of these reductions are hydroxy lactams made by monoreduction of the imide (Scheme 1-13, path A).

Speckamp and coworkers utilized the CBS catalyst **51** + BH$_3$·THF system to effect the enantioselective desymmetrization of *meso*-cyclic imides at 0 °C (Table 3-1).[74c] Reduction of imides using 10–50 mol% of **51**

and 0.60–0.75 equiv of BH$_3$·THF (i.e. 1.8-2.25 equiv BH), followed by addition of 5% HCl at 0 °C formed a mixture of *cis*- and *trans*-hydroxy lactams in 68–94% yield and 77–89% ee.

Table 3-1. Enantioselective desymmetrization of *meso*-cyclic imides via monoreduction by CBS catalyst **51** + BH$_3$·THF system.
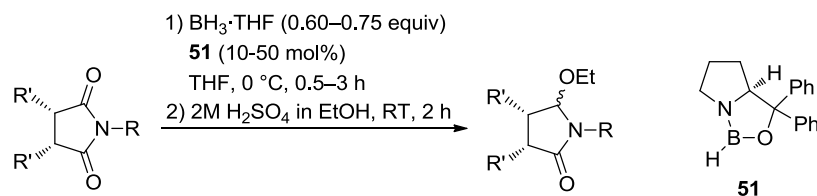
entry	imide	product	yield (%)	ee (%)
1			87	80
2			85	77
3			68	89
4			94	88

The authors found that all the *cis*-isomers converted into the thermodynamically more stable *trans*-isomers upon transformation into the corresponding ethoxy lactams. The *trans*-ethoxy lactam is favoured by thermodynamics because it has less steric repulsion between the ethoxy

group and the imide backbone. The authors proposed that the *cis*-hydroxy lactam is the kinetic product resulting from hydride attack from the least hindered convex face of the carbonyl group. The observed enantiogroup-selectivity was explained with transition state steric arguments (Figure 3-1). Specifically, the authors proposed that the bulky *N*-benzyl group is situated on the convex side of the catalyst **51** in the transition state to minimize steric repulsions. This explanation also accounts for the increase in ee that occurs when the steric size of the imide backbone is decreased (entries 1 and 2 vs. 3 and 4) because a smaller backbone will enhance the steric recognition between the *N*-benzyl group and the backbone.

favoured   unfavoured
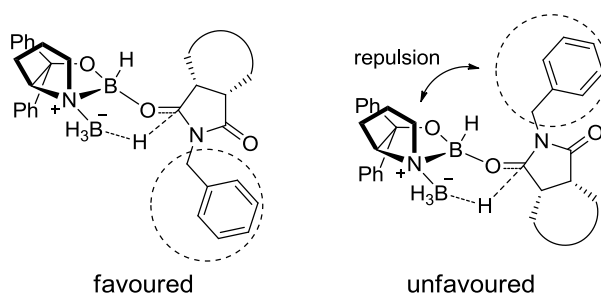
Figure 3-1. A proposed transition state for the enantioselective desymmetrization of *meso*-cyclic imides via monoreduction by the CBS catalyst **51** + BH$_3$·THF system.

Matsuki and co-workers utilized the BINAL-H(MeOH) system to effect the enantioselective desymmetrization of *meso*-bicyclic imides at −78 °C.[74a] Reduction of imides using 3.5 equiv of (*R*)-BINAL-H(MeOH),

followed by addition of 10% HCl at −78 °C followed by warming to 0 °C

formed a mixture of *cis*- and *trans*-hydroxy lactams in 55–86% yield and

88–91% ee (Table 3-2).

Table 3-2. Enantioselective desymmetrization of *meso*-cyclic imides via

monoreduction by (*R*)-BINAL-H(MeOH) system.
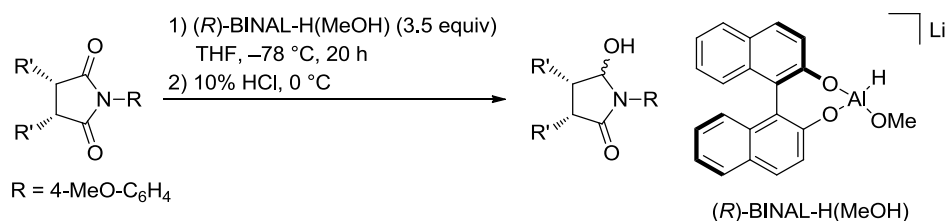
entry	imide	yield (%)	cis:trans ratio	ee (%)
1		86	9:1	88
2		79	10:1	88
3		55	10:1	91

The cis/trans ratio was dependent on the conditions utilized for the

reaction work-up. Work-up by addition of 10% HCl at 0 °C formed mixtures

of the *cis*- and *trans*-hydroxy lactams in ~9:1 ratios (Table 3-2). However,

work-up by addition of 10% HCl at −78 °C resulted in exclusive formation of

the *cis*-isomer of the hydroxy lactam. As the convex faces of the carbonyls

are less sterically crowded than the concave faces, hydride delivery from

the convex face forms the unstable *cis*-alcohol. The *cis*-isomer was converted into the *trans*-isomer upon treatment with 10% HCl at RT for 1 h.

Hydroxy lactams, and their derivatives are versatile building blocks that have been used to prepare several potent and commercialized pharmaceutical compounds including vitamins, and EP4 antagonists such as (+)-biotin,[74d,f,75] and MF-310[76]. Numerous academically important alkaloids such as gelsemine,[77] have also been prepared from hydroxy lactams and their derivatives.

Unlike hemiacetals, hydroxy lactams are isolable, bench-stable, and can be stored under ambient conditions. Also, they are readily converted into the corresponding lactones or lactams by reduction. Most of the hydroxy lactams in the literature are prepared by $NaBH_4$ or DIBAL-H reduction of the corresponding imides. For example, MF-310, a potential new treatment for chronic inflammation, was prepared in >2 kg scale using lactam **54** by researchers at Merck.[76] The preparation involved the regioselective DIBAL-H reduction of the imide **52** carried out on a 3 kg scale. The hydroxy lactam **53** was then reduced by $SiHEt_3$ in the presence of trifluoroacetic acid (TFA) to form **54** (Scheme 3-1).

Scheme 3-1. Preparation of MF-310 developed by Merck.
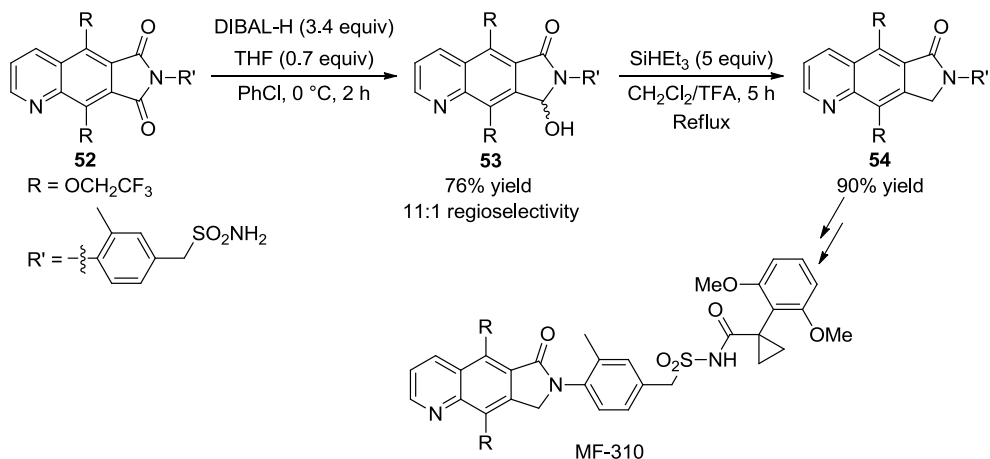
Hydroxy lactams form *N*-acyliminium ions upon the addition of Lewis or Brønsted acids.[78] *N*-acyliminium ions undergo a myriad of C–C bond forming reactions with a variety of nucleophiles such as organometallic reagents, alkenes, and arenes.[78d] Furthermore, they are frequently utilized to prepare nitrogen-containing polycyclic compounds such as alkaloids via intramolecular cyclizations. For example, Speckamp and coworkers synthesized (+)-biotin starting from L-cysteine (Scheme 3-2).[75b] They prepared the hydroxy lactam derivative **56** from the imide **55** using excess DIBAL-H. The corresponding *N*-acyliminium ion was then generated *in situ* by the addition of TMSOTf to **56**. Intramolecular addition between the enol C=C bond and the iminium ion formed the bicyclic compound **57**, which was then transformed into (+)-biotin. Recent advances in *N*-acyliminium ion chemistry include organocatalytic, enantioselective Morita–Baylis–Hillman-type reactions,[79] and Pictet–Spengler-type cyclizations.[80]

Scheme 3-2. Synthetic route to (+)-biotin developed by Speckmap et al..
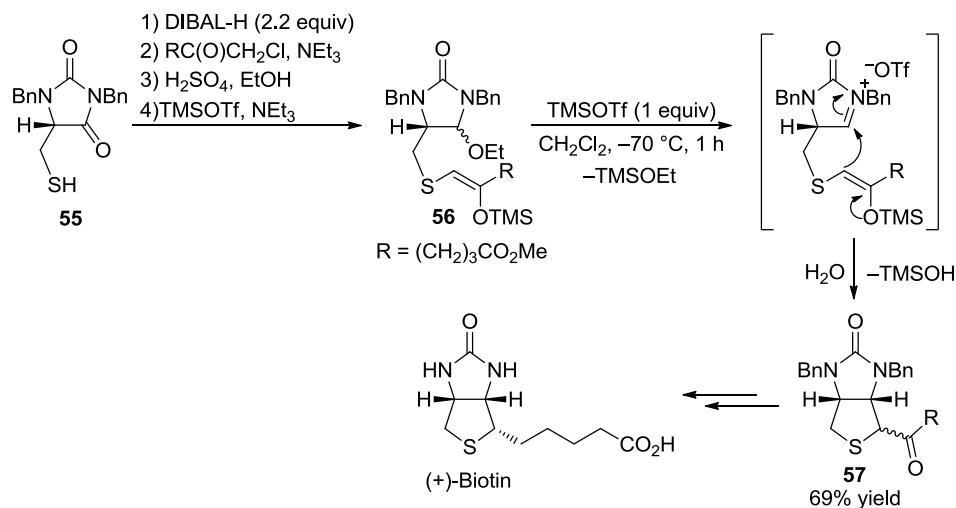
Jacobsen and co-workers recently reported enantioselective Pictet–Spengler-type cyclizations using a chiral thiourea catalyst (Scheme 3-3). These authors synthesized an alkaloid, (+)-harmicine, using an intermolecular *N*-acyliminium cyclization of the corresponding hydroxy lactam.[80] Their hydroxy lactam was prepared from $NaBH_4$ reduction of the corresponding imide. They proposed that the chiral thiourea catalyst induces enantioselectivity by the formation of *N*-acyliminium chloride–thiourea complex via hydrogen bonds between the thiourea and chloride anion.

Scheme 3-3. Synthetic route to (+)-harmicine developed by Jacobsen et al..
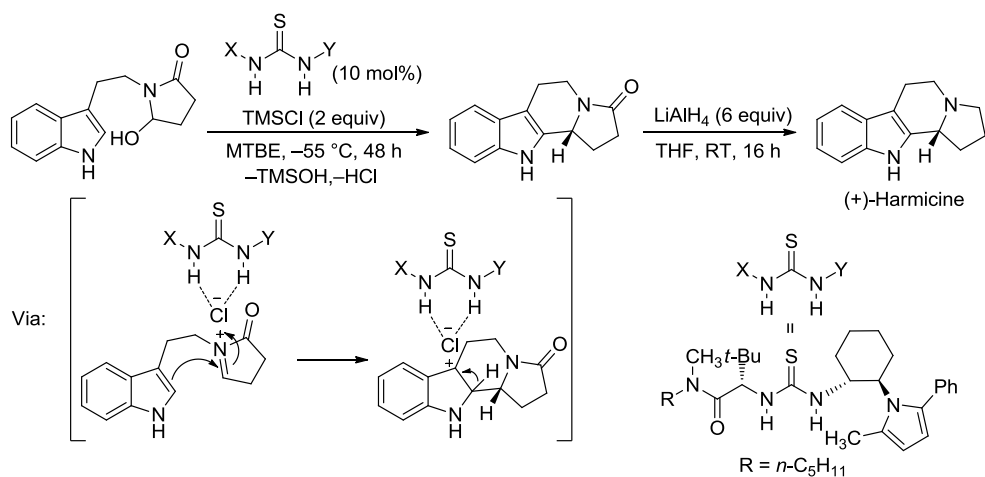
As described in Chapter 1, the hydrogenation of imides is rare in both heterogeneous and homogeneous catalysis. Indeed, only one enantioselective imide hydrogenation is reported to date. Ikariya and co-workers reported Ru-Cp*(P–N) complexes that hydrogenate cyclic imides in the absence of base (Typical reaction conditions: 10 mol % catalyst, 80 °C, 30 atm H_2, 18-24 h, in 2-PrOH, >99 % yield) (Figure 3-2).[63] Further, they reported the first enantioselective desymmetrization of cyclic imides by dihydrogenation using a chiral Ru-Cp*(P–N) catalyst (10 mol%). They observed moderate to excellent ee (62–98%) in high yields (>99%). The TOF was, however, low (0.42/h).
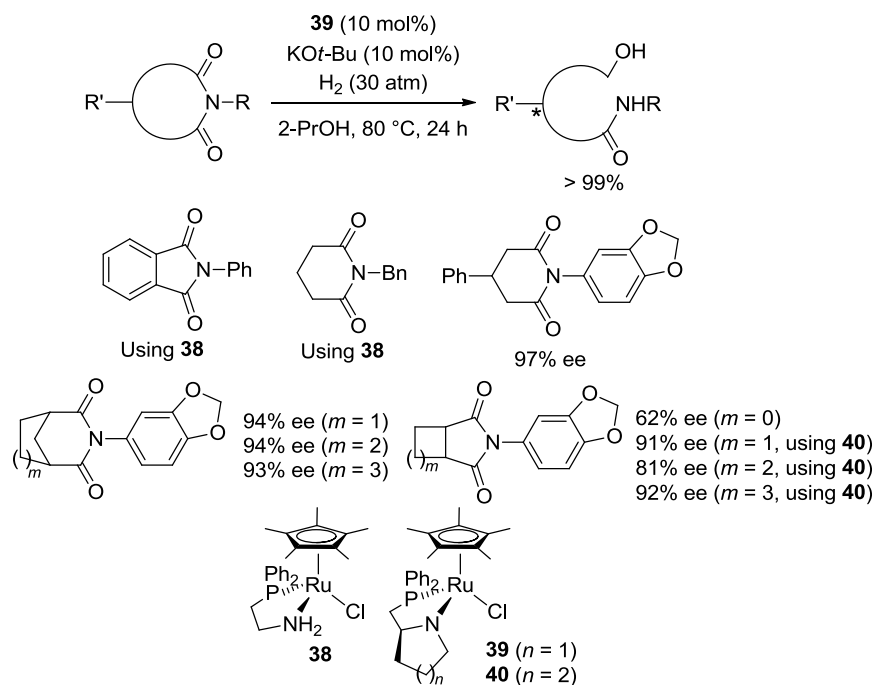
Figure 3-2. Dihydrogenation of imides reported by Ikariya and co-workers.

This hydrogenation produces the ring-opened, chiral alcohol–amides (Figure 3-1), as a result of dihydrogenation. Dihydrogenation presumably occurred via monohydrogenation to form hydroxyl lactams, followed by tautomerization to form the ring-opened aldehyde–amides that were subsequently hydrogenated to form alcohol–amides. The equilibrium position between the hydroxy lactam and the aldehyde–amide depends significantly on the substituents on the imide backbone, and upon the reaction conditions. Thus, the desired monohydrogenation is favoured under conditions that favour ring closing, such as lower reaction temperatures and bulky substituents on the backbone ring. For example, although NaBH$_4$ reduction generally forms direduced products, Speckamp and co-workers reported monoreduction of

several succinimides using NaBH$_4$ at lower temperatures (typically 0 °C) in ethanol.[82] The reduction of *N*-methylsuccinimide (**58**) at low temperature is sluggish. The authors found, however, that portion-wise addition of 2M HCl accelerates the reaction to form a monoreduced hydroxy lactam **59** as a ethoxy compound in 80% yield (Equation 3-1). The rate enhancement by HCl may arise from protonation of an imide oxygen, and/or formation of borane that activates the imide by coordination to the imide oxygen.

$$\text{(3-1)}$$
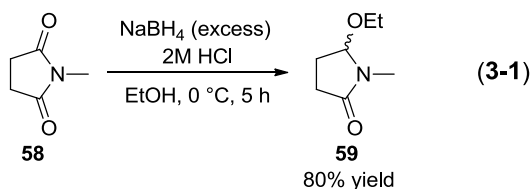
Imides such as **60** can be monoreduced to the hydroxy lactam **61** in near quantitative yield without activation by acids (Equation 3-2). The phenyl substituents on the imide backbone favour the ring closed hydroxy lactam tautomers (*gem*-disubstituent effect).[83] Also, the phenyl substituents may activate the adjacent imide C=O bond toward hydride addition by an overlap between the forming σ$_{C-H}$ orbital and the σ* orbital of the antiperiplanar C–Ph bond (stereoelectronic effect).[84]

$$\text{(3-2)}$$
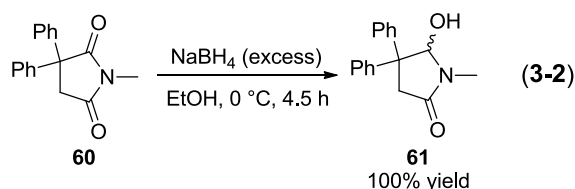
The effect of backbone rigidity on the rates and equilibrium constants for related lactonization of alcohol–acids was studied by Koshland and Storm.[85] They reported that both the rate constant and the equilibrium constant (K_{eq}) for the lactonization increased significantly by increasing the rigidity of the backbone (Table 3-3).

Table 3-3. Effect of the backbone rigidity in alcohol–acid lactonization.
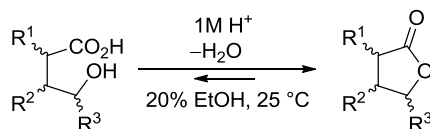
Entry	alcohol–acid	rate constant of lactonization ($M^{-1}min^{-1}$)	K_{eq}
1		0.086	6.15
2		0.344	data not available
3		7.23	2810
4		1120	12740

For example, the rate of ring closure for an alcohol–acid with a structurally rigid norbornane backbone is $\sim 10^4$ times faster than the non-substituted alcohol-acid (entry 1 vs. 4). The corresponding equilibrium constant is also ~2000 times larger. This effect is due to the restricted rotation around C–C bonds and the proximity of the OH and C=O functionalities.

These examples from the literature predict that monohydrogenation of imides to the corresponding hydroxy lactams is possible under the appropriate combination of reaction conditions and imide structures.[61] In fact, McCrindle and McAlees reported the heterogeneous, achiral monohydrogenation of imides under mild reaction conditions (20 °C, 1 atm H_2) with activated pseudo-bicyclic imides e.g. *N*-acylphthalimides (Equation 3-3).

$$Pt_2O \ (0.3 \ g)$$
$$H_2 \ (1 \ atm)$$
$$AcOEt, \ 20 \ ^\circ C, \ 24 \ h$$

1 g
R = Me, OEt, OMe, NMe$_2$

(Racemate)
0.21–0.80 g

(3-3)
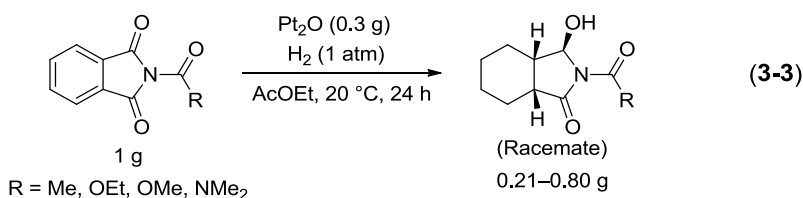
Monohydrogenation of unactivated imides, however, has not been reported with either heterogeneous or homogeneous catalysis to date. Based upon these literature results, it was hypothesized that the enantioselective desymmetrization of *meso*-cyclic imides by monohydrogenation would be possible if the catalyst was active enough to hydrogenate imides with structures that favour ring closing under mild conditions. In addition, this kind of hydrogenation is a desymmetrization that will catalytically produce multiple, adaptive stereogenic centres in the hydroxy lactam products.

This chapter discusses the application of the active Ru-dihydride catalyst **6** towards the monohydrogenation of a series of *meso*-cyclic imides. The mechanism of the reaction is investigated using low

temperature NMR experiments. A hydroxy lactam with 5 stereogenic centres is prepared in high ee, and transformed into a heteropolycyclic compound with 7 stereogenic centres using *N*-acyliminium ion chemistry.

Results and discussions

Solutions of the Ru-dihydride **6**, the en analogue **41**, the *N,N*-dimethylethylenediamine analogue **62**, and the (*R*)-daipen (daipen is 1,1-bis(4-methoxyphenyl)-3-methyl-1,2-butanediamine)[86] analogue **63** were prepared for this study by reacting mixtures of *trans*-[Ru((*R*)-BINAP)-(H)(η^2-H$_2$)(diamine)](BF$_4$) with 1–100 equiv of KO*t*-Bu or KN(Si(CH$_3$)$_3$)$_2$, under H$_2$ (~2 atm) at −78 °C in THF.[35e] As 1 equiv base is consumed to prepare these Ru-dihydrides the amount of base quoted in this text is that remaining after the dihydrides are prepared. We found the common catalyst precursor *trans*-[Ru((*R*)-BINAP)(Cl)$_2$((*R,R*)-dpen)][87] was inactive towards this imide hydrogenation under these conditions. Figure 3-3 shows structures of catalysts and imide substrates used in this chapter.
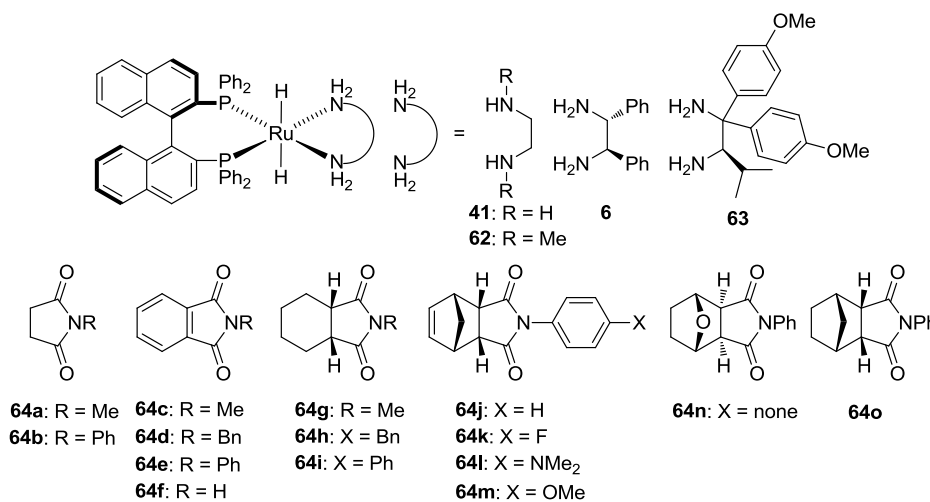
Figure 3-3. Structures of catalysts and cyclic Imides.

Table 3-4. Achiral hydrogenation of imides.[a]
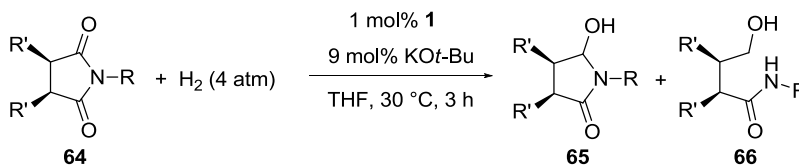
entry	catalyst	Imide	64 (%)[b]	65 (%)[b]	66 (%)[b]
1[c]	**41**	**64a**	100	0	0
2	**62**	**64a**	100	0	0
3	**41**	**64a**	0	0	100
4	**41**	**64c**	30	70	0
5	**41**	**64d**	34	66	0
6[d]	**41**	**64e**	24	76	0
7[e]	**41**	**64f**	100	0	0
8[f]	**6**	**64c**	45	55	0
9[g]	**6**	**64c**	50	30	20

[a] [Imide] = 0.33 M unless otherwise noted. [b] Determined by ^{1}H NMR. [c] Imide/**41**/KOt-Bu = 200:1:9, [imide] = 0.5 M in THF/2-PrOH = 3:1, . [d] [imide] = 0.11 M in THF/CH$_2$Cl$_2$ = 2:1 due to solubility of **64c**. [e] [Imide] = 0.17M due to solubility of **64e**. [f] Racemic product. [g] At 60 ºC.

Table 3-4 summarizes results from achiral hydrogenations under mild conditions (30 °C, 4 atm H$_2$, 3h) using 1 mol% catalyst, 9 mol% KOt-Bu, and 4 atm of H$_2$. In preliminary experiments, it was found that the catalyst **41** was inactive towards hydrogenation of N-methylsuccinimide (**64a**) using 2-PrOH as solvent, likely due to the formation of Ru-2-propoxide **12** (Table 3-4, entry 1). The use of a secondary diamine ligand also suppressed the catalytic activity (entry 2). The secondary diamine ligand likely deactivated the catalyst by increasing its steric bulk and/or by weakening hydrogen bonds that would occur between the substrate carbonyl oxygen and the catalyst NH bond during a bifunctional type addition. The imide **64a** was, however, dihydrogenated exclusively to the alcohol–amide product **66a** in THF using **41** (entry 3) as a catalyst. A

98

TOF of 33 h^{-1} was observed in the presence of 1 mol% **41** and 9 mol% KO*t*-Bu at 30 °C, 4 atm H$_2$ for 3 h in THF. This result shows that the Ru-dihydride catalyst has among the highest reactivities towards imide hydrogenation. By comparison, Ikariya's system requires harsher conditions (1 mol% catalyst, 80 °C,10 atm H$_2$, 18 h) to dihydrogenate the *N*-benzyl analogue of **64a** (>99% yield, TOF = 5.6 h^{-1}). The *N*-substituted phthalimides (**64c–e**) were monohydrogenated exclusively to form the corresponding hydroxy lactams in moderate yields (entries 4–6). Thus, as predicted, substituents on the imide backbone have a significant influence on ring-chain tautomerization, and thereby are a determining factor in mono/dihydrogenation selectivity. In contrast, the nature of the *N*-substituent has little influence upon the yield and upon the mono/dihydrogenation selectivity for this system. Phthalimide **64f** was inactive towards the hydrogenation. This inactivity may be due to the acidity of the imide NH group that would consume the added base (entry 7). The enantioselective hydrogenation of **64c** was attempted using **6**, however all the hydrogenations resulted in the formation of racemic products due to base catalyzed epimerization of the hydroxy lactam product **65c** (entry 8). Increasing the reaction temperature resulted in partial dihydrogenation (entry 9). These results suggest that monohydrogenation is favoured under mild conditions when the backbone of the cyclic imide favours ring-closing.

Table 3-5 summarizes results from optimization of the reaction conditions and imide structures for enantioselective hydrogenations using **6** as a catalyst. The cyclohexyl imides **64g–i** (Figure 3-3) were chosen to optimize the extent of hydrogenation (mono/di), the catalyst loadings, the diastereo- (cis/trans), and the enantioselectivity of the hydrogenation.

Table 3-5. Optimization of the reaction conditions and structure of imides[a]

entry	imide	T (°C)	time (h)	**65** (%)[b]	**66** (%)[b]	d.r. of **65**[b]	ee of **65** (%)[c]
1[d]	**64g**	30	3	8	68	n.d.	n.d.
2[d]	**64h**	30	3	26	59	n.d.	n.d.
3	**64i**	30	3	88	6	97:3	90
4	**64i**	0	4	95	0	98:2	90
5[e]	**64i**	0	57	90	trace	97:3	88
6[f]	**64i**	0	4	76	0	98:2	87

[a] Imide/**6**/KOt-Bu = 100:1:9, [imide] = 0.125 M, 50 atm H_2 in THF unless otherwise noted. [b] Determined by ^{1}H NMR. d.r.: diastereomeric ratio, n.d.: not determined. [c] Determined by HPLC analysis using Daicel CHIRALPAK IB column. [d] 40 atm H_2. [e] Imide/**6**/KOt-Bu = 1000:1:99, [imide] = 0.25 M. [f] 10 atm H_2.

Hydrogenation (40–50 atm) of **64g–i** at 30 °C formed a mixture of mono- and dihydrogenation products in a wide range of ratios (entries 1–3). The *N*-phenyl substituted imide **64i** showed the highest selectivity towards monohydrogenation. The selectivity of the hydrogenation towards monohydrogenation was increased by lowering the temperature (entry 4). The activity of the catalyst was sufficient to effect the reaction at a reasonable rate at this lower temperature, and the ee was high. In fact the catalyst loading could be decreased to 0.1 mol% without a significant decrease in yield (entry 5). Lowering the pressure of H_2 gas decreased the TOF at this temperature (entry 6). The optimal reaction conditions were

thus chosen to be at 0 °C under 50 atm H_2 using *N*-phenylimides. Table 3-6 summarizes the results from the enantioselective hydrogenation of several *N*-phenyl *meso*-cyclic imides using these reaction conditions.

Table 3-6. Enantioselective desymmetrization of *meso*-cyclic imides via monohydrogenation under optimized conditions.[a]

entry	imide	T (°C)	time (h)	65 (%)[b]	66 (%)[b]	d.r. of 65[b]	ee of 65 (%)[c]
1[d]	**64j**	0	17	98	0	>99:1	96
2	**64k**	0	17	99	0	>99:1	97
3	**64l**	0	17	92	0	>99:1	97
4	**64m**	0	17	98	0	>99:1	95
5[e]	**64n**	0	6	97	trace	93:7	92
6	**64o**	0	17	44	0	>99:1	92
7[f]	**64b**	0	6	0	100	n.a.	n.a.

[a] Imide/**6**/KO*t*-Bu = 500:1:9, [imide] = 0.625 M, 50 atm H_2 in THF unless otherwise noted. [b] Determined by ^{1}H NMR. d.r.: diastereomeric ratio, n.a.: not applicable. [c] Determined by HPLC analysis using Daicel CHIRALPAK IB column. [d] Imide/**6**/KO*t*-Bu = 1000:1:9, [imide] = 1.25 M. [e] Imide/**63**/KO*t*-Bu = 100:1:4, [imide] = 0.125 M. [f] Imide/**6**/KO*t*-Bu = 100:1:4, [imide] = 0.125 M.

The imide **64j** was hydrogenated exclusively to the corresponding hydroxy lactam **65j** in 98% yield and in 96% ee, without hydrogenating the reactive olefin backbone using 0.1 mol% **6** (entry 1). This observation indicates an outer coordination sphere mechanism. High preferences for C=O over C=C hydrogenations are well established for ketone and ester hydrogenations using Noyori-type Ru(diphosphine)(X)$_2$(diamine) catalysts.[87,57] One recrystallization of **65j** increased the ee to >99%. Thus, this desymmerization reaction formed five stereogenic centres in >99% ee in one step after one recrystallization. The 4-F, -NMe$_2$, and -OMe variants **64k–m** reacted in 92–99% yield and 95–99% ee, using 0.2 mol% of **6** as

catalyst (entries 2–4). The *exo-O*-bridged imide **64n** was hydrogenated in 97% yield and 92% ee using 1 mol% **63** (entry5). The norbornane imide **64o** reacted in 44% yield and in 92% ee (entry 6). The lower reactivity of the imide **64o** towards Al–H reduction was also reported by Matsuki et al (Table 3-2, entry 3)[74a], and is most likely a result of steric hindrance from the norbornane backbone.[88] *N*-phenlysuccinimide **64b** was dihydrogenated exclusively under the optimized conditions (entry 7). Thus, the structure of the imide backbone has a significant effect on mono/dihydrogenation selectivity even under optimized conditions.
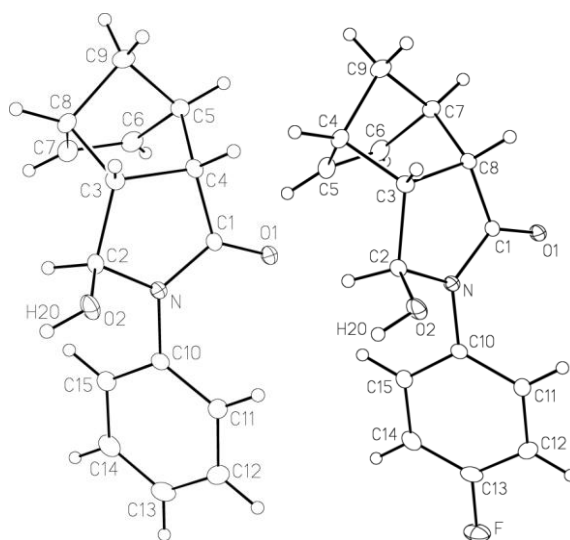
Figure 3-4. ORTEP drawings of hydroxy lactam *trans*-**65j** (left) and *trans*-**65k** (right) with 20% probability ellipsoids except hydrogen atoms. The absolute configuration was not determined.

The stereochemistry at the hydroxy carbon of the hydroxy lactam products was determined using ^{1}H NMR, and X-ray crystallography. The relative stereochemistry was almost exclusively *trans*. Figure 3-4 shows

the solid-state structures of hydroxy lactam *trans*-**65j** and *trans*-**65k**. The absolute configurations of these hydroxy lactams were not determined.

A control experiment was carried out using the *cis*-isomer of **65j** which was prepared by DIBAL-H reduction of **64j** followed by workup at low temperature under neutral conditions.[74a] Treatment of *cis*-**65j** with 5 mol% of KO*t*-Bu in THF at 0 °C for 4 h resulted in isomerization to *trans*-**65j** in quantitative yield. Cis-trans isomerization is thus catalyzed by base under the conditions of these hydrogenations. Speckamp et al. also reported complete conversion of *cis*-**65g** to *trans*-**65g** upon mixing with excess NaOEt.[82b] Therefore, the enantiogroup selectivity is preserved under the conditions of these hydrogenations, but the cis-trans selectivity at the hydroxy carbon is not.

To investigate the hydrogenation mechanism, stoichiometric reactions between the dihydride **6** and the imide **64j** were investigated using NMR spectroscopy. We prepared solutions of the dihydride **6** for this purpose as described previously[35e] by reacting mixtures of the Ru-dihydrogen compound **5** with 1–1.5 equiv of $KN(Si(CH_3)_3)_2$, under H_2 (~2 atm) at −78 °C in THF-d_8 in a NMR tube. When 1 equiv of $KN(Si(CH_3)_3)_2$ was used, **6** formed in ~70% yield along with ~30% of the Ru-hydroxide **43** caused by the presence of trace amounts of water in the THF-d_8. This trace of water likely accumulated during the numerous weighing, hydrogenation, and transfer steps involved in the preparation of **6**.

The effects of the $HN(Si(CH_3)_3)_2$ and KOH by-products formed during the preparation of **6** were investigated because these bases could catalyze the cis-trans isomerization of the hydroxy lactam product. We found that in the control experiment the cis-trans isomerization was completed on mixing at –80 °C when *cis*-**65g** was mixed with 1 equiv of $HN(Si(CH_3)_3)_2$ and 1 equiv of KOH prepared from water and $KN(Si(CH_3)_3)_2$. In another control experiment, $HN(Si(CH_3)_3)_2$ did not isomerize *cis*-**65g** even at 0 °C. Thus, the isomerization is catalyzed by KOH, and is fast under the conditions of stoichiometric reactions discussed in the following pages. The effect of KBF_4 that forms during the preparation of **6** was assumed to be negligible.

The reaction between imide **64j** and **6** prepared using 1.5 equiv of $KN(Si(CH_3)_3)_2$ in THF-d_8 proceeded at –80 °C to form the Ru-alkoxide of *trans*-**65j**, *trans*-**67**, quantitatively within an hour via the net hydride insertion (Equation 3-4). This net insertion is analogous to the addition reactions observed previously with ketones and lactams as substrates.

trans-**67**
100% yield

(3-4)
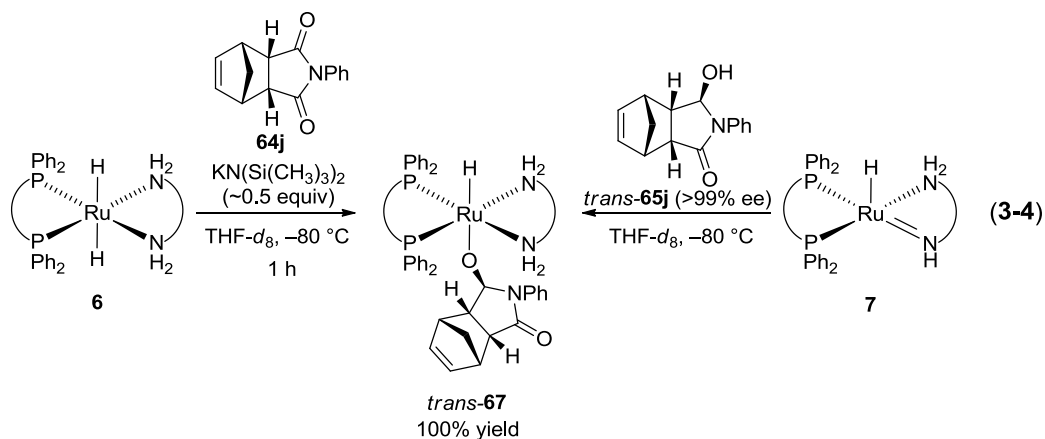
The rate of the net hydride insertion was slower than the corresponding rates of reactions with acetophenone (complete on mixing at −80 °C), or γ-butyrolactone (~83% conversion after ~3 min). The lower rate of addition between **6** and **64j** is likely due to the lower electrophilicity of the imide carbonyl groups relative to acetophenone, and γ-butyrolactone and steric hindrance around the carbonyl groups in **64j**. No other intermediates were observed during the addition.

The identity of *trans*-**67** was determined using ^{1}H, ^{31}P, ^{1}H–^{13}C gHSQC, and ^{1}H–^{1}H gCOSY NMR experiments, and confirmed by addition of the hydroxy lactam *trans*-**65j** (>99% ee) to the Ru-amide **7** at −80 °C (Equation 3-4). Figure 3-5 shows the key C–H correlation within the Ru-alkoxide group (RuOCH) of *trans*-**67** in the ^{1}H–^{13}C gHSQC NMR correlation plot. The ^{1}H and ^{13}C signals from the coordinated alkoxide OC–H group are at δ 6.13 and 96.24 ppm, respectively. These signals are shifted down-field by 1.11 and 9.66 ppm respectively from the corresponding signals in the spectra of the free hydroxy lactam *trans*-**65j** in THF-d_8 at −80 °C. Such downfield shifts by the formation of Ru–O bonds are previously reported, and are likely due to electron donation from oxygen to the Ru centre.[38]
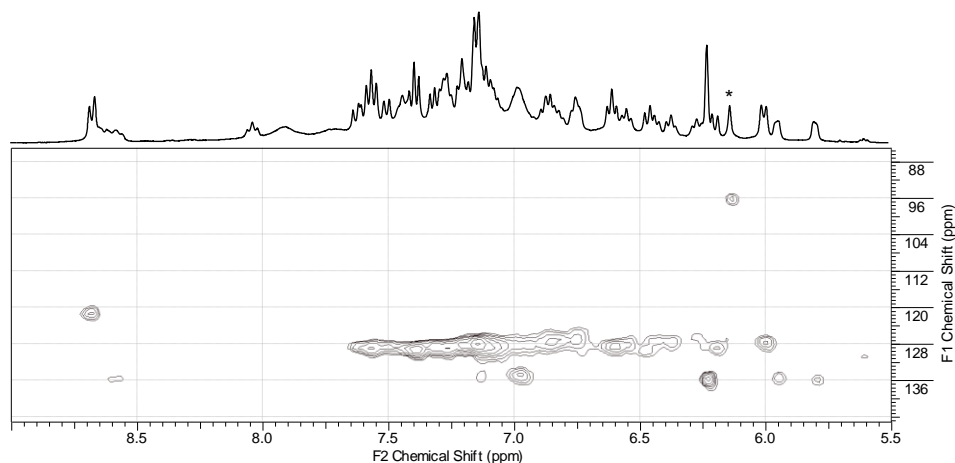
Figure 3-5. The C–H correlation (marked by *) of the Ru-alkoxide group (RuOCH) in the ^1H–^{13}C gHSQC NMR spectra of *trans*-**67**.

The formation of the *trans*-Ru-alkoxide *trans*-**67** by the addition at −80 °C is unexpected because it is a Ru-alkoxide that results from addition of the dihydride **6** from the more crowded, concave face of the imide carbonyl. All reports of monoreduction of imides by M–H reagents to date show that addition to the least hindered, convex face of a carbonyl group is kinetically favoured.[74] For example, Speckamp et al. and Matsuki et al. reported that *cis*-hydroxy lactams are the kinetic products in the monoreduction of imides using a CBS catalyst system and BINAL-H, respectively.[74a,c] Further, Speckamp reported that the reduction of imide **64g** by $NaBH_4$ at 0 °C formed *cis*-**65g** in quantitative yield if the reaction was quenched at low temperature.[82b] Thus, even a sterically less crowded M–H reagent prefers addition to the least hindered face of one of the imide carbonyl groups. The formation of *trans*-**67** is thus, likely a result of an

initial addition of the dihydride **6** to the least hindered, convex face of one of the imide carbonyls, followed by cis-trans isomerization.

Previously we reported that additions between the dihydride **6** and acetophenone or lactones formed the corresponding Ru-alkoxides or Ru-hemiacetaloxides.[35f] We thus assumed that addition of **6** to the least hindered convex face of one of the imide carbonyls would form the *cis*-Ru-alkoxide *cis*-**67**. Inspection of molecular models of *cis*-**67**, however, shows that an olefin group in the *cis*-alkoxide ligand is held within close proximity of the bulky *trans*-[Ru((*R*)-BINAP)(H)((*R*,*R*)-dpen)] group. This steric crowding is severe, and destabilizes *cis*-**67** relative to *trans*-**67** (Figure 3-6).
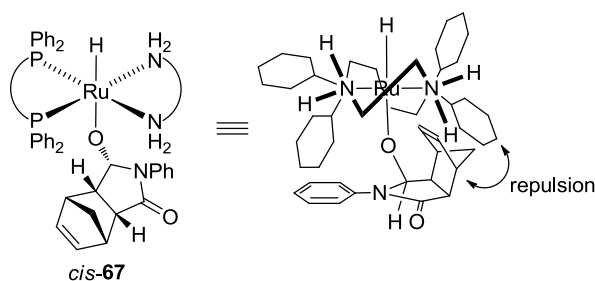
cis-**67**

Figure 3-6. Steric crowding in *cis*-**67**.

A possible mechanism for the formation of *trans*-**67** is one that proceeds via the formation of *cis*-**67** as a kinetic product. Rapid base catalyzed elimination and isomerization of the *cis*-alkoxide would form the thermodynamic product *trans*-**67**. Another possible mechanism is one that proceeds via the formation of Ru-amide **7** and the *cis*-hydroxy lactam *cis*-**65j**. This is the conventional bifunctional addition that forms Ru-amide

and alcohol as products. Base catalyzed isomerization of *cis*-**65j** and subsequent reaction between **7** and *trans*-**65j** forms the thermodynamic product *trans*-**67**.

To investigate whether *cis*-**67** is stable in the absence of base, **6** and imide **64j** were reacted in the absence of excess $KN(Si(CH_3)_3)_2$. This addition reaction proceeded at –80 °C at approximately the same rate as in the presence of $KN(Si(CH_3)_3)_2$ to form a new hydride species along with a small amount of *trans*-**67** (Equation 3-5). This new species transformed into *trans*-**67** upon warming to –40 °C.
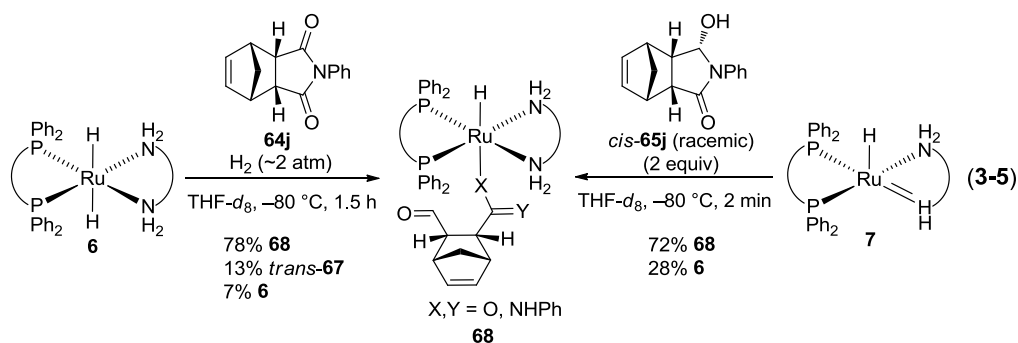
Characterization of the new species by low temperature NMR experiments, however, did not show evidence for the expected *cis*-**67**. Specifically, the expected alkoxide C–H peak of *cis*-**67** could not be detected in ^1H–^{13}C gHSQC NMR experiments, even though other structural features such as ^1H and ^{13}C signals from the Ru-hydride, (*R*,*R*)-dpen, the norbornene group, as well as ^{31}P signals from (*R*)-BINAP ligand were observed using ^1H, ^{31}P, ^1H–^{13}C gHSQC, and ^1H–^1H gCOSY NMR experiments. In addition, a broad signal was observed in the ^1H NMR

spectra at 16.5 ppm. ^{1}H–^{13}C gHSQC, and ^{1}H–^{1}H gCOSY NMR experiments could not characterize this peak unambiguously due to broad signal.

This compound was also independently prepared from the reaction between the Ru-amide **7** and two equiv of racemic *cis*-**65j** in the absence of excess $KN(Si(CH_3)_3)_2$. This reaction was complete after 2 min at –80 °C to form the new species and Ru-dihydride **6** in 72% and 28 % yield, respectively (Equation 3-5). The formation of **6** indicates that the addition between **6** and imide **64j** to form the Ru-amide **7** and *cis*-**65j** is, to some extent, reversible. In contrast, the formation of the Ru-dihydride is not observed during the reaction of the amide **7** and *trans*-**65j**. In a control experiment, this new complex was quenched using 2-PrOH-d_8 to form Ru-2-propoxide compound **12** and *trans*-**65j**. However, no significant deuteration on CH signal next to the CHOH group in *trans*-**65j** was observed. Thus, formation of a Ru-enolate complex[35b] via deprotonation of α-CH group in aldehyde-amide tautomer is not likely.

From this spectroscopic and experimental evidence, the identity of the new Ru-hydride species is proposed to be the N- or O-coordinated Ru-amidate **68**. The formation of Ru-amidate **68** can be explained by ring-chain tautomerization of the alkoxide *cis*-**67** within the coordination sphere (Scheme 3-4). Generally, late transition metal–alkoxide bonds are highly polar covalent bonds that exhibit ionic bond character.[89] This ionic character, together with the steric repulsions in *cis*-**67** will weaken the

Ru–oxygen bond. Thus, *cis*-**67** could exist as a weakly coordinated compound as depicted in Scheme 3-4. Therefore, it is possible that the *cis*-**67** tautomerizes to the amidate **68** within the coordination sphere via formation of the corresponding aldehyde–amide tautomer.

Scheme 3-4. Proposed pathways for the formation of the amidate **68**.
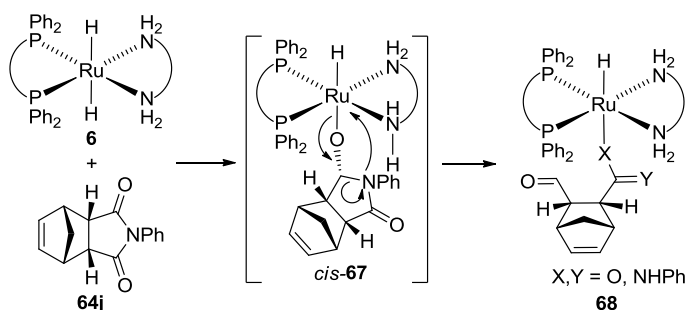
Detection of *cis*-**65j** was attempted by the stoichiometric addition of **6** and **64j** in the absence of $KN(Si(CH_3)_3)_2$ at –80 °C. *Cis*-**65j** would be trapped if the trapping reaction is faster than ring-chain tautomerization to form **68**. In the first attempt, 2 equiv of $HBF_4 \cdot OEt_2$ was added after the stoichiometric addition between **6** and **64j** at –80 °C. Matuki et al. reported that *cis*-hydroxy lactams formed exclusively by quenching the BINAL-H reduction by 10% HCl at –78 °C.[74a] Contrary to expectations, the trapped product was *trans*-**65j** exclusively (Scheme 3-5). The cationic Ru-dihydrogen complex **5** was generated upon addition of $HBF_4 \cdot OEt_2$ under H_2 (~2 atm). The ee and the absolute configuration of the *trans*-**65j** (96% ee) were the same as that of the catalytic reaction (Table 3-4, entry

1). Thus, the Ru–H insertion step is the enantioselective step in the catalytic cycle.

Scheme 3-5. Trapping experiments using $HBF_4 \cdot OEt_2$ and BSA.
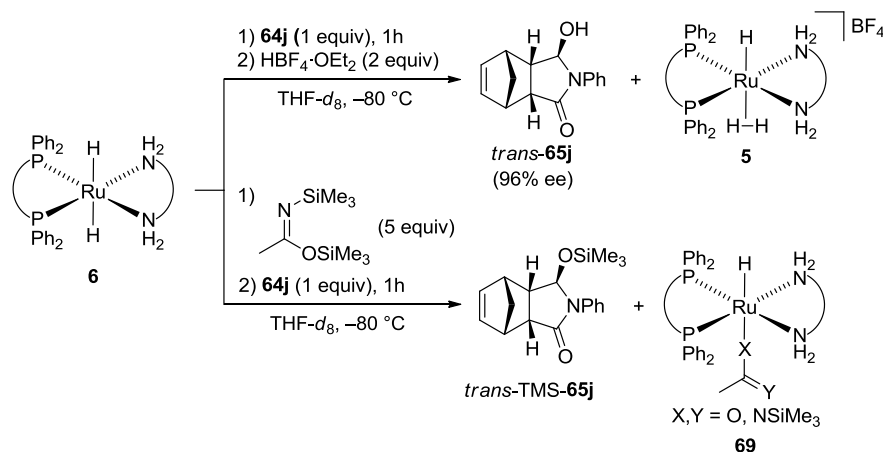
In another attempt, the stoichiometric addition was conducted at −80 °C in the presence of *N,O*-bis(trimethylsilyl)acetamide (BSA)[90] to trap *cis*-**64j** by silylation. The trapped product was, however silylated *trans*-**65j**, *trans*-TMS-**65j** (Scheme 3-5). In a control experiment, we found that racemic *cis*-**65j** reacts slowly with excess BSA at 60 °C to form *trans*-TMS-**65j** in neutral $CDCl_3$ solution. Thus, *cis*-TMS-**65j** does not form due to the steric repulsion between TMS group and imide backbone. This observation indicates that the Ru-alkoxide *cis*-**67** would possess a great deal of steric strain that weakens the Ru-O bond.

Trans-TMS-**65j** was characterized by ^1H, ^{29}Si, ^{31}P, ^1H–^{13}C gHSQC, ^1H–^{29}P gHSQC, ^1H–^{13}C gHMBC, and ^1H–^1H gCOSY NMR experiments, and by independent synthesis from *trans*-**65j** and BSA. The Ru-amidate

complex **69** formed upon Ru–H insertion. It is known that the silylation of alcohols by BSA forms *N*-trimethylsilylacetamide as a byproduct.[90] The amidate **69** was partially characterized by ^{1}H, ^{29}Si, ^{31}P, ^{1}H–^{13}C gHSQC, ^{1}H–^{29}Si gHSQC, ^{1}H–^{13}C gHMBC, and ^{1}H–^{1}H gCOSY NMR experiments. However, the coordination mode of the amidate ligand, N- or O-coordination, could not be determined.

The absolute configuration of the hydroxy lactam *trans*-**65j** was determined by transforming *trans*-**65j** into bromocarbamate **70** using 4-bromophenyl isocyanate.[91] The absolute configuration was one that resulted from addition to the convex face of the carbonyl group on the *S*-side (Figure 3-7). The reduced side of the hydroxy lactam *trans*-**65j** in Figure 3-7 is called the *S*-side because the absolute configurations of two stereogenic centres on this side of the norbornene backbone are both S.[92]
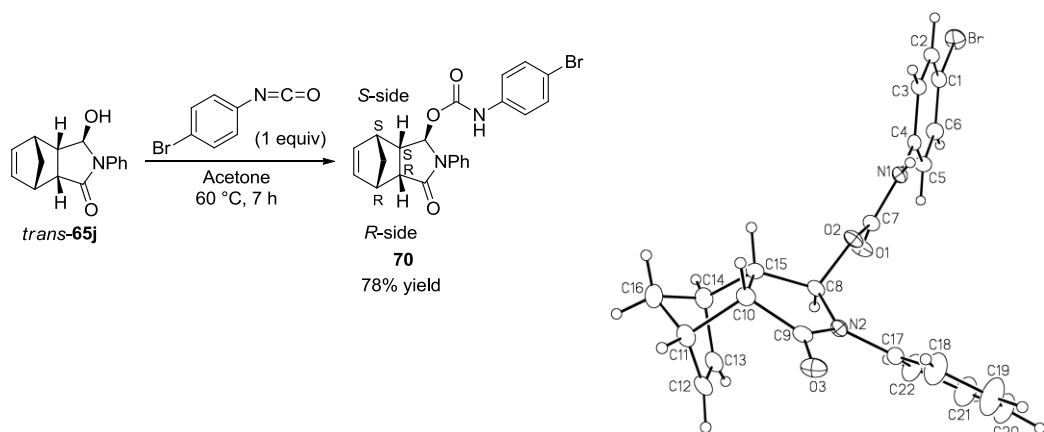
Figure 3-7. Preparation and ORTEP drawing of **70** with 20% probability ellipsoids except hydrogen atoms. The absolute configuration was determined, with a Flack parameter of 0.013(6).

112

The high enantioselectivity at −80 °C (Equation 3-7) can be explained by the steric interactions within the transition state for the addition step. There are two proposed transition states for the addition of Ru-dihydride to carbonyl groups in aprotic solvent. Noyori et al. proposed a a six membered pericyclic transition state that contains partial formation of Ru=N double bond (Figure 3-8, Ru−N transition state).[35c] Another transition state was proposed by us to account for the observation of Ru-alkoxides via the addition between the dihydride **6** and acetophenone or lactones at −80 °C.[35e] This transition state contains an interaction between the Ru centre and the carbonyl oxygen instead of the Ru=N interaction (Figure 3-7, Ru−O transition state).

Ru–N transition state   Ru–O transition state

6
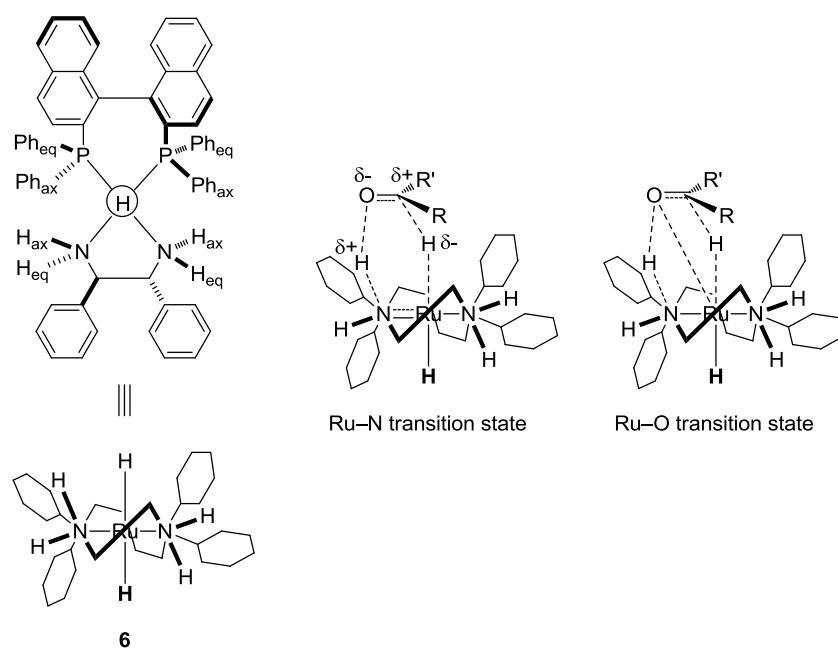
Figure 3-8. Possible transition states for the addition between the Ru-dihydride **6** and carbonyl compounds.

Both of these transition states will have the same or very similar steric interactions and thereby enantioselectivity during the Ru-dihydride addition. It is known that the dihydride **6** takes the conformation shown in Figure 3-8. Specifically, both (*R*)-BINAP and (*R*,*R*)-dpen ligands take the λ conformation to minimize the axial–axial steric repulsions. As a result, the four phenyl groups on the phosphine atoms and the four NH groups take a fixed spatial arrangement, and the two hydrides become spatially equivalent. The optimal geometry for the pericyclic six-membered transition state has been calculated for the *trans*-[Ru(diphosphine)(X)$_2$(diamine)] catalyzed ketone hydrogenation. All of the calculations to date show that the small H–Ru–N–H dihedral angle stabilizes the pericyclic six-membered transition state since it forms a strong dipole-dipole interaction with the carbonyl C=O dipole.[35b,37] Noyori et al. proposed that the carbonyl C=O bond reacts with Ru–H and the axial NH groups via the six-membered pericyclic transition state because H–Ru–N–H$_{ax}$ has the smaller H–Ru–N–H dihedral angle than H–Ru–N–H$_{eq}$.[35c] This proposed steric requirement would also be applicable for the Ru–O transition state because it also contains the dipole interaction between the dihydride and carbonyl group. In the next few pages, the high enantioselectivity of *trans*-**65j** at –80 °C is explained using the Ru–O transition state.

In theory there are four possible geometries for the transition states since the imide **64j** has four carbonyl C=O faces with different steric geometries. The four possible isomers that form via these transition states

are the two enantiomers of *cis*-**65j** and the two enantiomers of *trans*-**65j**. These isomers are named (*R*)- or (*S*)-*cis*-**65j** and (*R*)- or (*S*)-*trans*-**65j**. (*S*)-*Trans*-**65j** is the major product observed in both the stoichiometric and catalytic reactions in the presence of excess base. The addition reaction between the dihydride **6** and imide **64j** will likely occur from the least hindered convex face of the carbonyl groups.[74,82] Figure 3-9 shows two possible geometries of the transition state for the addition to the convex face of **64j**, **TS$_A$** and **TS$_B$**.[27a] The norbornene backbone in **64j** has smaller effective steric bulk than the *N*-phenyl group due to the *endo*-conformation. **TS$_A$** is thereby favoured over **TS$_B$** because **TS$_B$** suffers from severe steric repulsions between a phenyl group on (*R*)-BINAP and the *N*-phenyl group of imide **64j**. (*S*)-*Cis*-**65j** thus forms preferentially. The base-catalyzed isomerization of (*S*)-*cis*-**65j** then forms (*S*)-*trans*-**65j**. This model explains the high enantioselectivity (96% ee) observed for the catalytic hydrogenation of **64j**.
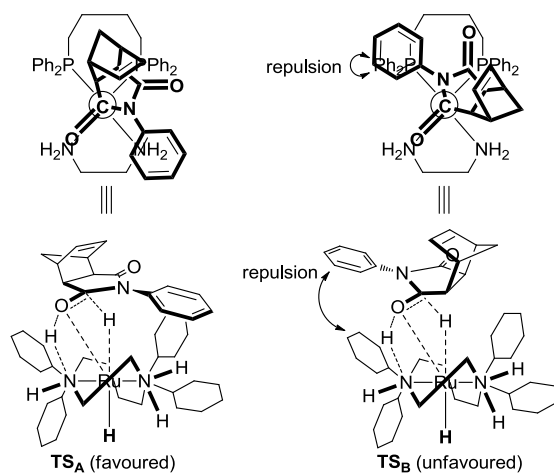
Figure 3-9. Favoured and unfavoured geometries of the transition state.

The enantioselectivity of a catalytic system often depends on the relative rates and reversibility of the steps in the catalytic cycle.[93] Such a situation was clearly demonstrated in the [Rh((S,S)-Chiraphos)(solvent)$_2$]$^+$ (see Scheme 3-6 for the structure of (S,S)-Chiraphos) catalyzed enantioselective hydrogenation of alkenes (Scheme 3-6).[93]

Scheme 3-6. Catalytic cycle for the [Rh((S,S)-Chiraphos)(solvent)$_2$]$^+$ catalyzed enantioselective alkene hydrogenation.
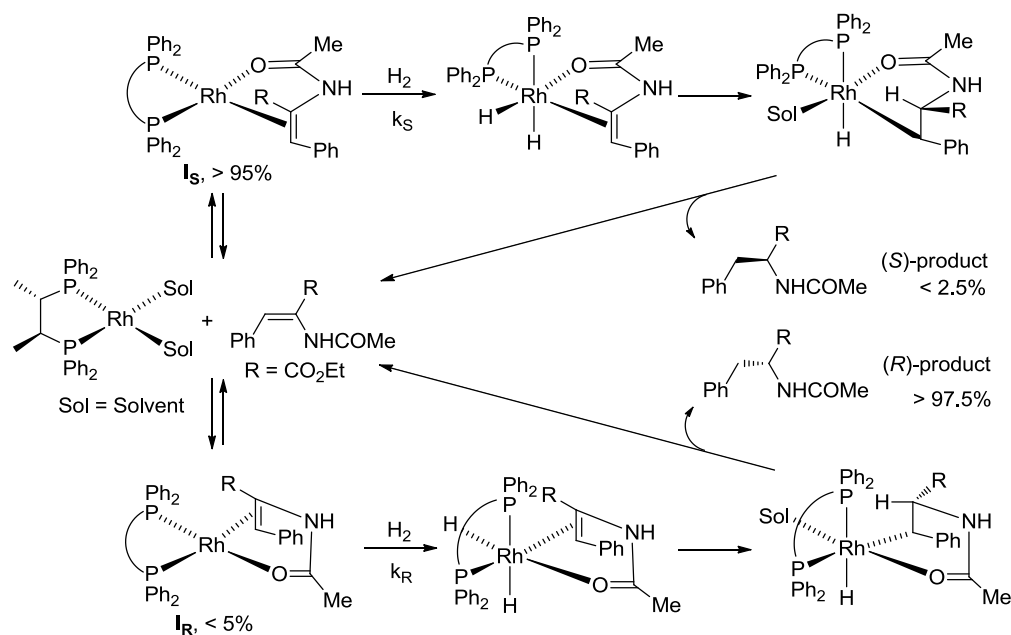
Halpern et al. reported that the reaction of [Rh((S,S)-Chiraphos)(solvent)$_2$]$^+$ and (Z)-α-acetamidocinnamate forms diastereomeric alkene-amide coordinated complex **I$_S$** and **I$_R$** in a >95:5 diastereomeric ratio.[93] However, this ratio is opposite to the enantioselection observed in a catalytic reaction (S product : R product > 2.5:97.5). Hence, the substrate coordination is not the only step that

116

determines the overall enantioselectivity of the catalytic reaction. Further study showed that the minor intermediate $\mathbf{I_R}$ oxidatively adds H_2 much faster than the major intermediate $\mathbf{I_S}$. Thus, overall enantioselectivity depends only the relative rates of H_2 addition to $\mathbf{I_R}$ and $\mathbf{I_S}$.

In a case of the Noyori ketone hydrogenation, Hamilton et al. reported that the stoichiometric reaction of Ru-dihydride **6** and acetophenone at –80 °C in THF forms the corresponding diastereomeric Ru-alkoxide **14** in a 91.5:8.5 diastereomeric ratio.[35f] These authors found that this diastereomeric ratio is roughly the same as the enantiomeric ratio of product alcohols observed in a catalytic reaction in 2-PrOH. The enantiomeric ratio of the product alcohol, however, quickly deteriorates to ~50:50 in the presence of **6** (10 mol%) in THF at 30 °C under ~2 atm H_2. The proposed origin of this racemization is the reversibility of both the Ru-dihydride addition step and the following product liberation step in THF (Scheme 3-7).

Scheme 3-7. Proposed mechanism for the racemization in ketone hydrogenation in THF.

117
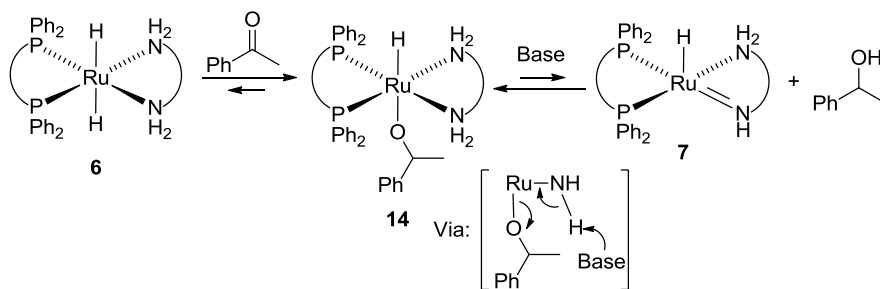
Thus, if the insertion step is irreversible, the high intrinsic enantioselectivity can be preserved. Alternatively, the intrinsic enantioselectivity can be preserved if the liberation step is irreversible and much faster than the reversible formation of the dihydride **6** from the alkoxide **14**. Indeed, the authors found that the use of 2-PrOH solvent preserves the enantioselectivity because 2-PrOH intercepts the amide **7** to form the Ru-isopropoxide complex before it reversibly reacts with the product alcohol.

Scheme 3-8. Possible explanation for the high overall enantioselectivity in THF.
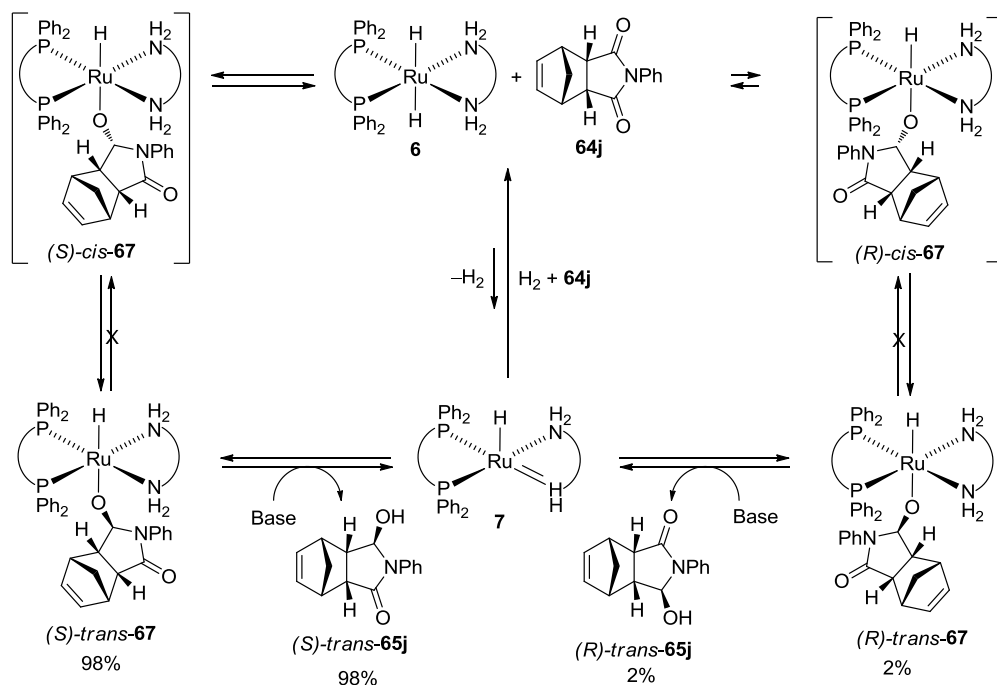
In the case of the imide hydrogenation, similar high intrinsic enantioselectivity (96% ee) was observed in the stoichiometric reaction of **6** and the imide **64j** at −80 °C in THF. Unlike ketone hydrogenations, this

enantioselectivity was preserved in the presence of **6** in THF for prolonged periods of time (Table 3-6, entry 1, 96% ee after 17 h). Scheme 3-8 shows a possible explanation for this high overall enantioselectivity in THF. Reaction of the dihydride **6** with imide **64j** in the presence of excess base forms *trans*-hydroxy lactam (*S*)-*trans*-**67** (96 % ee at –80 °C) via initial addition of the dihydride from the convex face to form *cis*-**67**, followed by cis-trans isomerization to form (*S*)-*trans*-**67** (98 %), and (*R*)-*trans*-**67** (2 %). The alkoxide *trans*-**67** reversibly forms the Ru-amide **7**, and (*S*)- and (*R*)-*trans*-**65j** in a 98:2 ratio via the base-assisted elimination. The amide **7** then reacts with H_2 and regenerates the dihydride **6**.

As seen in Equation 3-4, the hydroxy lactam *trans*-**65j** is less prone to reversibly form **6** and imide **64j** at –80 °C upon reaction with the Ru-amide **7**. This is likely due to the thermodynamic stability of *trans*-**65j**. The reaction pathways for the addition between **6** and **64j** to form *trans*-**67** and dehydrogenation of *trans*-**67** to form **6** and **64j** are the same because of the principle of microscopic reversibility. Thus, the reverse reaction requires the formation of alkoxide *cis*-**67** from alkoxide *trans*-**67** prior to the dehydrogenation. However, the formation of *cis*-**67** is almost negligible because equilibrium between *cis*- and *trans*-**67** almost exclusively forms the thermodynamically stable *trans*-**67** in the presence of base. Thus, formation of (*S*)-*trans*-**67** (96% ee) is virtually irreversible, and hence prevents racemization of the product. The origins for the high overall enantioselectivity in THF are thus the high intrinsic enantioselectivity of the

net hydride insertion observed at –80 °C, and rapid irreversible formation of *trans*-**67**. Additionally, the base catalyzed product liberation of the alkoxide *trans*-**67** is the turnover limiting step at –80 °C since all the other steps shown in Scheme 3-8 are observable at –80 °C.

Another factor that would contribute to the high enantioselectivity is precipitation of hydroxy lactams observed in the reactions conducted at 0 °C (Table 3-5, entries 4–6, and Table 3-6, entries 1–6). However, the effect of precipitation is not a significant factor because deterioration in ee was not observed when the reaction was conducted at higher temperature, lower concentration, or prolonged reaction times (Table 3-5, entries 3–5). However, precipitation of the product will have a positive influence on reaction rate because it limits [product] which will cause product inhibition in a similar manner as discussed in Chapter 2. The proposed origin of the overall enantioselectivity could be further investigated using kinetic and control experiments that elucidate effects of solvents, temperature, [H_2], [imide], [hydroxy lactam], and reversibility of the four possible isomers of the product hydroxy lactams.

To demonstrate the utility of this hydrogenation two experiments were conducted. First, a potential (+)-biotin precursor *N*-benzyl hydroxy lactam **72** was prepared from the corresponding imide **71** using 2 mol% of **6** (Equation 3-6).[74f] The trans isomer of **72** was obtained in 95% yield with low ee and d.r. (89:11). The low ee is probably because of the reversibility of the hydrogenation that originates from high temperature and a weaker

120

steric bias to trap the *trans*-hydroxy lactam. Further optimization of catalyst

structures as well as reaction conditions would improve the

enantioselectivity.

$$(3\text{-}6)$$
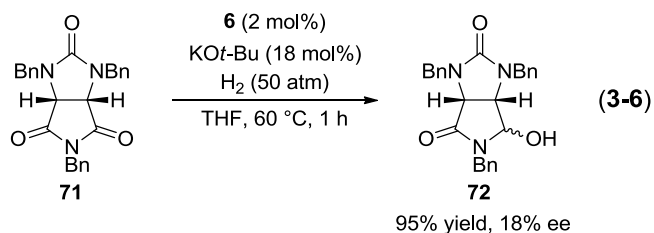
Secondly, we converted the hydroxy lactam **65j** into the

corresponding iminium ion by treatment with $BF_3 \cdot OEt_2$ at 22 °C in toluene.

Either *cis*- or *trans*-**65j** would form this iminium ion. This species reacted

with indene to form the heteropolycyclic compound **73** containing 7

stereogenic centres in 90% yield and in 91:9 diastereomeric ratio (d.r.)

(Scheme 3-9). Further, one recrystallization increased the d.r. to >99%.

Figure 3-10 shows the solid-state structure of the major diastereomer of

73. This reaction likely occurred by addition of indene to the convex face of

the iminum ion to form the benzylic carbocation, followed by intramolecular

cyclization with the *N*-phenyl ring, and rearomatization.[94]

Scheme 3-9. Intermolecular cyclization of **65j** and indene.
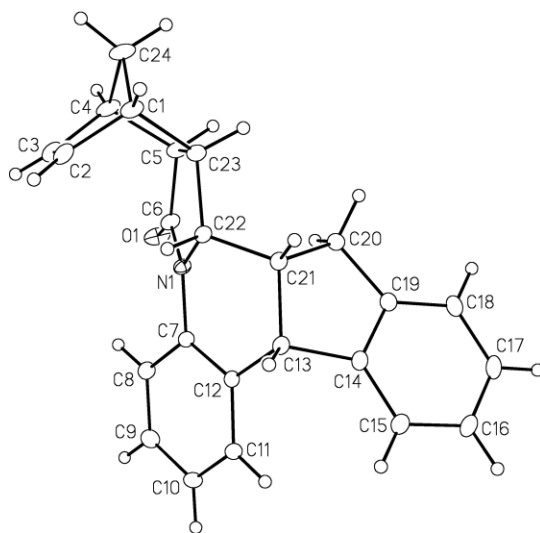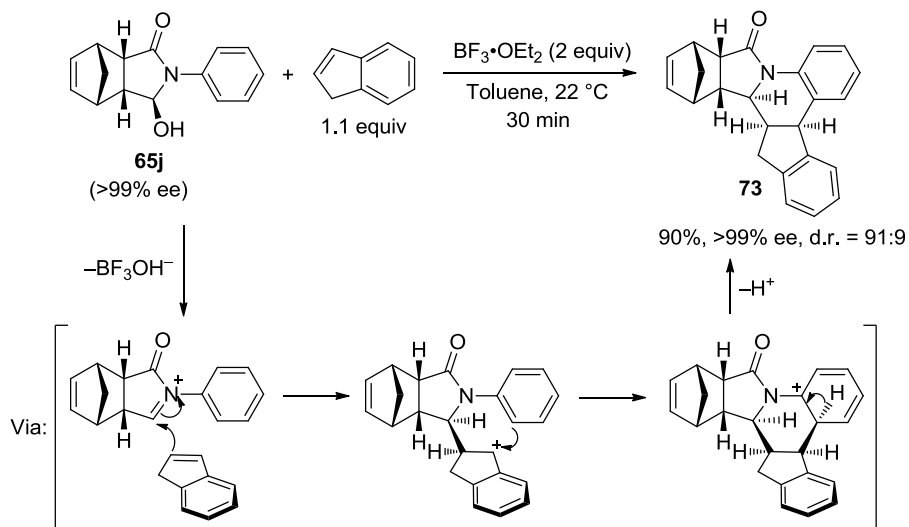
Figure 3-10. An ORTEP drawing of the major diastereomer of **73** with 20% probability ellipsoids except hydrogen atoms. The absolute configuration was not determined.

Analogs of **65j** were also used in the literature to prepare indolizidine, and pyrrolizidine alkaloids.[95] For example, (+)-indolizidine was

synthesized from a hydroxy lactam **74** using the cyclization of the corresponding *N*-acyliminium ion, followed by a retro-Diels-Alder reaction (Scheme 3-10).

Scheme 3-10. An enantioselective synthesis of (+)-indolizidine.
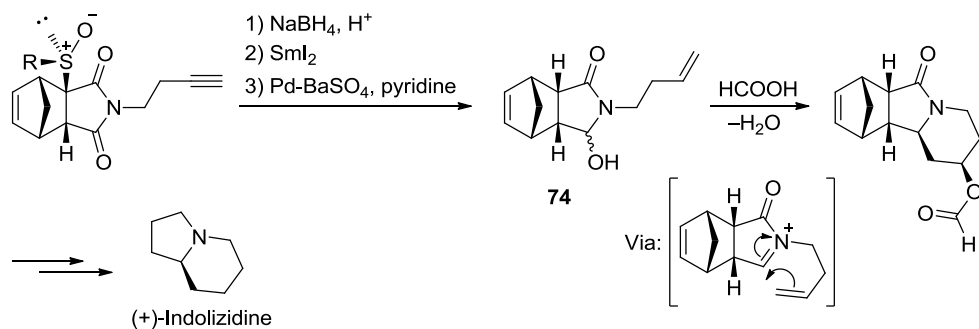
Conclusions

This chapter presents the first enantioselective desymmetrization of *meso*-imides using chemo-, diastereo-, and enantiogroup-selective monohydrogenations. These desymmetrization reactions formed up to five stereogenic centres in high enantioselectivity with one hydrogenation. The mechanistic investigation showed that the addition between the dihydride **6** and imide **64j** at –80 °C in the presence of excess base forms the Ru-alkoxide *trans*-**67**, the product of net hydride insertion from the hindered face of the carbonyl groups. All attempts to form or detect the kinetically favoured alkoxide *cis*-**67** resulted in the formation of Ru-amidate **68** or trapped *trans*-hydroxy lactams. In the absence of excess base, the Ru-amidate **68** formed upon the addition between dihydride **6** and imide

64j. Based on these observations and reported stereochemistry for M–H reduction of imides, we propose that the hydride addition proceeds from the less hindered face of the imide **64j** to form either the Ru-amide **7** and hydroxy lactam *cis*-**65j** or the alkoxide *cis*-**67**. These species collapse into either the alkoxide *trans*-**67** (in the presence of base) or the Ru-amidate **68** (in the absence of base). Thus, both the conventional six-membered pericyclic transition state with a Ru=N interaction (Ru–N transition state), and our proposed transition state with a Ru–O interaction (Ru–O transition state) can explain the observation. We proposed that the high enantioselectivity induced by the addition between **6** and **64j** is preserved by the rapid irreversible cis-trans isomerization of the net Ru-hydride insertion product *cis*-**67**. The utility of this hydrogenation and its product were demonstrated using the preparation of a potential (+)-biotin precursor **72**, and *N*-acyliminium ion chemistry that readily increases the number of stereogenic centres.

Experimental

Materials and Methods. All pressure reactions were carried out in a glass (for 4 atm H_2) or stainless steel (for 50 atm H_2) autoclave equipped with a stirring bar. Deuterated solvents were obtained from Cambridge Isotope Laboratories, and Aldrich. Common solvents were distilled over appropriate drying reagents. THF was distilled over sodium/benzophenone before each experiment. 2-PrOH, toluene, and CH_2Cl_2 were distilled over CaH_2. Common chemicals were obtained from Aldrich, TCI America, and

Strem, and were used as received unless stated otherwise. Potassium

tert-butoxide (KO*t*-Bu) was sublimed before use. Ethylenediamine was

distilled over KOH. *N*-methylsuccinimide (**64a**) was purchased from Aldrich,

and used as received. Phthalimide (**64f**) was purchased from General

Intermediates of Canada, and used as received. Indene was purchased

from Matheson Coleman & Bell, and fractionally distilled. Hydrogen gas

was ultra high purity grade purchased from Praxair. ^{1}H, ^{13}C, ^{19}F, ^{29}Si and

^{31}P NMR spectra were taken using Varian Inova (300 and 400 MHz), and

Varian DirectDrive (500 MHz) spectrometers. ^{1}H, ^{13}C, ^{29}Si NMR chemical

shifts are reported in parts per million (δ) relative to TMS with the solvent

as the internal reference. ^{31}P chemical shifts are reported in parts per

million (δ) relative to 85% H_3PO_4 as the external reference. ^{19}F chemical

shifts are reported in parts per million (δ) relative to CCl_3F as the external

reference. NMR peak assignments were made using ^{1}H–^{13}C gHSQC,

^{1}H–^{29}Si gHSQC, ^{1}H–^{13}C gHMBC, and ^{1}H–^{1}H gCOSY NMR experiments.

Abbreviations for NMR spectra are s (singlet), d (doublet), t (triplet), q

(quartet), dd (doublet of doublet), ddd (doublet of doublet of doublet), dt

(doublet of triplet), tt (triplet of triplet), m (multiplet), and br (broad). IR

spectra were taken using Nic-Plan FTIR microscope, and are reported in

wavenumbers (cm^{-1}). High resolution mass spectra were taken using

Applied BioSystems Mariner BioSpectrometry Workstation oaTOF mass

spectrometer. Elemental analysis data were obtained using Carlo Erba

CHNS-O EA1108 elemental analyzer. Optical rotations ($[\alpha]_D^{23}$) were

measured using Perkin Elmer 241 polarimeter. Melting points (M.p.) were measured using Perkin Elmer Pyris 1 differential scanning calorimeter. HPLC analysis was performed using a Waters 600E multisolvent delivery system equipped with Waters 715 Ultra WISP sample processor, Waters temperature control system, Waters 990 photodiode array detector, Waters 410 differential refractometer, Waters 5200 printer plotter, and Daicel CHIRALPAK IB (4.6 mm i.d. × 250 mm) chiral column. All ee's were confirmed by comparing the HPLC chromatogram of the hydrogenation product to that of the racemic product prepared by $NaBH_4$ or DIBAL-H reduction, followed by acidic work-up at RT.[74a,82a] HPLC grade hexanes (Min. 99.5%) and 2-propanol (Min. 99.7%) were obtained from Caledon Laboratories Ltd.

A general procedure for preparation of imides 64.[96] Under argon, the corresponding anhydride (10 mmol), primary amine (10 mmol), and THF (15 mL) were added to a 200 mL round bottom flask equipped with a 1 inch Teflon® coated stirring bar. The solution was stirred for 30 min at 40 °C. Removal of the solvent using a rotary evaporator gave the corresponding carboxylic acid–amide as a white solid. The carboxylic acid–amide was then heated at 150–200 °C under argon using a silicon oil bath. After complete melting, the melt was stirred at 150–200 °C from 5 min to 4 h. The extent of reaction was monitored using TLC. The crude, faint-yellow product was cooled to room temperature, solidified, and purified by flash chromatography using 230–400 mesh silica gel (ethyl acetate/hexanes)

followed by recrystallization. As imides **64b–e**, **64g–k**, and **64m–o** are well known in the literature, only the ^{1}H NMR data are reported.

64b[97] Heating conditions: 170 °C, 2 h. Recrystallization solvents: CH_2Cl_2/ethanol. Yield: 70%. ^{1}H NMR (399.80 MHz, $CDCl_3$, 27.0 °C): δ 2.91 (4H, s, 2CH_2), 7.28 (2H, m, aromatic 2CH), 7.42 (1H, m, aromatic CH), 7.50 (2H, m, aromatic 2CH).

64c[98] Heating conditions: 190 °C, 1.5 h. Recrystallization solvents: acetone/water. 40 w% $MeNH_2$ in water was used as an amine. Yield: 78%. ^{1}H NMR (399.79 MHz, $CDCl_3$, 27.0 °C): δ 3.19 (3H, s, CH_3), 7.71 (2H, m, aromatic 2CH), 7.85 (2H, m, aromatic 2CH).

64d[98] Heating conditions: 150 °C, 30 min. Recrystallization solvents: acetone/water. Yield: 81%. ^{1}H NMR (399.79 MHz, $CDCl_3$, 27.0 °C): δ 4.86 (2H, s, CH_2), 7.30 (3H, m, aromatic 3CH), 7.43 (2H, m, aromatic 2CH), 7.72 (2H, m, aromatic 2CH), 7.86 (2H, m, aromatic 2CH).

64e[98] Heating conditions: 200 °C, 1 h. Recrystallization solvents: acetone/water. Yield: 81%. ^{1}H NMR (399.79 MHz, $CDCl_3$, 27.0 °C): δ 7.41-7.55 (5H, m, aromatic 5CH), 7.80 (2H, m, aromatic 2CH), 7.97 (2H, m, aromatic 2CH).

64g[99] Heating conditions: 170 °C, 10 min under vacuum. Not recrystallized. Yield: 56%. ^{1}H NMR (399.79 MHz, $CDCl_3$, 27.0 °C): δ 1.41 (4H, m, 2CH_2), 1.71 (2H, m, CH_2), 1.84 (2H, m, CH_2), 2.82 (2H, m, 2CH), 2.94 (3H, s, CH_3)

64h[100] Heating conditions: 150 °C, 5 min. Recrystallization solvent: hot ethanol. Yield: 46%. ^{1}H NMR (399.79 MHz, $CDCl_3$, 27.0 °C): δ 1.38 (4H, m,

2CH_2), 1.72 (2H, m, CH_2), 1.84 (2H, m, CH_2), 2.85 (2H, m, CH), 4.64 (2H, s, CH_2), 7.26-7.38 (5H, m, aromatic 5CH).

64i[99] Heating conditions: 190 °C, 4 h. Recrystallization solvent: hot ethanol. Yield: 90%. ^{1}H NMR (399.79 MHz, CDCl$_3$, 27.0 °C): δ 1.53 (4H, m, 2CH_2), 1.93 (4H, m, 2CH_2), 3.05 (2H, m, 2CH), 7.29 (2H, m, aromatic 2CH), 7.38 (1H, m, aromatic 1CH), 7.47 (2H, m, aromatic 2CH).

64j[101] Heating conditions: 160 °C, 15 min under vacuum. Recrystallization solvents: acetone/water. Yield: 80%. ^{1}H NMR (399.79 MHz, CDCl$_3$, 27.0 °C): δ 1.61 (1H, m, CH_2), 1.79 (1H, dt, J = 1.6 and 8.8 Hz CH_2), 3.43 (2H, m, 2CH), 3.51 (2H, m, bridgehead 2CH), 6.27 (2H, t, J = 1.8 Hz 2CH), 7.13 (2H, m, aromatic 2CH), 7.36 (1H, m, aromatic CH), 7.44 (2H, m, aromatic 2CH).

64k[102] Heating conditions: 200 °C, 15 min. Recrystallization solvents: hot ethyl acetate/hexanes. Yield: 85%. ^{1}H NMR (399.79 MHz, CDCl$_3$, 27.0 °C): δ 1.61 (1H, d, J = 8.8 Hz, CH_2), 1.79 (1H, dt, J = 1.6 and 8.8 Hz, CH_2), 3.42 (2H, m, 2CH), 3.50 (2H, m, bridgehead 2CH), 6.25 (2H, t, J = 1.6 Hz, 2CH), 7.10 (2H, d, J = 2.0 Hz, aromatic 2CH), 7.12 (1H, s, aromatic 2CH). ^{19}F NMR (376.15 MHz, CDCl$_3$, 27.0 °C): δ -112.83 (tt, J = 6.0 and 7.5 Hz).

64l Heating conditions: 190 °C, 1 h. Recrystallization solvent: hot ethyl acetate. Yield: 80%. ^{1}H NMR (399.79 MHz, CDCl$_3$, 27.0 °C): δ 1.57 (1H, m, CH_2), 1.74 (1H, m, CH_2), 2.94 (6H, s, 2CH_3), 3.37 (2H, m, 2CH), 3.47 (2H, m, bridgehead 2CH), 6.23 (2H, m, 2CH), 6.69 (2H, m, aromatic, 2CH), 6.93 (2H, m, aromatic 2CH). ^{13}C{^{1}H} NMR (100.5 MHz, CDCl$_3$, 27.0 °C): δ 40.5

(2CH_3), 45.4 (bridgehead 2CH), 45.6 (2CH), 52.1 (CH_2), 112.4 (aromatic), 120.4 (aromatic), 127.2 (aromatic), 134.5 ($C=C$), 150.4 (aromatic), 177.4 ($C=O$). IR (solid): 2877, 1708, 1568, 1354, 1179 cm^{-1}. HRMS (ESI$^+$) m/z calcd for $C_{17}H_{19}N_2O_2{}^+$ ([M + H]$^+$): 283.1441. Found: 283.1435. Elemental analysis calcd for $C_{17}H_{18}N_2O_2$: N 9.92, C 72.32, H 6.43. Found: N 9.99, C 72.55, H 6.49. M.p.: 175.0 °C.

64m[101] Heating conditions: 170 °C, 1 h. Recrystallization solvent: hot ethyl acetate. Yield: 60%. ^{1}H NMR (399.79 MHz, CDCl$_3$, 27.0 °C): δ 1.57 (1H, m, CH_2), 1.74 (1H, m, CH_2), 3.37 (2H, m, 2CH), 3.46 (2H, m, bridgehead 2CH), 3.78 (3H, s, CH_3), 6.23 (2H, m, 2CH), 6.90 (2H, m, aromatic, 2CH), 7.02 (2H, m, aromatic 2CH).

64n[103] Heating conditions: 180 °C, 1 h. Recrystallization solvent: hot ethanol. Yield: 86%. ^{1}H NMR (399.79 MHz, CDCl$_3$, 27.0 °C): δ 1.66 (2H, m, CH_2), 1.91 (2H, m, CH_2), 3.04 (2H, s, bridgehead 2CH), 5.00 (2H, m, 2CH), 7.25 (2H, m, aromatic 2CH), 7.36-7.50 (3H, m, aromatic 3CH).

64o[104] Heating conditions: 200 °C, 30 min. Recrystallization solvent: hot ethanol/water. Yield: 62%. ^{1}H NMR (399.79 MHz, CDCl$_3$, 27.0 °C): δ 1.49 (2H, m, CH_2), 1.68 (4H, m, 2CH_2), 2.88 (2H, m, bridgehead 2CH), 3.25 (2H, m, 2CH), 7.25 (2H, m, aromatic 2CH), 7.39 (1H, m, aromatic CH), 7.48 (2H, m, aromatic 2CH).

A procedure for preparation of imides 71.[96] Under argon, *cis*-1,3-dibenzyl-2-oxo-4,5-imidazolidinedicarboxylic anhydride (3.3652 g, 10 mmol)[74a], benzylamine (1.1 mL, 10 mmol), acetic anhydride (0.95 mL,

10 mmol), and toluene (70 mL) were added to a 200 mL round bottom flask equipped with a 1 inch Teflon® coated stirring bar. The solution was stirred for 5 h under reflux. Removal of the solvent using a rotary evaporator gave yellow oil. The crude product was then purified by flash chromatography using 230–400 mesh silica gel (ethyl acetate:hexanes = 1:2). A white solid was obtained upon removal of the solvents. Yield: 86%. As imide **71** is well known in the literature[74f], only the ^{1}H NMR data are reported. ^{1}H NMR (299.97 MHz, CDCl$_3$, 27.0 °C): δ 4.00 (2H, s, 2C*H*), 4.26 (2H, d, J = 18.0 Hz, C*H$_2$*), 4.66 (2H, s, C*H$_2$*), 5.07 (2H, d, J = 15.0 Hz, C*H$_2$*), 7.35 (15H, m, aromatic 15C*H*).

Typical preparation of the catalyst [Ru((*R*)-BINAP)(diamine)(H)$_2$] with 4-99 equiv KO*t*-Bu.[35e] A solution of [Ru((*R*)-BINAP)((1-5-η)-C$_8$H$_{11}$)]BF$_4$ (0.005 or 0.010 mmol) in THF (0.50 mL) was shaken under H$_2$ (~2 atm) in a NMR tube at 0 °C for 3 min. The resulting solution containing [Ru((*R*)-BINAP)(H)(THF)$_3$]BF$_4$ was then cooled in a –78 °C dry ice/acetone bath, and the diamine (0.005 or 0.010 mmol) in THF (0.20 mL) was then added by cannula under H$_2$ pressure (~2 atm) at –78 °C. The NMR tube was shaken for ~5 sec outside the –78 °C bath, and then returned to the bath. This process was repeated nine times. KO*t*-Bu (0.050–0.50 mmol) in THF (0.30 mL) was then added by cannula under H$_2$. The NMR tube was shaken for ~5 sec outside the –78 °C bath and then returned to the bath. This process was repeated nine times. The solution color changed from yellow to red during the addition of KO*t*-Bu to form a mixture containing

trans-[Ru((*R*)-BINAP)(diamine)(H)$_2$] and 4-99 equiv KO*t*-Bu. This mixture was used directly for the catalytic hydrogenation as described in the next section.

Typical procedure for hydrogenation using [Ru((*R*)-BINAP)(diamine)(H)$_2$] as prepared above. A solution of the imide (1.0–10.0 mmol) in THF (3–19 mL), prepared under argon, was added to a stainless steel autoclave equipped with a magnetic stir bar. The atmosphere in the autoclave was then flushed with H$_2$ gas for ~3 min at 0 °C, and a solution of *trans*-[Ru((*R*)-BINAP)(diamine)(H)$_2$] (0.005 or 0.010 mmol) and KO*t*-Bu (0.045–0.495 mmol) in THF (1.0 mL), prepared typically as described above, was then added by cannula under H$_2$ pressure. The autoclave was then pressurized with H$_2$ to 50 atm. The reaction mixture was stirred at 0 °C under 50 atm H$_2$ for 6–57 h. The autoclave was then vented slowly at 0 °C. Precipitation of the product hydroxy lactam was observed (Table 3-5, entries 4–6, and Table 3-6, entries 1–6). The reaction yield, diastereomeric ratio, and enantiomeric excess were determined by ^{1}H NMR and HPLC. As compound **65c–e**, **66a**, **66b**, and **72** are known in the literature, only the ^{1}H NMR data and HPLC data (if applicable) are reported here. Only major spectrometric data of major isomers (trans isomers) are reported if applicable.

65c[105] (Table 3-4, entry 4, 8, and 9: 1.0 mmol of **64c** was used.) ^{1}H NMR (399.79 MHz, CDCl$_3$, 27.0 °C): δ 2.94 (3H, s, C*H*$_3$), 3.66 (1H, br, O*H*), 5.61 (1H, s, C*H*), 7.42 (1H, m, aromatic C*H*), 7.60 (3H, m, aromatic 3C*H*).

65d[106] (Table 3-4, entry 5: 1.0 mmol of **64d** was used.) ^{1}H NMR (399.79

MHz, CDCl$_3$, 27.0 °C): δ 3.43 (1H, d, J = 12.0 Hz, OH), 4.27 (1H, d, J =

14.8 Hz, CH_2), 4.89 (1H, d, J = 14.8 Hz, CH_2), 5.60 (1H, d, J = 11.6 Hz, CH),

7.2–7.6 (8H, m, aromatic 8CH), 7.69 (1H, m, aromatic CH).

65e[106] (Table 3-4, entry 6: 1.0 mmol of **64e** was used.) ^{1}H NMR (399.79

MHz, CDCl$_3$, 27.0 °C): δ 3.25 (1H, br, OH), 6.38 (1H, br, CH), 7.22 (1H, m,

aromatic CH), 7.4–7.8 (8H, m, aromatic 8CH).

65i (Table 3-5, entry 3, 4, 6 and 7: 1.0 mmol of **64i** was used. Table 3-5,

entry 5: 5.0 mmol of **64i** was used.) ^{1}H NMR (399.79 MHz, CDCl$_3$, 27.0 °C):

δ 1.12 (3H, m, CH_2), 1.55 (3H, m, CH_2), 1.86 (1H, m, CH_2), 2.17 (1H, m,

CH_2), 2.28 (1H, dt, J = 6.4 and 11.3 Hz, CH), 2.99 (1H, m, CH), 3.47 (1H, br

d, J = 5.9 Hz, OH), 5.10 (1H, d, J = 4.6 Hz, CHOH), 7.18 (1H, m, aromatic

CH), 7.35 (2H, m, aromatic 2CH), 7.54 (2H, m, aromatic 2CH). ^{13}C{^{1}H}

NMR (100.5 MHz, CDCl$_3$, 27.0 °C): δ 22.8 (CH$_2$), 23.0 (CH$_2$), 23.4 (CH$_2$),

26.5 (CH$_2$), 39.5 (CH), 41.1 (CH), 88.5 (CHOH), 122.3 (aromatic), 125.6

(aromatic), 129.0 (aromatic), 138.2 (aromatic), 175.6 (C=O). IR (CHCl$_3$

cast film): 3315, 2935, 2855, 1666, 1599, 1501, 1409, 1060, 759 cm^{-1}.

HRMS (ESI$^+$) m/z calcd for C$_{14}$H$_{17}$NNaO$_2^+$ ([M + Na]$^+$): 254.11515. Found:

254.11489. Elemental analysis calcd for C$_{14}$H$_{17}$NO$_2$: N 6.06, C 72.70, H

7.41. Found: N 6.01, C 72.85, H 7.56. $[\alpha]_D^{23}$ –34.07 (c = 1.00 g/100 mL,

CHCl$_3$, 93% ee). M.p.: 133.8 °C. HPLC analysis conditions: Daicel

CHIRALPAK IB column (4.6 mm i.d. × 250 mm), Hexanes:2-Propanol =

97:3, 30 °C, flow rate = 0.8 mL/min, detection (UV, 210 nm). Retention times: 27.0 min (minor enantiomer), 50.8 min (major enantiomer).

65j (Table 3-6, entry 1: 10.0 mmol of **64j** was used.) ^{1}H NMR (399.79 MHz, acetone-d_6, 27.0 °C): δ 1.47 (2H, m, CH_2), 2.76 (1H, m, CH), 3.21 (3H, overlapping multiplet, CH and bridgehead 2CH), 5.04 (1H, d, J = 8.1 Hz, CHOH), 5.23 (1H, d, J = 8.7 Hz, OH), 6.08 (1H, dd, J = 2.8 and 5.6 Hz, CH), 6.19 (1H, dd, J = 2.8 and 5.6 Hz, CH), 7.12 (1H, m, aromatic CH), 7.28 (2H, m, aromatic 2CH), 7.50 (2H, m, aromatic 2CH). ^{13}C{^{1}H} NMR (100.5 MHz, ~0.7 mL of acetone-d_6 with ~0.1 mL of MeOH-d_4, 27.0 °C): δ 46.0 (bridgehead CH), 46.5 (bridgehead CH), 47.5 (CH), 50.4 (CH), 51.7 (CH$_2$), 87.5 (CHOH), 125.3 (aromatic), 126.7 (aromatic), 129.4 (aromatic), 134.7 (aromatic), 136.6 (C=C), 138.9 (C=C), 176.1 (C=O). IR (CHCl$_3$ cast film): 3187, 2968, 1666, 1594, 1502, 1428, 1330, 1228, 1076, 721 cm^{-1}. HRMS (ESI$^+$) m/z calcd for C$_{15}$H$_{15}$NNaO$_2^+$ ([M + Na]$^+$): 264.0995. Found: 264.09938. Elemental analysis calcd for C$_{15}$H$_{15}$NO$_2$: N 5.81, C 74.67, H 6.27. Found: N 5.86, C 74.8, H 6.11. $[\alpha]_D^{23}$ −168.65 (c = 1.00 g/100 mL of methanol, >99% ee). M.p.: 120.5 °C. HPLC analysis conditions: Daicel CHIRALPAK IB column (4.6 mm i.d. × 250 mm), Hexanes:2-Propanol = 97:3, 30 °C, flow rate = 0.8 mL/min, detection (UV, 210 nm). Retention times: 41.1 min (minor enantiomer), 49.7 min (major enantiomer). Product with >99% ee was obtained upon single recrystallization from hot ethanol. Yield after single recrystallization (recrystallization conditions not optimized): 73%. This crystal was used for X-ray diffraction analysis.

65k (Table 3-6, entry 2: 2.5 mmol of **64k** was used.) ^{1}H NMR (399.80 MHz, acetone-d_6, 27.0 °C): δ 1.44 (1H, br dt, J = 1.6 and 8.4 Hz, CH_2), 1.50 (1H, dt, J = 1.6 and 8.4 Hz, CH_2), 2.76 (1H, m, CH), 3.18 (1H, m, CH), 3.23 (2H, overlapping multiplet, CH and bridgehead CH), 5.00 (1H, d, J = 8.0 Hz, CHOH), 5.26 (1H, d, J = 8.8 Hz, OH), 6.09 (1H, dd, J = 3.2 and 5.6 Hz, CH), 6.20 (1H, dd, J = 3.2 and 5.6 Hz, CH), 7.05 (2H, m, aromatic 2CH), 7.50 (2H, m, aromatic 2CH). ^{13}C{^{1}H} NMR (100.5 MHz, acetone-d_6, 27.0 °C): δ 46.0 (bridgehead CH), 46.5 (bridgehead CH), 47.4 (CH), 50.0 (CH), 51.6 (CH$_2$), 87.2 (CHOH), 115.6 (aromatic), 115.8 (aromatic), 126.4 (aromatic), 126.5 (aromatic), 134.5 (C=C), 136.6 (C=C), 159.7 (aromatic), 162.1 (aromatic), 174.8 (C=O). ^{19}F NMR (376.15 MHz, acetone-d_6, 27.0 °C): δ −119.27 (tt, J = 5.3 and 8.3 Hz). IR (methanol cast film): 3219, 2975, 1667, 1514, 1436, 1254, 1074 cm^{-1}. HRMS (ESI$^+$) m/z calcd for $C_{15}H_{14}FNNaO_2^+$ ([M + Na]$^+$): 282.0901. Found: 282.0899. Elemental analysis calcd for $C_{15}H_{14}FNO_2$: N 5.40, C 69.49, H 5.44. Found: N 5.42, C 69.47, H 5.45. $[\alpha]_D^{23}$ −151.13 (c = 1.00 g/100 mL of methanol, >99% ee). M.p.: 219.0 °C. HPLC analysis conditions: Daicel CHIRALPAK IB column (4.6 mm i.d. × 250 mm), Hexanes:2-Propanol = 97:3, 30 °C, flow rate = 0.8 mL/min, detection (UV, 210 nm). Retention times: 28.1 min (minor enantiomer), 31.5 min (major enantiomer). Product with >99% ee was obtained upon single recrystallization from hot ethyl acetate. This crystal was used for X-ray diffraction analysis.

65l (Table 3-6, entry 3: 2.5 mmol of **64l** was used.) ^{1}H NMR (399.79 MHz, CDCl$_3$, 27.0 °C): δ 1.44 (1H, m, CH_2), 1.61 (1H, dt, J = 1.6 and 8.4 Hz, CH_2), 2.71 (1H, ddd, J = 1, 4.2, and 8.6 Hz , CH), 2.86 (1H, br, CHOH), 2.93 (6H, s, 2CH_3), 3.23 (1H, br, CH), 3.28 (1H, m, CH), 3.35 (1H, br, CH), 4.84 (1H, d, J = 5.6 Hz, CHOH), 6.16 (1H, dd, J = 2.8 and 5.6 Hz, CH), 6.24 (1H, dd, J = 2.8 and 5.6, CH), 6.72 (2H, d, J = 8.4 Hz, aromatic 2CH), 7.14 (2H, d, J = 8.8 Hz, aromatic 2CH). ^{13}C{^{1}H} NMR (125.27 MHz, ~0.7 mL of CDCl$_3$ with ~0.1 mL of MeOH-d_4, 27.0 °C): δ 40.5 (CH_3), 44.9 (bridgehead CH), 45.3 (bridgehead CH), 46.3 (CH), 49.2 (CH), 51.1 (CH_2), 87.6 (CHOH), 112.8 (aromatic), 126.0 (aromatic), 126.5 (aromatic), 133.3 (C=C), 136.0 (C=C), 149.5 (aromatic), 176.1 (C=O). IR (CHCl$_3$ cast film): 3332, 3001, 1661, 1565, 1320, 1227, 1067, 801, 758 cm^{-1}. HRMS (ESI[+]) m/z calcd for C$_{17}$H$_{21}$N$_2$O$_2^+$ ([M + H][+]): 285.1598. Found: 285.1592. Elemental analysis calcd for C$_{17}$H$_{20}$N$_2$O$_2$: N 9.85, C 71.81, H 7.09. Found: N 9.56, C 71.41, H 6.80. $[\alpha]_D^{23}$ −147.69 (c = 0.50 g/100 mL of MeOH, 97% ee). M.p.: 237.13 °C. HPLC analysis conditions: Daicel CHIRALPAK IB column (4.6 mm i.d. × 250 mm), Hexanes:2-Propanol = 92:8, 30 °C, flow rate = 1.6 mL/min, detection (UV, 210 nm). Retention times: 28.1 min (minor enantiomer), 31.1 min (major enantiomer).

65m (Table 3-6, entry 4: 2.5 mmol of **64m** was used.) ^{1}H NMR (399.79 MHz, CDCl$_3$, 27.0 °C): δ 1.43 (1H, d, J = 8.4 Hz, CH_2), 1.61 (1H, d, J = 8.4 Hz, CH_2), 2.71 (1H, dd, J = 4.2 and 8.6 Hz, CH), 3.05 (1H, br, CHOH), 3.23 (1H, br, CH), 3.28 (1H, m, CH), 3.34 (1H, br, CH), 3.78 (3H, s, CH_3),

4.83 (1H, s, C*H*OH), 6.14 (1H, dd, J = 2.8 and 5.6 Hz, C*H*), 6.23 (1H, dd, J = 2.8 and 5.6 Hz, C*H*), 6.86 (2H, m, aromatic 2C*H*), 7.20 (2H, m, aromatic 2C*H*). $^{13}C\{^1H\}$ NMR (125.69 MHz, CDCl$_3$, 27.0 °C): δ 45.1 (bridgehead *C*H), 45.6 (bridgehead *C*H), 46.3 (CH), 49.2 (*C*H), 51.3 (*C*H$_2$), 55.5 (*C*H$_3$), 87.3 (*C*HOH), 114.4 (aromatic), 126.6 (aromatic), 129.7 (aromatic), 133.2 (*C*=C), 136.6 (C=*C*), 158.3 (aromatic), 175.0 (*C*=O). IR (CHCl$_3$ cast film): 3194, 2976, 1644, 1514, 1249, 1069, 1035, 829, 727 cm^{-1}. HRMS (ESI$^+$) m/z calcd for C$_{16}$H$_{17}$NNaO$_3^+$ ([M + Na]$^+$): 294.1101. Found: 294.1099. Elemental analysis calcd for C$_{16}$H$_{15}$NO$_3$: N 5.20, C 71.36, H 5.61. Found: N 5.03, C 70.88, H 6.22. $[\alpha]_D^{23}$ −151.93 (c = 0.50 g/100 mL of MeOH, 95% ee). M.p.: 205.62 °C. HPLC analysis conditions: Daicel CHIRALPAK IB column (4.6 mm i.d. × 250 mm), Hexanes:2-Propanol = 97:3, 30 °C, flow rate = 0.8 mL/min, detection (UV, 210 nm). Retention times: 82.68 min (minor enantiomer), 112.85 min (major enantiomer).

65n (Table 3-6, entry 5: 1.0 mmol of **64n** was used.) ^1H NMR (399.79 MHz, CDCl$_3$, 27.0 °C): δ 1.36 (2H, m, C*H*$_2$), 1.55 (2H, m, C*H*$_2$), 2.22 (1H, dd, J = 0.9 and 7.9 Hz, C*H*), 2.72 (1H, d, J = 7.9 Hz, C*H*), 4.48 (1H, d, J = 4.8 Hz, bridgehead C*H*), 4.57 (1H, d, J = 4.8 Hz, bridgehead C*H*), 5.02 (1H, br, O*H*), 5.21 (1H, d, J = 1.0 Hz, C*H*OH), 7.00 (1H, m, aromatic C*H*), 7.12 (2H, m, aromatic 2C*H*), 7.29 (2H, m, aromatic 2C*H*). $^{13}C\{^1H\}$ NMR (100.5 MHz, acetone-d_6, 27.0 °C): δ 29.0 (*C*H$_2$), 29.1 (*C*H$_2$), 50.9 (*C*H), 53.4 (*C*H), 79.8 (bridgehead *C*H), 81.6 (bridgehead *C*H) 88.9 (*C*HOH), 124.3 (aromatic), 126.3 (aromatic), 129.3 (aromatic), 138.9 (aromatic), 174.0 (*C*=O). IR

(CHCl$_3$ cast film): 3315, 2982, 2957, 1658, 1599, 1502, 1419, 1314, 1284, 1056, 747 cm^{-1}. HRMS (ESI$^+$) m/z calcd for C$_{14}$H$_{15}$NNaO$_3^+$ ([M + Na]$^+$): 268.09441. Found: 268.09411. Elemental analysis calcd for C$_{14}$H$_{15}$NO$_3$: N 5.71, C 68.56, H 6.16. Found: N 5.69, C 68.54, H 6.30. [α]$_D^{23}$ −133.33 (c = 1.00 g/100 mL of methanol, 87 % ee). M.p.: 178.2 °C. HPLC analysis conditions: Daicel CHIRALPAK IB column (4.6 mm i.d. × 250 mm), Hexanes:2-Propanol = 95:5, 30 °C, flow rate = 1.0 mL/min, detection (UV, 210 nm). Retention times: 38.9 min (minor enantiomer), 46.6 min (major enantiomer).

65o (Table 3-6, entry 6: 2.5 mmol of **64o** was used.) ^{1}H NMR (399.79 MHz, CDCl$_3$, 27.0 °C): δ 1.3-1.6 (6H, m, 3CH_2), 2.45 (1H, ddd, J = 1.1, 4.9 and 10.5 Hz, CH), 2.57 (1H, br t, J = 3.8 Hz, bridgehead CH), 2.71 (1H, br, bridgehead CH), 3.03 (1H, dd, J = 5.5 and 10.5 Hz, CH), 3.28 (1H, d, J = 8.3 Hz, OH), 5.33 (1H, d, J = 7.3 Hz, CHOH), 7.24 (1H, m, aromatic CH), 7.36 (2H, m, aromatic 2CH), 7.48 (2H, m, aromatic 2CH). ^{13}C{^{1}H} NMR (100.5 MHz, CDCl$_3$, 27.0 °C): δ 22.9 (CH$_2$), 24.8 (CH$_2$), 39.5 (bridgehead CH), 39.9 (bridgehead CH), 41.2 (CH$_2$), 48.07 (CH), 48.10 (CH) 86.0 (CHOH), 124.0 (aromatic), 126.4 (aromatic), 129.1 (aromatic), 137.2 (aromatic), 175.9 (C=O). IR (CHCl$_3$ cast film): 3347, 2960, 2881, 1673, 1597, 1500, 1409, 1066, 759 cm^{-1}. HRMS (ESI$^+$) m/z calcd for C$_{15}$H$_{17}$NNaO$_2^+$ ([M + Na]$^+$): 266.11515. Found: 266.11509. Elemental analysis calcd for C$_{15}$H$_{17}$NO$_2$: N 5.76, C 74.05, H 7.04. Found: N 5.61, C 74.04, H 7.49. [α]$_D^{23}$ −113.73 (c = 1.00 g/100 mL of CHCl$_3$, 93 % ee). M.p.:

153.5 °C. HPLC analysis conditions: Daicel CHIRALPAK IB column (4.6 mm i.d. × 250 mm), Hexanes:2-Propanol = 97:3, 30 °C, flow rate = 0.8 mL/min, detection (UV, 210 nm). Retention times: 27.8 min (minor enantiomer), 39.1 min (major enantiomer).

66a[107] (Table 3-4, entry 3: 1.0 mmol of **64a** was used.) ^{1}H NMR (399.79 MHz, CDCl$_3$, 27.0 °C): δ 1.81 (2H, tt, J = 6.2 and 6.8 Hz, CH_2), 2.30 (2H, t, J = 6.8 Hz, CH_2), 2.74 (3H, d, J = 4.8 Hz, CH_3), 3.61 (2H, br dt, J = 4.4 and 5.4 Hz, CH_2OH), 4.07 (1H, br, OH), 6.62 (1H, br, NH).

66b[108] (Table 3-6, entry 7: 1.0 mmol of **64b** was used.) ^{1}H NMR (299.97 MHz, CDCl$_3$, 27.0 °C): δ 1.95 (2H, tt, J = 8.6 and 8.4 Hz, CH_2), 2.51 (2H, t, J = 9.0 Hz, CH_2), 2.96 (1H, br, OH), 2.72 (2H, t, J = 7.6 Hz, CH_2OH), 7.09 (2H, m, aromatic 2CH), 7.29 (1H, m, aromatic 1CH), 7.49 (2H, m, aromatic 2CH), 7.92 (1H, br, NH).

72[74f] (Equation 3-7: 0.52 mmol of **71** was used. [**71**] = 0.065 M) ^{1}H NMR (399.80 MHz, DMSO-d_6, 27.0 °C): δ 3.79, (1H, d, J = 9.0 Hz, CH) 4.09 (1H, overlapping with a CH peak, d, J = 16.2 Hz, CH_2) 4.13 (1H, overlapping with a CH$_2$ peak, d, J = 9.2 Hz, CH) 4.33 (1H, AB patterned d, J = 15.7, CH_2), 4.44 (1H, overlapping with a CH$_2$ peak, AB patterned d, J = 15.7, CH_2), 4.48 (1H, overlapping with a CH$_2$ peak, d, J = 15.3, CH_2), 4.67 (1H, d, J = 15.2, CH_2), 4.76 (1H, overlapping with a CH$_2$ peak, d, J = 8.5, CHOH), 4.48 (1H, overlapping with a CHOH peak, d, J = 16.6, CH_2), 6.43 (1H, d, J = 8.1, CHOH),7.1–7.4 (15H, m, aromatic 15CH). HPLC analysis conditions: Daicel CHIRALPAK IB column (4.6 mm i.d. × 250 mm),

Hexanes:2-Propanol = 95:5, 30 °C, flow rate = 0.8 mL/min, detection (UV, 210 nm). Retention times: 35.2 min (major enantiomer), 44.8 min (minor enantiomer).

Preparation of racemic *cis*-65j.[74a] Under argon, imide **64j** (478.4 mg, 2.00 mmol), and 20 mL of CH_2Cl_2 were placed in a 100 mL Schlenk flask equipped with a stirring bar. DIBAL-H (1.5 M in toluene, 1.4 mL, 2.1 mmol) was slowly added at –78 °C. The reaction mixture was then stirred for 2 h at –78 °C. After 2 h, 5 mL of acetone and 2 mL of water was added to the reaction mixture at –78 °C. The cooling bath was removed, and the reaction mixture was stirred for ~10 min while it warmed to ~ RT. Formation of a white precipitate was observed. The reaction mixture was then dried by addition of $MgSO_4$, filtered using Celite® 545, and concentration of the clear colorless solution gave a white solid. The white solid was passed through 150 mesh, neutral, activated alumina (Brockmann I) using ethyl acetate as solvent. Evaporation of the ethyl acetate gave a white solid of racemic *cis*-**65j**. No formation of the *trans* isomer was observed. Yield: 70% (isolated yield). Diastereomeric ratio: > 99:1 (based on ^1H NMR). ^1H NMR (399.80 MHz, ~ 0.7 mL acetone-d_6 + ~0.1 mL $CDCl_3$, 27.0 °C): δ 1.45 (2H, m, CH_2), 3.11 (1H, m, bridgehead C*H*), 3.17 (3H, overlapping multiplet, 2C*H* and bridgehead C*H*), 5.05 (1H, d, J = 6.0 Hz, O*H*), 5.85 (1H, m, C*H*OH), 6.03 (1H, dd, J = 2.8 and 5.6 Hz, C*H*), 6.29 (1H, dd, J = 2.8 and 5.6 Hz, C*H*), 7.11 (1H, m, aromatic C*H*), 7.29 (4H, m, aromatic 4C*H*). $^{13}C\{^1H\}$ NMR (125.69 MHz, $CDCl_3$, 27.0 °C): δ 42.6 (*C*H), 44.9 (*C*H), 46.3

(CH), 50.0 (CH), 51.8 (CH_2), 83.0 ($CHOH$), 124.5 (aromatic), 126.5 (aromatic), 129.1 (aromatic), 135.0 (C=C), 135.2 (C=C), 136.4 (aromatic), 173.2 (C=O). IR (solid): 3297, 2984, 1651, 1469, 1406, 1302, 1097 cm^{-1}. HRMS (ESI$^+$) m/z calcd for $C_{15}H_{16}NO_2^+$ ([M + H]$^+$): 242.1176. Found: 242.1177. Elemental analysis calcd for $C_{15}H_{15}NO_2$: N 5.81, C 74.67, H 6.27. Found: N 5.86, C 74.8, H 6.29. M.p.: 177.9 °C.

Isomerization of racemic *cis*-65j into racemic *trans*-65j in the presence of KO*t*-Bu. Under argon, racemic *cis*-**65j** (51.5 mg, 0.21 mmol) and 3 mL of THF were placed in a 50 mL Schlenk flask equipped with a stirring bar forming a white suspension. KO*t*-Bu (1.2 mg, 0.010 mmol) in THF 1 mL was then added to the flask at 0 °C. The white suspension became a clear colorless solution upon addition of KO*t*-Bu. The reaction mixture was stirred for 4 h at 0 °C. After 4h, an aliquot of the reaction mixture was concentrated under vacuum, and analyzed by ^{1}H NMR. Complete isomerization from *cis*-**65j** to *trans*-**65j** was observed.

Reaction of *trans*-[Ru((*R*)-BINAP)(H)$_2$((*R,R*)-dpen)] (6) with the imide 64j in the presence of 0.5 equiv. of KN(Si(CH$_3$)$_3$)$_2$. A solution of **6** (0.015 mmol) was prepared in THF-d_8 (0.60 mL) using KN(Si(CH$_3$)$_3$)$_2$ (4.6 mg, 0.023 mmol) at –78 °C under H$_2$ as described previously,[35e] and frozen in a liquid N$_2$ bath. A solution of imide **64j** (3.6 mg, 0.015 mmol) in THF-d_8 (0.20 mL) was then added at –78 °C by cannula under argon pressure. The frozen solution was partially melted and mixed by shaking once outside the bath. The partially melted sample was then introduced into the NMR probe

pre-cooled to –80 °C. The first ^{1}H NMR spectrum (~2 min at –80 °C) showed that ~46% of the dihydride **6** had reacted to form the alkoxide *trans*-**67** as the sole detectable product. All dihydride **6** was converted into alkoxide *trans*-**67** after an hour. The alkoxide *trans*-**67** was characterized at –80 °C using ^{1}H, ^{31}P{^{1}H}, ^{1}H–^{1}H gCOSY and ^{1}H–^{13}C gHSQC NMR experiments. ^{1}H NMR (399.95 MHz, THF-d_8, –80 °C): δ –19.0 (1H, t, $^2J_{\text{P-H}}$ = 27.0 Hz, Ru-H), 0.59 (1H, broad doublet, J = 8.0 Hz, C$_H$H*H*), 0.89 (1H, overlapping with a hexane peak, C$_H$H*H*), 1.90 (1H, br, C$_a$HNH*H*), 2.09 (1H, br, overlapping with a C$_B$H peak, C$_G$*H*), 2.15 (1H, br, overlapping with a C$_G$H peak, C$_B$*H*), 2.27 (1H, s, C$_C$*H*), 2.73 (1H, s, C$_F$*H*), 3.27 (1H, br, overlapping with a peak from **64j**, C$_b$HNH*H*), 3.38 (1H, overlapping with a peak from **64j**, C$_a$HNH*H*), 3.52 (1H, overlapping with a residual THF-d_8 peak, C$_a$*H*NHH), 4.74 (1H, br t, C$_b$*H*NHH),   3.94 (1H, br, C$_b$HNH*H*), 5.80 (1H, br, C$_E$*H*), 5.94 (1H, br, overlapping with a aromatic peak, C$_D$*H*), 6.13 (1H, s, C$_A$*H*), 6-10 (overlapping peaks, aromatic). ^{13}C{^{1}H} NMR (100.6 MHz, THF-d_8, –80 °C, determined using ^{1}H–^{13}C HSQC): δ 46.3 (*C*$_C$H), 47.1 (*C*$_F$H), 49.8 (*C*$_B$H), 50.6 (*C*$_H$H$_2$), 53.3 (*C*$_G$H), 65.4 (*C*$_a$HNH$_2$), 67.7 (*C*$_b$HNH$_2$), 96.2 (*C*$_A$H), 135.1 (*C*$_D$H), 135.3 (*C*$_E$H), 120-140 (aromatic). ^{31}P{^{1}H} NMR (161.91 MHz, THF-d_8, –80 °C): δ68.03 (2P, AB quartet, $^2J_{\text{P–P}}$ = 45.4 Hz). See Figures 3-11 to 3-13.

Preparation of the alkoxide *trans*-76 by the reaction between [Ru((*R*)-BINAP)(H)((*R,R*)-NH(CH(Ph))$_2$NH$_2$)] (7) and hydroxy lactam *trans*-65j. A solution of **7** (0.011 mmol) was prepared in THF-d_8 (0.60 mL)

as we described previously using KN(Si(CH$_3$)$_3$)$_2$ (4.1 mg, 0.021 mmol), and frozen in a liquid nitrogen bath. A solution of *trans*-**65j** (2.5 mg, 0.010 mmol, >99% ee) in THF-*d$_8$* (0.20 mL) was then added to the frozen solution of **7** at −78 °C by cannula under dinitrogen. The frozen solution was partially melted and mixed by shaking once outside the bath. The partially melted sample was then introduced into the NMR probe pre-cooled to −80 °C. ^{1}H, and ^{31}P{^{1}H} NMR spectra showed formation of the alkoxide *trans*-**76** (51%) and *trans*-[((*R*)-BINAP)(H)(OH)((*R*,*R*)-dpen)] (**43**) (49%) (based on ^{31}P{^{1}H} NMR) due to water in the solution.[35e]

Reaction of the Ru-dihydride 6 with imide 64j in the absence of excess KN(Si(CH$_3$)$_3$)$_2$. A mixture of the Ru-dihydride **6** (55%) with the Ru-hydroxide **43** (45%) in THF-*d$_8$* (0.7 mL) in a NMR tube was prepared using [Ru((*R*)-BINAP)((1-5-η)-C$_8$H$_{11}$)]BF$_4$ (13.8 mg, 0.0150 mmol) and KN(Si(CH$_3$)$_3$)$_2$ (2.7 mg, 0.014 mmol) as reported previously,[35e] and kept in a liquid N$_2$ bath. A solution of the imide **64j** (1.9 mg, 0.0079 mmol, 1 equiv with respect to **6**) in THF-*d$_8$* (0.1 mL) was then added to the tube in the liquid N$_2$ bath under H$_2$ (~1 atm). The frozen solution was partially thawed in a −78 °C dry ice/acetone bath. The NMR tube was then introduced into a NMR probe pre-cooled at −80 °C, and completely thawed inside the probe. ^{1}H and ^{31}P NMR spectra recorded after ~3 min showed broadening of hydride peak of **6** (70%), and **68** (30%). All **6** was converted into **68** (93%) and *trans*-**67** (7%) after 4 h at −80 °C. Broadening of **64j** signals was observed in ^{1}H NMR. **68** was stable up to −60 °C. The identity of **68** was

investigated using ^{1}H, ^{31}P{^{1}H}, ^{1}H–^{1}H gCOSY and ^{1}H–^{13}C gHSQC NMR experiments. ^{1}H NMR (399.95 MHz, THF-d_8, −80 °C): δ −17.5 (1H, br, Ru-H), 1.46 (2H, overlapping with a cyclooctane peak, CH_2), 2.20 (1H, br, C$_a$HNHH), 3.1–3.4 (4H, br, bridgehead 2CH and 2CH), 3.31 (1H, overlapping with peaks from **64j**, C$_b$HNHH), 3.94 (2H, overlapping with a excess (R,R)-dpen peak, C$_a$$H$NHH and C$_b$$H$NHH), 4.40 (1H, br, C$_bHNHH$), 4.64 (1H, br, C$_aHNHH$), 6.12 (2H, m, 2C$H$), 6-10 (overlapping peaks, aromatic), 16.5 (1H, br). ^{13}C{^{1}H} NMR (100.6 MHz, THF-d_8, −80 °C, determined using ^{1}H–^{13}C HSQC): δ 46.6 (bridgehead 2C H), 51.1 (CH$_2$) 51.2 (2C H), 62.8 (C$_a$HNH$_2$), 69.0 (C$_b$HNH$_2$), 134.5 (C H), 135.5 (C H), 120-140 (aromatic). ^{31}P{^{1}H} NMR (161.91 MHz, THF-d_8, −80 °C): δ 67.67 (d, overlapping with *trans*-**67** peaks, $^2J_{P–P}$ = 39.5 Hz), 73.16 (d, $^2J_{P–P}$ = 39.5 Hz). See Figures 3-14 to 3-16.

Reaction of the Ru-amide 7 and racemic *cis*-65j in the absence of excess KN(Si(CH$_3$)$_3$)$_2$. A mixture of the Ru-amide **7** (66%) with the Ru-hydroxide **43** (26%) and trans-[Ru((R)-BINAP)-(H)(THF-d_8)((R,R)-dpen)]BF$_4$ (8%) in THF-d_8 (0.7 mL) in a NMR tube was prepared using [Ru((R)-BINAP)((1-5-η)-C$_8$H$_{11}$)]BF$_4$ (13.3 mg, 0.0145 mmol) and KN(Si(CH$_3$)$_3$)$_2$ (1.8 mg, 0.090 mmol) as reported previously, and kept in a liquid N$_2$ bath. A solution of racemic *cis*-**65j** (3.0 mg, 0.012 mmol, 2 equiv relative to **7**) in THF-d_8 (0.1 mL) was then added to the tube in the liquid N$_2$ bath under H$_2$ (~1 atm). The frozen solution was partially thawed in a −78 °C dry ice/acetone bath. The NMR tube was then introduced into a

NMR probe pre-cooled at –80 °C, and completely thawed inside the probe. ^{1}H and ^{31}P NMR spectra recorded after 2 min showed formation of **6** (28% yield), and **68** (72% yield).

Quenching of the Ru-amidate 68 with excess 2-PrOH-d_8. A mixture of the Ru-dihydride **6** (80%) with the Ru-hydroxide **43** (20%) in THF-d_8 (0.7 mL) in a NMR tube was prepared using [Ru((*R*)-BINAP)((1-5-η)-C$_8$H$_{11}$)]BF$_4$ (14.3 mg, 0.0156 mmol) and KN(Si(CH$_3$)$_3$)$_2$ (2.8 mg, 0.014 mmol) as reported previously,[35e] and kept in a liquid N$_2$ bath. A solution of the imide **64j** (2.5 mg, 0.010 mmol, 1 equiv with respect to **6**) in THF-d_8 (0.1 mL) was then added to the tube in the liquid N$_2$ bath under H$_2$ (~1 atm). The frozen solution was partially thawed in a –78 °C dry ice/acetone bath. The NMR tube was then introduced into a NMR probe pre-cooled at –80 °C, and completely thawed inside the probe. ^{1}H and ^{31}P NMR spectra recorded after ~1 h showed formation of the amidate **68** (55%) and *trans*-**67** (45%). 2-PrOH-d_8 (~0.2 mL) was then added to the solution at –78 °C. ^{1}H and ^{31}P NMR spectra recorded after ~10 min showed formation of Ru-2-propoxide **12** and *trans*-**65j**. No significant deuteration of CH signal next to the CHOH group in *trans*-**65j** was observed based on integration of the ^{1}H NMR signals.

Reaction of Racemic *cis*-65j with mixture of KOH and HN(Si(CH$_3$)$_3$)$_2$. Under N$_2$, reacemic *cis*-**65j** (4.8 mg, 0.020 mmol) and THF-d_8 (0.2 mL) were placed in a NMR tube, and frozen in a liquid N$_2$ bath. Distilled water (0.35 µL, 0.019 mmol) was added to KN(Si(CH$_3$)$_2$)$_2$ (3.9 mg, 0.020 mmol) in

THF-d_8 (0.5 mL). This mixture was then added to the solution of *cis*-**65j** in the liquid N_2 bath under N_2. The frozen solution was partially thawed in a –78 °C dry ice/acetone bath. The sample was then introduced into a NMR probe pre-cooled at –80 °C, and completely thawed inside the probe. ^{1}H NMR spectrum recorded after ~3 min showed complete isomerization from *cis*-**65j** to *trans*-**65j**.

Reaction of Racemic *cis*-65j with HN(Si(CH$_3$)$_3$)$_2$. Under N_2, racemic *cis*-**65j** (2.4 mg, 0.010 mmol) and CD_2Cl_2 (0.6 mL) were placed in a NMR tube, and frozen in a liquid N_2 bath. $HN(Si(CH_3)_2)_2$ (3 μL, 0.014 mmol) in THF-d_8 (0.1 mL) was then added to the solution of *cis*-**65j** in the liquid N_2 bath under N_2. The frozen solution was partially thawed in a –78 °C dry ice/acetone bath. The sample was then introduced into a NMR probe pre-cooled at –80 °C, and completely thawed inside the probe. ^{1}H NMR spectrum recorded after at –80 and 0 °C showed no isomerization of *cis*-**65j**.

Trapping experiment of *cis*-65j using HBF$_4$·OEt$_2$ as a trapping reagent. A mixture of the Ru-dihydride **6** (68%) with the Ru-hydroxide **43** (32%) in THF-d_8 (0.7 mL) in a NMR tube was prepared using [Ru((*R*)-BINAP)((1-5-η)-C_8H_{11})]BF$_4$ (18.6 mg, 0.0203 mmol) and KN(Si(CH$_3$)$_3$)$_2$ (3.8 mg, 0.019 mmol) as reported previously, and kept in a liquid N_2 bath. A solution of the imide **64j** (2.8 mg, 0.012 mmol, 1 equiv with respect to **6**) in THF-d_8 (0.1 mL) was then added to the tube in the liquid N_2 bath under H_2 (~1 atm). The frozen solution was partially thawed in a –78

°C dry ice/acetone bath. The NMR tube was then introduced into a NMR probe pre-cooled at –60 °C, and completely thawed inside the probe. ^{1}H and ^{31}P NMR spectra recorded after ~20 min showed unreacted **6** (10%), and formation of new Ru-hydride species (70%) and *trans*-**67** (20%).

This mixture was then frozen in the liquid N$_2$ bath. HBF$_4$·OEt$_2$ (54 w% in Et$_2$O, 5.0 µL, 0.036 mmol) was then added to the frozen solution under H$_2$ (~1 atm). The frozen solution was partially thawed in a –78 °C dry ice/acetone bath. The NMR tube was then introduced into a NMR probe pre-cooled at –80 °C, and completely thawed inside the probe. ^{1}H and ^{31}P NMR spectra recorded after ~3 min showed formation of the Ru-dihydrogen **5** and *trans*-**65j** (96% ee) exclusively.

Trapping experiment of *cis*-65j using BSA as a trapping reagent. A mixture of the Ru-dihydride **6** (87%) with the Ru-hydroxide **43** (13%) in THF-d_8 (0.7 mL) in a NMR tube was prepared using [Ru((R)-BINAP)((1-5-η)-C$_8$H$_{11}$)]BF$_4$ (14.6 mg, 0.0159 mmol) and KN(Si(CH$_3$)$_3$)$_2$ (3.1 mg, 0.016 mmol) as reported previously. *N*,*O*-bis(trimethylsilyl)acetamide (BSA, 20 µL, 0.082 mmol) was then added to the NMR tube using a micro-liter syringe at –78 °C under H$_2$ (~1 atm). The solution was mixed by shaking the NMR tube once outside of the –78 °C bath. The ^{1}H and ^{31}P{^{1}H} NMR taken at –80 °C showed mixture of the dihydride **6** (78%) and Ru-amidate **69** (22%). All Ru-hydroxide **43** was converted into **69**. This mixture was then kept in a liquid N$_2$ bath. A solution of the imide **64j** (2.6 mg, 0.011 mmol, ~1 equiv with respect to **6**) in THF-d_8

(0.1 mL) was then added to the tube in the liquid N_2 bath under H_2 (~1 atm). The frozen solution was partially thawed in a –78 °C dry ice/acetone bath. The NMR tube was then introduced into a NMR probe pre-cooled at –80 °C, and completely thawed inside the probe. The first ^{1}H and ^{31}P NMR spectra recorded after ~3 min showed unreacted **6** (56%), and formation of the Ru-amidate **69** (44%) and *trans*-TMS-**65j**. 95% of the dihydride **6** was converted into **69** after 1 h, and more *trans*-**68** formed. *Trans*-TMS-**65j** and **69** were characterized using ^{1}H, ^{31}P{^{1}H}, ^{1}H–^{1}H gCOSY and ^{1}H–^{13}C gHSQC NMR experiments. **69**: ^{1}H NMR (399.95 MHz, THF-d_8, –80 °C): δ –18.6 (1H, t, J = 25.4 Hz, Ru-H), –0.51 (9H, s, Si*ME₃*), 1.28 (1H, overlapping with hexanes peaks, C_aHN*H*H), 2.24 (3H, s, C*H₃*), 2.37 (1H, br, C_bHN*H*H), 3.39 (1H, overlapping with a peak from **64j**, C_a*H*NHH), 3.93 (1H, overlapping with an excess (*R,R*)-dpen peak, C_b*H*NHH), 4.60 (1H, overlapping with an excess H_2 peak, C_bHNH*H*), 10.08 (1H, br, C_aHNH*H*), 6-9 (overlapping peaks, aromatic). ^{13}C{^{1}H} NMR (100.6 MHz, THF-d_8, –80 °C, determined using ^{1}H–^{13}C HSQC and ^{1}H–^{13}C HMBC): δ 1.83 (Si*Me₃*), 29.3 (C*H₃*), 63.7 (C_a*H*NH₂), 68.5 (C_b*H*NH₂), 120-140 (aromatic), 177.6 (*C*=N). ^{29}Si{^{1}H} NMR (79.46 MHz, THF-d_8, –80 °C): δ –13.15 (s). ^{31}P{^{1}H} NMR (161.91 MHz, THF-d_8, –80 °C): δ 67.67 (2P, AB quartet, $^2J_{P–P}$ = 41.3 Hz). See Figures 3-17 to 3-19.

Independent synthesis of *Trans*-TMS-65j by the reaction between *trans*-65j (>99% ee) and BSA. *Trans*-**65j** (>99% ee, 3.6 mg, 0.015 mmol) and BSA (20 µL, 0.082 mmol) were mixed in THF-d_8 (0.7 mL) for 1 min. ^{1}H

NMR taken at –80 °C showed quantitative formation of *trans*-TMS-**65j**. ^{1}H NMR (399.95 MHz, THF-d_8, –80 °C): δ 0.046 (9H, s, Si*Me₃*), 1.48 (2H, AB quartet, *J* = 8.8 Hz, C*H₂*), 2.68 (1H, dd, *J* = 4.0 and 8.8 Hz, C*H*), 3.21 (2H, s, bridgehead 2C*H*), 3.31 (1H, dd, *J* = 4.8 and 8.5 Hz, C*H*), 5.27 (1H, s, C*H*OSiMe₃), 6.10 (1H, m, C*H*), 6.24 (1H, m, C*H*), 7.14 (1H, t, *J* = 7.5 Hz, aromatic C*H*), 7.30 (2H, t, *J* = 7.5 Hz, aromatic 2C*H*), 7.42 (2H, d, *J* = 8.1 Hz, aromatic 2C*H*). ^{13}C{^{1}H} NMR (100.5 MHz, THF-d_8, –80 °C, determined using ^{1}H–^{13}C HSQC and ^{1}H–^{13}C HMBC): δ 3.97 (Si*Me₃*), 45.9 (bridgehead 2*C*H), 47.6 (*C*H), 50.0 (*C*H), 51.2 (*C*H₂), 86.1 (*C*HOH), 120-140 (aromatic), 134.1 (*C*=C), 135.8 (C=*C*), 174.1 (*C*=O). ^{29}Si{^{1}H} NMR (79.46 MHz, THF-d_8, –80 °C): δ 16.38 (s).

Reaction of Racemic *cis*-65j with BSA. Racemic *cis*-**65j** (4.4 mg, 0.018 mmol) and BSA (8.9 μL, 0.032 mmol) were mixed in CDCl₃ (0.7 mL) for 5 min at 40 °C. ^{1}H NMR spectra recorded at 27.0 °C showed formation of *trans*-TMS-**65j** in <5% yield. Further heating at 60 °C for 2 h resulted in formation *trans*-TMS-**65j** quantitatively.

Preparation of the bromocarbamate (70) Under argon, *trans*-**65j** (>99% ee, 10.8 mg, 0.045 mmol) and 4-bromophenyl isocyanate (9.3 mg, 0.047 mmol) were placed in a NMR tube. 0.7 mL of acetone-d_6 was then added to the tube. The tube was heated at 60 °C for 7 h. 78 % (^{1}H NMR) of *trans*-**65j** was converted into **70**. Formation of 4-bromophenyl carbamic acid was observed as insoluble crystals due to trace water in the solvent. The mixture was concentrated using rotary evaporator, extracted from CH₂Cl₂,

and dried over $MgSO_4$. Concentration of the extract gave a colorless oil. Crystals suitable for the X-ray diffraction analysis were grown upon cooling the hexanes/ethyl acetate solution at –20 °C. ^{1}H NMR (499.82 MHz, acetone-d_6, 27.0 °C): δ 1.52 (1H, m, CH_2), 1.57 (1H, m, CH_2), 2.96 (1H, ddd, J = 1.0, 4.5, and 8.5 Hz, CH), 3.27 (1H, m, bridgehead CH), 3.34 (1H, m, bridgehead CH), 3.36 (1H, ddd, J = 0.5, 5.0, and 8.5 Hz, CH), 6.03 (1H, s, CHO), 6.17 (1H, dd, J = 3.0 and 6.0 Hz, CH), 6.36 (1H, dd, J = 3.0 and 6.0 Hz, CH), 7.19 (1H, m, aromatic CH), 7.33 (2H, m, aromatic 2CH), 7.40 (2H, m, aromatic 2CH), 7.44 (2H, m, aromatic 2CH), 7.48 (2H, br m, aromatic 2CH). ^{13}C{^{1}H} NMR (125.69 MHz, acetone-d_6, 27.0 °C): δ 45.3 (CH), 46.0 (bridgehead CH), 46.8 (bridgehead CH), 49.4 (CH), 51.6 (CH_2), 89.0 (CHO), 115.7 (aromatic C), 121.0 (appear as doublet due to the slow rotation of carbamate C-N bond, aromatic CH), 124.5 (aromatic CH), 126.9 (aromatic CH), 129.6 (aromatic CH), 132.6 (aromatic CH), 134.4 (C=C), 136.8 (C=C), 138.3 (aromatic C), 139.1 (appear as doublet due to the slow rotation of carbamate C-N bond, aromatic C), 153.0 (appear as doublet due to the slow rotation of carbamate C-N bond, C=O), 175.5 (C=O). IR ($CHCl_3$ cast film): 3283, 1712, 1599, 1539, 1492, 1213, 1033 cm^{-1}. HRMS (ESI[+]) m/z calcd for $C_{22}H_{19}BrN_2NaO_3^+$ ([M + Na][+]): 461.0471. Found: 461.0464. Elemental analysis calcd for $C_{22}H_{19}BrN_2O_3$: N 6.38, C 60.15, H 4.36. Found: N 6.38, C 60.38, H 4.39. $[\alpha]_D^{23}$ –108.40 (c = 1.00 g/100 mL of acetone, > 99% ee,). M.p.: 167.3 °C.

Cyclization of the hydroxy lactam *trans*-65j with indene to form polycyclic lactam 73. Under argon, *trans*-**65j** (>99% ee) (95.8 mg, 0.40 mmol), indene (0.05 mL, 0.43 mmol), and 10 mL of toluene were placed in a 50 mL Schlenk flask equipped with a stirring bar. *Trans*-**65j** was scarcely soluble in toluene. $BF_3 \cdot OEt_2$ (0.1 mL, 0.79 mmol) was then added to the flask at 22 °C. Dissolution of *trans*-**65j** was observed as soon as $BF_3 \cdot OEt_2$ was added. The clear faint yellow solution was stirred for 30 min at 22 °C. The reaction was then quenched by addition of sat. $NaHCO_3$ (5 mL) at 22 °C, followed by stirring at 22 °C for 5 min. The faint yellow solution became colorless upon quenching. The reaction mixture was extracted using CH_2Cl_2 (100 mL), dried over $MgSO_4$, and concentrated under vacuum. The resulting colorless oil was analyzed by ^{1}H NMR and HPLC to determine the yield, diastereomeric ratio, and enantiomeric excess. The HPLC chromatogram was compared to that of racemic **73** prepared from racemic *trans*-**65j**. Crystals of the major diastereomer formed upon slow evaporation of ethyl acetate solution. This crystal was used for X-ray diffraction analysis. Yield: 90% (based on ^{1}H NMR). Diastereomeric ratio: 91:9 (based on ^{1}H NMR). Enantiomeric excess: >99%. **73** ^{1}H NMR (399.79 MHz, $CDCl_3$, 27.0 °C): δ 1.47 (1H, d, $J = 8.4$ Hz, C*H*₂), 1.66 (1H, dt, $J = 1.6$ and 8.4 Hz, C*H*₂), 2.75 (1H, m, C*H*), 2.87 (1H, dd, $J = 10.6$ and 15.4 Hz, C*H*₂), 3.02 (1H, dd, $J = 8.2$ and 15.4 Hz, C*H*₂), 3.19 (1H, br m, bridgehead C*H*), 3.21-3.30 (2H, m, 2CH), 3.41 (1H, br m, bridgehead C*H*), 3.60 (1H, t, $J = 3.0$ Hz, C*H*), 4.46 (1H, d, $J = 8.8$ Hz, C*H*), 6.17 (1H, dd, $J = 3.2$ and 5.6

Hz, C*H*), 6.35 (1H, dd, *J* = 3.2 and 5.6 Hz, C*H*), 7.04 (1H, m, aromatic C*H*),

7.14 (4H, m, aromatic 4C*H*), 7.47 (2H, m, aromatic 2C*H*), 8.01 (1H, dd, *J* =

1.4 and 8.2 Hz, aromatic C*H*). ^{13}C{^{1}H} NMR (100.5 MHz, CDCl$_3$, 27.0 °C): δ

32.1 (benzylic *C*H$_2$), 40.0 (*C*H), 45.5 (*C*H), 45.7(bridgehead *C*H), 46.1

(bridgehead *C*H), 46.8 (*C*H), 51.0 (*C*H$_2$), 51.1 (*C*H), 60.8 (*C*HN), 121.3

(aromatic), 124.8 (aromatic), 124.9 (aromatic), 125.0 (aromatic), 126.4

(aromatic), 126.8 (aromatic), 127.3 (aromatic), 128.6 (aromatic), 130.1

(aromatic), 134.3 (*C*=C), 135.2 (aromatic), 136.8 (C=*C*), 141.8 (aromatic),

145.4 (aromatic), 173.3 (*C*=O). IR (CHCl$_3$ cast film): 2981, 1683, 1492,

1397, 755 cm^{-1}. HRMS (ESI$^+$) m/z calcd for C$_{24}$H$_{22}$NO ([M + H]$^+$): 340.1696.

Found: 340.1701. Elemental analysis calcd for C$_{24}$H$_{21}$NO: N 4.13, C 84.92,

H 6.24. Found: N 3.92, C 84.12, H 6.30. $[\alpha]_D^{23}$ 124.76 (c = 1.00 g/100 mL of

CHCl$_3$, >99% ee). M.p.: 211.2 °C. HPLC analysis conditions: Daicel

CHIRALPAK IB column (4.6 mm i.d. × 250 mm), Hexanes:2-Propanol =

97:3, 30 °C, flow rate = 0.8 mL/min, detection (UV, 210 nm). Retention

times: 19.7 min (minor enantiomer), 24.7 min (major enantiomer).

Table 3-7. Crystallographic Experimental Details for **65j**.

A.   Crystal Data

formula	C$_{15}$H$_{15}$NO$_2$
formula weight	241.28
crystal dimensions (mm)	0.48 × 0.33 × 0.23
crystal system	orthorhombic
space group	*P*2$_1$2$_1$2$_1$ (No. 19)
unit cell parameters*a*	
a (Å)	6.1618 (7)
b (Å)	12.7291 (14)
c (Å)	15.3398 (17)

V (Å^3)	1203.2 (2)
Z	4
ρ_{calcd} (g cm^{-3})	1.332
μ (mm^{-1})	0.089

B.   Data Collection and Refinement Conditions

diffractometer	Bruker PLATFORM/SMART 1000 CCD[b]
radiation (λ [Å])	graphite-monochromated Mo Kα (0.71073)
temperature (°C)	–80
scan type	ω scans (0.4°) (10 s exposures)
data collection 2θ limit (deg)	54.96
total data collected	9693 (-7 $\leq h \leq$ 8, -16 $\leq k \leq$ 16, -19 $\leq l \leq$ 19)
independent reflections	2738 (R_{int} = 0.0247)
number of observed reflections (NO)	2478 [$F_o^2 \geq 2\sigma(F_o^2)$]
structure solution method	direct methods (SHELXS–97[c])
refinement method	full-matrix least-squares on F^2 (SHELXL–97[c])
absorption correction method	multi-scan (SADABS)
range of transmission factors	0.9799–0.9587
data/restraints/parameters	2738 [$F_o^2 \geq -3\sigma(F_o^2)$] / 0 / 164
Flack absolute structure parameter[d]	1.4 (11)
goodness-of-fit (S)[e]	1.062 [$F_o^2 \geq -3\sigma(F_o^2)$]
final R indices[f]	
R_1 [$F_o^2 \geq 2\sigma(F_o^2)$]	0.0358
wR_2 [$F_o^2 \geq -3\sigma(F_o^2)$]	0.0866
largest difference peak and hole	0.248 and –0.132 e Å^{-3}

[a]Obtained from least-squares refinement of 5008 reflections with 5.32° < 2θ < 54.84°.

[b]Programs for diffractometer operation, data collection, data reduction and absorption correction were those supplied by Bruker.

[c]Sheldrick, G. M.   *Acta Crystallogr.* **2008**, *A64*, 112–122.

[d]Flack, H. D.   *Acta Crystallogr.* **1983**, *A39,* 876–881;   Flack, H. D.; Bernardinelli, G.   *Acta Crystallogr.* **1999**, *A55*, 908–915;   Flack, H. D.; Bernardinelli, G.   *J. Appl. Cryst.* **2000**, *33*, 1143–1148.   The Flack parameter will refine to a value near zero if the structure is in the correct configuration and will refine to a value near one for the inverted configuration.   However, the low anomalous scattering power of the atoms in this structure (none heavier than oxygen) implies that the data

cannot be used for absolute structure assignment, thus the Flack parameter is provided for informational purposes only. The present structural study should only be used for assignment of relative stereochemistry.

[e]$S = [\Sigma w(F_o^2 - F_c^2)^2/(n - p)]^{1/2}$ (n = number of data; p = number of parameters varied; $w = [\sigma^2(F_o^2) + (0.0427P)^2 + 0.2201P]^{-1}$ where $P = [\text{Max}(F_o^2, 0) + 2F_c^2]/3)$.

[f]$R_1 = \Sigma||F_o| - |F_c||/\Sigma|F_o|$; $wR_2 = [\Sigma w(F_o^2 - F_c^2)^2/\Sigma w(F_o^4)]^{1/2}$.

Table 3-8. Selected Interatomic Distances (Å) for **65j**.

Atom1	Atom2	Distance	Atom1	Atom2	Distance
O1	O2^a	2.6608(14)^b	C5	C6	1.508(2)
O1	C1	1.2321(16)	C5	C9	1.538(2)
O1	H2O^a	1.83^b	C6	C7	1.329(2)
O2	C2	1.4034(17)	C7	C8	1.509(2)
N	C1	1.3582(16)	C8	C9	1.543(2)
N	C2	1.4700(17)	C10	C11	1.386(2)
N	C10	1.4330(18)	C10	C15	1.388(2)
C1	C4	1.5018(19)	C11	C12	1.387(2)
C2	C3	1.533(2)	C12	C13	1.380(3)
C3	C4	1.5442(19)	C13	C14	1.378(3)
C3	C8	1.561(2)	C14	C15	1.392(2)
C4	C5	1.568(2)			

^{a}At 1−x, $^1/_2$+y, $^1/_2$−z. ^{b}Nonbonded distance.

Table 3-9. Selected Interatomic Angles (deg) for **65j**.

Atom1	Atom2	Atom3	Angle	Atom1	Atom2	Atom3	Angle
C1	N	C2	114.73(11)	C6	C5	C9	99.98(13)
C1	N	C10	122.91(11)	C5	C6	C7	107.96(14)
C2	N	C10	122.28(10)	C6	C7	C8	107.60(14)
O1	C1	N	124.33(13)	C3	C8	C7	107.05(12)
O1	C1	C4	126.42(12)	C3	C8	C9	99.64(13)
N	C1	C4	109.24(12)	C7	C8	C9	100.15(13)
O2	C2	N	109.68(12)	C5	C9	C8	93.83(12)
O2	C2	C3	111.91(12)	N	C10	C11	120.02(14)
N	C2	C3	103.62(10)	N	C10	C15	119.61(14)
C2	C3	C4	106.93(11)	C11	C10	C15	120.36(14)
C2	C3	C8	116.57(13)	C10	C11	C12	119.67(16)
C4	C3	C8	102.64(11)	C11	C12	C13	120.21(16)
C1	C4	C3	105.07(11)	C12	C13	C14	120.09(15)
C1	C4	C5	114.45(11)	C13	C14	C15	120.41(17)
C3	C4	C5	103.43(11)	C10	C15	C14	119.25(16)
C4	C5	C6	106.83(12)	O2	H2O	O1^a	169.0^b
C4	C5	C9	99.05(12)				

^{a}At 1−x, −$^1/_2$+y, $^1/_2$−z. ^{b}Angle includes nonbonded O–H···O interaction.

Table 3-10. Crystallographic Experimental Details for **65k**.

A. Crystal Data

formula	$C_{15}H_{14}FNO_2$
formula weight	259.27
crystal dimensions (mm)	$0.46 \times 0.27 \times 0.21$
crystal system	orthorhombic
space group	$P2_12_12_1$ (No. 19)
unit cell parameters[a]	
a (Å)	6.1944 (4)
b (Å)	12.7213 (8)
c (Å)	15.5031 (9)
V (Å^3)	1221.66 (13)
Z	4
ρ_{calcd} (g cm^{-3})	1.410
μ (mm^{-1})	0.104

B. Data Collection and Refinement Conditions

diffractometer	Bruker D8/APEX II CCD[b]
radiation (λ [Å])	graphite-monochromated Mo Kα (0.71073)
temperature (°C)	−100
scan type	ω scans (0.3°) (20 s exposures)
data collection 2θ limit (deg)	55.02
total data collected	10802 (-8 $\leq h \leq$ 8, -16 $\leq k \leq$ 16, -20 $\leq l \leq$ 20)
independent reflections	1633 (R_{int} = 0.0136)
number of observed reflections (NO)	1587 [$F_o^2 \geq 2\sigma(F_o^2)$]
structure solution method	direct methods (SHELXS–97[c])
refinement method	full-matrix least-squares on F^2 (SHELXL–97[c])
absorption correction method	Gaussian integration (face-indexed)
range of transmission factors	0.9781–0.9539
data/restraints/parameters	1633 / 0 / 173
Flack absolute structure parameter[d]	1.7(10)
goodness-of-fit (S)[e] [all data]	1.071
final R indices[f]	
R_1 [$F_o^2 \geq 2\sigma(F_o^2)$]	0.0295
wR_2 [all data]	0.0810
largest difference peak and hole	0.231 and −0.148 e Å^{-3}

[a]Obtained from least-squares refinement of 9934 reflections with 5.26° <

$2\theta < 54.96°$.

[b]Programs for diffractometer operation, data collection, data reduction and absorption correction were those supplied by Bruker.

[c]Sheldrick, G. M. *Acta Crystallogr.* **2008**, *A64*, 112–122.

[d]Flack, H. D. *Acta Crystallogr.* **1983**, *A39*, 876–881; Flack, H. D.; Bernardinelli, G. *Acta Crystallogr.* **1999**, *A55*, 908–915; Flack, H. D.; Bernardinelli, G. *J. Appl. Cryst.* **2000**, *33*, 1143–1148. The Flack parameter will refine to a value near zero if the structure is in the correct configuration and will refine to a value near one for the inverted configuration. The low anomalous scattering power of the atoms in this structure (none heavier than oxygen) implies that the data cannot be used for absolute structure assignment, thus the Flack parameter is provided for informational purposes only.

[e]$S = [\Sigma w(F_o^2 - F_c^2)^2/(n - p)]^{1/2}$ (n = number of data; p = number of parameters varied; $w = [\sigma^2(F_o^2) + (0.0490P)^2 + 0.2124P]^{-1}$ where $P = [\mathrm{Max}(F_o^2, 0) + 2F_c^2]/3$).

[f]$R_1 = \Sigma||F_o| - |F_c||/\Sigma|F_o|$; $wR_2 = [\Sigma w(F_o^2 - F_c^2)^2/\Sigma w(F_o^4)]^{1/2}$.

Table 3-11. Selected Interatomic Distances (Å) for **65k**.

Atom1	Atom2	Distance	Atom1	Atom2	Distance
F	C13	1.3572(17)	C4	C5	1.507(3)
O1	O2^a	2.7003(15)^b	C4	C9	1.545(2)
O1	H2O^a	1.86^b	C5	C6	1.334(3)
O1	C1	1.2302(17)	C6	C7	1.513(2)
O2	C2	1.3995(18)	C7	C8	1.567(2)
N	C1	1.3578(16)	C7	C9	1.539(2)
N	C2	1.4703(17)	C10	C11	1.388(2)
N	C10	1.4276(18)	C10	C15	1.387(2)
C1	C8	1.5041(19)	C11	C12	1.390(2)
C2	C3	1.537(2)	C12	C13	1.373(3)
C3	C4	1.559(2)	C13	C14	1.369(3)
C3	C8	1.5484(18)	C14	C15	1.390(2)

^{a}At $1-x$, $1/2+y$, $1/2-z$. ^{b}Nonbonded distance.

Table 3-12. Selected Interatomic Angles (deg) for **65k**.

Atom1	Atom2	Atom3	Angle	Atom1	Atom2	Atom3	Angle
C1	N	C2	115.16(12)	C6	C7	C9	100.33(13)
C1	N	C10	122.84(12)	C8	C7	C9	98.80(12)
C2	N	C10	121.98(10)	C1	C8	C3	105.03(11)
O1	C1	N	124.53(13)	C1	C8	C7	114.52(12)
O1	C1	C8	126.35(12)	C3	C8	C7	103.18(11)
N	C1	C8	109.11(12)	C4	C9	C7	93.69(12)
O2	C2	N	108.85(12)	N	C10	C11	120.30(13)
O2	C2	C3	112.33(12)	N	C10	C15	119.73(14)
N	C2	C3	103.41(10)	C11	C10	C15	119.97(14)
C2	C3	C4	116.11(12)	C10	C11	C12	120.25(16)
C2	C3	C8	107.00(11)	C11	C12	C13	118.17(16)
C4	C3	C8	102.73(12)	F	C13	C12	118.64(17)
C3	C4	C5	107.30(12)	F	C13	C14	118.29(17)
C3	C4	C9	99.63(13)	C12	C13	C14	123.07(14)
C5	C4	C9	100.18(14)	C13	C14	C15	118.42(16)
C4	C5	C6	107.73(16)	C10	C15	C14	120.10(16)
C5	C6	C7	107.59(16)	O2	H2O	O1^a	174.3^b
C6	C7	C8	107.26(12)				

^{a}At $1-x$, $-1/2+y$, $1/2-z$. ^{b}Angle includes nonbonded O–H···O interaction.

Table 3-13. Crystallographic Experimental Details for **70**.

A. Crystal Data

formula	$C_{22}H_{19}BrN_2O_3$
formula weight	439.30
crystal dimensions (mm)	$0.63 \times 0.37 \times 0.21$
crystal system	orthorhombic
space group	$P2_12_12$ (No. 18)
unit cell parameters[a]	
a (Å)	12.7403 (5)
b (Å)	25.8323 (10)
c (Å)	12.1352 (5)
V (Å³)	3993.8 (3)
Z	8
ρ_{calcd} (g cm⁻³)	1.461
μ (mm⁻¹)	2.084

B. Data Collection and Refinement Conditions

diffractometer	Bruker D8/APEX II CCD[b]
radiation (λ [Å])	graphite-monochromated Mo Kα (0.71073)
temperature (°C)	-100
scan type	ω scans (0.3°) (20 s exposures)
data collection 2θ limit (deg)	55.00
total data collected	35335 ($-16 \le h \le 16$, $-33 \le k \le 33$, $-15 \le l \le 15$)
independent reflections	9140 ($R_{int} = 0.0204$)
number of observed reflections (*NO*)	8033 [$F_o^2 \ge 2\sigma(F_o^2)$]
structure solution method	direct methods (*SHELXD*[c])
refinement method	full-matrix least-squares on F^2 (*SHELXL–97*[d])
absorption correction method	Gaussian integration (face-indexed)
range of transmission factors	0.6688–0.3545
data/restraints/parameters	9140 / 0 / 505
Flack absolute structure parameter[e]	0.013(6)
goodness-of-fit (*S*)[f] [all data]	1.028
final *R* indices[g]	
R_1 [$F_o^2 \ge 2\sigma(F_o^2)$]	0.0354
wR_2 [all data]	0.0921
largest difference peak and hole	0.621 and -0.444 e Å⁻³

[a]Obtained from least-squares refinement of 9772 reflections with $4.50° < 2\theta < 51.00°$.

[b]Programs for diffractometer operation, data collection, data reduction and absorption correction were those supplied by Bruker.

[c]Schneider, T. R.; Sheldrick, G. M. *Acta Crystallogr.* **2002**, *D58*, 1772-1779.

[d]Sheldrick, G. M. *Acta Crystallogr.* **2008**, *A64*, 112–122.

[e]Flack, H. D. *Acta Crystallogr.* **1983**, *A39*, 876–881; Flack, H. D.; Bernardinelli, G. *Acta Crystallogr.* **1999**, *A55*, 908–915; Flack, H. D.; Bernardinelli, G. *J. Appl. Cryst.* **2000**, *33*, 1143–1148. The Flack parameter will refine to a value near zero if the structure is in the correct configuration and will refine to a value near one for the inverted configuration.

[f]$S = [\Sigma w(F_o^2 - F_c^2)^2/(n - p)]^{1/2}$ (n = number of data; p = number of parameters varied; $w = [\sigma^2(F_o^2) + (0.0479P)^2 + 1.0597P]^{-1}$ where $P = [\text{Max}(F_o^2, 0) + 2F_c^2]/3$).

[g]$R_1 = \Sigma||F_o| - |F_c||/\Sigma|F_o|$; $wR_2 = [\Sigma w(F_o^2 - F_c^2)^2/\Sigma w(F_o^4)]^{1/2}$.

Table 3-14. Selected Interatomic Distances (Å) for **70**.

(a) within molecule A			*(b) within molecule B*		
Atom1	Atom2	Distance	Atom1	Atom2	Distance
Br	C1	1.898(2)	Br	C1	1.906(3)
O1	C7	1.202(3)	O1	C7	1.208(3)
O2	C7	1.370(3)	O2	C7	1.372(3)
O2	C8	1.439(3)	O2	C8	1.448(3)
O3	C9	1.219(3)	O3	C9	1.228(3)
N1	C4	1.415(3)	N1	C4	1.415(3)
N1	C7	1.350(3)	N1	C7	1.342(3)
N2	C8	1.452(3)	N2	C8	1.455(3)
N2	C9	1.373(3)	N2	C9	1.355(3)
N2	C17	1.420(3)	N2	C17	1.418(4)
C1	C2	1.366(4)	C1	C2	1.379(4)
C1	C6	1.378(4)	C1	C6	1.370(4)
C2	C3	1.386(3)	C2	C3	1.382(4)
C3	C4	1.387(3)	C3	C4	1.382(3)
C4	C5	1.396(3)	C4	C5	1.387(4)
C5	C6	1.387(3)	C5	C6	1.389(4)
C8	C15	1.525(4)	C8	C15	1.531(4)
C9	C10	1.506(4)	C9	C10	1.489(4)
C10	C11	1.571(4)	C10	C11	1.578(4)
C10	C15	1.528(4)	C10	C15	1.530(4)
C11	C12	1.506(5)	C11	C12	1.513(5)
C11	C16	1.510(6)	C11	C16	1.521(5)
C12	C13	1.323(5)	C12	C13	1.299(5)
C13	C14	1.510(4)	C13	C14	1.516(5)
C14	C15	1.566(4)	C14	C15	1.573(4)
C14	C16	1.549(6)	C14	C16	1.538(6)
C17	C18	1.382(4)	C17	C18	1.366(5)
C17	C22	1.373(4)	C17	C22	1.398(5)
C18	C19	1.404(6)	C18	C19	1.439(8)
C19	C20	1.350(6)	C19	C20	1.380(10)
C20	C21	1.343(5)	C20	C21	1.326(9)
C21	C22	1.378(5)	C21	C22	1.365(6)

Table 3-15. Selected Interatomic Angles (deg) for **70**.

(a) within molecule A

Atom1	Atom2	Atom3	Angle
C7	O2	C8	117.20(18)
C4	N1	C7	125.2(2)
C8	N2	C9	113.7(2)
C8	N2	C17	121.08(18)
C9	N2	C17	125.1(2)
Br	C1	C2	119.25(19)
Br	C1	C6	119.4(2)
C2	C1	C6	121.3(2)
C1	C2	C3	119.3(2)
C2	C3	C4	120.3(2)
N1	C4	C3	116.8(2)
N1	C4	C5	123.1(2)
C3	C4	C5	120.1(2)
C4	C5	C6	118.8(2)
C1	C6	C5	120.2(2)
O1	C7	O2	124.2(2)
O1	C7	N1	128.0(2)
O2	C7	N1	107.77(19)
O2	C8	N2	106.77(18)
O2	C8	C15	110.02(19)
N2	C8	C15	105.1(2)
O3	C9	N2	125.2(2)
O3	C9	C10	126.0(2)
N2	C9	C10	108.8(2)
C9	C10	C11	113.3(2)
C9	C10	C15	105.5(2)
C11	C10	C15	103.4(3)
C10	C11	C12	106.4(2)
C10	C11	C16	99.5(3)
C12	C11	C16	100.1(3)
C11	C12	C13	108.2(3)
C12	C13	C14	107.4(3)
C13	C14	C15	107.1(2)
C13	C14	C16	99.8(3)
C15	C14	C16	98.5(3)
C8	C15	C10	106.4(2)
C8	C15	C14	116.3(2)
C10	C15	C14	103.0(2)
C11	C16	C14	94.5(3)

(b) within molecule B

Atom1	Atom2	Atom3	Angle
C7	O2	C8	117.58(19)
C4	N1	C7	127.3(2)
C8	N2	C9	114.1(2)
C8	N2	C17	121.8(2)
C9	N2	C17	124.1(2)
Br	C1	C2	119.0(2)
Br	C1	C6	119.7(2)
C2	C1	C6	121.3(2)
C1	C2	C3	118.7(2)
C2	C3	C4	121.0(2)
N1	C4	C3	116.9(2)
N1	C4	C5	123.7(2)
C3	C4	C5	119.4(2)
C4	C5	C6	119.8(2)
C1	C6	C5	119.7(2)
O1	C7	O2	123.7(2)
O1	C7	N1	127.9(2)
O2	C7	N1	108.4(2)
O2	C8	N2	108.0(2)
O2	C8	C15	110.3(2)
N2	C8	C15	104.3(2)
O3	C9	N2	124.3(3)
O3	C9	C10	126.2(2)
N2	C9	C10	109.5(2)
C9	C10	C11	112.8(2)
C9	C10	C15	105.6(2)
C11	C10	C15	102.9(2)
C10	C11	C12	106.3(2)
C10	C11	C16	99.0(2)
C12	C11	C16	100.7(3)
C11	C12	C13	107.9(3)
C12	C13	C14	108.2(3)
C13	C14	C15	105.8(3)
C13	C14	C16	100.0(3)
C15	C14	C16	99.1(3)
C8	C15	C10	106.2(2)
C8	C15	C14	116.0(3)
C10	C15	C14	103.1(2)
C11	C16	C14	94.1(3)

Table 3-15. Selected Interatomic Angles for **70** (continued)

(a) within molecule A

Atom1	Atom2	Atom3	Angle
N2	C17	C18	121.3(2)
N2	C17	C22	120.1(2)
C18	C17	C22	118.5(3)
C17	C18	C19	119.3(3)
C18	C19	C20	121.2(4)
C19	C20	C21	118.7(3)
C20	C21	C22	122.1(3)
C17	C22	C21	120.0(3)

(b) within molecule B

Atom1	Atom2	Atom3	Angle
N2	C17	C18	120.6(3)
N2	C17	C22	118.9(3)
C18	C17	C22	120.5(4)
C17	C18	C19	117.0(5)
C18	C19	C20	119.6(5)
C19	C20	C21	122.2(5)
C20	C21	C22	119.3(6)
C17	C22	C21	121.3(4)

Table 3-16. Crystallographic Experimental Details for **73**.

A.   Crystal Data

formula	$C_{24}H_{21}NO$
formula weight	339.42
crystal dimensions (mm)	$0.49 \times 0.36 \times 0.10$
crystal system	monoclinic
space group	$P2_1$ (No. 4)
unit cell parameters[a]	
a (Å)	8.7288 (3)
b (Å)	11.5872 (4)
c (Å)	17.5810 (6)
β (deg)	103.4409 (4)
V (Å^3)	1729.48 (10)
Z	4
ρ_{calcd} (g cm^{-3})	1.304
μ (mm^{-1})	0.079

B.   Data Collection and Refinement Conditions

diffractometer	Bruker D8/APEX II CCD[b]
radiation (λ [Å])	graphite-monochromated Mo Kα (0.71073)
temperature (°C)	–100
scan type	ω scans (0.3°) (20 s exposures)
data collection 2θ limit (deg)	55.00
total data collected	15335 (-11 $\leq h \leq$ 11, -15 $\leq k \leq$ 15, -22 $\leq l \leq$ 22)
independent reflections	4162 (R_{int} = 0.0182)
number of observed reflections (NO)	3948 [$F_o^2 \geq 2\sigma(F_o^2)$]
structure solution method	direct methods (*SHELXD*[c])
refinement method	full-matrix least-squares on F^2 (*SHELXL–97*[d])
absorption correction method	Gaussian integration (face-indexed)
range of transmission factors	0.9923–0.9624
data/restraints/parameters	4162 / 0 / 469
Flack absolute structure parameter[e]	2.6(12)
goodness-of-fit (S)[f] [all data]	1.052
final R indices[g]	
R_1 [$F_o^2 \geq 2\sigma(F_o^2)$]	0.0302
wR_2 [all data]	0.0841
largest difference peak and hole	0.185 and –0.159 e Å^{-3}

[a]Obtained from least-squares refinement of 5507 reflections with 4.76° < 2θ < 43.02°.

[b]Programs for diffractometer operation, data collection, data reduction and absorption correction were those supplied by Bruker.

[c]Schneider, T. R.; Sheldrick, G. M. *Acta Crystallogr.* **2002**, *D58*, 1772-1779.

[d]Sheldrick, G. M. *Acta Crystallogr.* **2008**, *A64*, 112–122.

[e]Flack, H. D. *Acta Crystallogr.* **1983**, *A39*, 876–881; Flack, H. D.; Bernardinelli, G. *Acta Crystallogr.* **1999**, *A55*, 908–915; Flack, H. D.; Bernardinelli, G. *J. Appl. Cryst.* **2000**, *33*, 1143–1148. The Flack parameter will refine to a value near zero if the structure is in the correct configuration and will refine to a value near one for the inverted configuration. The low anomalous scattering power of the atoms in this structure (none heavier than oxygen) implies that the data cannot be used for absolute structure assignment, thus the Flack parameter is provided for informational purposes only.

[f]$S = [\Sigma w(F_o^2 - F_c^2)^2/(n - p)]^{1/2}$ (n = number of data; p = number of parameters varied; $w = [\sigma^2(F_o^2) + (0.0523P)^2 + 0.2269P]^{-1}$ where $P = [\mathrm{Max}(F_o^2, 0) + 2F_c^2]/3$).

[g]$R_1 = \Sigma||F_o| - |F_c||/\Sigma|F_o|$; $wR_2 = [\Sigma w(F_o^2 - F_c^2)^2/\Sigma w(F_o^4)]^{1/2}$.

Table 3-17. Selected Interatomic Distances (Å) for **73**.

(a) Molecule A			*(b) Molecule B*		
Atom1	Atom2	Distance	Atom1	Atom2	Distance
O1	C6	1.221(2)	O1	C6	1.226(2)
N1	C6	1.364(2)	N1	C6	1.362(2)
N1	C7	1.420(2)	N1	C7	1.413(2)
N1	C22	1.474(2)	N1	C22	1.465(2)
C1	C2	1.510(3)	C1	C2	1.522(3)
C1	C23	1.561(3)	C1	C23	1.563(3)
C1	C24	1.550(3)	C1	C24	1.537(3)
C2	C3	1.331(3)	C2	C3	1.326(3)
C3	C4	1.515(3)	C3	C4	1.514(3)
C4	C5	1.564(3)	C4	C5	1.573(3)
C4	C24	1.542(3)	C4	C24	1.538(3)
C5	C6	1.509(3)	C5	C6	1.512(3)
C5	C23	1.549(3)	C5	C23	1.551(3)
C7	C8	1.396(2)	C7	C8	1.393(2)
C7	C12	1.404(2)	C7	C12	1.396(2)
C8	C9	1.382(3)	C8	C9	1.388(3)
C9	C10	1.388(3)	C9	C10	1.382(3)
C10	C11	1.385(3)	C10	C11	1.387(3)
C11	C12	1.394(2)	C11	C12	1.393(3)
C12	C13	1.531(2)	C12	C13	1.531(2)
C13	C14	1.523(2)	C13	C14	1.521(2)
C13	C21	1.544(2)	C13	C21	1.565(3)
C14	C15	1.386(3)	C14	C15	1.386(3)
C14	C19	1.394(3)	C14	C19	1.389(3)
C15	C16	1.398(3)	C15	C16	1.395(3)
C16	C17	1.382(3)	C16	C17	1.380(3)
C17	C18	1.391(3)	C17	C18	1.387(3)
C18	C19	1.389(3)	C18	C19	1.397(3)
C19	C20	1.512(2)	C19	C20	1.505(3)
C20	C21	1.551(2)	C20	C21	1.550(3)
C21	C22	1.520(2)	C21	C22	1.527(2)
C22	C23	1.544(2)	C22	C23	1.537(3)

Table 3-18. Selected Interatomic Angles (deg) for **73**.

	(a) Molecule A				(b) Molecule B		
Atom1	Atom2	Atom3	Angle	Atom1	Atom2	Atom3	Angle
C6	N1	C7	126.12(15)	C6	N1	C7	128.25(15)
C6	N1	C22	114.90(14)	C6	N1	C22	115.50(15)
C7	N1	C22	118.44(14)	C7	N1	C22	116.19(14)
C2	C1	C23	107.54(15)	C2	C1	C23	106.86(14)
C2	C1	C24	100.46(16)	C2	C1	C24	100.21(19)
C23	C1	C24	99.67(15)	C23	C1	C24	99.75(17)
C1	C2	C3	107.57(19)	C1	C2	C3	107.6(2)
C2	C3	C4	107.66(19)	C2	C3	C4	107.7(2)
C3	C4	C5	107.01(15)	C3	C4	C5	105.70(16)
C3	C4	C24	100.56(17)	C3	C4	C24	100.30(19)
C5	C4	C24	99.01(17)	C5	C4	C24	99.76(17)
C4	C5	C6	113.91(17)	C4	C5	C6	111.95(16)
C4	C5	C23	103.41(15)	C4	C5	C23	103.19(16)
C6	C5	C23	106.52(14)	C6	C5	C23	105.62(15)
O1	C6	N1	126.31(17)	O1	C6	N1	125.79(17)
O1	C6	C5	125.32(16)	O1	C6	C5	125.95(18)
N1	C6	C5	108.36(15)	N1	C6	C5	108.25(16)
N1	C7	C8	120.58(15)	N1	C7	C8	121.35(16)
N1	C7	C12	118.73(15)	N1	C7	C12	117.04(15)
C8	C7	C12	120.67(16)	C8	C7	C12	121.34(16)
C7	C8	C9	119.97(17)	C7	C8	C9	119.17(18)
C8	C9	C10	120.38(18)	C8	C9	C10	120.54(17)
C9	C10	C11	119.33(18)	C9	C10	C11	119.62(17)
C10	C11	C12	121.94(17)	C10	C11	C12	121.35(18)
C7	C12	C11	117.70(16)	C7	C12	C11	117.91(16)
C7	C12	C13	122.41(15)	C7	C12	C13	122.29(16)
C11	C12	C13	119.89(15)	C11	C12	C13	119.79(16)
C12	C13	C14	110.90(14)	C12	C13	C14	110.86(14)
C12	C13	C21	113.10(13)	C12	C13	C21	114.20(14)
C14	C13	C21	102.05(14)	C14	C13	C21	103.26(14)
C13	C14	C15	128.84(17)	C13	C14	C15	128.16(17)
C13	C14	C19	110.35(15)	C13	C14	C19	111.17(17)
C15	C14	C19	120.77(17)	C15	C14	C19	120.66(18)
C14	C15	C16	118.63(19)	C14	C15	C16	119.38(19)
C15	C16	C17	120.66(18)	C15	C16	C17	119.9(2)
C16	C17	C18	120.60(18)	C16	C17	C18	121.10(19)
C17	C18	C19	119.03(19)	C17	C18	C19	119.1(2)
C14	C19	C18	120.27(17)	C14	C19	C18	119.8(2)
C14	C19	C20	110.56(15)	C14	C19	C20	111.70(17)

Table 3-18. Selected Interatomic Angles for **73** (continued)

	(a) Molecule A				*(b) Molecule B*		
Atom1	Atom2	Atom3	Angle	Atom1	Atom2	Atom3	Angle
C18	C19	C20	129.15(17)	C18	C19	C20	128.45(19)
C19	C20	C21	102.74(14)	C19	C20	C21	104.27(16)
C13	C21	C20	105.03(13)	C13	C21	C20	106.45(15)
C13	C21	C22	111.41(14)	C13	C21	C22	110.16(14)
C20	C21	C22	115.90(14)	C20	C21	C22	114.41(16)
N1	C22	C21	108.96(13)	N1	C22	C21	108.29(14)
N1	C22	C23	104.47(13)	N1	C22	C23	103.90(14)
C21	C22	C23	115.69(14)	C21	C22	C23	117.84(15)
C1	C23	C5	102.40(14)	C1	C23	C5	102.50(16)
C1	C23	C22	117.20(15)	C1	C23	C22	115.01(16)
C5	C23	C22	105.55(14)	C5	C23	C22	106.22(14)
C1	C24	C4	93.20(15)	C1	C24	C4	93.99(16)
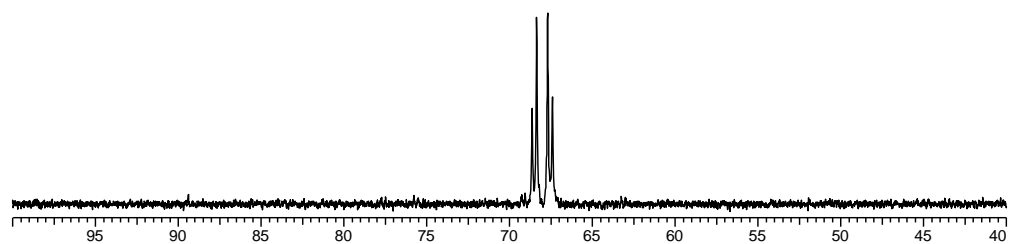
Figure 3-11. ^{31}P NMR spectrum (δ 100 to 40) of *trans*-**67** prepared from **6** and **64j** in the presence of 0.5 equiv KN(Si(CH$_3$)$_3$)$_2$ at −80 °C.
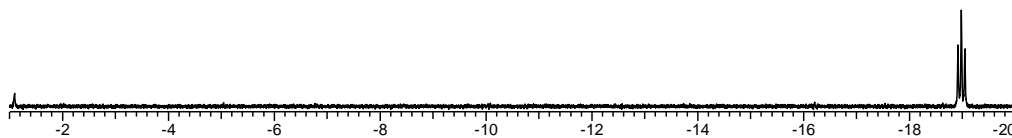
Figure 3-12. ^{1}H NMR spectrum (δ −1 to −20) of *trans*-**67** prepared from **6** and **64j** in the presence of 0.5 equiv KN(Si(CH$_3$)$_3$)$_2$ at −80 °C.
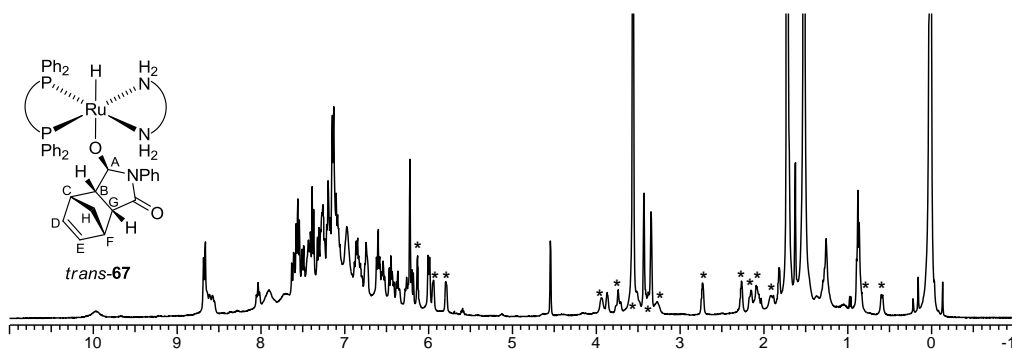
Figure 3-13. ^{1}H NMR spectrum (δ 11 to −1) of *trans*-**67** prepared from **6** and **64j** in the presence of 0.5 equiv KN (Si(CH$_3$)$_3$)$_2$ at −80 °C. The non-aromatic peaks assigned to *trans*-**67** are marked with an asterisk. The remaining peaks are due to excess **64j**, residual protons in THF-d_8,

168

HN(SiC(CH$_3$)$_3$)$_2$, KN(SiC(CH$_3$)$_3$)$_2$, cyclooctane and cyclooctene (formed during the hydrogenation of [Ru((R)-BINAP)((1-5-η)-C$_8$H$_{11}$)]BF$_4$) and hexanes, if present.
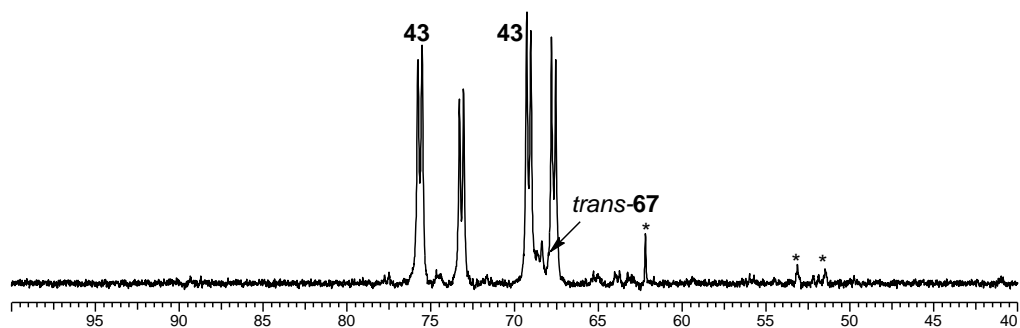
Figure 3-14. ^{31}P NMR spectrum (δ 100 to 40) of **68** prepared from **6** and **64j** in the absence of KN(Si(CH$_3$)$_3$)$_2$ at −80 °C. * is Ru species formed during preparation of **6**.
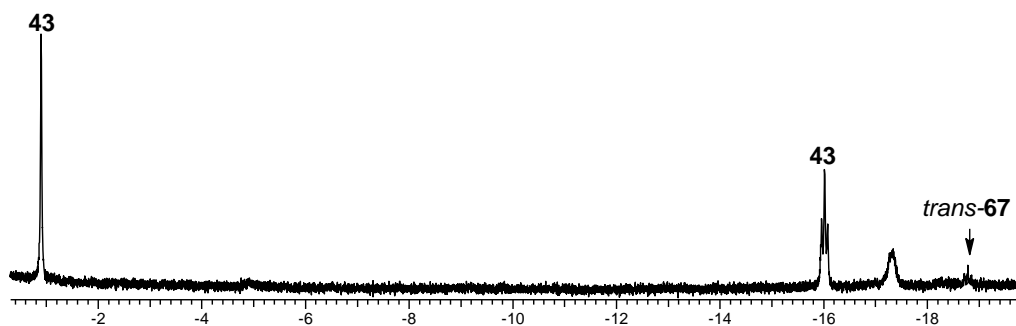
Figure 3-15. ^{1}H NMR spectrum (δ −0.5 to −20) of **68** prepared from **6** and **64j** in the absence of KN(Si(CH$_3$)$_3$)$_2$ at −80 °C.

169
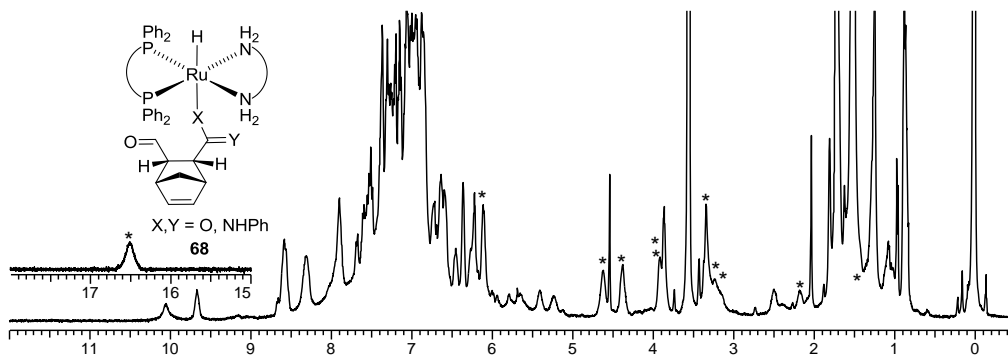
Figure 3-16. ^{1}H NMR spectrum (δ 18 to 15 and 12 to –0.5) of **68** prepared from **6** and **64j** in the absence of KN(Si(CH$_3$)$_3$)$_2$ at –80 °C. The non-aromatic peaks assigned to **68** are marked with an asterisk except the amidate OCH peak. The remaining peaks are due to excess (R,R)-dpen, the Ru-hydroxide **43**, residual protons in THF-d_8, HN(SiC(CH$_3$)$_3$)$_2$, cyclooctane and cyclooctene (formed during the hydrogenation of [Ru((R)-BINAP)((1-5-η)-C$_8$H$_{11}$)]BF$_4$) and hexanes, if present.
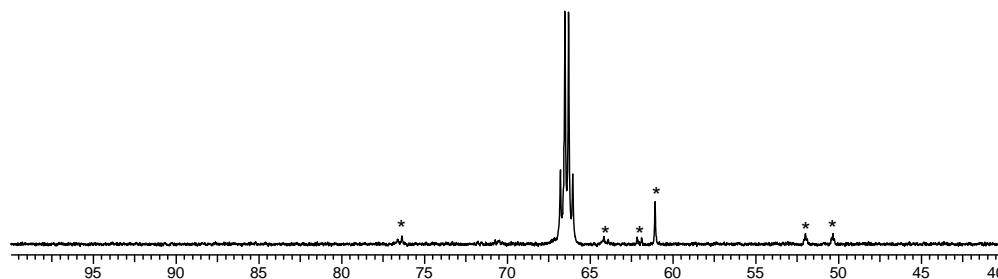
Figure 3-17. ^{31}P NMR spectrum (δ 100 to 40) of **69** formed from the reaction between **6** and **64j** in the presence of 5 equiv BSA at –80 °C. * is Ru species formed during preparation of **6**.
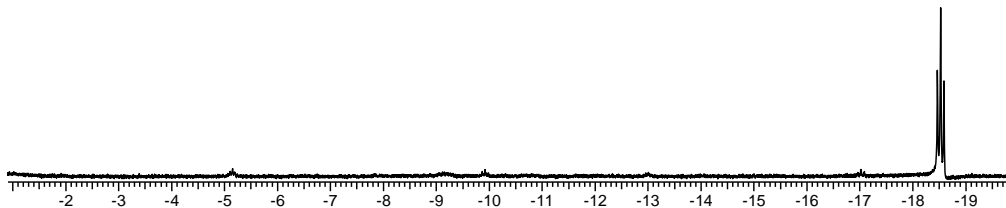
Figure 3-18. ^{1}H NMR spectrum (δ –1 to –20) of **69** formed from the reaction between **6** and **64j** in the presence of 5 equiv BSA at –80 °C.
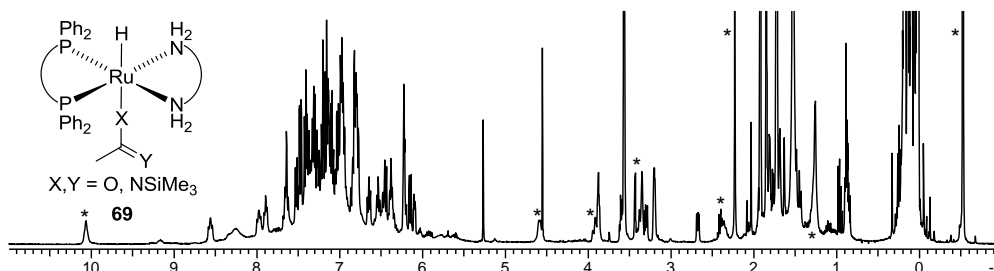
Figure 3-19. ^{1}H NMR spectrum (δ 14 to –0.5) of **69** formed from the reaction between **6** and **64j** in the presence of 5 equiv BSA at –80 °C. The non-aromatic peaks assigned to **69** are marked with an asterisk. The remaining peaks are due to excess BSA, excess (*R,R*)-dpen, excess **64j**, *trans*-TMS-**65j**, residual protons in THF-d_8, HN(SiC(CH$_3$)$_3$)$_2$, H$_2$, cyclooctane and cyclooctene (formed during the hydrogenation of [Ru((*R*)-BINAP)((1-5-η)-C$_8$H$_{11}$)]BF$_4$) and hexanes, if present.

171

Chapter 4

Intramolecular Trapping Experiments to Investigate the Bifunctional Addition Step in Noyori-type Enantioselective Ketone Hydrogenations.

Introduction

The Noyori catalyst system *trans*-[Ru(diphosphine)(X)$_2$(diamine)] + base and its variants are extremely active towards the hydrogenation of carbonyl compounds.[27] Many enantioselective ketone hydrogenations with this catalyst system have been developed in both academic and industrial laboratories.[25,87] In recent developments, less reactive carbonyl compounds including esters and imides have also been hydrogenated.[57,58] The majority of examples use *trans*-[Ru(diphosphine)(Cl)$_2$(diamine)] and a base such as KO*t*-Bu to generate the active catalyst *trans*-[Ru(diphosphine)(H)$_2$(diamine)] *in situ*. The mechanism of this hydrogenation is being studied by several research groups using methods that include kinetics of product formation, computational studies, and stoichiometric reactions of putative intermediates and model compounds.[35] Scheme 4-1 shows the generally accepted steps in the catalytic cycle for ketone hydrogenations. The distinguishing feature of this mechanism is the proposed metal-ligand assisted bifunctional addition between the carbonyl and the active catalyst. Specifically, the hydridic hydrogen on Ru, and the protic hydrogen on nitrogen add to the carbon and oxygen of the carbonyl via a six-membered, pericyclic transition state without pre-coordination of the ketone to the Ru centre (Scheme 4-1, TS1). An alcohol-assisted variant

of this mechanism is proposed to occur in the presence of alcohol solvent or product (Scheme 4-1, TS2).[35c,45] The direct products of the proposed addition are a Ru-amide and the alcohol. The Ru-amide is then proposed to add dihydrogen through a four membered transition state (TS3) to regenerate the dihydride active catalyst. A variant of this addition involves an alcohol-assisted pathway via a six-membered transition state (TS4).[45,112] The details of these steps are proposed based upon gas-phase DFT calculations using model compounds such as *trans*-[Ru-(PH$_3$)$_2$(H)$_2$(en)] in order to simplify the calculations.[35b,37]

Scheme 4-1. The generally accepted catalytic cycle for Noyori-type ketone hydrogenations.
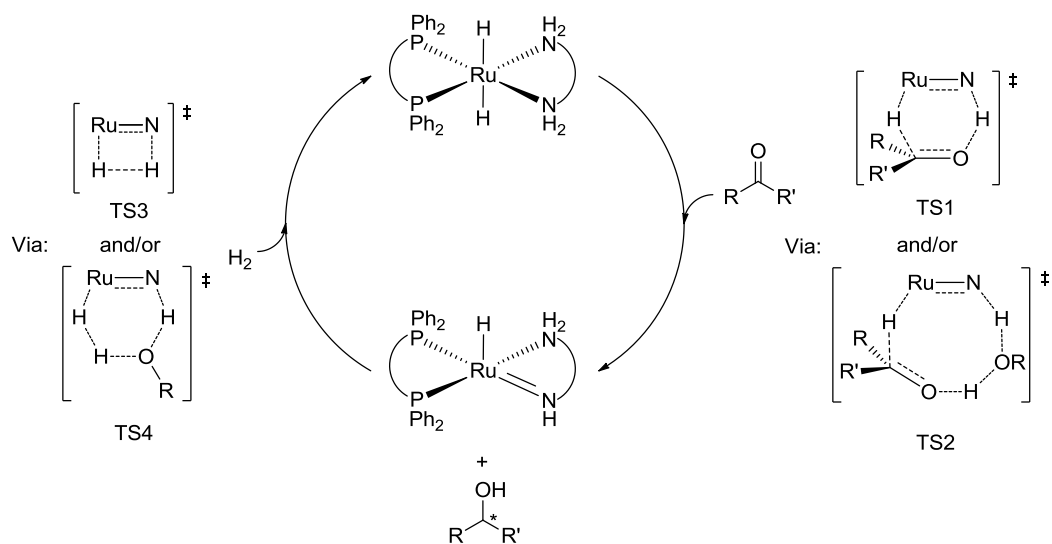
Direct experimental studies of this catalytic cyclic with the actual, proposed catalytic intermediates are rare because the intermediates are usually unstable at room temperature in the absence of substrate or

173

hydrogen, and because the key hydrogen atoms on N and Ru rapidly exchange with deuterated alcohol solvents.[35d] In fact, there are only two direct studies of the bifunctional addition between *trans*-[Ru(diphosphine)-(H)$_2$(diamine)] and ketones.[35a,b,d-f] The first was carried out by Morris et al. using the model dihydride *trans*-[Ru((*R*)-BINAP)(H)$_2$(NH$_2$CMe$_2$CMe$_2$NH$_2$)] (**9**) and acetophenone.[35a,b] These authors reported that the addition between the dihydride **9** and 1 equiv of acetophenone formed the corresponding Ru-amide compound **10** and free 1-phenyl ethanol in C$_6$D$_6$ at room temperature (Equation 4-1).[35a] This result is consistent with the proposed bifunctional, concerted transfer of Ru–H and N–H via a six-membered pericyclic transition state.
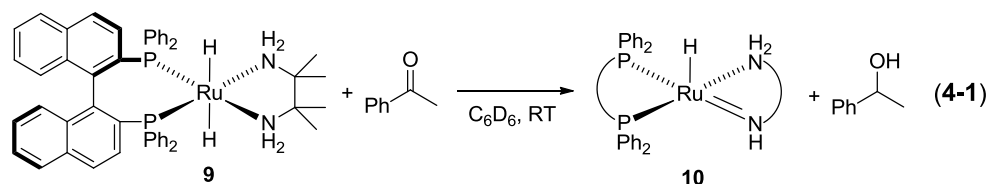
In another study, the Bergens group reported a low temperature preparation of the actual active catalyst *trans*-[Ru((*R*)-BINAP)-(H)$_2$((*R*,*R*)-dpen)] (**6**), and found that the dihydride **6** was remarkably active towards carbonyl reductions in THF.[35f] For example, the stoichiometric reaction between **6** and acetophenone (under ~2 atm H$_2$, in THF-*d$_8$*) was complete on mixing at –80 °C. Unlike the result from the model compound **9** reported by Morris et al., the addition of acetophenone to **6** was extremely rapid, and it formed the Ru-alkoxide **14**, the net product of a ketone-hydride insertion (Equation 4-2).

$$\text{(4-2)}$$
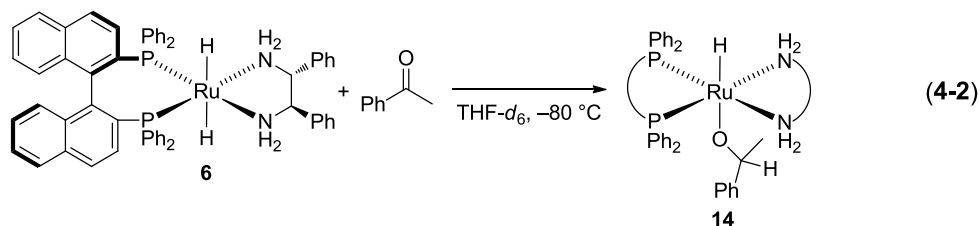
The three major differences between the experiments reported by the groups of Morris and Bergens are the steric and electronic properties of the diamine ligands ($NH_2CMe_2CMe_2NH_2$ vs. (R,R)-dpen), the reaction temperatures (RT vs. –80 °C), and solvents (benzene vs. THF). The most likely explanation of their apparently contradictory results is that the bulkier, more electron rich diamine $NH_2CMe_2CMe_2NH_2$ favours the formation of Ru-amide **10** instead of the corresponding Ru-alkoxide.[109] In other words, increased electron density and steric crowding on Ru would destabilize the Ru-OR bond, and favour the five-coordinate Ru-amide **10**. Comparison between Equations 4-1 and 4-2 suggests higher intrinsic activity of **6** than **9**. However, it is difficult to compare the activity because the activity of **9** at low temperature is not reported.

The electronic effect on the stability of late transition metal alkoxide compounds has been studied intensely by Bergman and co-workers.[89b,c] Generally, electron-withdrawing substituents on the alkoxide ligand stabilize the bond to late transition metal centres. There are two theories that have been put forward to explain this general trend. Bergman proposes that the metal-alkoxide bond has covalent and ionic character, with some negative charge on oxygen.[110] The presence of electron-withdrawing groups on the alkoxide ligand stabilizes this build up

of negative charge. The other theory is the pπ/dπ repulsion theory, in which electron repulsions between the lone pairs of the alkoxide ligand and the filled d orbitals on the metal centre are reduced by the electron-withdrawing groups on the alkoxide.[111] Such pπ/dπ repulsions would also explain why the greater electron-donating ability of the $NH_2CMe_2CMe_2NH_2$ ligand, relative to $NH_2C(H)PhC(H)PhNH_2$, would destabilize the Ru-alkoxide bond.[109]

The higher temperature used by Morris et al. might lead to the formation of Ru-amide **10** and 1-phenylethanol via an intramolecular elimination of the alkoxide and an amine proton from the corresponding Ru-alkoxide **75** (Equation 4-3). In fact, Morris et al. proposed that two diastereomers of the Ru-alkoxide **75** formed upon mixing the dihydride **9** and (S)-1-phenylethanol (90% ee).[35b] It is worth noting that the spectroscopic evidence for **75** was incomplete, with only the hydride peak listed in the ^{1}H NMR data, and two sets of doublets listed in the ^{31}P NMR data. They proposed that the reaction between **9** and (S)-1-phenylethanol proceeds via a pathway that involves hydrogen bonding between the alcohol hydrogen and the hydride ligand.
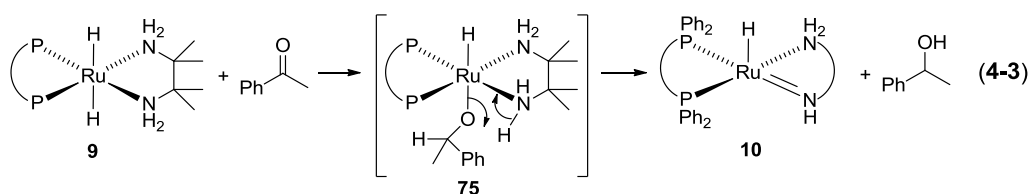
Morris also proposed that the reaction between the amide,

[Ru(PPh$_3$)$_2$(H)(NHCMe$_2$CMe$_2$NH$_2$)] (**76**), and 20 equiv of (*S*)-1-phenylethanol forms an equilibrium mixture of **76**, alcohol adduct **77**, and the corresponding alkoxide **78** via a rapid pre-equilibrium between **76** and **77**, followed by a slow establishment of equilibrium between **77** and **78** to form a 1:1 mixture of **76+77** and **78** (Equation 4-4).[35b] Spectroscopic evidence for **78** was incomplete with no signals from the alkoxide ligand reported in the ^{1}H NMR data.

(4-4)

76 + 77 : **78** = 1:1
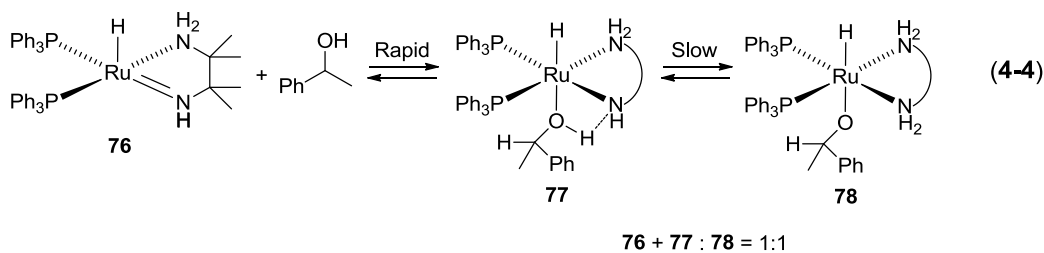
The nature and identity of the solvent will also have an influence on the reaction mechanism. For example, Morris et al. studied the influence of 2-PrOH solvent molecules on the bifunctional addition using gas-phase DFT calculations.[45] Specifically, they studied the model Ru-dihydride complex *trans*-[Ru(PH$_3$)$_2$(H)$_2$(pica)] (**79**) (pica is 2-aminomethylpyridine) as a catalyst for the hydrogenation of acetone. Scheme 4-2 shows the predicted reaction pathways for the addition between **79** and acetone in the presence (paths B and C) and absence (path A) of 2-PrOH. In path A, the addition proceeds via a six-membered, pericyclic transition state. The concerted addition of Ru–H and N–H to acetone forms pseudo-Ru-alkoxide species **80** as the most stable species in the absence of 2-PrOH solvent.

Scheme 4-2. Proposed pathways for the addition between **79** and acetone.
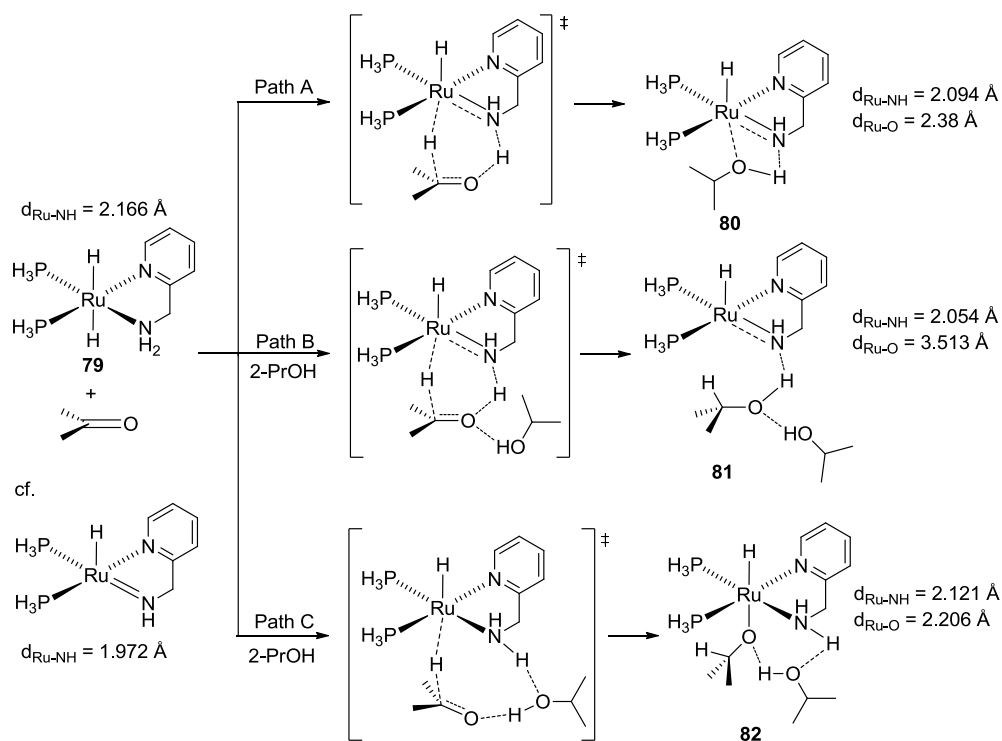
The pseudo-alkoxide **80** contains a hydrogen bond between the product 2-PrOH and the Ru-amide nitrogen. The Ru–NH bond in **80** (2.094 Å) is longer than the corresponding Ru–NH bond of the hydrogen-bond-free Ru-amide (1.972 Å), and shorter than the Ru–NH_2 bond in the dihydride **79** (2.166 Å). This is likely due to the donation of electron density from the Ru-amide nitrogen to the OH group to form the hydrogen bond. The Ru–O distance in **80** was short (2.38 Å) because of the electron deficiency of the Ru centre originating from a hydrogen bond between the Ru-amide nitrogen and product OH group. This Ru–O interaction was not observed in the transition state in these gas phase model calculations.

In path B, the addition proceeds via a six-membered transition state containing a hydrogen bond between the oxygen of acetone and 2-PrOH. The concerted transfer of Ru–H and N–H forms Ru species **81**. The amide derivative **81**, product 2-PrOH, and solvent 2-PrOH are linked via hydrogen bonds as shown in Scheme 4-2. Similar to the Ru species **80**, the Ru–NH bond in **81** (2.054 Å) is longer than the corresponding Ru–NH bond of the hydrogen-bond-free Ru-amide (1.972 Å), and shorter than the Ru–NH$_2$ bond in the dihydride **79** (2.166 Å). This is likely because formation of the hydrogen bond between the Ru-amide nitrogen and the product OH group removes electron density from the amide nitrogen, decreasing the Ru–N double bond character. Unlike path A, there is no interaction between the Ru centre and the product 2-PrOH because both the lone pairs on oxygen are involved in hydrogen bonding.

In path C, the addition proceeds via an eight-membered transition state linked by hydrogen bonds to the solvent. In this path, only the hydride on Ru was transferred to the acetone carbonyl carbon to form the hydrogen-bonded Ru-alkoxide **82** as the most stable species in the presence of 2-PrOH solvent. The Ru–O bond in **82** (2.206 Å) was shorter than that in species **80** (2.38 Å). A possible inner coordination sphere interaction between the Ru centre and the oxygen of acetone was not observed in the transition state of path C. These effects of 2-PrOH solvent predicted by calculations illustrate the large influence that solvent can have on the bifunctional addition. THF solvent, used by Bergens et al., is a better hydrogen bond acceptor than benzene solvent, used by Morris et al..

Combination of the differences in the steric and electronic properties of the diamine ligands, the reaction temperature, and the solvents likely caused the difference between Morris and Bergens' experiments. An additional important finding from Morris and Bergens' direct experimental studies is observation of rapid H_2 activation by the amides **7** and **9** at low temperatures (–80 °C for **7**, –60 °C for **9**) to form the dihydrides **6** and **9**.[35a,d] This result is unexpected because it is believed that the slowest step in the catalytic cycle is the H_2 activation step based upon the activation energies calculated by DFT methods. [35b,37]

The formation of a Ru-alkoxide compound was also reported by Baratta et al. using the Ru–CNN pincer complex $[Ru(PPh_2(CH_2)_4PPh_2)(H)(CNN)]$ (**15**) (see Scheme 4-3 for the structure of the CNN ligand).[38]

Scheme 4-3. Proposed reaction mechanism for the formation of Ru-alkoxide **16**.
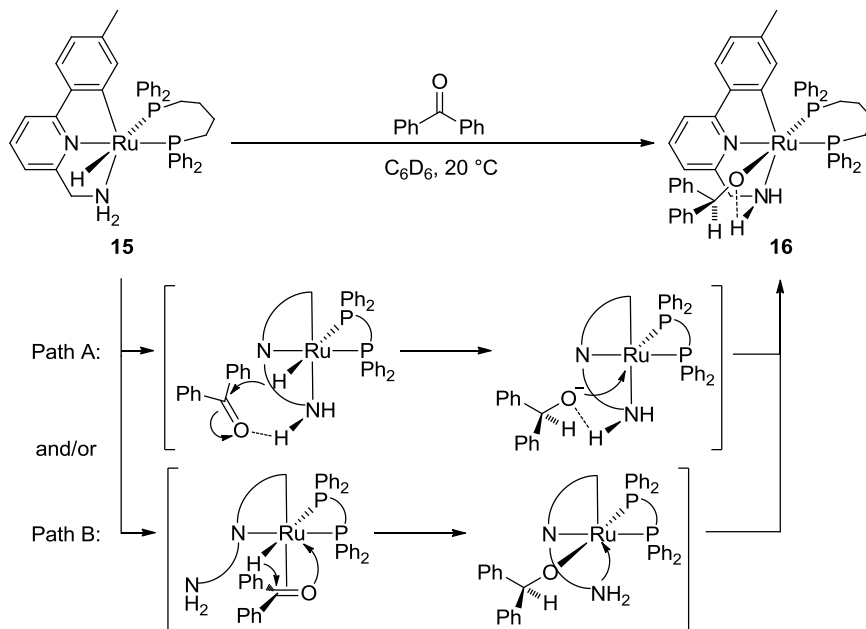
Compound **15** reacted with 1 equiv of benzophenone at 20 °C in C_6D_6 to form the Ru-alkoxide **16**. It was proposed that **16** contains a hydrogen bond between the alkoxide oxygen atom and one NH group because one NH signal in the ^{1}H NMR spectrum is shifted downfield relative to the other NH signal. The authors proposed that the alkoxide **16** formed via a mechanism that begins with formation of a hydrogen bond between the NH_2 group on the catalyst and the oxygen of benzophenone, which activates the carbonyl group towards the nucleophilic attack. Nucleophilic attack by Ru–H on the benzophenone carbonyl carbon to form an alkoxide anion that remains hydrogen-bonded to the NH_2 group, and then followed by migration of the alkoxide anion to the Ru centre (Scheme

4-3, path A). The authors did not explain why the second and third steps were not part of a concerted step, although in principle, electron deficiency is formed on Ru simultaneously with transfer of the hydride.

Another possible pathway for the formation of **16** involves dissociation of an NH_2 group to form a vacant coordination site on Ru. The η^1- or η^2-coordination of benzophenone to the vacant coordination site followed by hydride addition via an inner coordination sphere mechanism forms the Ru-alkoxide **16** (Scheme 4-3, path B). The analogue of the path B is proposed by Milstein et al. for the mechanism of ester hydrogenation catalyzed by Ru-PNN pincer complex (Chapter 1, Scheme 1-12).[55]

Scheme 4-4. Possible mechanisms for the formation of Ru-alkoxide **14**.
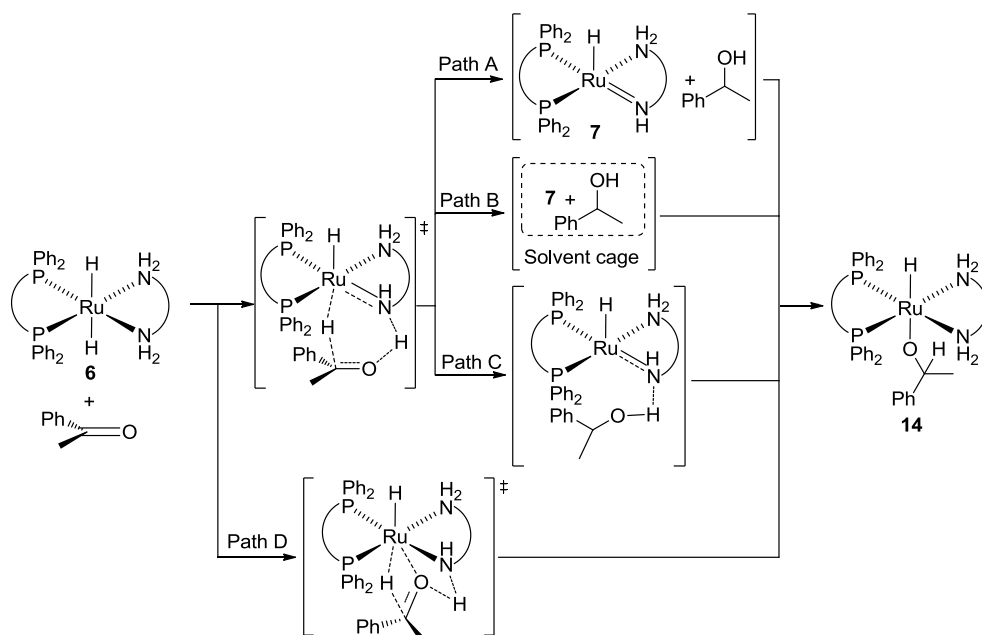
The four most likely reaction pathways for the formation of **14** are shown in Scheme 4-4. Paths A–C are classified as the outer coordination

sphere mechanisms because the ketone does not coordinate to Ru during the addition, and proceed via the conventional six-membered pericyclic transition state for the bifunctional addition. Path D is classified as an inner coordination sphere mechanism because partial coordination of the ketone to Ru occurs during the addition. Path A is the most widely accepted pathway for hydrogenation/transfer hydrogenations using catalysts such as *trans*-[Ru(diphosphine)(X)$_2$(diamine)],[35a-c,37]

RuH(arene)(XCH$_2$CH$_2$NH$_2$),[39,40] Shvo's,[41] and the RuCp*(P–N)[112] systems discussed in Chapter 1. Path A forms the Ru-amide **7** and free product alcohol. Paths B and C are variations of path A that were proposed by Casey et al. for the imine hydrogenation catalyzed by Shvo's catalyst.[41b-g] These paths form the Ru-amide **7** and the product alcohol either in a solvent cage with a weak hydrogen bond between the alcohol and the amide nitrogen, (path B), or as a hydrogen-bonded species (path C). The Ru-amide and the product alcohol in paths A through C then react to form the Ru-alkoxide. Path D, in contrast, forms the Ru-alkoxide in a concerted manner without formation of the Ru-amide. The Ru–amide bond in the hydrogen-bonded species (path C) would have reduced Ru=N double bond character because of partial electron donation from amide nitrogen to the product alcohol OH as observed in Scheme 4-2. This hydrogen bonded species would not be an 18 electron compound because of the reduced double bond character of the Ru-amide bond. Thus, path C would proceed in a concerted manner similar to path D forming the Ru-alkoxide **14**.

Analogues of path D have been studied previously for electrophilic insertion reactions of unsaturated bonds into metal–alkyl and metal–hydride bonds.[113,114] Addition of the dihydride **6** and acetophenone to form the alkoxide **14** is formally electrophilic insertion of a carbonyl C=O bond into a Ru–H bond of 18 electron species **6**. It is not migratory insertion because coordination of ketone substrate by substitution of diamine or diphosphine ligands at –80 °C is unlikely. In general, there are two types of reaction mechanisms for the electrophilic insertion reaction between an electrophile (E) and a metal–ligand (M–L) bond of a coordinatively saturated 18 electron species.[93] One type is an S_E2 mechanism (Scheme 4-5, (a)) via 1) electrophilic attack of a non-coordinated electrophile to the ligand to form an electrophile–ligand (E–L) bond, 2) subsequent dissociation of E–L complex from metal centre 3) re-coordination of E–L complex to form 18 electron M–E–L complex. In the S_E2 mechanism, an electrophile inserts into a metal–alkyl bond with inversion of stereoconfiguration at the carbon centre of the alkyl ligand. The other mechanism is a concerted mechanism (Scheme 4-5, (b)) where insertion of an electrophile and dissociation of ligand proceed in a concerted manner to form the M–E–L complex. In this case, an insertion into the metal–alkyl bond proceeds via retention of stereoconfiguration at the carbon centre of the alkyl ligand.

Scheme 4-5. General mechanisms for electrophilic insertion reaction.
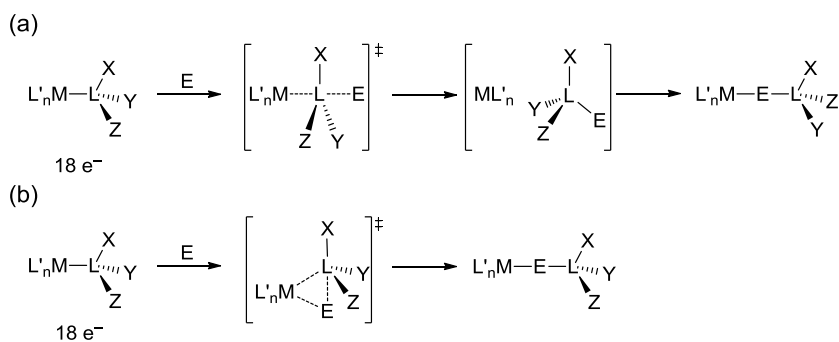
Two of the most extensively studied electrophilic insertion reactions of 18 electron species involve insertion of SO_2[113] and CO_2[114] into metal-alkyl, and metal-hydride bonds. The reaction mechanism of electrophilic insertion of SO_2 into a metal–alkyl bond was studied extensively by several research groups.[113] For example, Whitesides et al. investigated stereochemistry of this reaction using an iron complex, **83**, that has a *threo*-alkyl ligand.[113a] They reported that the *erythro*-sulfinate, **84**, was obtained upon insertion of SO_2 (Equation 4-5). The same stereochemical outcome was also observed for SO_2 insertion of *cis*-[Mn(PEt$_3$)(CO)$_4$(*threo*-PhCHDCHD)], and W(η^5-C$_5$H$_5$)(CO)$_3$(*threo*-PhCHDCHD).[113c] Additionally, the rate of SO_2 insertion was independent of CO pressure. Thus, a migratory insertion pathway via dissociation of CO is not likely. Based on these stereochemical investigations and kinetic experiments, an S_E2 mechanism was proposed for the SO_2 insertion reaction.

$$(4\text{-}5)$$
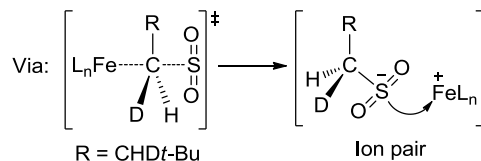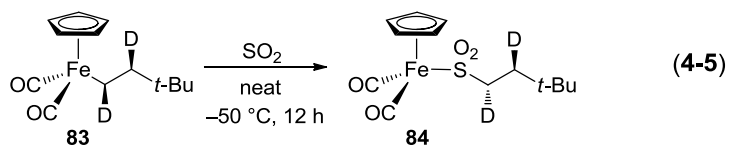
Darensbourg et al. investigated the reaction mechanism of electrophilic insertion of CO_2 into the tungsten–alkyl bond of an anionic tungsten complex **85**.[114a-b] In this case, stereochemical analysis showed retention of stereoconfiguration at the carbon centre upon the insertion. Additionally, the rate of CO_2 insertion was independent of CO pressure. Based on these results and kinetic experiments, the authors proposed a concerted mechanism (Equation 4-6). An analogous concerted mechanism is also proposed for the Ru(phosphine)$_4$(X)(Y) (X, Y = H, Cl, OAc) catalyzed CO_2 hydrogenation,[114f-h] and CO_2 insertion reaction of *fac*-[Re(bipy)(CO)$_3$- (H)] (bipy is 2,2'-bipyridine).[114e] However it is difficult to distinguish between S_E2 and concerted mechanisms in these cases since stereochemical analysis is unavailable.

$$(4\text{-}6)$$
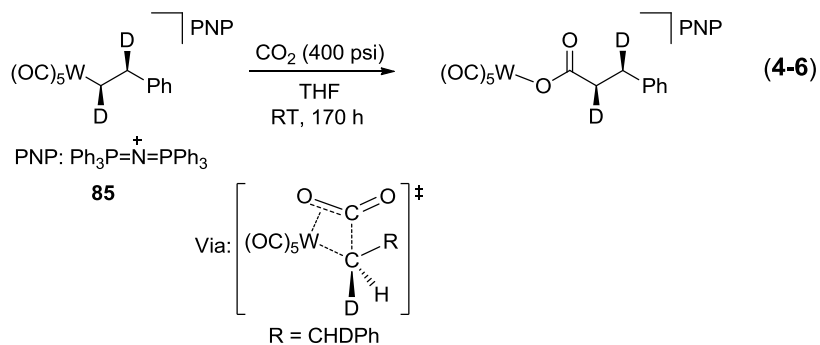
Further, Darensbourg et al. reported that the W-hydride *cis*-PNP[W(CO)$_4$(P(OMe)$_3$)(H)] (**86**) (see Equation 4-7 for the structure of PNP) reacts with aldehydes stoichiometrically to form the corresponding W-alkoxides.[114c,d] For example, the W-hydride **86** reacts with benzaldehyde instantaneously at RT to form the corresponding W-alkoxide, PNP[W(CO)$_4$(P(OMe)$_3$)(OCH$_2$Ph)] (**87**). Addition of 1 equiv of acetic acid to a solution of alkoxide **87** formed benzyl alcohol (Equation 4-7). The insertion did not proceed with ketones unless 1 equiv of acid was added. A proposed effect of acid is activation of ketones towards electrophilic insertion by protonation of the carbonyl oxygen. The mechanism of aldehyde and ketone insertion is similar to that of CO$_2$ insertion in Equation 4-6 because the reaction under CO pressure did not retard the rate. Thus it is possible that the coordinatively saturated Ru-dihydride **6** and acetophenone form the Ru-alkoxide **14** in a similar concerted manner with a Ru–oxygen interaction during the insertion. Path D in Scheme 4-4 represents such concerted mechanisms.
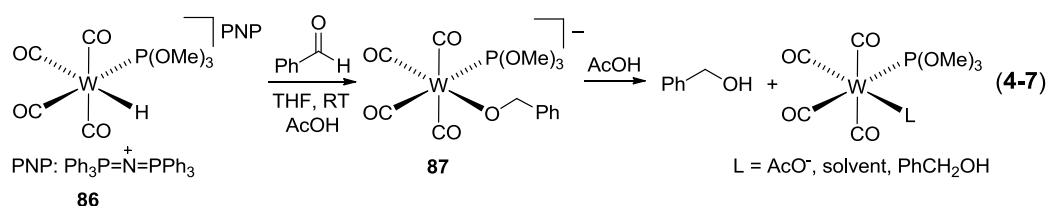
Casey and Bäckvall have investigated bifunctional additions similar to paths A through D as part of the mechanism of imine hydrogenations catalyzed by Shvo's catalysts.[41,42] The focus of their investigation is the

formation of Ru(0)-amine complexes such as **88** as the product of the bifunctional addition between imines and Shvo's catalysts. The formation of **88** could be explained using paths A through D as shown in Scheme 4-6. Paths A through C are outer coordination sphere mechanisms that proceed via the concerted transfer of the hydridic Ru–H and the protic O–H to the imine carbon and nitrogen atoms respectively. Pathway D is an inner coordination sphere mechanism wherein the imine substrate coordinates to the 16 electron, Ru-η^3-Cp complex before subsequent insertion into the Ru-hydride bond. Path A forms a 16 electron Ru(0) species **20** and the product amine. Paths B and C are variations of path A where the 16 electron species **20** and the product amine exist either in a solvent cage (path B), or as a hydrogen bonded species (path C).

Scheme 4-6. Possible mechanisms for the formation of Ru-amine complex **88**.
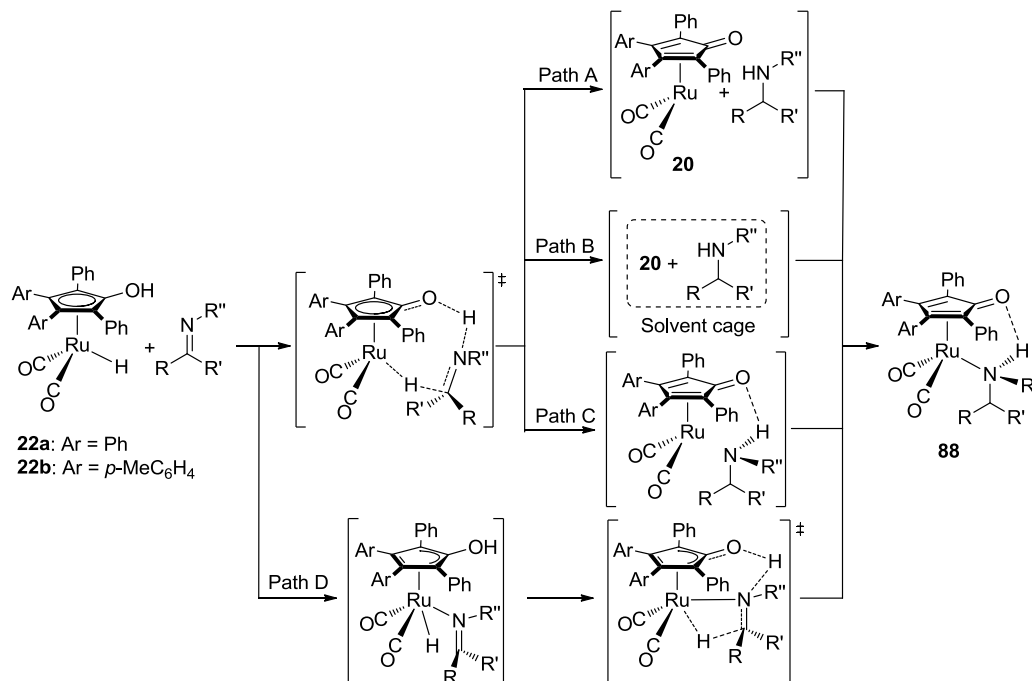
The mixture of **20** and the product amine formed by paths A through C then reacts to form the 18 electron Ru-amine complex **88**. In contrast, Path D does not proceed via the 16 electron species **20**. Note, path D in Schemes 4-4 and 4-6 are not exactly parallel mechanisms because path D in Scheme 4-6 is the classical inner coordination sphere mechanism whereas path D in Scheme 4-4 is not. The concerted reaction mechanism that corresponds to path D in Scheme 4-4 is not proposed for Shvo's system. Casey and Bäckval reported inter- and intramolecular trapping experiments to distinguish between pathways A through D.

The intermolecular experiment carried out by Bäckvall et al. is shown in Equation 4-8.[42e] The reaction between the Ru-hydride **22a** and

the imine **24** in the presence of the intermolecular trapping amine **25** formed the Ru-amine complex of the product amine **26** quantitatively. This result supports paths B through D because if the addition between the Ru-hydride **22a** and the imine **24** proceeds via path A, the 16 electron species **20a** should be trapped by both the product amine and the trapping amine **25**. Similar results were also reported by Casey et al. using the reduction of MeN=CHPh in the presence of isopropylamine, or the reduction of PhN=CHPh in the presence of aniline.[41d] Both experiments showed formation of the Ru-product amine complexes in >95% yield in the temperature range between –60 and 0 °C.
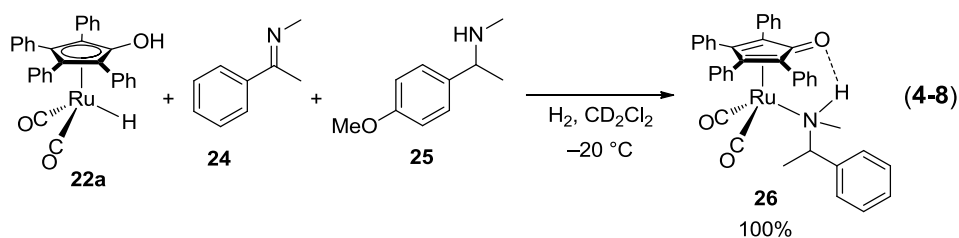
Intramolecular trapping experiments were carried out to distinguish between paths B and C or D. If path B is operative, the 16 electron species **20**a will be trapped by both the intramolecular trap and by the product amine group due to molecular tumbling within the solvent cage. Conversely, if path C operates, **20a** will be trapped only by the product amine because molecular tumbling within the cage would be restricted by the strong hydrogen bond. Similarly, pathway D forms only the product Ru-amine complex because the coordination between Ru and the imine nitrogen does not break during the addition. Casey and Bäckvall used imines with

190

the trapping amine functionality within the same molecule as an intramolecular trap. Such an intramolecular trapping experiment was first reported by Casey et al. with the reaction between the imine **89a** and Shvo's catalyst **22b**.[41d] The authors reported formation of the product and the trapped Ru-amine complexes **90a** and **91a** in a 1:1 ratio (Equation 4-9).
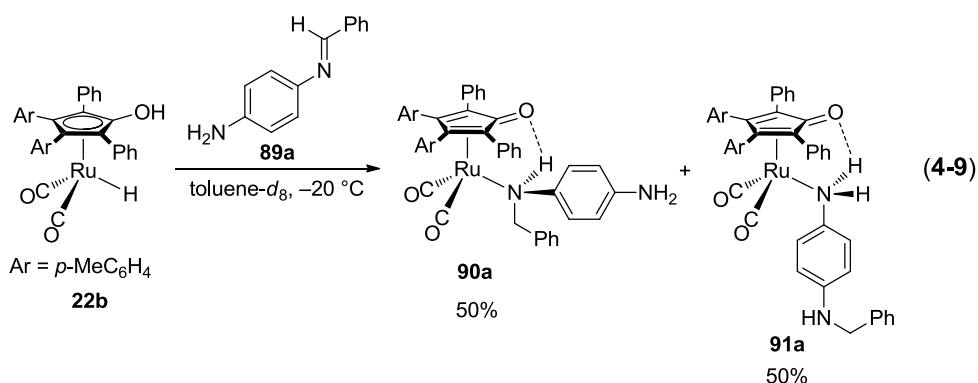
In a control experiment, Casey observed that a dimer of the 16 electron intermediates **20b** reacted with 2 equiv of the product diamine **92a** to form the Ru-amine complexes **90a** and **91a** in a 1:3 ratio (Equation 4-10).
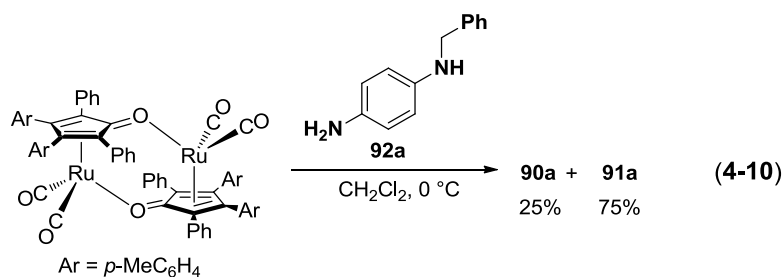
Thus, if the addition between **22b** and the imine **89a** forms the product diamine **91a** and the 16 electron species **20b** without any interaction between each other, the Ru-amine complexes **90a** and **91a**

should form in about a 1:3 ratio. Casey et al. explained the observed formation of **90a** and **91a** in a 1:1 ratio (Equation 4-9) using the outer coordination sphere mechanism. They explained that the larger amount of the product Ru-amine complex **90a** indicates the solvent cage mechanism with a weak hydrogen bond between **92a** and the 16 electron species **20b**, that is, path B. Conversely Bäckvall et al. explained Casey's observation as an intramolecular exchange reaction between Ru-amine complex **90a** and **91a** via slippage of the π-system, and concluded that these results do not differentiate between the outer and inner coordination mechanisms. To eliminate the possible intramolecular exchange via π-slippage, Bäckvall carried out an intramolecular trapping experiment using the imine **89b**.[42f] The addition between the Ru-hydride **22a** and the imine **89b** formed only the Ru-amine complex **90b** as a cis/trans mixture between –80 and –8 °C (Equation 4-11).
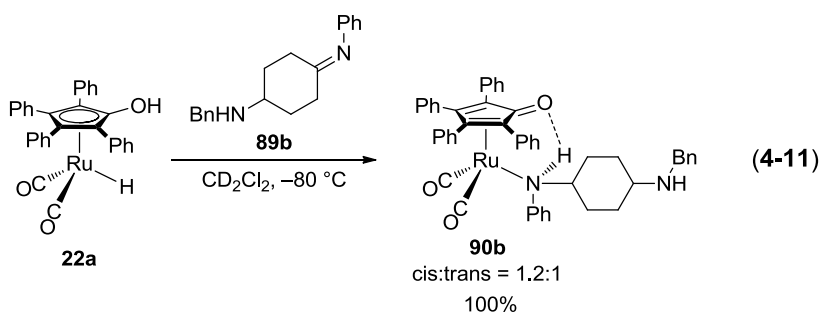
In a control experiment, Bäckvall et al. observed that the reaction between the dimer of **20a** and the product diamine **92b** formed a mixture of cis/trans isomers of the Ru-amine complex **91b** as the sole detectable products (Equation 4-12). The selective formation of **91b** is likely because

the benzylamine side of the intramolecular trapping agent is more basic

than the aniline side. Thus, if the 16 electron species **20a** and **92b** forms as

free products, or in a solvent cage with a weak hydrogen bond, the trapped

Ru-amine species **91b** should form as the major product. The exclusive

formation of **90b** in Equation 4-11 thus indicates reaction paths C or D

operate as shown in Scheme 4-6.
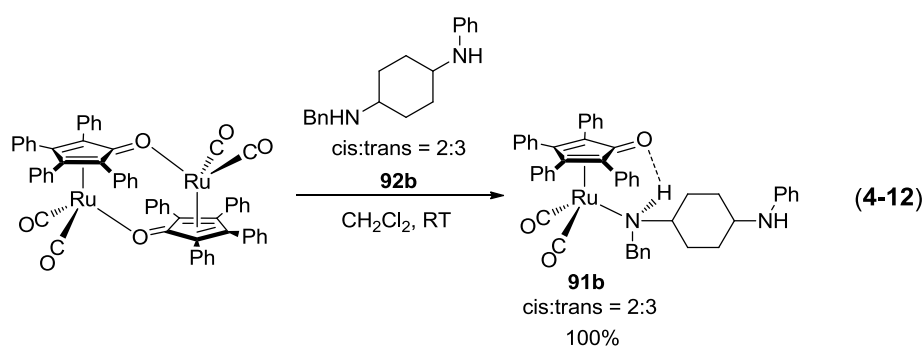
Bäckvall interpreted these results as evidence for the inner coordination

sphere mechanism, path D. In contrast, Casey explained these results

using the outer coordination sphere mechanism with a strong hydrogen

bond between the **20a** and the aryl amine side of diamine **92a**, path C.

Specifically, the aryl amine group would hydrogen bond more strongly to

the oxygen than the alkyl amine side, preventing exchange. Casey et al.

then carried out a similar intramolecular trapping experiment using imine

89c.[41f] In the case of **89c**, both amines in the reduced product are now

expected to hydrogen bond equally to the oxygen in **20b**. The reaction

between **22b** and **89c**, at temperatures ranging between –45 and 0 °C,

formed a mixture of the cis/trans isomers of the Ru-amine complexes **90c**

and **91c** in an 85:15 ratio (Equation 4-13). A significant change in this ratio was not observed until the solution was heated at 50 °C for 4 h, showing that intramolecular exchange between **90c** and **91c** in the temperature range between –45 and 0 °C does not occur, and cannot explain the product ratio. Based upon these observations, Casey insisted that the outer coordination sphere mechanism with a hydrogen bond between the 16 electron species **20b** and the product diamine **92c**, path C in Scheme 4-6, was in operation for the addition. This mechanism explains all three results from the intramolecular trapping experiments. Thus, if the hydrogen bond between **20b** and the diamine product is weak, more **20b** is trapped by the trapping side of the product diamine (Equations 4-9 and 4-13). If the hydrogen bond is strong, only the product side of the diamine is trapped by **20b** (Equation 4-11).
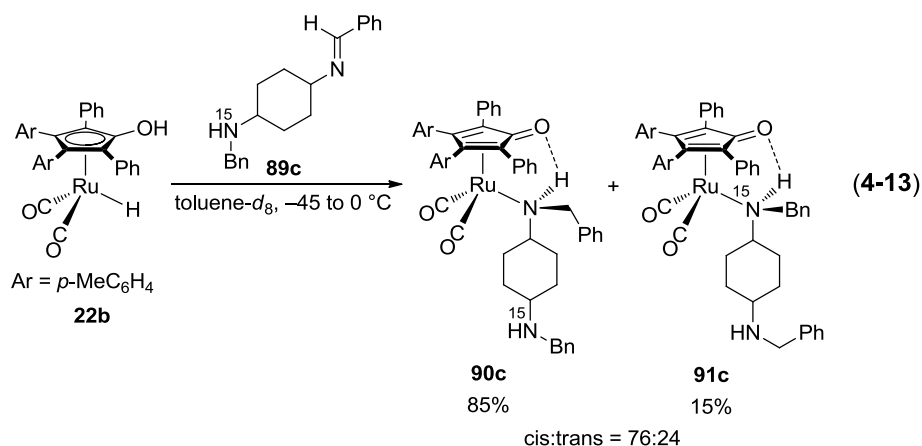
The result shown in Equation 4-13 is thus best explained by the outer coordination sphere mechanism with a strong hydrogen bond (path C, Scheme 4-6). However, it is also possible that the observed formation of

85% of **90c** is partially due to the inner coordination sphere mechanism. In other words, Casey's results do not rule out a parallel, direct pathway. A simple comparison of reaction mechanisms of Shvo's system discussed above and Noyori's system based upon these trapping experiments is not appropriate because catalysts structure and activity is very different, and more importantly reduction/oxidation of the Ru centre does not occur in Noyori's system.

In the case of formation of the Ru-alkoxide **14** from the addition of the Ru-dihydride **6** and acetophenone, Hamilton and Bergens reported intermolecular trapping experiments using 2-PrOH as the trapping agent (Equation 4-14).[35f] 2-PrOH was chosen because the reaction of Ru-amide **7** and 2-PrOH rapidly forms the Ru-2-propoxide compound **12** at −80 °C.[35e] Thus, if the addition proceeds via path A, the free Ru-amide **7** formed will be trapped by 2-PrOH. The addition between Ru-dihydride **6** and acetophenone at −80 °C in the presence of ~5 equiv of 2-PrOH formed **14** as the sole product. In a control experiment, addition between the Ru-amide **7** and a mixture of 5 equiv of 2-PrOH and 1 equiv of 1-phenylethanol resulted in the formation of **14** and Ru-2-propoxide **12** as a ~1:1 mixture. Thus, the exclusive formation of **14** from **6** and acetophenone proved that path A is not operative at −80 °C.

Ph$_2$ H H$_2$
P,,,,, N
Ru
P N
Ph$_2$ H H$_2$
6

+

O
Ph
(1 equiv)

+

OH
(~5 equiv)

$\xrightarrow{\text{THF-}d_8,\ -80\ ^\circ\text{C}}$

Ph$_2$ H H$_2$
P,,,,, N
Ru
P O H N
Ph$_2$ H$_2$
Ph
100%
14

(4-14)
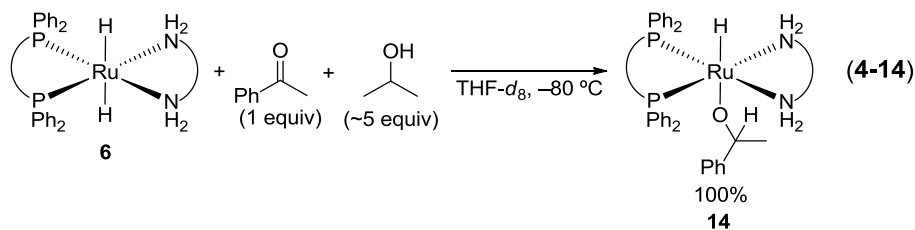
This chapter discusses intramolecular trapping experiments that were carried out in order to distinguish between paths B through D for the formation of Ru-alkoxide **14**. A carbonyl compound modeled by **93** with a trapping hydroxy functionality as an intramolecular trap was utilized for this purpose (Scheme 4-7). If the addition proceeds via path B, a mixture of the product Ru-alkoxide **94** and the trapped Ru-alkoxide **95** will form due to molecular tumbling within the solvent cage. Conversely, if the addition proceeds via path C or D, only **94** will form as long as hydrogen bonding between Ru-amide **7** and a product alcohol is strong enough to prevent tumbling of the product alcohol.

This chapter discusses the first such intramolecular trapping experiments for the Noyori hydrogenation using hydroxy carbonyl compounds to elucidate the reaction mechanism of the Ru-alkoxide formation. The intramolecular trapping agents utilized for this study are shown in Figure 4-1.

Scheme 4-7. Intermolecular trapping experiments to distinguish between paths B and C or D.
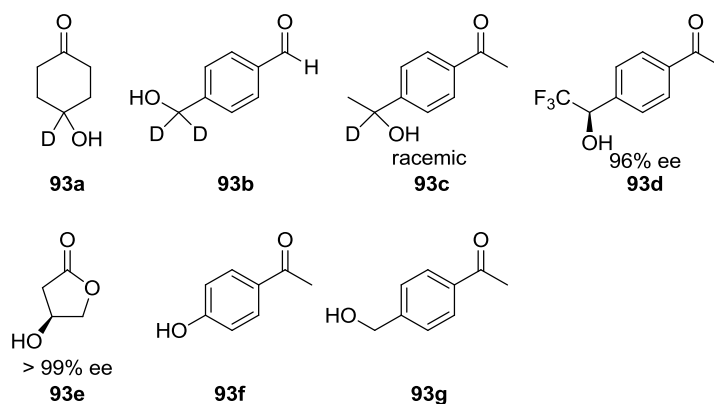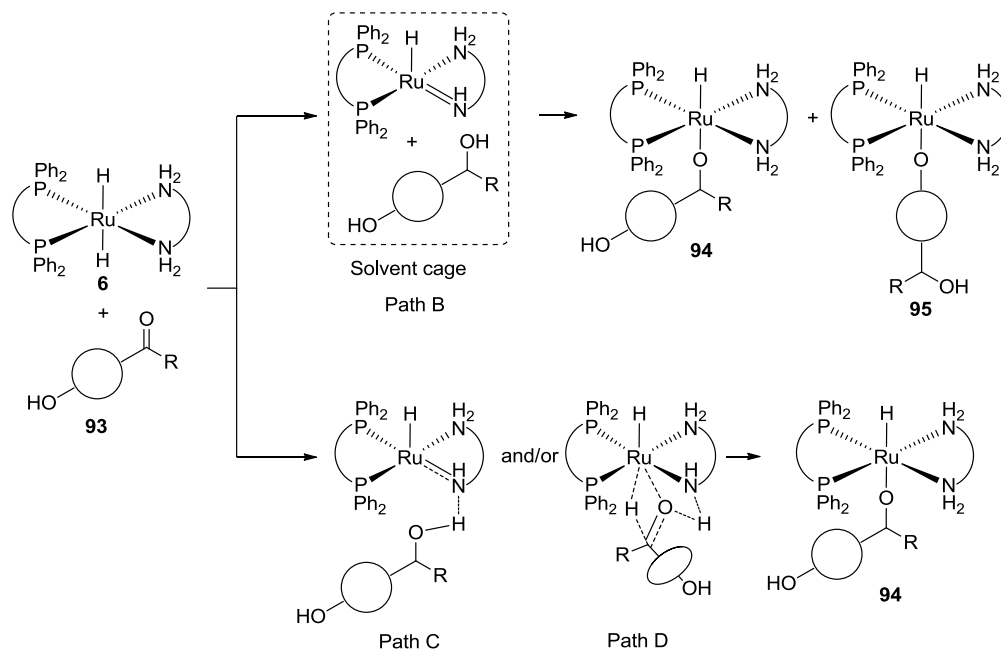
Figure 4-1. Structures of the Intramolecular trapping carbonyl compounds utilized in Chapter 4.

197

Results and discussion

We prepared solutions of Ru-dihydride **6** for this study by reacting mixtures of the cationic dihydrogen compound **5** with 0.7 – 1 equiv of KN(Si(CH$_3$)$_3$)$_2$ and H$_2$ (~2 atm) at −78 °C in THF-d_8 in an NMR tube.[35e] Less than 1 equiv of KN(Si(CH$_3$)$_3$)$_2$ was used to avoid the presence of excess base after the preparation. An excess of base was avoided to prevent the base-assisted elimination of alkoxide from the Ru-alkoxide products of the bifunctional addition between **6** and the intramolecular alcohol–carbonyl trapping reagents. Such base-assisted eliminations are rapid, even at –78 °C, and they would erase the kinetic regiochemistry of the bifunctional addition.[35e] Hamilton et al. reported a base-assisted elimination from the Ru-2-propoxide compound **12** using 1 equiv of KO*t*-Bu as base in THF at −78 °C. The yield of **6** was ~85% when prepared under these conditions using <1 equiv of KN(Si(CH$_3$)$_3$)$_2$. The remaining Ru species consists of small amounts of decomposition side-products that form during the steps required to prepare **6**, and the Ru-hydroxide compound **43** formed from trace amounts of water.[35e] The trace water likely accumulated during the numerous weighing, hydrogenation, and transfer steps involved in the preparation of **6**.

For the intramolecular trapping experiments in this chapter, layers of frozen THF-d_8 solutions of the intramolecular trapping agent (top) and the dihydride **6** (bottom) were thawed and mixed at –80 °C in a pre-cooled NMR probe. More specifically, a solution of **6** in THF-d_8 was prepared first, and characterized by NMR. This solution was frozen by immersing the

NMR tube in liquid nitrogen. A THF-d_8 layer containing 1 equiv (relative to the amount of **6** in the bottom layer determined by NMR) of the carbonyl-alcohol intramolecular trapping agent was placed on top of the bottom layer, and also quickly frozen by liquid nitrogen. The tube was transferred (without thawing) to a NMR probe pre-cooled to –80°C, and NMR spectra were recorded as soon as possible after the layers thawed, as indicated by increase in the lock signal.

A series of intramolecular trapping agents were prepared and screened to find a suitable candidate. The deuterium and fluorine labelled carbonyl-alcohols **93a–d** were studied first. The trapping agent **93a** is the ketone analogue of the imine-amine **90c** utilized by Casey to study Shvo's system (Equation 4-13). The trapping agent **93b** is an aldehyde-primary alcohol trapping system whereas **93c** (racemic) and **93d** are chiral, ketone-secondary alcohol traps. The ee of the trifluoro-substituted trap **93d**¸ was 96 %. This species was prepared by hydrogenation of a trifluoromethyl ketone precursor using Noyori's catalyst system. The absolute configuration was thereby the same as would be formed by the bifunctional addition. Consistent with the high activity of **6** towards the reduction of ketones and aldehydes, all of the trapping agents **93a–d** underwent the bifunctional addition instantaneously with the Ru-dihydride **6** upon thawing at –80 °C to form the corresponding Ru-alkoxide species with hydride signals at ~ –17 ppm. It proved, however, impossible to determine the ratios of the corresponding product alkoxide **94** and the

trapped alkoxide **95** because of overlapping of broad signals in the ^{1}H, ^{2}H, and ^{19}F NMR (**93d**) spectra of the products.

Interestingly, reaction between the hydroxy-lactone trapping agent **93e** (99 % ee) and **6** resulted in exclusive formation of the Ru-alkoxide **96e** and H$_2$ as soon as the solution was thawed (Equation 4-15). **96e** was characterized by ^{1}H, ^{31}P, ^{1}H–^{13}C gHSQC, and ^{1}H–^{1}H gCOSY NMR experiments.

$$(4\text{-}15)$$
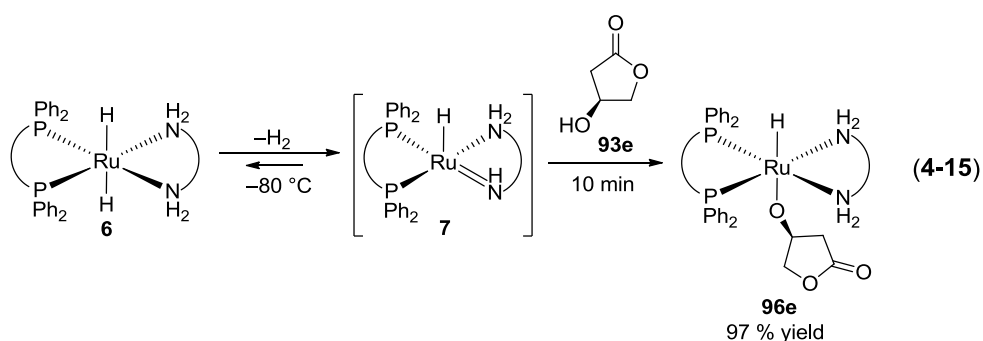
It is likely that **96e** formed via a reversible formation of the Ru-amide **7** from elimination of hydrogen from **6**, followed by reaction of the amide **7** with the hydroxy group in **93e**. The reversible addition of H$_2$ to form **6** from the amide **7** at –80 °C was previously demonstrated by the Bergens group using H$_2$/D$_2$ exchange experiments.[35d] Although the addition is reversible, it strongly favours the dihydride. More specifically, Hamilton et al. reported H-D exchange at the Ru–H and at the axial N–H groups on dpen in **6** upon bubbling D$_2$ (1 atm) through a THF-d_8 solution of **6** at –80 °C. The reactivity of the lactone carbonyl in **93e** towards the bifunctional addition with **6** is lower than that of ketones. This decreased

reactivity at the lactone carbonyl explains why this trapping agent reacted with the amide **7** instead of undergoing the expected bifunctional addition.

In a manner similar to hydroxy-lactone **93e** the phenolic ketone **93f** also reacted with **6** to form the Ru-phenoxide **96f** via reaction with the amide **7** (Equation 4-16). The relatively high acidity of the phenolic OH group in **93f** is the likely cause of the formation of **96f**. The phenoxide **96f** was characterized by ^{1}H, ^{31}P, ^{1}H–^{13}C gHSQC, and ^{1}H–^{1}H gCOSY NMR experiments, and it was independently synthesized by addition of the ketone **96f** to the Ru-amide **7**.
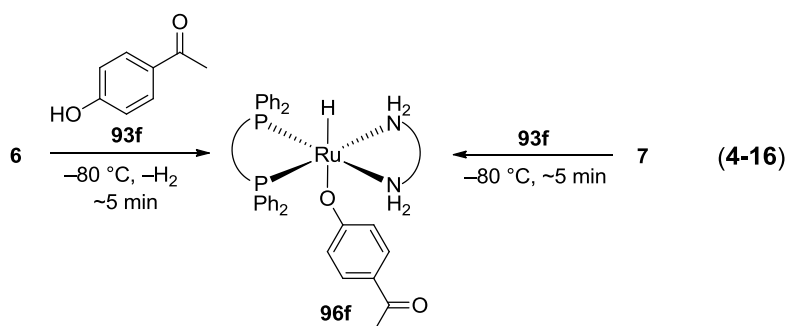
These screening experiments showed that a balance had to be found that favoured the irreversible addition reaction between the dihydride **6** and the carbonyl group in the trapping agent over the reaction between the small amounts of the amide **7**, in equilibrium with **6**, and the hydroxy group. Further, the products had to be unambiguously distinguishable by NMR spectroscopy. It was found that the ketone-primary alcohol trapping agent 4-hydroxymethylacetophenone (**93g**) fulfilled these requirements. The ketone carbonyl in **93g** is more reactive than the lactone carbonyl in **93e**, and the hydroxide in **93g** is less acidic than the the phenolic ketone

93f. The bifunctional addition reaction between the Ru-dihydride **6** and the ketone **93g** proceeded instantaneously upon thawing at –80 °C to form the Ru-alkoxides **96g** and **94g** in 57% and 43% yield respectively (Scheme 4-8). This reaction was carried out a total of four times with the same result.

Scheme 4-8. Reaction of **6** and hydroxy ketone **93g**.
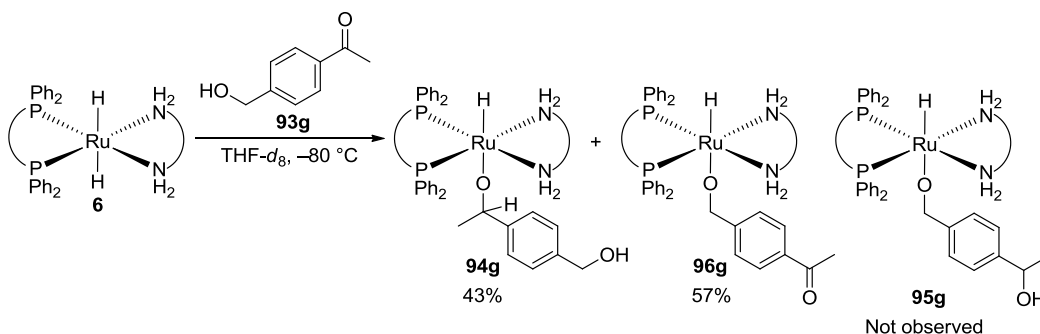
*Most importantly, no formation of trapped alkoxide **95g** was observed.* The alkoxide **96g** formed most likely via the same mechanism discussed for the formation of **96e** and **96f** (Equations 4-15 and 4-16). Thus, **96g** formed via elimination of H_2 from **6** to form the Ru-amide **7** followed by reaction with the alcohol group in unreduced ketone-alcohol **93g**. Despite the rapid nature of the addition of ketone groups to **6**, more than 50% of **6** reacted through addition of the primary alcohol trap in **93g** with the amide **7**. This bias towards alcohol addition is explained by two factors. The first is the relatively high strength of the Ru-primary alkoxide bond in **96g**. This relatively high bond strength, compared to Ru-secondary alkoxide bonds that would form during ketone hydrogenations, contributed

to the product inhibition observed during ester hydrogenations (Chapter 2). The second factor is that primary alcohols are more acidic than secondary alcohols.[68] Note, however, that the formation of **96g** as the major product (53 %) does not impact the mechanism of formation of **94g** (43 %), the product of the addition of the ketone group to **6**. The identities of the Ru-alkoxides **94g**, **95g**, and **96g** were determined unambiguously with ^{1}H, ^{31}P, ^{1}H–^{13}C gHSQC, and ^{1}H–^{1}H gCOSY NMR experiments. The ketone-primary alkoxide **95g** was prepared independently by the reactions between the Ru-amide **7** and **93g** (Equation 4-17).

(4-17)
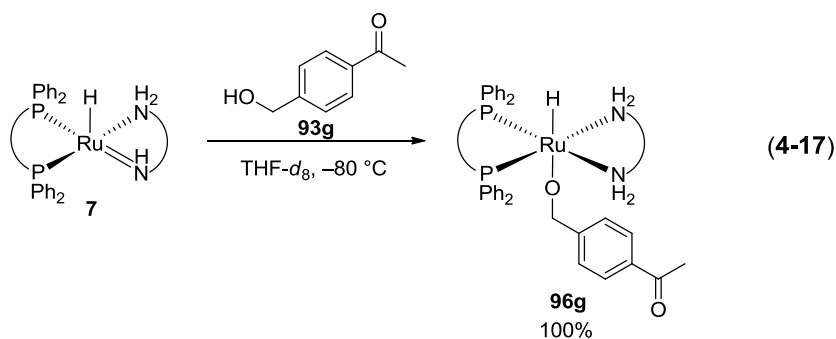
The absence of any primary alkoxide **95g**, the product of intramolecular trapping of the amide **7** by the diol product of ketone reduction **97,** is a startling result. As a control competition experiment, the Ru-amide **7** and 1 equiv of the product diol **97** (97% ee) were combined in THF-d_8 at –80 °C. Enantiomerically enriched **97** was utilized for this experiment in order to prevent complication of analysis due to the formation of two possible diastereomers for both **94g** and **95g**. The absolute configuration of **97** was chosen to match the expected major absolute

configuration that will form upon addition of **6** and **93g** at –80 °C in THF-d_8.
This was accomplished by the catalytic hydrogenation of **93g**. Previously,
the Bergens group reported that the stoichiometric addition between **6** and
acetophenone at –80 °C in THF-d_8 forms (*S*)-(–)-1-phenylethanol in the
same enantioselectivity as the catalytic hydrogenation.[35f] Surprisingly, the
reaction of the amide **7** and the enantioenriched diol **97** at –80 °C in THF-d_8
exclusively formed **95g**, the product of addition of the primary alcohol group,
and the species *not* formed by the bifunctional addition of **93g** to **6**
(Equation 4-18).

(**4-18**)
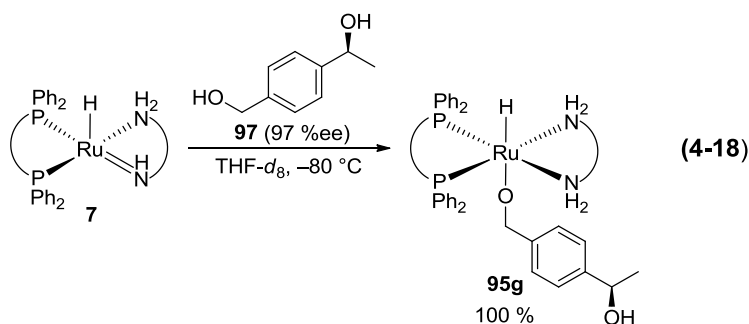
As discussed above, the high selectivity towards the formation of
the primary alkoxide is explained by the higher acidity and lower steric
crowding of the primary alcohol. Thus there exists a strong bias towards
the formation of **95g** over **94g** for this reaction. Therefore, if the free amide
Ru-amide **7** and the diol **97** were formed within a solvent cage during the
bifunctional addition between **6** and **93g** , **95g** should form as a major
product. The exclusive formation of **94g** upon addition between **6** and **93g**,
is strong evidence that the reaction path via the formation of Ru-amide **7**
and **93g** within a solvent cage (Scheme 4-7, path B) is *not* operative during

the hydrogenation of **93g** by **6**. The independent synthesis of **94g** from **7**

and the product diol **97** was not possible due to the exclusive formation of

95g. The methyl ether analogue of **94g**, **Me-94g**, was prepared using

reaction of **7** and the methyl ether, **98** ((*S*)-enantiomer, 87% ee), and was

used to confirm NMR assignments of **94g** (Equation 4-19).

(4-19)

Me-94g
78 % yield
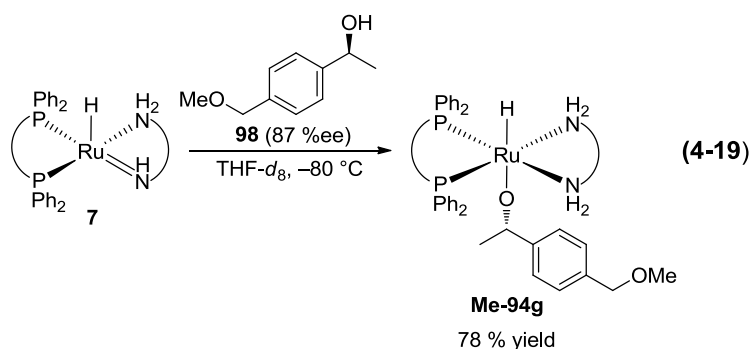
Based on the intramolecular trapping experiments discussed

above and the intermolecular trapping experiment reported previously by

the Bergens group, the most probable reaction mechanisms for the

formation of Ru-alkoxides by the bifunctional addition between the

Ru-dihydride **6** and ketones are either a reaction path via the formation of a

strong hydrogen bond between amido nitrogen in **7** and the product alcohol

(Scheme 4-7, path C), or a reaction path via a concerted formation of the

alkoxide without cleaving a catalyst N–H bond (path D).

Conclusions

In conclusion, this chapter presents the first intramolecular trapping

experiments to elucidate a reaction mechanism for the formation of

Ru-alkoxides in Noyori-type ketone hydrogenations. The addition between

the dihydride **6** and the trapping ketone **93g** at –80 °C formed the product alcohol alkoxide **94g** exclusively. In the competition experiment, the addition between Ru-amide **7** and the product diol **97**, showed exclusive formation of **94g**. These results prove that the solvent cage mechanism containing free amide **7** and product alcohol is not operative during the addition of **6** and **93g**. Thus, the current, most probable mechanisms are either via the formation of a strong hydrogen bond between the amide **7** and a product alcohol (Scheme 4-7, path C), or via the concerted formation of a Ru-alkoxide without N–H bond cleavage (path D). Note that the existence of a strong hydrogen bond between the amido nitrogen and the alcohol product will diminish the N to Ru π donation, generating net coordination unsaturation on Ru. Also, Darensbourg has established precedent for partial Ru–O formation during the electrophilic attack of carbonyl carbon centres on 18 electron metal-hydrides.[114a-d] It is thereby reasonable to propose that partial Ru–oxygen bond formation occurs during the bifunctional addition of ketones to **6** (path D). It is also likely that other catalyst systems and substrates can react by either pathway C or D, and the preference depends upon the particulars of each system.

Experimental

Materials and Methods. Deuterated solvents were obtained from Cambridge Isotope Laboratories, and Aldrich. Common solvents were distilled over appropriate drying reagents. THF-d_8 was distilled over sodium before each experiment. 2-PrOH was distilled over CaH_2. Common chemicals were obtained from Aldrich, TCI America, and Strem, and were

used as received unless stated otherwise. Potassium *tert*-butoxide (KO*t*-Bu) was sublimed before use. (*S*)-3-Hydroxy-γ-butyrolactone (>99% ee) (**93e**) was purchased from TCI America and used as received. 4-Hydroxyacetophenone (**93f**) was purchased from Aldrich, and used as received. Hydrogen gas was ultra high purity grade purchased from Praxair. ^{1}H, ^{2}H, ^{13}C, ^{19}F, and ^{31}P NMR spectra were taken using Varian Inova (300 and 400 MHz), and Varian DirectDrive (500 MHz) spectrometers. ^{1}H, and ^{13}C NMR chemical shifts are reported in parts per million (δ) relative to TMS with the solvent as the internal reference. ^{31}P chemical shifts are reported in parts per million (δ) relative to 85% H_3PO_4 as the external reference. NMR peak assignments were made using ^{1}H–^{1}H gCOSY, and ^{1}H–^{13}C gHSQC NMR experiments. Abbreviations for NMR spectra are s (singlet), d (doublet), t (triplet), q (quartet), dd (doublet of doublet), ddd (doublet of doublet of doublet), dt (doublet of triplet), dq (doublet of quartet), tt (triplet of triplet), m (multiplet), and br (broad). IR spectra were taken using Nic-Plan FTIR microscope, and are reported in wavenumbers (cm^{-1}). High resolution mass spectra were taken using Applied BioSystems Mariner BioSpectrometry Workstation oaTOF mass spectrometer for ESI-MS, and Kratos MS50 with Agilent 6890GC (MS50B) for EI-MS. Elemental analysis data were obtained using Carlo Erba CHNS-O EA1108 elemental analyzer. Optical rotations ($[\alpha]_D^{23}$) were measured using Perkin Elmer 241 polarimeter. Melting points (M.p.) were measured using Perkin Elmer Pyris 1 differential scanning calorimeter. GC analysis was performed using a Hewlett-Packard 5890A gas

chromatograph equipped with a flame ionization detector, a Hewlett-Packard 3392A integrator, and a Supelco β-DEX^{TM} 120 fused silica capillary column (30 m × 0.25 mm i.d. × 0.25 μm film thickness). 20 psi He was used as carrier gas. All ee's were confirmed by comparing the HPLC/GC chromatogram of the hydrogenation product to that of the racemic product prepared by NaBH$_4$ reduction. 4-hydroxymetylacetophenone (**93g**) and (*S*)-(–)-1-(4-hydroxymethylphenyl) ethanol (**97**) are well known in literature, only ^{1}H NMR data, optical rotations, and GC analysis conditions, are reported here.

Preparation of 4-hydroxymetylacetophenone (93g).[115] Under argon, 4-(2-Metyl-1,3-dioxolane-2-yl)-benzaldehyde (392.1 mg, 2.04 mmol)[116], and NaBH$_4$ (498.5, 13.2 mmol) were placed in a 100 mL round bottom flask equipped with a stirring bar. 10 mL of ethanol was then added to the flask at RT. The mixture was stirred for 1h at 60 °C. The reaction was quenched by the addition of 10 mL of 2M HCl at RT. The solution was then extracted with 100 mL of CH$_2$Cl$_2$. The collected organic layer was dried over MgSO$_4$, and concentrated using a rotary evaporator. A yellow solid was obtained upon concentration. The solid was purified by column chromatography (hexanes:ethyl acetate = 2:1, silica gel). A white solid formed upon purification. Yield: 303 mg, 99%. ^{1}H NMR (299.97 MHz, CDCl$_3$, 27.0 °C): δ 2.19 (1H, br, O*H*), 2.59 (3H, s, C*H*$_3$), 4.76 (2H, s, C*H*$_2$), 7.44 (2H, m, aromatic 2C*H*), 7.93 (2H, m, aromatic 2C*H*).

Preparation of (*S*)-(–)-1-(4-hydroxymethylphenyl) ethanol (97).[117] Under argon, **93g** (146.9 mg, 0.978 mmol) and *trans*-[Ru-

208

((*R*)-3,5-xylyl-BINAP)(Cl)$_2$((*R*)-daipen)][86] (9.5 μmol) were placed in a 20 mL Schlenk tube equipped with a stirring bar. Argon in the tube was flushed out by H$_2$. KO*t*-Bu (7.2 mg, 64 μmol) was then added to the tube using 3 mL of 2-PrOH under H$_2$. The mixture was stirred for 16 h at 30 °C under 1 atm of H$_2$. The crude mixture was concentrated using a rotary evaporator. Residual catalyst was removed by column chromatography (hexanes:ethyl acetate = 2:1, silica gel). A white solid was obtained upon purification. Yield: 146 mg, 98%. E.e.: 97%. ^{1}H NMR (299.79 MHz, CDCl$_3$, 27.0 °C): δ 1.49 (3H, d, *J* = 6.4 Hz, C*H*$_3$), 1.74 (2H, br, 2O*H*), 4.67 (2H, s, C*H*$_2$), 4.91 (1H, q, *J* = 6.4 Hz, C*H*), 7.36 (4H, m, aromatic 4C*H*). $[\alpha]_D^{23}$ −37.93 (c = 1.00 g/100 mL of CH$_3$OH, 97% ee). GC analysis conditions: initial oven temperature = 140 °C, held at 140 °C for 20 min, and increased at 0.5 °C/min to 200 °C. Retention times: 59.7 min (minor enantiomer), 60.6 min (major enantiomer).

Preparation of 4-methoxymetylacetophenone.[118] Under argon, KH (30w% in mineral oil, 414 mg, 3.10 mmol) was placed in a 50 mL Schlenk flask equipped with a stirring bar. KH was washed three times with 10 mL of hexanes. 3 mL of THF was then added to the flask. 4-(2-Metyl-1,3-dioxolane-2-yl)-benzyl alcohol (353 mg, 1.82 mmol) was added to the flask at 0 °C using 7 mL of THF. Formation of H$_2$ and white precipitate of the potassium alkoxide were observed as soon as the alcohol was added. The suspension of the salt was stirred for 30 min at 0 °C. CH$_3$I (0.23 mL, 3.69 mmol) was then added dropwise at 0 °C. The resulting suspension was stirred for 30 min at 0 °C. The reaction was quenched by

the addition of 3 mL of 2M HCl at 0 °C. The quenched solution was stirred

for 30 min at 0 °C to RT. The resulting yellow organic layer was extracted

with ether (100 mL), dried over $MgSO_4$, and concentrated using a rotary

evaporator. An orange oil formed. The crude mixture was purified by

column chromatography (hexanes:ethyl acetate = 5:1, silica gel). A

colorless oil was obtained upon purification. Yield: 117.9 mg, 40%. ^{1}H NMR

(499.82 MHz, $CDCl_3$, 27.0 °C): δ 2.60 (3H, s, CH_3), 3.42 (3H, s, OCH_3),

4.52 (2H, s, CH_2), 7.42 (2H, m, aromatic 2CH), 7.94 (2H, m, aromatic 2CH).

^{13}C{^{1}H} NMR (125.69 MHz, $CDCl_3$, 27.0 °C): δ 26.7 (CH_3), 58.5 (OCH_3),

74.1 (CH_2), 127.4 (aromatic CH), 128.5 (aromatic CH), 136.5 (aromatic C),

143.8 (aromatic C), 197.9 (C=C). HRMS (EI$^+$) m/z calcd for $C_{10}H_{12}O_2^+$(M$^+$):

164.08372. Found: 164.08387.

Preparation of (*S*)-(–)-1-(4-Methoxymethylphenyl) ethanol (98).[119]

Under argon, 4-methoxymetylacetophenone (104.9 mg, 0.639 mmol) was

placed in a glass autoclave equipped with a stirring bar using 6 mL of

2-PrOH. Argon in the tube was flushed out by H_2. *trans*-[Ru-

((*R*)-3,5-xylyl-BINAP)(Cl)$_2$((*R*)-daipen)]^{86} (1.8 μmol) in 1 mL of 2-PrOH was

added to the autoclave under H_2. KO*t*-Bu in 1 mL of 2-PrOH was

subsequently added to the autoclave under H_2. The mixture was stirred for

13 h at RT under 4 atm of H_2. The crude mixture was concentrated using a

rotary evaporator. Residual catalyst was removed by column

chromatography (hexanes:ethyl acetate = 5:1, silica gel). A colorless oil

was obtained upon purification. Yield: 102.7 mg, 97%. E.e.: 87%. ^{1}H NMR

(499.82 MHz, $CDCl_3$, 27.0 °C): δ 1.49 (3H, d, *J* = 6.5 Hz, CH_3), 1.86 (1H, d,

J = 3.5 Hz, O*H*), 3.38 (3H, s, OC*H*$_3$), 4.45 (2H, s, C*H*$_2$), 4.90 (1H, dq, *J* =

3.8 and 6.5 Hz, C*H*), 7.34 (4H, m, aromatic 4C*H*). ^{13}C{^{1}H} NMR (125.69

MHz, CDCl$_3$, 27.0 °C): δ 25.2 (*C*H$_3$), 58.1 (O*C*H$_3$), 70.3 (*C*H), 74.5 (*C*H$_2$),

125.5 (aromatic *C*H), 128.0 (aromatic *C*H), 137.5 (aromatic *C*), 145.3

(aromatic *C*). HRMS (EI$^+$) m/z calcd for C$_{10}$H$_{14}$O$_2$$^+$ (M$^+$): 166.09938. Found:

164.09943. $[\alpha]_D^{23}$ −37.63 (c = 0.98 g/100 mL of CHCl$_3$, 87% ee). GC

analysis conditions: initial oven temperature = 70 °C, increased at 1 °C/min

to 140 °C, and held at 140 °C for 60 min. Retention times: 81.0 min (minor

enantiomer), 82.2 min (major enantiomer).

Typical preparation of *trans*-[Ru((*R*)-BINAP)(H)$_2$((*R*,*R*)-dpen)] (6) in

THF-*d*$_8$ in the absence of excess KN(Si(CH$_3$)$_3$)$_2$.[35e] Under argon,

[Ru((*R*)-BINAP)((1-5-*η*)-C$_8$H$_{11}$)]BF$_4$ (0.015 mmol) and THF-*d*$_8$ (0.50 mL)

were placed in a NMR tube. The solution was cooled at 0 °C. Argon in the

tube was removed by H$_2$ (~2 atm). The tube was then shaken ten times

outside the 0 °C bath, and returned to the bath. This process was repeated

nine times. H$_2$ (~2 atm) was replenished three times at 0 °C after each

10×10 shaking. The resulting solution containing [Ru((*R*)-BINAP)-

(H)(THF)$_3$]BF$_4$ was then cooled in a −78 °C dry ice/acetone bath.

(*R*,*R*)-Dpen (0.015 mmol) in THF-*d*$_8$ (0.20 mL) was then added to the tube

at −78 °C under H$_2$ (~2 atm). The tube was shaken for ~5 sec outside the

−78 °C bath, and then returned to the bath. This process was repeated

nine times. The solution was then added to a NMR tube that contained

KN(Si(CH$_3$)$_3$)$_2$ (0.011-0.016 mmol) at −78 °C under H$_2$ (~2 atm). The tube is

shaken for ~5 sec outside the −78 °C bath and then returned to the bath.

This process was repeated nine times. The solution color changed from yellow to red during the addition of $KN(Si(CH_3)_3)_2$. NMR spectra recorded at −80 °C showed formation of the dihydride **6** (52-72%) and Ru-hydroxide compound **43** (28-48%). **43** formed due to trace water in the solution. Presence of **43** indicates the absence of excess $KN(Si(CH_3)_3)_2$.[35f]

Reaction of [*trans*-[Ru((*R*)-BINAP)(H)$_2$((*R*,*R*)-dpen)] (6) with (*S*)-3-Hydroxy-γ-butyrolactone (>99% ee) (93e) at −80 °C in the absence of excess $KN(Si(CH_3)_3)_2$. A solution of **6** (79%) with the hydroxide compound **43** (21%) in THF-d_8 (0.7 mL) in a NMR tube was prepared using $[Ru((R)\text{-BINAP})((1\text{-}5\text{-}\eta)\text{-}C_8H_{11})]BF_4$ (13.7 mg, 0.0149 mmol) and $KN(Si(CH_3)_3)_2$ (3.0 mg, 0.015 mmol), bubbled with N_2 for ~3 min to remove excess H_2, and kept in a liquid N_2 bath. **93e** (1 µL, ~0.010 mmol) was then added to the tube in the liquid N_2 bath under N_2. The frozen solutions were partially thawed in a −78 °C dry ice/acetone bath to prevent sudden accumulation of pressure inside the tube. The sample was then introduced into a NMR probe pre-cooled at −80 °C, and completely thawed inside the probe. The first ^{1}H NMR spectra recorded after ~10 min showed formation of **96e** and H_2. Yield: 97%. The alkoxide **96e** was characterized at −80 °C using ^{1}H, ^{31}P{^{1}H}, COSY and ^{13}C-^{1}H HSQC NMR experiments. ^{1}H NMR (399.95 MHz, THF-d_8, −80 °C): δ −17.7 (1H, br t, J = 23.0 Hz, Ru-H), 2.13 (1H, br, C$_a$HN*H*H), 2.39 (1H, d, J = 16.4 Hz, a α-C*H*$_2$ peak of the lactone ligand), 2.74 (1H, d, J = 13.6 Hz, a α-CH$_2$ peak of the lactone ligand), 3.56 (1H, overlapping with a residual THF-d_8 peak, C$_b$HN*H*H), 4.05 (2H, overlapping C$_a$HNH*H* and C$_b$*H*NHH peak), 4.18 (1H, br, a γ-CH$_2$ peak

of the lactone ligand), 4.23 (1H, br, a γ-CH_2 peak of the lactone ligand), 4.56 (1H, br, C$_b$HNHH), 4.60 (2H, br, overlapping C$_a$HNHH peak and CH peak of the lactone ligand), 6-9 (overlapping peaks, aromatic). ^{13}C{^{1}H} NMR (100.6 MHz, THF-d_8, −80 °C, determined using ^{13}C-^{1}H HSQC): δ 38.8 (α-CH_2), 62.6 (C$_a$HNH$_2$), 67.4 (CH), 69.5 (C$_b$HNH$_2$), 77.7 (γ-CH_2), 120-140 (aromatic). ^{31}P{^{1}H} NMR (161.91 MHz, THF-d_8, −80 °C): δ 66.07 (br d, $^2J_{P-P}$ = 30.5 Hz), 72.68 (d, $^2J_{P-P}$ = 41.4 Hz). See Figures 4-2 to 4-4.

Reaction of [$trans$-[Ru((R)-BINAP)(H)$_2$((R,R)-dpen)] (6) with 4-Hydroxyacetophenone (93f) at −80 °C in the absence of excess KN(Si(CH$_3$)$_3$)$_2$. A solution of **6** (72%) with the hydroxide compound **43** (28%) in THF-d_8 (0.7 mL) in a NMR tube was prepared using [Ru((R)-BINAP)((1-5-η)-C$_8$H$_{11}$)]BF$_4$ (13.8 mg, 0.0150 mmol) and KN(Si(CH$_3$)$_3$)$_2$ (3.0 mg, 0.015 mmol), bubbled with N$_2$ for ~3 min to remove excess H$_2$, and kept in a liquid N$_2$ bath. **93f** (1.5 mg, 0.011 mmol) in THF-d_8 (0.1 mL) was then added to the tube in the liquid N$_2$ bath under N$_2$. The frozen solutions were partially thawed in a −78 °C dry ice/acetone bath to prevent sudden accumulation of pressure inside the tube. The sample was then introduced into a NMR probe pre-cooled at −80 °C, and completely thawed inside the probe. The first ^{1}H NMR spectra recorded after ~3min showed formation of **96f** and H$_2$. Yield: 83%. Identity of **96f** was confirmed by comparing spectra of **96f** prepared independently from [Ru((R)-BINAP)(H)((R,R)-NH(CH(Ph))$_2$NH$_2$)] (**7**) and **93f** (See next section). The alkoxide **96f** was characterized at −80 °C using ^{1}H, ^{31}P{^{1}H}, COSY and ^{13}C-^{1}H HSQC NMR experiments. ^{1}H NMR (399.95 MHz, THF-d_8, −80 °C):

δ −18.7 (1H, t, J = 25.8 Hz, Ru-H), 2.19 (3H, s, CH_3), 2.34 (1H, overlapping with a CH$_3$ peak of unreacted **93f**, C$_a$HNHH), 2.48 (1H, br, C$_b$HNHH), 2.97 (1H, br, C$_a$HNHH), 3.14 (1H, br, C$_a$$H$NHH), 3.80 (1H, br, C$_b$$H$NHH), 4.69 (1H, br, C$_bHNHH$), 6-9 (overlapping peaks, aromatic). ^{13}C{^{1}H} NMR (100.6 MHz, THF-d_8, −80 °C, determined using ^{13}C-^{1}H HSQC): δ 33.0 (*C*H$_3$), 62.6 (*C*$_a$HNH$_2$), 65.7 (*C*$_b$HNH$_2$), 120-140 (aromatic). ^{31}P{^{1}H} NMR (161.91 MHz, THF-d_8, −80 °C): δ 67.66 (d, $^2J_{P–P}$ = 44.4 Hz), 69.21 (d, $^2J_{P–P}$ = 41.9 Hz).

Reaction of [Ru((R)-BINAP)(H)((R,R)-NH(CH(Ph))$_2$NH$_2$)] (7) with 4-hydroxyacetophenone (93f) at −78 °C. A solution of **7** (0.0175 mmol) was prepared in THF-d_8 (0.70 mL) in a NMR tube using KN(Si(CH$_3$)$_3$)$_2$ (7.1 mg, 0.036 mmol) as described previously.[35e] A solution of **93f** (2.7 mg, 0.020 mmol) in THF-d_8 (0.10 mL) was then added to the tube at −78 °C under argon. The solution was mixed by shaking once outside the bath. The sample was then introduced into the NMR probe pre-cooled at −80 °C. ^{1}H, and ^{31}P{^{1}H} NMR spectra showed formation of the alkoxide **96f** (74%) and *trans*-[((R)-BINAP)(H)(OH)((R,R)-dpen)] (36%) due to water in the solution. See Figures 4-5 to 4-7.

Reaction of *trans*-[Ru((R)-BINAP)(H)$_2$((R,R)-dpen)] (6) with 4-hydroxymetylacetophenone (93g) at −80 °C in the absence of excess KN(Si(CH$_3$)$_3$)$_2$. A solution of **6** (71%) with the hydroxide compound **43** (29%) in THF-d_8 (0.7 mL) in a NMR tube was prepared using [Ru((R)-BINAP)((1-5-η)-C$_8$H$_{11}$)]BF$_4$ (14.4 mg, 0.0157 mmol) and KN(Si(CH$_3$)$_3$)$_2$ (3.2 mg, 0.016 mmol), and kept in a liquid N$_2$ bath. A solution of **93g** (1.7 mg, 0.011 mmol, 1 equiv with respect to Ru dihydride) in

THF-d_8 (0.1 mL) was then added to the tube in the liquid N_2 bath under H_2 (~1 atm). The solution of **93g** froze on the upper part of the tube. The frozen solutions were partially thawed in a –78 °C dry ice/acetone bath to prevent sudden accumulation of pressure inside the tube. The sample was then introduced into a NMR probe pre-cooled at –80 °C, and completely thawed inside the probe. ^{1}H and ^{31}P NMR spectra recorded after ~3 min showed formation of **96g** (61%), and **94g** (39%). No formation of **95g** was observed. Ru-hydroxide (**43**) formed during the preparation of **6** was remained intact. The alkoxide **94g** was characterized at –50 °C using ^{1}H, ^{31}P{^{1}H}, COSY and ^{13}C-^{1}H HSQC NMR experiments. ^{1}H NMR (399.95 MHz, THF-d_8, –50 °C): δ –17.0 (1H, br t, J = 23.8 Hz, Ru-H), 1.32 (3H, overlapping with a cyclooctane peak, CH_3), 2.13 (1H, br, C$_a$HNHH), 4.04 (2H, overlapping C$_b$HNHH and C$_b$$H$NHH), 4.18 (2H, overlapping C$_a$$H$NHH and C$_bHNHH$), 4.64 (3H, overlapping CH_2 and C$_a$HNHH), 4.80 (1H, br, CHORu), 6-9 (overlapping peaks, aromatic). ^{13}C{^{1}H} NMR (100.6 MHz, THF-d_8, –50 °C, determined using ^{13}C-^{1}H HSQC): δ 30.47 (CH_3), 62.9 (C$_a$HNH), 64.1 (CH_2), 69.0 (CHORu), 69.6 (C$_b$HNH$_2$), 120-140 (aromatic). ^{31}P{^{1}H} NMR (161.91 MHz, THF-d_8, –80 °C): δ 66.27 (d, $^2J_{P-P}$ = 40.6 Hz), 72.36 (d, $^2J_{P-P}$ = 40.2 Hz). See Figures 4-8 to 4-10.

Reaction of [Ru((*R*)-BINAP)(H)((*R*,*R*)-NH(CH(Ph))$_2$NH$_2$)] (7) with 4-hydroxymetylacetophenone (93g) at –78 °C. A solution of **7** (0.0151 mmol) was prepared in THF-d_8 (0.70 mL) in a NMR tube using KN(Si(CH$_3$)$_3$)$_2$ (6.0 mg, 0.030 mmol) as we described previously. A solution of **93g** (6.9 mg, 0.046 mmol) in THF-d_8 (0.20 mL) was then added to the

tube at –78 °C under argon. The solution was mixed by shaking once outside the bath. The sample was then introduced into the NMR probe pre-cooled at –80 °C. ^{1}H, and ^{31}P$\{^1$H$\}$ NMR spectra showed formation of the alkoxide **96g** (100%). The alkoxide **96g** was characterized at –80 °C using ^{1}H, ^{31}P$\{^1$H$\}$, COSY and ^{13}C-^{1}H HSQC NMR experiments. ^{1}H NMR (399.95 MHz, THF-d_8, –80 °C): δ –17.7 (1H, br, Ru-H), 2.55 (3H, s, overlapping with a CH$_3$ peak of unreacted **93g**, CH_3), 2.64 (1H, overlapping with a CH$_3$ peak, C$_a$HNHH), 4.23 (3H, overlapping peaks, C$_a$$HNHH, C_b$$H$NHH, and C$_bHNH$H), 4.46 (1H, br, C$_aHNHH$), 4.77 (1H, overlapping with a CH_2 peak of unreacted **93g**, CH_2), 5.27 (1H, d, J = 19.5 Hz, CH_2), 5.52 (1H, br, C$_b$HNHH), 6-10 (overlapping peaks, aromatic). ^{13}C$\{^1$H$\}$ NMR (100.6 MHz, THF-d_8, –80 °C, determined using ^{13}C-^{1}H HSQC): δ 26.7 (*C*H$_3$), 64.0 and 69.9 (*C*$_a$HNH$_2$ and *C*$_b$HNH$_2$), 64.7 (*C*H$_2$), 120-140 (aromatic). ^{31}P$\{^1$H$\}$ NMR (161.91 MHz, THF-d_8, –80 °C): δ 67.44 (br d, $^2J_{P–P}$ = 36.9 Hz), 74.72 (br). See Figures 4-11 to 4-13.

Reaction of [Ru((*R*)-BINAP)(H)((*R,R*)-NH(CH(Ph))$_2$NH$_2$)] (7) with (–)-1-(4-hydroxymethylphenyl) ethanol (97) at –78 °C. A solution of **7** (0.0203 mmol) was prepared in THF-d_8 (0.70 mL) in a NMR tube using KN(Si(CH$_3$)$_3$)$_2$ (7.0 mg, 0.035 mmol) as we described previously. A solution of **97** (3.4 mg, 0.023 mmol, 97% ee) in THF-d_8 (0.20 mL) was then added to the tube at –78 °C under argon. The solution was mixed by shaking once outside the bath. The sample was then introduced into the NMR probe pre-cooled at –80 °C. ^{1}H, and ^{31}P$\{^1$H$\}$ NMR spectra showed formation of the alkoxide **95g** (100%). The alkoxide **95g** was characterized at –80 °C

using ^1H, $^{31}P\{^1H\}$, COSY and ^{13}C-^1H HSQC NMR experiments. ^1H NMR (399.95 MHz, THF-d_8, –80 °C): δ –17.5 (1H, br t, $J = 25.2$ Hz, Ru-H), 1.54 (3H, overlapping with a cyclooctane peak, CH_3), 2.68 (1H, br, C$_a$HNHH), 3.57 (1H, overlapping with a residual THF-d_8 peak, C$_b$HNHH), 4.28 (1H, br, CH_2) 4.43 (1H, br, C$_b$$H$NHH), 4.63 (1H, overlapping with a CH$_2$ peak of unreacted **97**, C$_a$$H$NHH), 4.78 (1H, br, C$_aHNHH$), 5.00 (2H, C$H_2$ and C$_b$HNHH), 5.28 (1H, s, CH), 6-9 (overlapping peaks, aromatic), 12.2 (1H, br, OH). $^{13}C\{^1H\}$ NMR (100.6 MHz, THF-d_8, –80 °C, determined using ^{13}C-^1H HSQC): δ 27.7(CH_3), 63.2 (C$_a$HNH$_2$),69.29 (α-CH), 70.38 (C$_b$HNH$_2$), 74.24 (CH_2), 120-140 (aromatic). $^{31}P\{^1H\}$ NMR (161.91 MHz, THF-d_8, –80 °C): δ 65.85 (d, $^2J_{P–P} = 40.8$ Hz), 73.09 (d, $^2J_{P–P} = 41.9$ Hz). See Figures 4-14 to 4-16.

Reaction of [Ru((R)-BINAP)(H)((R,R)-NH(CH(Ph))$_2$NH$_2$)] (7) with (–)-1-(4-methoxymethylphenyl) ethanol (98) at –78 °C. A solution of **7** (0.0151 mmol) was prepared in THF-d_8 (0.70 mL) in a NMR tube using KN(Si(CH$_3$)$_3$)$_2$ (3.7 mg, 0.019 mmol) as we described previously. A solution of **98** (6.2 mg, 0.037 mmol, 87% ee) in THF-d_8 (0.20 mL) was then added to the tube at –78 °C under argon. The solution was mixed by shaking once outside the bath. The sample was then introduced into the NMR probe pre-cooled at –80 °C. ^1H, and $^{31}P\{^1H\}$ NMR spectra showed formation of the alkoxide **Me-94g** (78%) and *trans*-[((R)-BINAP)(H)(OH)((R,R)-dpen)] (22%) due to water in the solution. The alkoxide **Me-94g** was characterized at –80 °C using ^1H, $^{31}P\{^1H\}$, COSY and ^{13}C-^1H HSQC NMR experiments. ^1H NMR (399.95 MHz, THF-d_8, –80 °C): δ –17.1 (1H, br, Ru-H), 1.32 (3H,

overlapping with a CH_3 peak of unreacted **98**, CH_3), 2.09 (1H, overlapping with a cyclooctene peak, C$_a$HNHH), 3.28 (3H, overlapping with a OCH_3 peak of unreacted **98,** OCH_3), 3.61 (1H, overlapping with a THF-d_7 peak, C$_b$HNHH), 3.98 (1H, br t, C$_b$$H$NHH), 4.15 (1H, br, C$_a$$H$NHH), 4.38 (2H, overlapping with a CH_2 peak of unreacted **98**, CH_2), 4.43 (1H, overlapping with a CH_2 peak of unreacted **98**, C$_b$HNHHH), 4.84 (2H, overlapping with a CH peak of unreacted **98**, CH and C$_a$HNHHH), 6-9 (overlapping peaks, aromatic). ^{13}C{^{1}H} NMR (100.6 MHz, THF-d_8, −80 °C, determined using ^{13}C-^{1}H HSQC): δ 27.3 (CH_3), 57.08 (OCH_3), 62.8 (C$_a$HNH_2), 69.14 (C$_b$HNH_2), 69.16 (CH), 74.46 (CH_2), 120-140 (aromatic). ^{31}P{^{1}H} NMR (161.91 MHz, THF-d_8, −80 °C): δ 65.2 (br), 71.91 (d, $^2J_{P-P}$ = 40.6 Hz). See Figures 4-17 to 4-19.

Figure 4-2. ^{31}P NMR spectrum (δ 100 to 40) of **96e** prepared from **6** and **93e** at −80 °C.
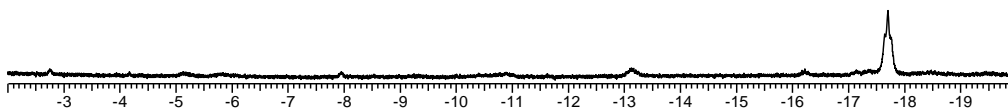
Figure 4-3. ^{1}H NMR spectrum (δ –2 to –20) of **96e** prepared from **6** and **93e** at –80 °C.

Figure 4-4. ^{1}H NMR spectrum (δ 11 to –2) of **96e** prepared from **6** and **93e** at –80 °C. The non-aromatic peaks assigned to **96e** are marked with an asterisk. The remaining peaks are due to excess **93e**, residual protons in THF-d_8, HN(SiC(CH$_3$)$_3$)$_2$, KN(SiC(CH$_3$)$_3$)$_2$, excess (*R,R*)-dpen, cyclooctane and cyclooctene (formed during the hydrogenation of [Ru((*R*)-BINAP)((1-5-*η*)-C$_8$H$_{11}$)]BF$_4$) and hexanes, if present.
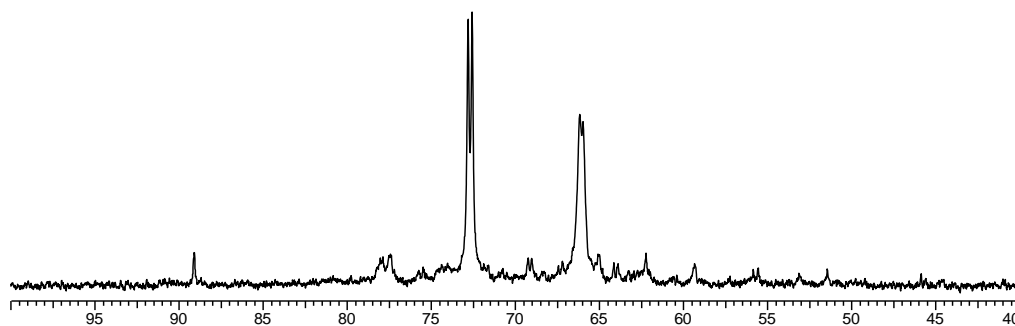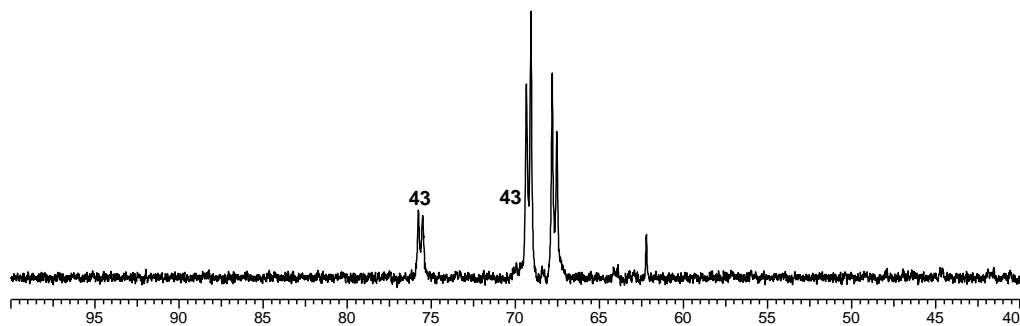
Figure 4-5. ^{31}P NMR spectrum (δ 100 to 40) of **96f** prepared from **7** and **93f** at –80 °C.
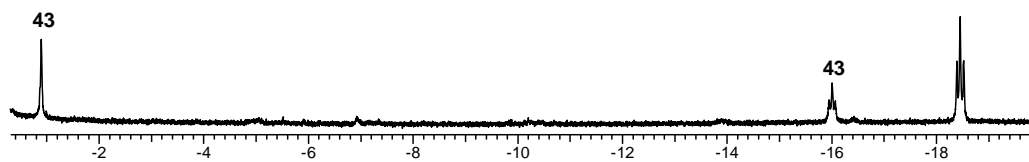
Figure 4-6. ^{1}H NMR spectrum (δ –0.5 to –20) of **96f** prepared from **7** and **93f** at –80 °C.

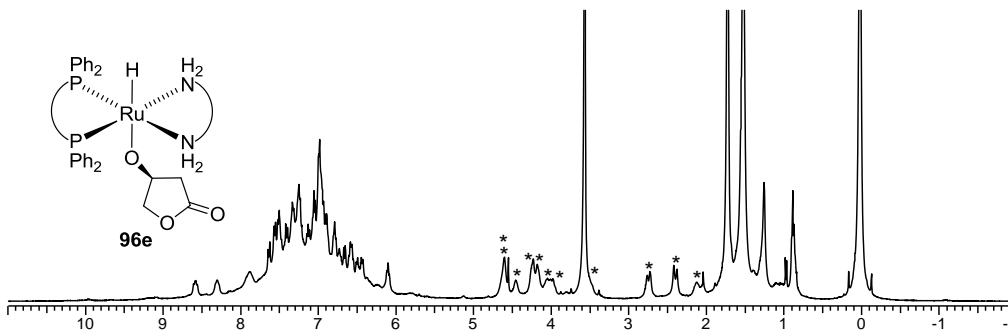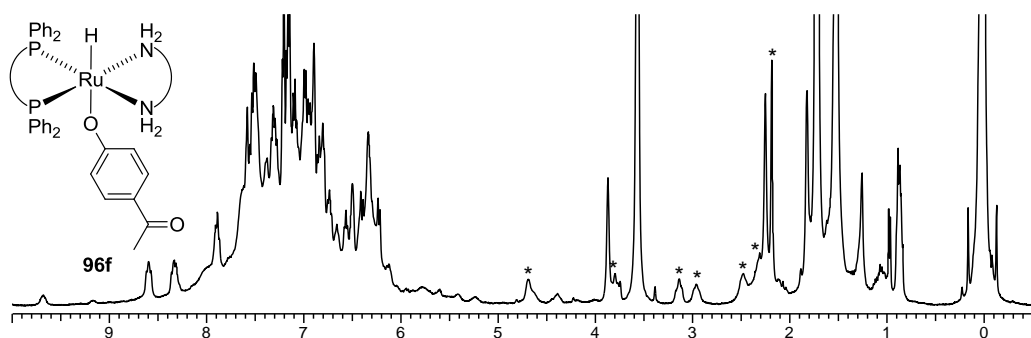**Figure 4-7.** ^{1}H NMR spectrum (δ 11 to –0.5) of **96f** prepared from **7** and **93f** at –80 °C. The non-aromatic peaks assigned to **96f** are marked with an asterisk. The remaining peaks are due to **43**, excess **93f**, residual protons

in THF-d_8, HN(SiC(CH$_3$)$_3$)$_2$, KN(SiC(CH$_3$)$_3$)$_2$, excess (*R*,*R*)-dpen, cyclooctane and cyclooctene (formed during the hydrogenation of [Ru((*R*)-BINAP)((1-5-η)-C$_8$H$_{11}$)]BF$_4$) and hexanes, if present.
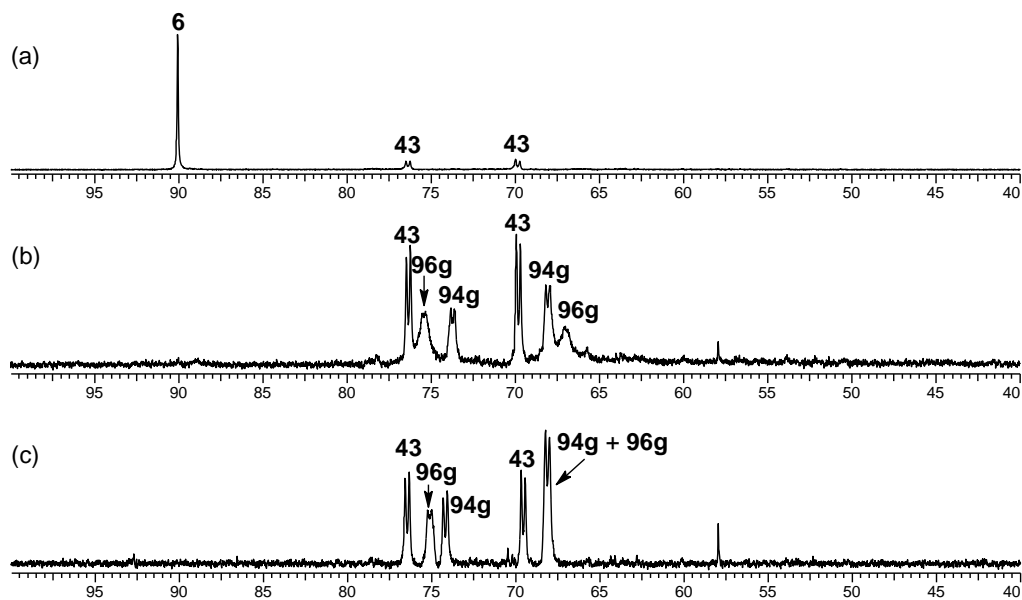
Figure 4-8. ^{31}P NMR spectra (δ 100 to 40) of the reaction between **6** and **93g** in the absence of KN(Si(CH$_3$)$_3$)$_2$ at −80 °C. (a) Before the addition of **93g**. (b) First spectrum taken ~5 min after the addition of **93g** at −80 °C. (c) Spectrum taken at −50 °C.

(a)

(b)

(c)
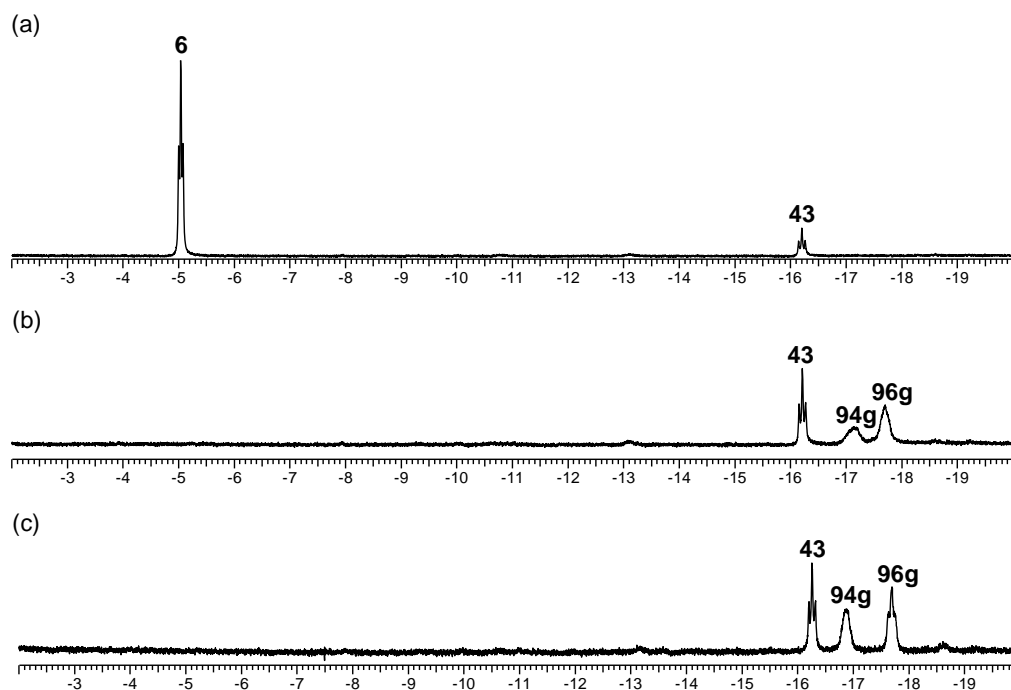
Figure 4-9. ^{1}H NMR spectra (δ –2 to –20) of the reaction between **6** and **93g** in the absence of KN(Si(CH$_3$)$_3$)$_2$ at –80 °C. (a) Before the addition of **93g**. (b) First spectrum taken ~5 min after the addition of **93g** at –80 °C. (c) Spectrum taken at –50 °C.
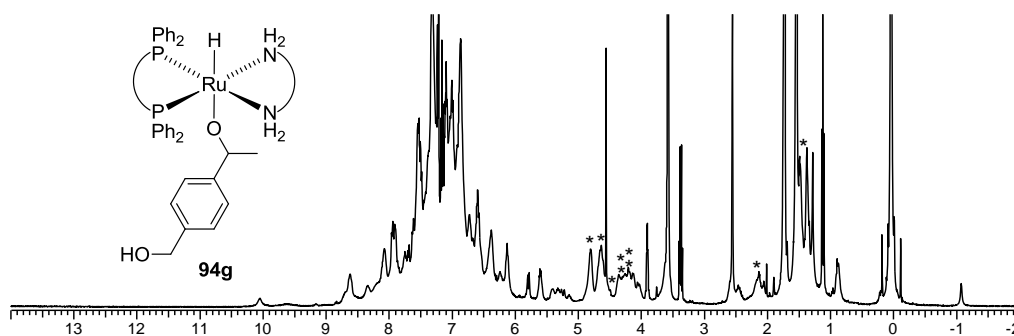
Figure 4-10. ^{1}H NMR spectrum (δ 14 to –2) of the reaction between **6** and **93g** in the absence of KN(Si(CH$_3$)$_3$)$_2$ at –50 °C. The non-aromatic peaks assigned to **94g** are marked with an asterisk. The remaining peaks are due

222

to **43**, **96g**, excess (*R*,*R*)-dpen, the Ru-hydroxide **43**, residual protons in THF-d_8, HN(SiC(CH$_3$)$_3$)$_2$, cyclooctane and cyclooctene (formed during the hydrogenation of [Ru((*R*)-BINAP)((1-5-*η*)-C$_8$H$_{11}$)]BF$_4$) and hexanes, if present.

Figure 4-11. ^{31}P NMR spectrum (δ 100 to 40) of **96g** formed from the reaction between **7** and **93g** at –80 °C. * is Ru species formed during preparation of **7**.

Figure 4-12. ^{1}H NMR spectrum (δ –2 to –20) of **96g** formed from the reaction between **7** and **93g** at –80 °C.
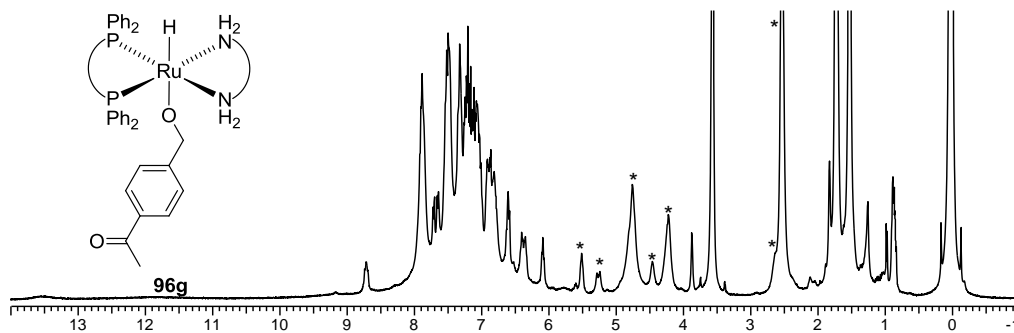
Figure 4-13. ^{1}H NMR spectrum (δ 14 to -1) of **96g** formed from the reaction between **7** and **93g** at $-80\ °C$. The non-aromatic peaks assigned to **96g** are marked with an asterisk. The remaining peaks are due to excess **93g**, residual protons in THF-d_8, KN(Si(CH$_3$)$_3$)$_2$, HN(Si(CH$_3$)$_3$)$_2$, excess (*R*,*R*)-dpen, cyclooctane and cyclooctene (formed during the hydrogenation of [Ru((*R*)-BINAP)((1-5-η)-C$_8$H$_{11}$)]BF$_4$), ether, and hexanes, if present.
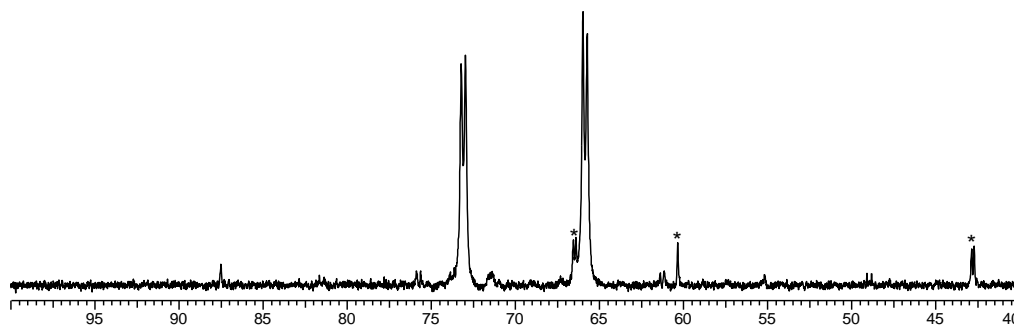
Figure 4-14. ^{31}P NMR spectrum (δ 100 to 40) of **95g** formed from the reaction between **7** and **97** at $-80\ °C$. * is Ru species formed during preparation of **7**.

224
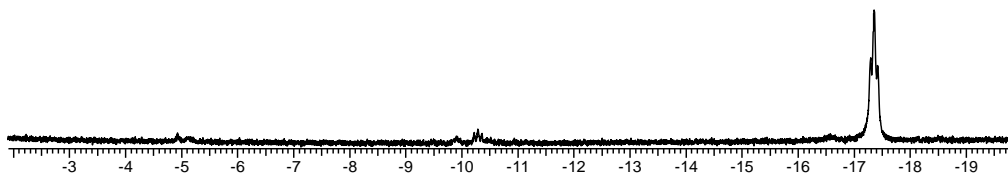
Figure 4-15. ^{1}H NMR spectrum (δ −2 to −20) of **95g** formed from the reaction between **7** and **97** at −80 °C.
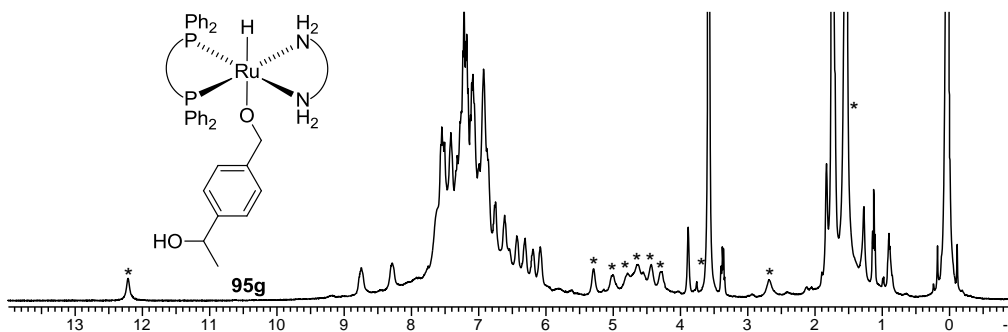
Figure 4-16. ^{1}H NMR spectrum (δ 14 to −1) of **95g** formed from the reaction between **7** and **93g** at −80 °C. The non-aromatic peaks assigned to **95g** are marked with an asterisk. The remaining peaks are due to excess **97**, residual protons in THF-d_8, KN(Si(CH$_3$)$_3$)$_2$, HN(Si(CH$_3$)$_3$)$_2$, excess (R,R)-dpen, cyclooctane and cyclooctene (formed during the hydrogenation of [Ru((R)-BINAP)((1-5-η)-C$_8$H$_{11}$)]BF$_4$), ether, and hexanes, if present.

225
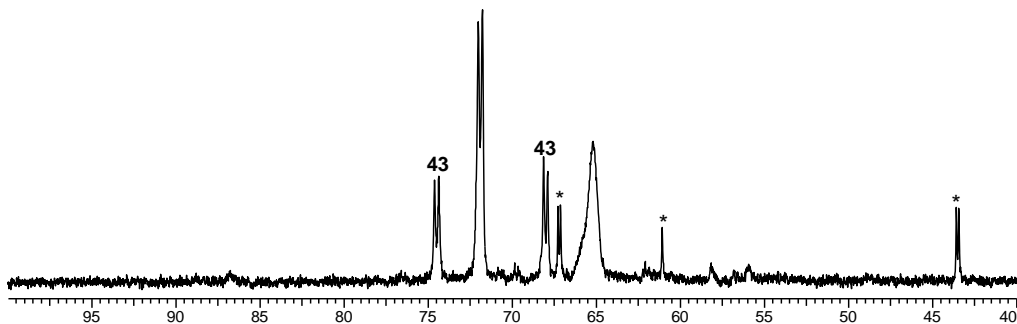
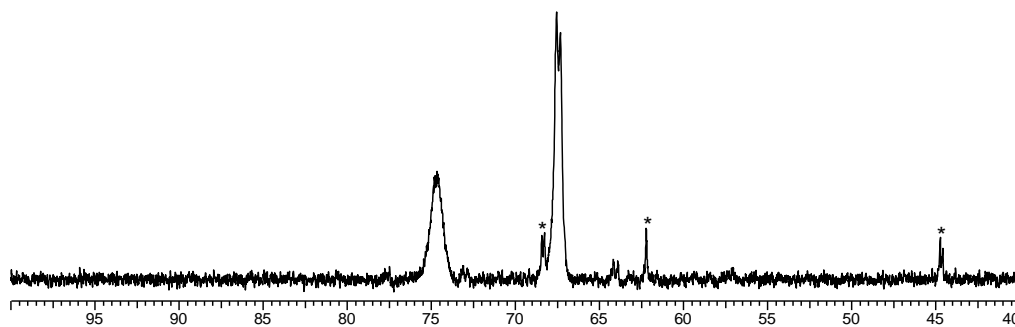**Figure 4-17.** ^{31}P NMR spectrum (δ 100 to 40) of **Me-94g** formed from the reaction between **7** and **98** at −80 °C. * is Ru species formed during preparation of **7**.
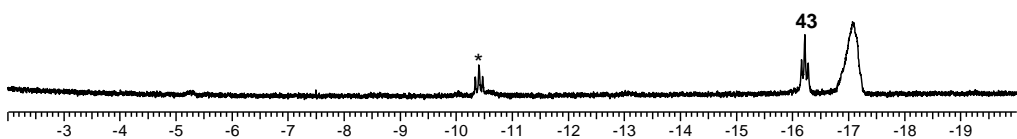
Figure 4-18. ^{1}H NMR spectrum (δ −2 to −20) of **Me-94g** formed from the reaction between **7** and **98** at −80 °C. * is Ru species formed during preparation of **7**.
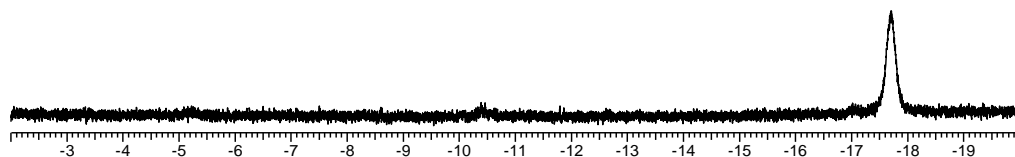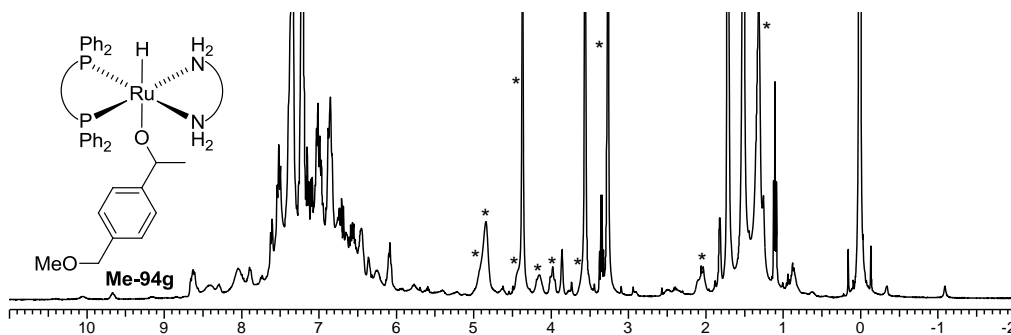
Figure 4-19. ^{1}H NMR spectrum (δ 11 to –2) of **Me-94g** formed from the reaction between **7** and **98** at –80 °C. The non-aromatic peaks assigned to **Me-94g** are marked with an asterisk. The remaining peaks are due to **43**, excess **98**, residual protons in THF-d_8, KN(Si(CH$_3$)$_3$)$_2$, HN(Si(CH$_3$)$_3$)$_2$, excess (R,R)-dpen, cyclooctane and cyclooctene (formed during the hydrogenation of [Ru((R)-BINAP)((1-5-η)-C$_8$H$_{11}$)]BF$_4$), ether, and hexanes, if present.

Chapter 5

Conclusions and Future Directions

Conclusions

The increasing health and environmental regulations on the production of pharmaceuticals is motivating the development of highly selective and environmentally benign industrial syntheses. The Noyori-type ketone hydrogenation system *trans*-[Ru(diphosphine)(X)$_2$(diamine)] + base and its base-free analogues are among the most important discoveries that can address health and environmental regulations without losing economic competency.[27a,87] This catalyst system is already utilized in the pharmaceutical and fine chemical industries, and has proven to be among the most reliable methods to hydrogenate ketones with practical TOF and enantioselectivities.[21,30] The major focus in the development of this catalyst system in academia has been hydrogenation of variety of ketones in high TOF and enantioselectivity since its discovery in the 90's. There was no application of this catalyst system in the hydrogenation of less reactive carbonyl compounds such as esters and amides when this research began.

Although M–H reductions of esters, amides, and related carbonyl compounds, are used more frequently than reduction of ketones,[120] there was no corresponding hydrogenation method that is compatible with multi-functionalized pharmaceutical precursors on production scales. As a result industrial scale synthetic pathways that involve these reductions were either carried out using wasteful M–H reagents or they were

228

avoided.[120a] Most of the homogeneous catalytic systems for these hydrogenations reported prior to this research require high temperatures and pressures that are less economical and are often detrimental to multi-functionalized substrates. Further, mechanistic understanding of these high pressure hydrogenations was limited due to the harsh reaction conditions.

Previously, the mechanism of Noyori ketone hydrogenations was studied in our group utilizing the first stoichiometric reactions of putative intermediates.[35d-f] One of the most surprising discoveries made during this study is the facile net insertion reaction between the dihydride, *trans*-[Ru((*R*)-BINAP)(H)$_2$((*R*,*R*)-dpen)] (**6**) and acetophenone to form the Ru-alkoxide, *trans*-[Ru((*R*)-BINAP)(H)(OCH(CH$_3$)(Ph))((*R*,*R*)-dpen)] (**14**). This addition occurred essentially on mixing at –80 °C. The primary goal of the research described in this dissertation was to utilize the high reducing power of **6** in the hydrogenation of esters, amides, and related less reactive carbonyl compounds. Further, the high reactivity of **6** enabled us to carry out the most detailed mechanistic investigations to date for these hydrogenations. The research presented in this thesis provides the most detailed mechanistic information to date on the hydrogenation of esters and imides. Further, the origin of the formation of the alkoxide **14** was investigated using intramolecular trapping experiments.

Hydrogenation of esters

Before this research, all the homogeneous ester hydrogenation catalyst systems in the literature operated via the inner coordination sphere

mechanism. High temperatures (>100 °C) and/or H_2 pressures (>50 atm) were typically required[55,57,58] for such systems because of the low electrophilicity of esters,[47] and because η^2-coordination of esters to a metal centre is less favoured than ketones.[48] The idea behind this research was thus to overcome such requirements by using the highly active dihydride intermediate **6** that hydrogenates ketones via the outer coordination sphere mechanism.

In this work, the high reducing power of the dihydride **6** and its en analogue *trans*-[Ru((*R*)-BINAP)(H)$_2$(en)] (**41**) was successfully utilized to hydrogenate several esters under mild conditions (30 °C, 4 atm). Further, the hydrogenation of the unactivated ester ethyl hexanoate proceeded catalytically even at –20 °C under 4 atm H_2 to form 1-hexanol and ethanol. However, we discovered that accumulation of the product alcohols or use of 2-PrOH solvent deactivated the catalyst system. For example, TOF(h^{-1}) for the hydrogenation of methyl benzoate decreased from 49 (for the first hour) to 3 (calculated for after 3–4 h). The stoichiometric addition of the dihydride **6** to the ester substrates was carried out to investigate origins of the high initial TOF and product inhibition. The addition of the dihydride to the lactones proceeded unexpectedly fast at –80 °C to form mixtures of Ru-hemiacetaloxides and Ru-alkoxides of product diols. This is the first observation of a transition metal-hemiacetaloxide and -alkoxide compound formed from addition of a lactone or ester substrate. These low temperature experiments demonstrated the exceptionally high intrinsic activity of Noyori-type catalysts towards hydrogenation of esters. Further,

these low temperature NMR experiments showed that these Ru-alkoxides of primary alcohols are stable, and regeneration of the dihydride from these alkoxides is likely the slow step in the catalytic cycle. Thus, the proposed origin of the product inhibition is the formation of stable primary alcohol alkoxides that inhibit regeneration of the active dihydride species. The mechanistic knowledge obtained through this research will help to develop an ester hydrogenation system that is operative under mild conditions with economic competency.

Enantioselective desymmetrization of meso-Cyclic Imides

In this research, initially, hydrogenation of *N*-substituted succinimides and phthalimides were investigated to determine the catalysts' activity and mono/dihydrogenation selectivity. These test hydrogenations revealed that the dihydride **6** dihydrogenates succinimides under mild reaction conditions (30 °C, 4 atm H_2). In contrast, phthalimides were mostly monohydrogenated as long as the reaction temperature was low (30 °C). Based upon these results a monohydrogenation of succinimides was developed with the appropriate imide backbone structure and reaction conditions. Indeed, we found that the dihydride **6** monohydrogenates *meso*-bicyclic imides at 0 °C under 50 atm of H_2. The monohydrogenation formed *trans*-hydroxy lactams in high enantioselectivity. This result was unexpected because the *trans*-hydroxy lactam is the product of net hydride insertion to the more hindered face of the carbonyl groups, and because the catalytic hydrogenation of ketones by the dihydride **6** typically forms product alcohols with low ee's in THF

solvent.

These results were further investigated with low temperature NMR studies. The origin of the *trans*-hydroxy lactam product was found to be the rapid, pseudo-irreversible base catalyzed cis-trans isomerization that favours the formation of thermodynamically more stable *trans*-isomers. This isomerization occurred rapidly even at –80 °C on mixing the solution of *cis*-isomer and mixture of KOH and $HN(Si(CH_3)_3)_2$. The origins of the high enantioselectivity were proposed based on low temperature NMR and X-ray diffraction study, as well as stereochemical analysis of diastereomeric transition states for the net hydride insertion step. The two major contributors for the high enantioselectivity were high intrinsic enantioselectivity of the dihydride addition step induced by highly ordered transition states, and by the irreversibility of the addition step because of the rapid, pseudo-irreversible formation of *trans*-hydroxy lactams under basic conditions. Finally, the utility of this reaction was demonstrated by the *N*-acyliminium ion chemistry that increases the number of stereogenic centres from 5 to 7 in a single step.

Origin of the formation of Ru-alkoxides

In this study, the mechanism for the formation of previously reported alkoxide **14** was investigated.[35f] Specifically, a transition state that leads to the formation of **14** from **6** and acetophenone was investigated using intramolecular trapping experiments. This study is important for two reasons; first, the alkoxide **14** was rarely considered in a catalytic cycle of Noyori-type ketone hydrogenation,[35a-c,37] and the understanding of the

transition state of the formation will have influence in the current understanding of this catalyst system; second, the previous study by Hamilton et al. as well as in Chapters 2 and 3 of this dissertation revealed that regeneration of the Ru-dihydride from Ru-alkoxides and H_2 is the turnover limiting step in ketone, ester, and imide hydrogenation. Thus, understanding of the alkoxide formation mechanism may help improving the catalyst activity.

One of the most difficult aspects of this study was to find a suitable hydroxy-carbonyl compound as an intramolecular trapping agent. After several disappointing results, it was found that 4-hydroxymethyl-acetophenone (**93g**) possess the right balance of trapping ability by the hydroxide group and reactivity at carbonyl group. The rapid reaction between the hydride **6** and **93g** at –80 °C formed an alkoxide of net hydride insertion **94g** and an alkoxide of unreacted **96g** in 43 and 57% yield respectively. Most importantly, no formation of trapped product **95g** was observed. Further, a control reaction between the Ru-amide **7** and the product diol **97** formed **95g** exclusively. Thus there exists a strong bias towards the formation of **95g** over **94g**. These results clearly showed that if the Ru-amide **7** and the product alcohol are the product of dihydride addition, these products must have a strong hydrogen bond between the amide nitrogen and product alcohol OH hydrogen which does not break before the formation of the alkoxide **14**. This strong hydrogen bond is translated into weakening of the electron donation from amide nitrogen to Ru centre, and hence electron deficiency on the Ru centre. Therefore, it is

proposed and likely that the hydrogen bonded species has an interaction between Ru and the alcohol oxygen (Scheme 5-1, left). Alternatively, the sequence of 1) transfer of RuH and NH to carbonyl C=O bond, 2) formation of the hydrogen bonded Ru-amide with Ru⋯O interaction and 3) formation of **14** could occur in concerted manner (Scheme 5-1, right). Indeed, this type of concerted transfer of hydride and formation of a metal oxygen bond was reported for the CO_2 insertion of 18 electron W-alkyl compounds.[114a,b]

Scheme 5-1. Proposed transition pathways for the formation of alkoxide **14**.
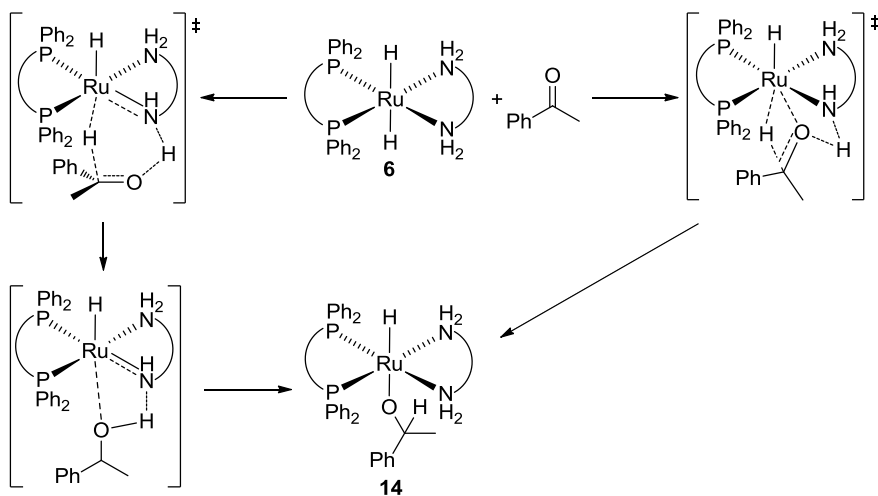
Future research

Chapter 2 showed the high activity of the Ru-dihydrides, and significant product inhibition by primary alcohols. Based on the mechanistic findings in Chapter 2, developments in ester hydrogenations should be directed toward catalyst systems that prevent product inhibition without diminishing the high intrinsic activity of the Ru-dihydride. One approach

234

would be to use of a flow reactor that allows high [product] by removing product from an immobilized catalyst after the reaction.[121] Another approach is to use bulkier ligands that disfavour the formation of Ru-alkoxides.[122] The use of bulky ligands would also stabilize the Ru-amide intermediate.[35a 122c] One possible disadvantage of this strategy is that the bulkier ligand could lower activity of the dihydrides due to the increased catalyst–substrate steric repulsion.[123] Electron-donating phosphine ligands could also destabilize Ru-alkoxides by stronger $p\pi/d\pi$ repulsion.[111,124]

Another solution to product inhibition would be trapping of the alcohol products. Use of silylating agents such as BSA would be one of such strategies.[125] This method, in principle, may form silylated hemiacetals in high enantioselectivity if the trapping of hemiacetal is faster than its racemization via tautomerization (Equation 5-1). Hydrogenation of norbornyl lactone **99** will also trap the product alcohol by the formation of *trans*-hemiacetal **100** in a similar manner to that discussed in Chapter 3. Further, if a racemic mixture of **99** is used, it may be possible to form **100** in high enantioselectivity via kinetic resolution. In this case, use of excess base would be beneficial because it speeds up the cis-trans isomerization of the product hemiacetal (Equation 5-2).

$(5\text{-}1)$

$(5\text{-}2)$

racemic **99**

100
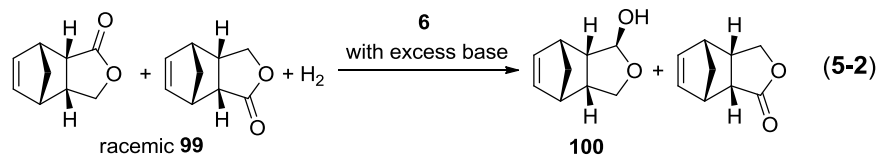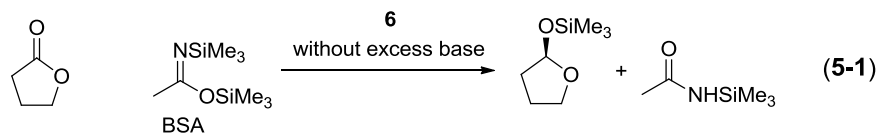
In Chapter 3, I found a catalyst system that hydrogenates imides at low temperature (0 °C). Thus, the next challenge for hydrogenation of carbonyl compounds is the homogeneous hydrogenation of less electrophilic amides. In fact preliminary studies of such homogeneous hydrogenation are already reported using Ru-triphos,[126] Milstein's Ru-PNN,[127] and Ikariya's Ru-Cp* [128] catalyst systems (Scheme 5-2). A common feature of these catalysts is the presence of strongly chelating ligands. The strongly chelating ligands likely prevent catalyst decomposition under the high reaction temperatures (100–164 °C) and long reaction time (14–90 h). All of these systems likely proceed via formation of hemiaminal intermediates.[129]

Scheme 5-2. Previously reported homogeneous amide hydrogenation systems.

1 mol% Ru(acac)$_3$
2 mol% Triphos
40 atm H$_2$
THF, 164 °C, 14 h

NHPh + H$_2$O

99 %

Triphos

1 mol% Ru-PNN
10 atm H$_2$
THF, 110 °C, 48 h

OH + PhNH$_2$

92%

Ru-PNN

10 mol% Ru-Cp*
3 mol% NaOMe
50 atm H$_2$
t-BuOH, 100 °C, 90 h

OH
HN   OMe

>99%

Ru-Cp*
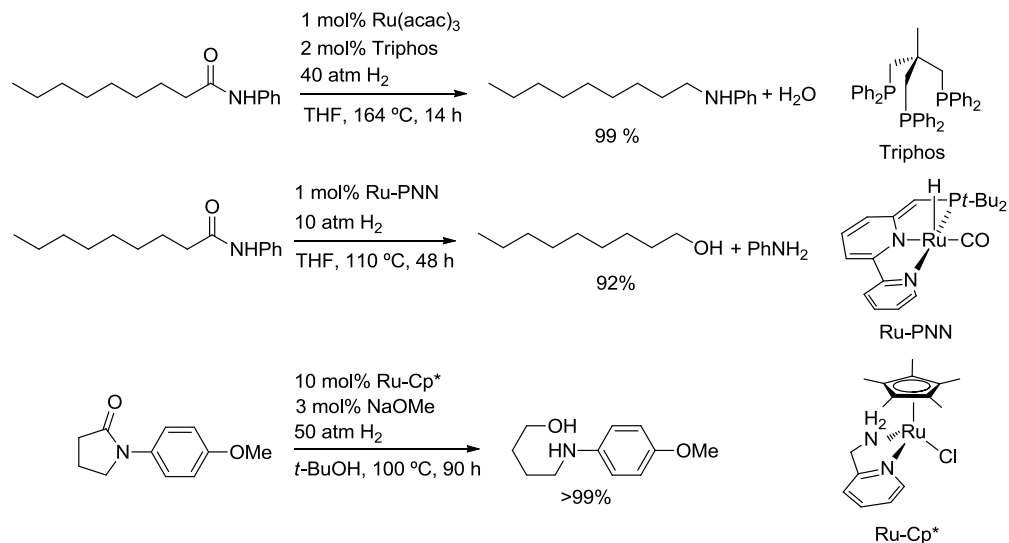
The products of these hydrogenations were either amine and water or primary alcohol and amine.[126,127] This product selectivity likely depends on the basicity of the solution. Thus, relatively less basic reaction conditions of the Ru-triphos system lead to the formation of imine and water from the corresponding hemiaminal intermediate via protonation of the hemiaminal OH group. Hydrogenation of the imine forms the corresponding amine (Scheme 5-2, top). In contrast, relatively basic reaction conditions used for the Ru-PNN and Ru-Cp* systems favour the base catalysed tautomerization of the hemiaminal intermediate to form the corresponding aldehyde and amine that is subsequently hydrogenated to form primary alcohol and amine products (Scheme 5-3, bottom). Hydrogenation of amides by Noyori-type catalysts, such as the dihydride **6**, will thus likely form primary alcohol and amine.

Scheme 5-3. Two pathways for the hydrogenation of amides.
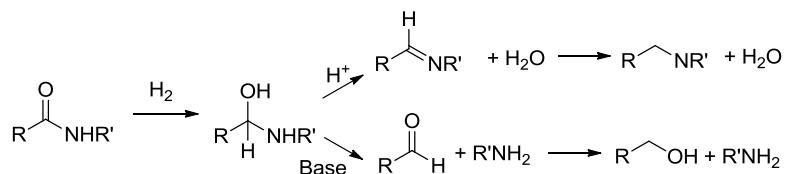
Based on these previous studies, Noyori-type catalysts for amide hydrogenation will require high thermal stability. Such thermal stability will be achieved by replacing relatively weakly coordinating diamine ligands with two equiv of P-N ligands or tetradentate N-P-P-N ligands, or by adding an excess amount of diamine ligands to prevent catalyst decomposition initiated by dissociation of the diamine ligands. The preparation and use of P-N[26,57a,130] and N-P-P-N[57a,131] ligands for Noyori-type and Ikaria's Ru-Cp* hydrogenation are well-studied by the groups of Morris and Ikariya. Further, removal of β-hydrogens on the diamine ligand will prevent the decomposition of the catalyst via β-hydrogen elimination.[132] Alternatively, one could also develop a catalyst system that does not require high temperatures by increasing nucleophilicity of the dihydride catalyst. The utilization of ligands such as **101,** or the *N*-heterocyclic carbene (NHC) ligand such as **102** are promising approaches (Figure 5-1).[60]
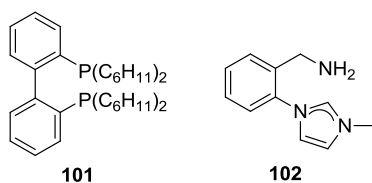
Figure 5-1. Potential electron donating ligands.

References

(1) Wöhler, F. *Ann. Phys-Berlin.* **1828**, *88*, 253.

(2) Mander, L.; Liu, H.-W. *Comprehensive Natural Products II: Chemistry and Biology*, Elsevier Science, Oxford, 2010.

(3) Smith, A. B., III; Freeze, S. *Tetrahedron* **2008**, *64*, 261.

(4) Mickel, A. J. et al. *Org. Process Res. Dev.* **2004**, *8*, 92, 101, 107, 113, and 112.

(5) Dunn, P.; Wells, A.; Williams, M. T. (eds.) *Green Chemistry in the Pharmaceutical Industry*, Wiley-VCH, Weinheim, 2010.

(6) Anastas, P. T.; Farris, C. A. (eds.) *Benign by Design: Alternative Synthetic Design for Pollution Prevention*, Americal Chemical Society, Washington, D.C., 1994.

(7) Trost, B. M. *Science* **1991**, *254*, 1471.

(8) Constable, D. J. C.; Curzons, A. D.; Cunningham, V. L. *Green Chem.* **2002**, *4*, 521.

(9) Sheldon, R. A. *Chem. Ind. (London)*, **1992**, 903.

(10) Harrington, P. J.; Lodewijk, E. *Org. Process Res. Dev.* **1997**, *1*, 72.

(11) Anderson, G. L. *J. Chem. Educ.* **2004**, *81*, 971.

(12) DiMasi, J. A.; Paquette, C. *Pharmacoeconomics* **2004**, *22*, 1.

(13) (a) Chauvin, Y. *Angew. Chem., Int. Ed.* **2006**, *45*, 3741. (b) Schrock, R. R. *Angew. Chem., Int. Ed.* **2006**, *45*, 3748. (c) Grubbs, R. H. *Angew. Chem., Int. Ed.* **2006**, *45*, 3760.

(14) (a) Burns, N. Z.; Baran, P. S.; Hoffmann, R. W. *Angew. Chem., Int. Ed.* **2008**, *48*, 2854. (b) Lin, R. W.; Herndon, R. C. Jr.; Allen, R. H.;

Chockalingham, K. C.; Focht, G. D.; Roy, R. K. WO Patent WO9830529, **1998**.

(15) de Vries, J. G. *Can. J. Chem.* **2001**, *79*, 1086.

(16) Taber, G. P.; Pfisterer, D. M.; Colberg, J. C. *Org. Process Res. Dev.* **2004**, *8*, 385.

(17) Varadaraj, E. et al. US Patent 4,981,995, 1991.

(18) (a) Jayasree, S.; Seayad, A.; Chaudhari, R. V. *Chem. Comm.* **1999**, 1067. (b) Seayad, A.; Jayasree, S.; Chaudhari, R. V. *J. Mol. Catal. A: Chem.* **2001**, *172*, 151.

(19) U.S. FDA Guidance (Drugs), *Development of New Stereoisomeric Drugs*, 1992.

(20) Farina, V.; Reeves, J. T.; Senanayake, C. H.; Song, J. J. *Chem. Rev.* **2006**, *106*, 2734.

(21) Blaser, H. U.; Spindler, F.; Studer, M. *Appl. Catal., A* **2001**, *221*, 119.

(22) Brown, H. C.; Krishnamurthy, S. *Tetrahedron* **1979**, *35*, 567.

(23) de Vries, J. G.; Elsevier, C. J. (eds.) *Handbook of Homogeneous Hydrogenation, Vol. 1, Chap. 15,* Wiley-VCH, Weinheim, 2007.

(24) Nishimura, S. *Handbook of Heterogeneous Catalytic Hydrogenation for Organic Synthesis,* Wiley-VCH, New York, 2001.

(25) (a) Studer, M.; Blaser, H.-U.; Exner, C. *Adv. Synth. Catal.* **2003**, *345*, 45. (b) Blaser, H.-U.; Malan, C.; Pugin, B.; Spindler, F.; Steiner, H.; Studer, M. *Adv. Synth. Catal.* **2003**, *345*, 103. (c) Osawa, T.; Harada, T.; Takayasu, O. *Curr. Org. Chem.* **2006**, *10*, 1513. (d) Bartók, M. *Curr. Org. Chem.* **2006**, *10*, 1533. (e) Heitbaum, M.; Glorius, F.; Escher, I. *Angew. Chem., Int. Ed.*

2006, *45*, 4732. (f) Mallat, T.; Orglmeister, E.; Baiker, A. *Chem. Rev.* **2007**, *107*, 4863.

(26) Ito, M.; Ikariya, T. *Chem. Comm.* **2007**, 5134, and references therein.

(27) (a) de Vries, J. G.; Elsevier, C. J. (eds.) *Handbook of Homogeneous Hydrogenation, Vol. 3, Chap. 32,* Wiley-VCH, Weinheim, 2007. (b) Kitamura, M.; Ohkuma, T.; Inoue, S.; Sayo, N.; Kumobayashi, H.; Akutagawa, S.; Ohta, T.; Takaya, H.; Noyori, R. *J. Am. Chem. Soc.* **1988**, *110*, 629.

(28) (a) Ohkuma, T.; Koizumi, M. Muñiz, K.; Hilt, G.; Kabuto, C.; Noyori, R. *J. Am. Chem. Soc.* **2002**, *124*, 6508. (b) Ohkuma, T.; Sandval, C. A.; Srinivasan, R.; Lin, Q.; Wei, Y.; Muñiz, K.; Noyori, R. *J. Am. Chem. Soc.* **2005**, *127*, 8288.

(29) Beck, G.; Jendralla, H.; Kesseler, K. *Synthesis* **1995**, 1014.

(30) Akutagawa, S. *Appl. Catal., A* **1995**, *128*, 171.

(31) (a) Sánchez-Delgado, R. A.; Valencia, N.; Márquez-Silva, R.-L.; Andriollo, A.; Medina, M. Inorg. Chem. **1986**, *25*, 1106. (b) Geraty, S. M.; Harkin, P.; Vos, J. G. *Inorg. Chim. Acta* **1987**, *131*, 217. (c) Mezzetti, A.; Tschumper, A.; Consiglio, G. *J. Chem. Soc., Dalton Trans.* **1995**, 49.

(32) Clapham, S. E.; Hazovic, A.; Morris, R. H. *Coord. Chem. Rev.* **2004**, *248,* 2201.

(33) (a) Shambayati, S.; Crowe, W. E.; Schreiber, S. L. *Angew. Chem., Int. Ed.* **1990**, *29*, 256. (b) Delbecq, F.; Sautet, P. *J. Am. Chem. Soc.* **1992**, *114*, 2446.

(34) Daley, C. J. A.; Bergens, S. H. *J. Am. Chem. Soc.* **2002**, *124*, 3680.

(35) (a) Abdur-Rashid, K.; Faatz, M.; Lough, A. J.; Morris, R. H. *J. Am. Chem. Soc.* **2001**, *123*, 7473. (b) Abdur-Rashid, K.; Clapham, S. E.; Hadzovic, A.; Harvey, J. N.; Lough, A. J.; Morris, R. H. *J. Am. Chem. Soc.* **2002**, *124*, 15104. (c) Sandoval, C. A.; Ohkuma, T.; Muñiz, K.; Noyori, R. *J. Am. Chem. Soc.* **2003**, *125*, 13490. (d) Hamilton, R. J.; Leong, C. G.; Bigam, G.; Miskolzie, M.; Bergens, S. H. *J. Am. Chem. Soc.* **2005**, *127*, 4152. (e) Hamilton, R. J.; Bergens, S. H. *J. Am. Chem. Soc.* **2006**, *128*, 13700. (f) Hamilton, R. J.; Bergens, S. H. *J. Am. Chem. Soc.* **2008**, *130*, 11979, and references therein.

(36) Farrer, N. J.; McDonald, R.; McIndoe, J. S. *J. Chem. Soc., Dalton Trans.* **2006**, 4570.

(37) (a) Tommaso, D. D.; French, S. A.; Catlow, R. A. *J. Mol. Struct. THEOCHEM*, **2007**, *812*, 39. (b) Leyssens, T.; Peeters, D.; Harvey, J. N. *Organometallics* **2008**, *27*, 1514.

(38) (a) Baratta, W.; Chelucci, G.; Gladiali, S.; Siega, K.; Toniutti, M.;Zanette, M.; Zangrando, E.; Rigo, P. *Angew. Chem., Int. Ed.* **2005**, *44*, 6214. (b) Baratta, W.; Siega, K.; Rigo, P. *Chem. Eur. J.* **2007**, *13*, 7479.

(39) (a) Alonso, D. A.; Brandt, P.; Nordin, S. J. M.; Andersson, P. G. *J. Am. Chem. Soc.* **1999**, *121,* 9580. (b) Yamakawa, M.; Ito, H.; Noyori, R. *J. Am. Chem. Soc.* **2000**, *122,* 1466. (c) Petra, D. G. I.; Reek, J. N. H.; Handgraaf, J.-W.; Meijer, E. J.; Dierkes, P.; Kamer, P. C. J.; Brussee, J.; Schoemaker, H. E.; van Leeuwen, P. W. N. M. *Chem. Eur. J.* **2000**, *15*, 2818. (d) Noyori, R.; Yamakawa, M.; Hashiguchi, S. *J. Org. Chem.* **2001**, *66*, 7931 (e) Handgraaf, J.-W.; Meijer, E. J. *J. Am. Chem. Soc.* **2007**, *129,* 3099.

(40) Casey, C. P.; Johnson, J. B. *J. Org. Chem.* **2003**, *68*, 1998.

(41) (a) Casey, C. P.; Singer, S. W.; Powell, D. R.; Hayashi, R. K.; Kavana, M. *J. Am. Chem. Soc.* **2001**, *123*, 1090. (b) Casey, C. P.; Johnson, J. B. *J. Am. Chem. Soc.* **2005**, *127*, 1883. (c) Casey, C. P.; Johnson, J. B.; Singer, S. W.; Cui, Q. *J. Am. Chem. Soc.* **2005**, *127*, 3100. (d) Casey, C. P.; Bikzhanova, G. A.; Cui, Q.; Guzei, I. A. *J. Am. Chem. Soc.* **2005**, *127*, 14062. (e) Casey, C. P.; Bikzhanova, G. A.; Guzei, I. A. *J. Am. Chem. Soc.* **2006**, *128*, 2286. (f) Casey, C. P.; Clark, T. B.; Guzei, I. A. *J. Am. Chem. Soc.* **2007**, *129*, 11821. (g) Casey, C. P.; Beetner, S. E.; Johnson, J. B. *J. Am. Chem. Soc.* **2008**, *130*, 2285.

(42) (a) Johnson, J. B.; Bäckvall, J.-E. *J. Org. Chem.* **2003**, *123*, 7681. (b) Éll, A. H.; Johnson, J. B.; Bäckvall, J.-E. *Chem. Commun.* **2003**, 1652. (c) Samec, J. S. M.; Éll, A. H.; Bäckvall, J.-E. *Chem. Commun.* **2004**, 2748. (d) Samec, J. S. M.; Éll, A. H.; Bäckvall, J.-E.; Andersson, P. G.; Brandt, P. *Chem. Soc. Rev.* **2006**, *35*, 237. (e) Samec, J. S. M.;E´ ll, A. H.; Åberg, J. B.; Privalov, T.; Eriksson, L.; Bäckvall, J.-E. *J. Am. Chem. Soc.* **2006**, *128*, 14293. (f) Privalov, T.; Samec, J. S. M.; Bäckvall, J.-E. *Organometallics* **2007**, *26*, 2840. (g) Åberg, J. B.; Bäckvall, J.-E. *Chem. Eur. J.* **2008**, *14*, 9169.

(43) Conley, B. L.; Pennington-Boggio, M. K.; Boz, E.; Williams, T. J. *Chem. Rev.* **2010**, *110*, 2294.

(44) Comas-Vives, A.; Ujaque, G.; Lledós, A. *Organometallics* **2007**, *26*, 4135.

(45) Hadzovic, A.; Song, D.; MacLaughlin, C. M.; Morris, R. H. *Organometallics* **2007**, *26*, 5987.

(46) Clapham, S. E.; Guo, R.; Iuliis, M. Z.-D.; Rasool, N.; Lough, A.; Morris, R. H. *Organometallics* **2006**, *25*, 5477.

(47) Carey, F. A.; Sundberg, R. J. *Advanced Organic Chemistry, 4th ed.*, Kluwer Academic/Plenum Publishers, New York, 2000.

(48) (a) Burkey, D. J.; Debad, J. D.; Legzdins, P. *J. Am. Chem. Soc.* **1997**, *119*, 1139. (b) Meiere, S. H.; Ding, F.; Friedman, L. A.; Sabat, M.; Harman, W. D. *J. Am. Chem. Soc.* **2002**, *124*, 13506. (c) Graham, P. M.; Meiere, S. H.; Sabat, M.; Harman, W. D. *Organometallics* **2003**, *22*, 4364. (d) Graham, P. M.; Mocella, C. J.; Sabat, M.; Harman, W. D. *Organometallics* **2005**, *24*, 911.

(49) (a) Rieke, R. D.; Thakur, D. S.; Roberts, B. D.; White, G. T. *J. Am. Oil Chem. Soc.* **1997**, *74*, 333. (b) Parmon, V. N. et al. *Russ. J. Gen. Chem.* **2008**, *78*, 2203.

(50) Grey, R. A.; Pez, G. P.; Wallo, A. *J. Am. Chem. Soc.* **1981**, *103*, 7536.

(51) Linn, Jr. D. E.; Halpern, J. *J. Am. Chem. Soc.* **1987**, *109*, 2969.

(52) Matteoli, U.; Menchi, G.; Bianchi, M.; Piacenti, F.; Ianelli, S.; Nardelli, M. *J. Organomet. Chem.* **1995**, *498*, 177, and references therein.

(53) (a) van Engelen, M. C.; Teunissen, H. T.; de Vries, J. G.; Elsevier, C. J. *J. Mol. Catal. A* **2003**, *206*, 185, and references therein. (b) Kilner, M.; Tyers, D. V.; Crabtree, S. P.; Wood, M. A. WO03093208 A1, **2003**. (c) Yamamoto, K.; Watanabe, T.; Abe, T. JP2004300131, **2004**.

(54) Geilen, F. M. A.; Engendahl, B.; Harwardt, A.; Marquardt, W.;

Klankermayer, J.; Leitner, W. *Angew. Chem., Int. Ed.* **2010**, *49*, 5510.

(55) Zhang, J.; Leitus, G.; Ben-David, Y.; Milstein, D. *Angew. Chem., Int. Ed.* **2006**, *45*, 1113.

(56) Strem's online catalogue (http://www.strem.com/catalog/)

(57) (a) Saudan, L.; Saudan,C. M.; Debieux, C.; Wyss, P. *Angew. Chem., Int. Ed.* **2007**, *46*, 7473. (b) Saudan, L.; Dupau, P.; Riedhauser, J.; Wyss, P. WO2006106484 A1, **2006**. (c) Saudan, L.; Saudan, C. WO2008065588 A1, **2008**. (d) Saudan, L.; Saudan, C. WO2010038209 A1, **2010**. (e) Saudan, L. *Acc. Chem. Res.* **2007**, *40*, 1309.

(58) (a) Ino, Y.; Yoshida, A.; Kuriyama, W. EP1970360 A1, **2008**. (b) Kuriyama, W.; Ino, Y.; Ogata, O.; Sayo, N.; Saito, T. *Adv. Synth. Catal.* **2010**, *352*, 92.

(59) Ikariya, T.; Ito, M.; Ootsuka, T. WO2010004883 A1, **2010**.

(60) O, W. W. N.; Lough, A.; Morris, R. H. *Chem. Commun.* **2010**, 8240.

(61) McAlees, A. J.; McCrindle, R. *J. Chem. Soc. C* **1969**, *19*, 2425.

(62) (a) Patton, D. E.; Drago, R. S. *J. Chem. Soc., Perkin Trans. 1* **1993**, 1611. (b) Aoun, R.; Renaud, J.-L.; Dixneuf, P. H.; Bruneau, C. *Angew. Chem., Int. Ed.* **2005**, *44*, 2021.

(63) Ito, M.; Sakaguchi, A.; Kobayashi, C.; Ikariya, T. *J. Am. Chem. Soc.* **2007**, *129*, 290.

(64) (a) Shambayati, S.; Crowe, W. E.; Schreiber, S. L. *Angew. Chem., Int. Ed.* **1990**, *29*, 256. (b) Evans, D. A.; Rovis, T.; Kozlowski, M. C.; Tedrow, J. S. *J. Am. Chem. Soc.* **1999**, *121*, 1994. (c) Daley, C. J.; Bergens, S. H. *J. Am. Chem. Soc.* **2002**, *124*, 3680.

(65) Kapoor, P.; Pathak, A.; Kapoor, R.; Venugopalan, P. *Inorg. Chem.* **2002**, *41*, 6153, and references therein.

(66) Kirby, A. J. *Stereoelectronic Effects*, Oxford University Press Inc., New York, 2007.

(67) Jeffrey, G. A. *An Introduction to Hydrogen Bonding*, Oxford University Press Inc., New York, 1997.

(68) Olmstead, W. N.; Margolin, Z.; Bordwell, F. G. *J. Org. Chem.* **1980**, *45*, 3295.

(69) Seyden-Penne, J. *Reductions by the Alumino- and Borohydrides in Organic Synthesis*, 2nd eds.; WILEY-VCH: New York, 1997.

(70) Barrett, A.G. M.; Broughton, H. B.; Attwood, S. V.; Gunatilaka, A. A. L. *J. Org. Chem.* **1986**, *51*, 495.

(71) Wiles, J. A.; Daley, C. J. A.; Hamilton, R. J.; Leong, C. G.; Bergens, S. H. *Organometallics* **2004**, *23*, 4564.

(72) (a) Speckamp, W. N.; Moolenaar, M. J. *Tetrahedron* **2000**, *56*, 3817. (b) Maryanoff, B. E.; Zhang, H-C.; Cohen, J. H.; Turchi, I. J.; Maryanoff, C. A. *Chem. Rev.* **2004**, *104*, 1431. (c) Royer, J.; Bonin, M.; Micouin, L. *Chem. Rev.* **2004**, *104*, 2311. (d) Atodiresei, I.; Schiffers, I.; Bolm, C. *Chem. Rev.* **2007**, *107*, 5683. (e) Yazici, A.; Pyne, S. G. *Synthesis* **2009**, *3*, 339.

(73) Ramón, D. J.;Guillena, G.; Seebach, D. *Helv. Chim. Acta*, **1996**, *79*, 875.

(74) (a) Matuki, K.; Inoue, H.; Ishida, A.; Takeda, M.; Nakagawa, M.; Hino, T. *Chem. Pharm. Bull.* **1994**, *42*, 9. (b) Kang, J.; Lee, J. W.; Kim, J. I.; Pyun, C. *Tetrahedron Lett.* **1995**, *36*, 4265. (c) Ostendorf, M.; Romagnoli, R.;

Pereiro, I. C.; Roos, E. C.; Moolenaar, M. J.; Speckamp, W. N.; Hiemstra, H. *Tetrahedron. Asymmetry* **1997**, *8*, 1773. (d) Shimizu, M.; Nishigaki, Y.; Wakabayashi, A. *Tetrahedron Lett.* **1999**, *40*, 8873. (e) Dixon, R. A.; Jones, S. *Tetrahedron: Asymmetry* **2002**, *13*, 1115. (f) Chen, F. E.; Dai, H. F.; Kuang, Y. Y.; Jia, H. Q. *Tetrahedron: Asymmetry* **2003**, *14*, 3667. (g) Oba, M.; Koguchi, S.; Nishiyama, K. *Tetrahedron* **2004**, *60*, 8089.

(75) (a) Corey, E. J.; Mehrotra, M. M. *Tetrahedron Lett.* **1988**, *29*, 57. (b) Moolneaar, J. M.; Speckamp, W. N.; Hiemstra, H.; Poetsch, E.; Casutt, M. *Angew. Chem., Int. Ed.* **1995**, *34*, 2391. (c) Bonrath, W.; Karge, R.; Netscher, T.; Roessler, F.; Spindler, F. *Chimia,* **2009**, *63*, 265.

(76) Molinaro, C.; Gauvreau, D.; Hughes, G.; Lau, S.; Lauzon, S.; Angelaud, R.; O'Shea, P. D.; Janey, J.; Palucki, M.; Hoerrner, S. R.; Raab, C. E.; Sidler, R. R.; Belley, M.; Han, Y. *J. Org. Chem.* **2009**, *74*, 6863.

(77) Danishefsky, S. J.; Lin, H. *Angew. Chem., Int. Ed.* **2003**, *42*, 36.

(78) (a) Speckamp, W. N.; Moolenaar, M. J. *Tetrahedron* **2000**, *56*, 3817. (b) Maryanoff, B. E.; Zhang, H.-C.; Cohen, J. H.; Turchi, I. J.; Maryanoff, C. A. *Chem. Rev.* **2004**, *104*, 1431. (c) Royer, J.; Bonin, M.; Micouin, L. *Chem. Rev.* **2004**, *104*, 2311. (d) Yazici, A.; Pyne, S. G. *Synthesis* **2009**, *3*, 339.

(79) Myers, E. L.; de Vries, J. G.; Aggarwal, V. K. *Angew. Chem., Int. Ed.* **2007**, *46*, 1893.

(80) Raheem, I. T.; Thiara, P. S.; Peterson, E. A.; Jacobsen, E. N. *J. Am. Chem. Soc.* **2007**, *129*, 13404.

(81) (a) Valters, R. Russ*. Chem. Rev.* **1982**, *51*, 1374. (b) Valters, R. E.; Flitsch, W. *Ring-Chain Tautomerism*, Plenum Press, Ney York, 1985.

(82) (a) Hubert, J. C.; Wunberg, J. B. P. A.; Speckamp, W. N. *Tetrahedron* **1975**, *31*, 1437. (b) Wunberg, J. B. P. A.; Schoemaker, H. E.; Speckamp, W. N. *Tetrahedron* **1978**, *34*, 179.

(83) Jung, M. E.; Piizzi, G. *Chem. Rev.* **2005**, *105*, 1735.

(84) Vejn, R. J.; Hiemstra, H.; Kok, J. J.; Knotter, M.; Speckamp, W. N. *Tetrahedron* **1987**, *43*, 5019.

(85) Storm, D. R.; Koshland, D. E. *J. Am. Chem. Soc.* **1972**, *96*, 5805 and 5815.

(86) Ohkuma, T.; Koizumi, M.; Doucet, H.; Pham, T.; Kozawa, M.; Murata, K.; Katayama, E.; Yokozawa, T.; Ikariya, T.; Noyori, R. *J. Am. Chem. Soc.* **1998**, *120,* 13529.

(87) Noyori, R.; Ohkuma, T. *Angew. Chem., Int. Ed.* **2001**, *40*, 41.

(88) Brown, H. C.; Kawakami, J. H. *J. Am. Chem. Soc.* **1970**, *92*, 1990.

(89) (a) Bryndza, H. E.; Tam, W. *Chem. Rev.* **1988**, *88*, 1163. (b) Bergman, R. G. *Polyhedron* **1995**, *14*, 3227. (c) Fulton, J. R.; Holland, A. W.; Fox, D. J.; Bergman, R. G. *Acc. Chem. Res.* **2002**, *35*, 44.

(90) El Gihani, M. T.; Heaney, H. *Synthesis* **1998**, 357.

(91) Nicolaou, K. C.; Li, A.; Ellery, S. P.; Edmonds, D. J. *Angew. Chem., Int. Ed.* **2009**, *48*, 6293.

(92) Lok, K. p.; Jakovac, I. J.; Jones, J. B. *J. Am. Chem. Soc.* **1985**, *107*, 2521.

(93) Hartwig, J. *Organotransition Metal Chemistry. From Bonding to Catalysis*, University Science Books, 2010.

(94) Zhang, W.; Zheng, A.; Liu, Z.; Yang, L.; Liu, Z. *Tetrahedron Lett.* **2005**, *46*, 5691.

(95) Arai, Y.; Kontani, T.; Koizumi, T. *J. Chem. Soc., Perkin Trans. 1*, **1994**, 15

(96) Sano, H.; Noguchi, T.; Tanatani, A.; Miyachi, H.; Hashimoto, Y. *Chem. Pharm. Bull.* **2004**, *52*, 1021.

(97) Liang, J.; Lv, J.; Fan, J.-C.; Shang, Z.-C. *Synth. Commun.* **2009**, *39*, 2822.

(98) Fraga-Dubreuil, J.; Comak, G.; Taylor, A. W.; Poliakoff, M. *Green Chem.* **2007**, *9*, 1067.

(99) Bilyard, K.; Garratt, P. J.; Hunter, R.; Lete, E. *J. Org. Chem.* **1982**, *47*, 4731.

(100) Barker, M. D.; Dixon, R. A.; Jones, S.; Marsh, B. J. *Tetrahedron* **2006**, *62*, 11663.

(101) Sauers, C. K.; Marikakis, C. A.; Lupton, M. A. *J. Am. Chem. Soc.* **1973**, *95*, 6792.

(102) Vargas, J.; Santiago, A. A.; Gaviño, R.; Cerda, A. M.; Tlenkopatchev, M. A. *eXPRESS Polym. Lett.* **2007**, *1*, 274.

(103) Hill, T. A.; Stewart, S. G.; Ackland, S. P.; Gilbert, J.; Sauer, B.; Sakoff, J. A.; McCluskey, A. *Bioorg. Med. Chem.* **2007**, *15*, 6126.

(104) Bentz, T.; Ryzhkov, L. R. *Spectrosc. Lett.* **2006**, *39*, 225.

(105) Yuan, X.-H.; Zhang, M.-J.; Kang, C.-Q.; Guo, H.-Q.; Qiu, X.-P.; Gao, L.-X.; *Synth. Commun.* **2006**, *36*, 435.

(106) Wang, J.; Johnson, D. M. *Polym. Int.* **2009**, *58*, 1234.

(107) Wilk, A.; Grajkowski, A.; Phillip, L. R.; Beaucage, S. L. *J. Org. Chem.* **1999**, *64*, 7515.

(108) Wang, X.; Guo, H.; Xie, G.; Zhang, Y. *Synthetic Commun.* **2004**, *34*, 3001.

(109) Hall, Jr. H. K. *J. Am. Chem. Soc.* **1957**, *79*, 5441.

(110) Holland, P. L.; Andersen, R. A.; Bergman, R. G. *Comments Inorg. Chem.* **1999**, *21*, 115.

(111) Mayer, J. M. *Comments Inorg. Chem.* **1988**, *8*, 125.

(112) Hedberg, C.; Källstöm, k.; Arvidsson, P. I.; Brandt, P.; Andersson, P. G. *J. Am. Chem. Soc.* **2005**, *127*, 15083.

(113) (a) Whitesides, G. M.; Boschetto, D. J. *J. Am. Chem. Soc.* **1971**, *93*, 1529. (b) Jacobson, S. E.; Wojcicki, A. *J. Am. Chem. Soc.* **1973**, *95*, 6962. (c) Miles, S. L.; Miles, D. L.; Bau, R.; Flood, T. C. *J. Am. Chem. Soc.* **1978**, *100*, 7278. (d) Dong, D.; Slack, D. A.; Baird, M. C. *J. Organomet. Chem.* **1975**, *153*, 219. (e) Su, S.-C. H.; Wojcicki, A. *Organometallics* **1983**, *2*, 1296.

(114) (a) Darensbourg, D. J.; Grötsch, G. *J. Am. Chem. Soc.* **1985**, *107*, 7473. (b) Darensbourg, D. J.; Hanckel, R. K.; Bauch, C. G.; Pala, M.; Simmons, D.; White, J. N. *J. Am. Chem. Soc.* **1985**, *107*, 7463. (c) Gaus, P. L.; Kao, S. C.; Youngdahl, K.; Darensbourg, M. Y. *J. Am. Chem. Soc.* **1985**, *107*, 2428. (d) Tooley, P. A.; Ovalles, C.; Kao, S. C.; Darensbourg, D. J.; Darensbourg, M. Y. *J. Am. Chem. Soc.* **1986**, *108*, 5465. (e) Sullivan, B. P.; Meyer, T. J. *Organometallics* **1986**, *5*, 1500. (f) Whittlesey, M. K.; Perutz, R. N.; Moore, M. H. *Organometallics* **1996**, *15*, 5516. (g) Jessop, P. G.; Hsiao,

Y.; Ikariya, T.; Noyori, R. *J. Am. Chem. Soc.* **1996**, *118*, 344. (h) Jessop, P. G.; Joó, F.; Tai, C.-C. *Coord. Chem. Rev.* **2004**, *248*, 2425.

(115) Ruan, J.; Li, X.; Saidi, O.; Xiao, J. *J. Am. Chem. Soc.* **2008**, *130*, 2424.

(116) Hyder, Z.; Mo, J.; Xiao, J. *Adv. Synth. Catal.* **2006**, *348*, 1699.

(117) Dijksman, A.; Marino-González, A.; Payeras, A. M. i.; Arends, I. W. C. E.; Sheldon, R. A. *J. Am. Chem. Soc.* **2001**, *123*, 6826.

(118) Tanaka, K.; Inoue, S.; Ito, D.; Murai, N.; Kaburagi, Y.; Shirotori, S. WO2006098270, **2006**.

(119) Arshady, R.; Ledwith, A. *Makromol. Chem.* **1978**, *179*, 819.

(120) (a) Carey, J. S.; Laffan, D.; Thomson, C.; Williams, M. T. *Org. Biomol. Chem.*, **2006**, *4*, 2337. (b) Constable, D. J C.; Dunn, P. J.; Hayler, J. D.; Humphrey, G. R.; Leazer, Jr. J. L.; Linderman, R. J.; Lorenz, K.; Manley, J.; Pearlman, B. A.; Wells, A.; Zaks, A.; Zhang, T. Y. *Green Chem.* **2007**, *9*, 411.

(121) (a) Mak, X. Y. Laurino, P. Seeberger, P. H. Beilstein *J. Org. Chem.* **2009**, *5*, No. 19. (b) Webb, D.; Jamison, T. F. *Chem. Sci.* **2010**, *1*, 675.

(122) (a) Tolman, C. A. *Chem. Rev.* **1977**, *77*, 313. (b) Bunten,K. A.; Chen, L.; Fernandez, A. L.; Poë, A. J. *Coord. Chem. Rev.* **2002**, *41*, 233. (c) Power, P. P. *J. Organometallic Chem.* **2004**, *689*, 3904.

(123) (a) Schrock, R. R. *Polyhedron* **1995**, *14*, 3177. (b) Sanford, M. S.; Henling, L. M.; Day, M. W.; Grubbs, R. H. *Angew. Chem., Int. Ed.* **2000**, *39*, 4351.

(124) Holland, P. L.;   Andersen, R. A.; Bergman, R. G.; Huang, J.; Nolan, S. P. *J. Am. Chem. Soc.* **1997**, *119,* 12800.

(125) (a) Hansen, K. B.; Rosner, T.; Kubryk, M.; Dormer, P. G.; Armstrong, III, J. D. *Org. Lett.* **2005**, *7*, 4935. (b) de Vries, J. G.; Elsevier, C. J. (eds.) *Handbook of Homogeneous Hydrogenation, Vol. 3, Chap. 44,* Wiley-VCH, Weinheim, 2007.

(126) Magro, A. A. N.; Eastham, G. R.; Cole-Hamilton, D. J. *Chem. Commun.* **2007**, 3154.

(127) Balaraman, E.; Gnanaprakasam, B.; Shimon, L. J. W.; Milstein, D. *J. Am. Chem. Soc.* **2010**, *132*, 16756.

(128) (a) Ito, M.; Koo, L. W.; Himizu, A.; Kobayashi, C.; Sakaguchi, A.; Ikariya, T. *Angew. Chem., Int. Ed.* **2008**, *48,* 1324. (b) Ikariya, T.; Ito, M.; Ootsuka, T. WO2010073974 A1, **2010**.

(129) Kawamichi, T.; Haneda, T.; Kawano, M.; Fujita, M. *Nature* **2009**, *461*, 633.

(130) (a) Guo, R.; Lough, A. J.; Morris, R. H.; Song, D. *Organometallics* **2004**, *23*, 5524. (b) Ito, M.; Osaku, A.; Kobayashi, C.; Shiibashi, A.; Ikariya, T. *Organometallics* **2009**, *28*, 390.

(131) (a) Gao, J.-X.,; Ikariya, T.,; Noyori, R. *Organometallics* **1996**, *15*, 1087. (b) Li, T.; Churlaud, R.; Lough, A. J.; Abdur-Rashid; Morris, R. H. *Organometallics* **2004**, *23*, 6239. (c) Sui-Seng, C.; Freutel, F.; Lough, A. J.; Morris, R. H. *Angew. Chem., Int. Ed.* **2008**, *47*, 940.

(132) Abbel, R.; Abdur-Rashid, K.; Faatz, M.; Hadzovic, A.; Lough, A. J.; Morris, R. H. *J. Am. Chem. Soc.* **2005**, *127*, 1870.